



# Linear Interference Cancellation Structures in DS- CDMA Systems

by

**Abdelouahab BENTRCIA**

**A dissertation submitted for the degree of**

**Doctor of Science**

**Departement of Electronics, College of Engineering, Batna University**

**June 2008**

République Algérienne Démocratique et Populaire  
Ministère de l'enseignement Supérieure et de la Recherche Scientifique  
Université de Batna

# Thèse

Présentée au Département d'électronique  
Faculté des sciences de l'ingénieur  
Pour l'obtention du diplôme de

Docteur en Science  
Option : Communication

par  
Abdelouahab BENTRCIA

Thème

## Les Structures d'Annulation Linéaire d'Interférence Dans les Systèmes Cellulaires DS-CDMA

Soutenue le : 29 Juin, 2008

Devant la commission d'examen composée de:

<b>Mohamed Boulemden</b>	Professeur	Université de Batna	Président
<b>Moussa Benyoucef</b>	Maître de conférences	Université de Batna	Rapporteur
<b>Azzedine Zerguine</b>	Professeur Associé	Université Roi Fahd du Pétrole et des minéraux (KFUPM)	Rapporteur (à l'étranger)
<b>Fauzi Soltani</b>	Professeur	Université de Constantine	Examineur
<b>Djamel Chikouche</b>	Professeur	Université de M'sila	Examineur
<b>Lamir Saidi</b>	Maître de conférences	Université de Batna	Examineur

## Dedication

To my family 😊

## **Acknowledgement**

First and foremost, my unconditional praise and thankfulness goes to Allah, the Most Compassionate, and the Most Merciful for his countless bounties and blessings.

I am grateful to my PhD advisor in Algeria Dr. Moussa Benyoucef for his encouragement and continuous support throughout different phases of this dissertation. His assistance and valuable support in all administrative details with the University is highly appreciated.

I am highly indebted to my PhD advisor in Saudi Arabia Dr. Azzedine Zerguine for the constant support and encouragement he provided through my graduate studies. I appreciate his great effort in improving my writing skills and in revising my papers. I would especially like to thank him for his helpful advice not only in my academic research but also in building my future career.

I would like to thank Prof. Mohamed Boulemden for being the president of the dissertation committee. Many thanks also go to the members of the dissertation committee, namely: Prof. Faouzi Soltani from the University of Constantine, Prof. Djamel Chikouche from the University of M'sila and Dr. Lamir Saidi from the University of Batna. I am grateful to them for sharing their time and expertise, each of them contributed to the final version of this dissertation in numerous ways.

The help of many people during different phases of my PhD is highly appreciated. Particularly, I am thankful to Prof. Jbabra and Prof. Azoui from Batna University for their assistance in all administrative details within the University.

Most importantly, I would like to express my deep gratitude to my family for their boundless support, priceless sacrifice and continuous prayers. The value that my parents placed on education and hard work gave me the ability to pursue my dreams. My special thanks to my brother Toufik for his constant help in all administrative aspects of my PhD dissertation within the University of Batna. The love and support of my wife had made all this worthwhile. Finally, I would be remiss not to thank my daughter for the extra bit of motivation she provided me with to finish my dissertation in a timely manner.

**Abdelouahab**

## Abstract

The main goal of this dissertation is to investigate linear interference cancellation structures that are appropriate for long-code CDMA systems. Motivated by the lack of such structures and exploiting the fact that for long-code CDMA systems, the major computational complexity burden comes from the frequent calculation of the cross-correlation matrix (it should be calculated each symbol period) and not from the interference cancellation itself, we examine the possibility of developing interference cancellation schemes that avoid the calculation of the cross-correlation matrix. Such structures are known as chip-level (wideband) interference cancellation schemes and they directly make use of the spreading codes instead of the cross-correlation coefficients, hence the additional burden of the cross-correlation computation is avoided. Our approach for developing such structures is based on the equivalence between some of the chip-level linear interference cancellation structures and linear iterative methods. Such mapping will not only enable the identification of new interference cancellation schemes that correspond to other iterative methods but will also facilitate the study of the convergence behavior of these structures based on the rich theory developed within the frame of iterative methods. In chapter 8, two new chip-level linear weighted SIC/weighted group-wise SIC structures that can converge not only to the decorrelator detector but also to the LMMSE detector are derived. They proved to exhibit less computational complexity than their symbol-level counterparts. In chapter 9, four novel chip-level linear weighted SIC/weighted group-wise SIC structures that are equivalent to linear SOR/linear BSOR iterative methods are derived. Their convergence behavior is analyzed and their conditions of convergence are determined using two different methods that lead to the same result. In chapter 10, using a matrix iterative analysis approach, the chip-level linear group-wise structure is shown to be equivalent to the linear BSOR iterative method but with a relaxation matrix rather than a relaxation factor. Establishing such connection allows the proposition of two new corollaries from which two conditions of convergence are determined. In chapter 11, a new chip-level linear group-wise PIC detector is proposed. Its inherent parallelism facilitates its implementation in a parallel multiprocessor structure and reduces considerably the algorithm time complexity. Other by-product contributions are also obtained in chapters 4, 5 and 7 respectively.

# Table of Contents

Dedication .....	III
Acknowledgement.....	IV
Abstract .....	V
Table of Contents .....	VI
List of Figures .....	X
List of Tables.....	XVI
Chapter 1 Introduction .....	1
1.1 Chapter's Contents .....	1
1.2 Aim of this Work .....	1
1.3 Thesis Organization.....	1
1.4 Thesis Contribution .....	3
Chapter 2 Cellular and CDMA Concepts.....	5
2.1 Chapter's Contents .....	5
2.2 Cellular Concept.....	5
2.3 Different Generations of Cellular Systems .....	9
2.4 CDMA History .....	10
2.5 Spread Spectrum Technique.....	12
2.6 Direct Sequence Spread Spectrum .....	14
2.7 Radio-Channel Access Schemes .....	15
2.8 Spreading Codes.....	19
2.9 Short-Code versus Long-Code CDMA Systems.....	21
2.10 Conclusion.....	22
Chapter 3 Wireless Fading Channels .....	23
3.1 Chapter's Contents .....	23
3.2 Introduction .....	23
3.3 Channel Model .....	27
3.4 Power-Delay Profile.....	29
3.5 Generation of Rayleigh Complex Channel Coefficients .....	33
3.6 Conclusion.....	39
Chapter 4 CDMA Channel Model .....	40
4.1 Chapter's Contents .....	40

---

VI

4.2 Introduction.....	41
4.3 Matrix Form of the Asynchronous CDMA AWGN Channel .....	42
4.4 Matrix Form of the Asynchronous CDMA Multi-Path Fading Channel .....	52
4.5 Conclusion.....	68
Chapter 5 Iterative Methods for Matrix Inversion .....	69
5.1 Chapter's Contents .....	69
5.2 Introduction.....	70
5.3 General Concepts .....	70
5.4 Iterative Methods.....	72
5.5 Convergence Issues .....	81
5.6 Simulation Results.....	92
5.7 Conclusion.....	96
Chapter 6 Multiuser Detection in CDMA .....	97
6.1 Chapter's Contents .....	97
6.2 Introduction .....	98
6.3 Performance Metrics and Computational Complexity .....	98
6.4 Classification of Multiuser Detectors.....	100
6.5 Multiuser Detection Structures for Asynchronous CDMA AWGN Channel .....	102
6.6 Multiuser Detection Structures for Asynchronous CDMA Multipath Fading Channel .....	109
6.7 The Linear Transformation of the Received Signal .....	116
6.8 The Linear Transformation of the Matched Filters/Rake Receivers' Outputs .....	117
6.9 Computational Complexity .....	119
6.10 Simulation Results.....	120
6.11 Conclusion.....	124
Chapter 7 Linear Interference Cancellation Structures .....	125
7.1 Chapter's Contents .....	125
7.2 Introduction .....	126
7.3 Symbol-level Linear SIC (SL-LSIC) Structure.....	127
7.4 Symbol-Level Linear SOR-SIC (SL-LSOR-SIC) Structure .....	128
7.5 Symbol-Level Linear Group-Wise SIC (SL-LGSIC) Structure .....	129
7.6 Symbol-Level Linear Block SOR Group-Wise SIC (SL-LBSOR-GSIC) Structure .....	132
7.7 Symbol-Level Linear PIC/Weighted PIC (SL-LPIC/SL-LWPIC) Structure .....	134
7.8 Chip-Level Linear SIC (CL-LSIC) Structure.....	136

7.9 Reduced Complexity Chip-Level Linear SIC (RC-CL-LSIC) Structure .....	138
7.10 Reduced Complexity Chip-Level Linear Group-Wise SIC (RC-CL-LGSIC) Structure.....	141
7.11 Case of CDMA Multi-Path Fading Channel .....	145
7.12 Chip-Level Linear PIC/Weighted PIC (CL-LPIC/CL-LWPIC) Structure .....	149
7.13 Computational Complexity .....	153
7.14 Simulation Results.....	157
7.15 Conclusion.....	167
Chapter 8 LMMSE-based Chip-level Linear SIC/GSIC Multiuser Detectors .....	168
8.1 Chapter's Contents .....	168
8.2 Introduction .....	168
8.3 The Chip-Level Linear Weighted SIC (CL-LWSIC) Structure .....	169
8.4 The CL-LWSIC Structure for Multi-Path Fading Channels .....	173
8.5 The Chip-Level Linear Weighted Group-Wise SIC (CL-LWGSIC) Structure.....	174
8.6 Simulation Results.....	178
8.7 Conclusion.....	184
Chapter 9 Chip-level Linear SOR-SIC and BSOR-GSIC Multiuser Detectors .....	185
9.1 Chapter's Contents .....	185
9.2 Introduction .....	186
9.3 Chip-Level Linear Successive Over-Relaxation SIC (CL-LSOR-SIC) Structure.....	186
9.4 Chip-Level Linear Block Successive Over-Relaxation Group-Wise SIC (CL-LBSOR-GSIC) Structure .....	193
9.5 Reduced-Complexity Chip-Level Linear Successive Over-Relaxation (RC-CL-LSOR-SIC) Structure .....	199
9.6 Reduced-Complexity Chip-Level Linear Block Successive Over-Relaxation Group-Wise SIC (RC-CL-LBSOR-GSIC) Structure .....	201
9.7 Simulation Results.....	203
9.8 Conclusion.....	209
Chapter 10 Analysis of the Reduced-Complexity Chip-level Linear GSIC Multi-user Detector Using a Matrix Iterative Approach .....	210
10.1 Chapter's Contents .....	210
10.2 Introduction .....	210
10.3 Convergence Behavior and Conditions of Convergence.....	211
10.4 Simulation Results.....	215

10.5 Conclusion.....	216
Chapter 11 Chip-level Linear GPIC Detectors.....	217
11.1 Chapter's Contents .....	217
11.2 Introduction .....	217
11.3 Structure of the Chip-Level Linear Group-Wise Parallel Interference Cancellation (CL-LGPIC) Detector .....	218
11.4 Algebraic Approach to the CL-LGPIC Detector.....	220
11.5 Convergence Behavior and Conditions of Convergence.....	222
11.6 The Chip-Level Linear Weighted Group-Wise PIC (CL-LWGPIC) Detector.....	223
11.7 The CL-LGPIC Detector for the Case of an Asynchronous CDMA Multi-Path Fading Channel .....	224
11.8 Computational Complexity .....	225
11.9 Simulation Results.....	226
11.10 Conclusion.....	233
Chapter 12 Conclusion and Future Work.....	234
12.1 Chapter's Contents .....	234
12.2 Conclusion.....	234
12.3 Future Work .....	235
Appendix A : Probability of error of a linear transformation of the received chip-matched signal/matched filter output.....	236
Appendix B : Asymptotic multiuser efficiency of a linear transformation of the received chip-matched signal/matched filter output.....	238
References .....	242

## List of Figures

Figure 2.1: A typical cellular system. ....	7
Figure 2.2: An illustration of the cellular frequency reuse concept. ....	8
Figure 2.3: Low probability of interception capability of the spread spectrum technique. ....	13
Figure 2.4: Anti-jamming capability of the spread spectrum technique. ....	14
Figure 2.5: Spreading process. ....	15
Figure 2.6: Frequency division multiple access. ....	16
Figure 2.7: Time division multiple access. ....	17
Figure 2.8: Code division multiple access. ....	18
Figure 3.1: Wave propagation mechanisms ....	24
Figure 3.2: Fading mechanisms. ....	25
Figure 3.3: Time-varying channel impulse response. ....	28
Figure 3.4: Uplink asynchronous CDMA system. ....	28
Figure 3.5: Time-varying fading channel for the $k^{th}$ user. ....	29
Figure 3.6: Equivalent Channel Model. ....	32
Figure 3.7: The simulated and theoretical autocorrelation of the inphase and quadrature components of the Rayleigh fading signal $c(t)$ for $M_o = 10$ . ....	35
Figure 3.8: The simulated and theoretical autocorrelation of the inphase and quadrature components of the Rayleigh fading signal $c(t)$ for $M_o = 100$ . ....	35
Figure 3.9: The simulated and theoretical crosscorrelation of the inphase and quadrature components of the Rayleigh fading signal $c(t)$ for $M_o = 10$ . ....	36
Figure 3.10: The simulated and theoretical cross-correlation of the in-phase and quadrature components of the Rayleigh fading signal $c(t)$ for $M_o = 100$ . ....	36
Figure 3.11: The simulated and theoretical cross-correlation of the in-phase components of two paths of the Rayleigh fading signal $c(t)$ and simulated and theoretical cross-correlation of the quadrature components of two paths of the Rayleigh fading signal $c(t)$ for $M_o = 10$ . ....	37
Figure 3.12: The simulated probability density function (PDF) of envelope and phase of the Rayleigh fading signal $c(t)$ . ....	38
Figure 3.13: The envelope of the Rayleigh fading signal $c(t)$ : slow versus fast fading. ....	38
Figure 4.1: The matrix $\tilde{\mathbf{S}}$ ....	43
Figure 4.2: The matrix $\bar{\mathbf{S}}$ ....	44
Figure 4.3: The matrix $\bar{\mathbf{A}}$ ....	45

---

Figure 4.4: The vector $\bar{\mathbf{b}}$ . . . . .	45
Figure 4.5: The vector $\mathbf{r}$ and the sliding window of length $PW$ chips and overlap $V$ chips. . . . .	46
Figure 4.6: The matrix $\mathbf{Q}$ . . . . .	47
Figure 4.8: The matrix $\bar{\mathbf{S}}_{eff}(w)$ . . . . .	48
Figure 4.9: The vectors $\mathbf{y}_{MF}$ (left) and $\mathbf{y}_{MF}^b$ (right). . . . .	49
Figure 4.10: The matrices $\bar{\mathbf{R}}$ and $\bar{\mathbf{R}}_{eff}$ for the asynchronous CDMA AWGN channel. . . . .	50
Figure 4.11: The matrix $\bar{\mathbf{A}}_{eff}$ . . . . .	51
Figure 4.12: The vectors $\bar{\mathbf{b}}^b$ and $\bar{\mathbf{b}}_w^b$ . . . . .	52
Figure 4.13: The matrix $\bar{\mathbf{H}}$ . . . . .	55
Figure 4.14: The matrix $\tilde{\mathbf{H}}^m$ . . . . .	55
Figure 4.15: The matrix $\mathbf{H}_k^m$ . . . . .	56
Figure 4.16: The matrix $\bar{\mathbf{S}}$ . . . . .	57
Figure 4.17: The matrix $\tilde{\mathbf{S}}$ . . . . .	57
Figure 4.18: The matrix $\bar{\bar{\mathbf{S}}}$ . . . . .	58
Figure 4.19: The matrix $\tilde{\mathbf{S}}(m)$ . . . . .	59
Figure 4.20: The matrix $\bar{\mathbf{A}}$ . . . . .	60
Figure 4.21: The vector $\bar{\mathbf{b}}$ . . . . .	60
Figure 4.22: The vector $\mathbf{r}$ and the sliding window of length $PW$ chips and overlap $V$ chips. . . . .	61
Figure 4.23: The matrix $\bar{\mathbf{H}}^b$ . . . . .	62
Figure 4.24: The matrix $\tilde{\mathbf{H}}^{w+W(b-1)}$ . . . . .	62
Figure 4.25: The matrix $\mathbf{H}_k^{w+W(b-1)}$ . . . . .	63
Figure 4.26: The matrix $\bar{\mathbf{S}}_{eff}$ . . . . .	64
Figure 4.27: The matrix $\bar{\bar{\mathbf{S}}}_{eff}^b$ . . . . .	65
Figure 4.28: The matrix $\bar{\bar{\mathbf{S}}}_{eff}^b(w)$ . . . . .	65
Figure 4.29: Structure of the matrix $\bar{\bar{\mathbf{R}}}$ and $\bar{\bar{\mathbf{R}}}_{eff}^b$ for the asynchronous CDMA multipath fading channel. . . . .	67
Figure 4.30: The matrix $\bar{\mathbf{A}}$ . . . . .	68
Figure 5.1: Convergence behavior of different point iterative methods. . . . .	93

Figure 5.2: Convergence behavior of different block iterative methods.....	94
Figure 5.3: Convergence behavior of different point relaxation iterative methods versus the relaxation factor. ....	95
Figure 5.4: Convergence behavior of different block relaxation iterative methods versus the relaxation factor. ....	96
Figure 6.1: Multi-user detection Receiver acting on the vector of matched filters outputs .....	102
Figure 6.2: Multi-user detection acting on the received chip-matched signal.....	103
Figure 6.3: Bank of matched filter detectors.....	104
Figure 6.4: Multi-user detection Receiver acting on the vector of Rake receivers outputs. ....	109
Figure 6.5: Multi-user detection acting on the received signal. ....	110
Figure 6.6: MRC Rake receiver .....	112
Figure 6.7: Conventional bank of Rake receivers. ....	113
Figure 6.8: Average BER versus SNR performance of different multiuser detectors in a synchronous CDMA AWGN channel.....	121
Figure 6.9: Average BER versus the number of users' performance of different multiuser detectors in a synchronous CDMA AWGN channel.....	122
Figure 6.10: Average BER versus near-far ratio performance of different multiuser detectors in a synchronous CDMA AWGN channel.....	123
Figure 6.11: Average BER versus SNR performance of different multiuser detectors in an asynchronous CDMA multipath Rayleigh fading channel.....	123
Figure 7.1: SL-LSIC unit of the $k^{th}$ effective user.....	127
Figure 7.2: SL-LSOR-SIC unit of the $k^{th}$ effective user.....	129
Figure 7.3: SL-LGSIC unit of the $g^{th}$ effective group of users.....	131
Figure 7.4: SL-LBSIC unit of the $w^{th}$ block of users.....	132
Figure 7.5: SL-LBSOR-GSIC unit of the $g^{th}$ effective group of users.....	133
Figure 7.6: SL-LBSOR-GSIC unit of the $w^{th}$ block of users.....	134
Figure 7.7: SL-LPIC/SL-LWPIC unit of the $k^{th}$ effective user. ....	135
Figure 7.8: Multistage structure of the CL-LSIC detector .....	137
Figure 7.9: $p^{th}$ stage, $k^{th}$ effective user's CL-LSIC unit (ICU) .....	137
Figure 7.10: Multistage structure of the RC-CL-LSIC detector.....	140
Figure 7.11: $p^{th}$ stage, $k^{th}$ effective user's RC-CL-LSIC unit (ICU). ....	140
Figure 7.12: Multistage structure of the RC-CL-LGSIC detector.....	142
Figure 7.13: $p^{th}$ stage, $g^{th}$ effective group RC-CL-LGSIC unit (GICU).....	143

Figure 7.14: The CL-LSIC unit for the CDMA multi-path fading channel .....	146
Figure 7.15: RC-CL-LSIC unit for the CDMA multi-path fading channel.....	146
Figure 7.16: RC-CL-LGMF-SIC unit for the CDMA multi-path fading channel.....	147
Figure 7.17: CL-LSIC unit for the CDMA multi-path fading channel using the under-relaxation principle.....	148
Figure 7.18: RC-CL-LSIC unit for the CDMA multi-path fading channel using the under-relaxation principle.....	149
Figure 7.19: RC-CL-LGMF-SIC unit for the CDMA multi-path fading channel using the under-relaxation principle.....	149
Figure 7.20: Multi-stage structure of the CL-LWPIC detector. ....	150
Figure 7.21: The $p^{th}$ stage interference cancellation unit of the CL-LWPIC detector.....	151
Figure 7.22: Convergence behavior of the CL-LSIC/CL-LPIC detectors. ....	158
Figure 7.23: Convergence behavior of the RC-CL-LGSIC detector.....	159
Figure 7.24: Convergence behavior of the RC-CL-LGDEC-SIC detector for $G = 2$ and $G = 10$ .....	160
Figure 7.25: Convergence behavior of the RC-CL-LGMMSE-SIC detector for $G = 2$ and $G = 10$ ....	160
Figure 7.26: Convergence behavior of the RC-CL-LGPIC-SIC detector for $G = 2$ and $G = 10$ .....	161
Figure 7.27: Convergence behavior of the RC-CL-LGMF-SIC detector for $G = 2$ and $G = 10$ .....	161
Figure 7.28: Divergence behavior of some chip-level linear interference cancellation detectors due to highly correlated codes.....	162
Figure 7.29: Divergence behavior of some chip-level linear interference cancellation detectors due to grouping. ....	163
Figure 7.30: Convergence behavior of the CL-LSIC/CL-LPIC detectors. ....	164
Figure 7.31: Convergence behavior of the RC-CL-LGSIC detector.....	164
Figure 7.32: Computational complexity of different symbol-level/chip-level LSIC detectors.....	165
Figure 7.33: Computational complexity of the SL-LGDEC-SIC/RC-CL-LGDEC-SIC detectors. ....	166
Figure 7.34: Computational complexity of different symbol-level/chip-level LPIC detectors.....	167
Figure 8.1: $p^{th}$ stage, $k^{th}$ effective user's CL-LWSIC unit (ICU) .....	169
Figure 8.2: $p^{th}$ stage, $k^{th}$ effective user's CL-LWSIC unit (ICU) for the case of asynchronous CDMA multipath fading channel.....	173
Figure 8.3: Multistage structure of the CL-LWGSIC detector.....	175
Figure 8.4: $p^{th}$ stage, $g^{th}$ effective GICU. ....	175
Figure 8.5: Impact of the weighting factor on the average BER of the proposed CL-LWSIC detector. ....	179

Figure 8.6: Convergence behavior of the proposed CL-LWSIC detector, converging to the Decorrelator/LMMSE detector. ....	180
Figure 8.7: Convergence behavior of the proposed CL-LGWSIC detector, converging to the Decorrelator/LMMSE detector. ....	181
Figure 8.8: Convergence behavior of the proposed CL-LWSIC detector, converging to the Decorrelator/LMMSE detector. ....	182
Figure 8.9: Convergence behavior of the proposed CL-LGWSIC detector, converging to the Decorrelator/LMMSE detector. ....	182
Figure 8.10: Computational complexity of the proposed CL-LWSIC structure versus that of the SL-LSIC structure. ....	183
Figure 8.11: Computational complexity of the proposed CL-LWGSIC structure versus that of the SL-LGSIC structure. ....	184
Figure 9.1: Basic interference cancellation unit (ICU). ....	187
Figure 9.2: Basic group interference cancellation unit (GICU) ....	194
Figure 9.3: $p^{th}$ stage, $k^{th}$ effective user RC-CL-LSOR-SIC's ICU. ....	200
Figure 9.4: $p^{th}$ stage, $g^{th}$ effective group RC-CL-LBSOR-GSIC's GICU ....	202
Figure 9.5: Average BER performance versus the relaxation factor of the proposed CL-LSOR-SIC detector for the case of a synchronous CDMA AWGN channel.....	203
Figure 9.6: Convergence behavior of the proposed CL-LSOR-SIC detector for different relaxation factor values for the case of a synchronous CDMA AWGN channel.....	204
Figure 9.7: Average BER performance versus the relaxation factor of the proposed CL-LBSOR-GSIC detector for the case of a synchronous CDMA AWGN channel.....	205
Figure 9.8: Convergence behavior of the proposed CL-LBSOR-GSIC detector for different relaxation factor values for the case of a synchronous CDMA AWGN channel.....	206
Figure 9.9: Average BER performance versus the relaxation factor of the proposed CL-LSOR-SIC/CL-LBSOR-GSIC detectors for the case of an asynchronous CDMA multipath fading channel.....	207
Figure 9.10: Computational complexity of the proposed CL-LSOR-SIC/RC-CL-LSOR-SIC structures versus that of the SL-LSOR-SIC structure.....	208
Figure 9.11: Computational complexity of the proposed CL-LBSOR-GSIC/RC-CL-LBSOR-GSIC structures versus that of the SL-LBSOR-GSIC structure.....	209
Figure 10.1: Convergence behavior of the RC-CL-LGSIC detector versus the determinant of the relaxation matrix. ....	216
Figure 11.1: Multi-stage structure of the CL-LGPIC detector. ....	218

Figure 11.2: The $p^{th}$ stage interference cancellation unit of the CL-LGPIC detector. ....	219
Figure 11.3: The $p^{th}$ stage interference cancellation unit of the CL-LWGPIC detector.....	224
Figure 11.4: SL-LWGPIC unit of the $g^{th}$ effective group of users.....	226
Figure 11.5: Convergence behavior of the CL-LGPIC detector. ....	227
Figure 11.6: Convergence behavior of the CL-LGDEC-PIC detector for $G = 2$ and $G = 10$ . ....	228
Figure 11.7: Convergence behavior of the CL-LGMMSE-PIC detector for $G = 2$ and $G = 10$ .....	229
Figure 11.8: Convergence behavior of the CL-LGPIC-PIC detector for $G = 2$ and $G = 10$ . ....	229
Figure 11.9: Convergence behavior of the CL-LGMF-PIC detector for $G = 2$ and $G = 10$ .....	230
Figure 11.10: Divergence behavior of some chip-level linear interference cancellation detectors due to highly correlated codes.....	231
Figure 11.11: Convergence behavior of the CL-LGPIC detector. ....	232
Figure 11.12: Computational complexity of the CL-LGDEC-PIC detector compared to that of the SL-LGDEC-PIC detector. ....	233

## List of Tables

Table 2.1: Sizes of cells and associated uses.....	7
Table 2.2: 3G Data Rate Requirements.....	10
Table 2.3: CDMA evolution.....	11
Table 3.1: Indoor channel power delay profile (5Km/h).....	30
Table 3.2: Indoor to outdoor channel power delay profile (5Km/h). ....	31
Table 3.3: Vehicular A outdoor channel power delay profile (120Km/h). ....	31
Table 3.4: Equivalent indoor channel amplitude delay profile of Table 3.1 at chip rate using the proposed interpolation method.....	32
Table 3.5: Equivalent indoor to outdoor channel amplitude delay profile of Table 3.2 at chip rate using the proposed interpolation method.....	32
Table 3.6: Equivalent vehicular A outdoor channel amplitude delay profile of Table 3.3 at chip rate using the proposed interpolation method. ....	33
Table 5.1: Splitting and iteration matrices of different iterative methods.....	81
Table 5.2: Conditions of convergence for different iterative methods.....	89
Table 5.3: Optimal relaxation factors for different iterative methods.....	90
Table 6.1: Simulation parameters.....	120
Table 7.1: Simulation parameters.....	157
Table 10.1: Conditions of convergence for different group detection schemes.....	215
Table 11.1: Simulation parameters.....	227

# Chapter 1

## Introduction

### 1.1 Chapter's Contents

1.1 Chapter's Contents .....	1
1.2 Aim of this Work.....	1
1.3 Thesis Organization.....	1
1.4 Thesis Contribution.....	3

### 1.2 Aim of this Work

The main goal of this dissertation is to investigate linear interference cancellation structures that are appropriate for long-code CDMA systems. Motivated by the lack of such structures and exploiting the fact that for long-code CDMA systems, the major computational complexity burden comes from the frequent calculation of the cross-correlation matrix (it should be calculated each symbol period) and not from the interference cancellation itself, we examine the possibility of developing interference cancellation schemes that avoid the calculation of the cross-correlation matrix. Such structures are known as chip-level (wideband) interference cancellation schemes and they directly make use of the spreading codes instead of the cross-correlation coefficients, hence the additional burden of the cross-correlation computation is avoided. Our approach for developing such structures is based on the equivalence between some of the chip-level linear interference cancellation structures and linear iterative methods. Such mapping will not only enable the identification of new interference cancellation schemes that correspond to other iterative methods but will also facilitate the study of the convergence behavior of these structures based on the rich theory developed within the frame of iterative methods.

### 1.3 Thesis Organization

The dissertation is divided into many chapters that can be roughly partitioned into introductory chapters and contributive chapters. This splitting is coarse, in the sense that some of the introductory chapters contain contributions, however, they can be considered as minor contributions.

- Chapter 1 describes the aim of the dissertation and its contribution to the literature.
- Chapter 2 introduces the cellular concept and discusses different generations of cellular systems. Moreover, it describes the spread spectrum technique, its advantages and disadvantages and finally it discusses different spreading codes used in CDMA systems and the advantages and disadvantages of both short-code and long-code spreading codes.
- Chapter 3 introduces different fading mechanisms arising in a wireless fading CDMA channel. Then, it proposes the channel model used for all simulations in the subsequent chapters. The power delay profile used in all simulations conducted in different chapters is then discussed. Finally, an enhanced Jakes model which is used to generate the Rayleigh fading complex coefficients is implemented and simulated.
- Chapter 4 develops CDMA models for both the synchronous CDMA AWGN and the asynchronous CDMA multi-path fading channels. Moreover, it proposes a new CDMA model for the asynchronous CDMA multi-path fading channel that allows the development of new multiuser detectors.
- Chapter 5 reviews various iterative methods covered in the literature. It details different point and block iterative methods, study their convergence behavior and determine their conditions of convergence. Two new iterative methods are developed and studied in detail. The latter will be used in the subsequent chapters to identify some chip-level linear interference cancellation structures. Finally, all the aforementioned iterative methods are simulated and compared together.
- Chapter 6 reviews and studies some basic multiuser detectors such as the matched filter detector, the optimal multiuser detector, the decorrelator detector and the LMMSE detector for both a synchronous CDMA AWGN channel and an asynchronous CDMA multipath fading channel. These detectors are assessed in terms of many performance metrics such as the probability of error, asymptotic multiuser efficiency, near-far resistance and the computational complexity.
- Chapter 7 introduces the two main categories of linear interference cancellation structures, namely the symbol-level and chip-level schemes. Different structures covered in the literature are restudied here and furthermore three new structures using the principle of under-relaxation are developed for the case of an asynchronous CDMA multipath fading channel. Finally, the computational complexity of both symbol-level and chip-level linear interference cancellation structures are compared and commented.
- Chapter 8 presents a chip-level linear weighted SIC structure that can converge to either the decorrelator detector or the LMMSE detector. Another new structure is obtained by extending the

previous scheme to group-wise SIC detection. The convergence behavior of these two novel structures is analyzed and conditions of convergence are determined. Finally, simulation results supporting the theoretical findings are obtained.

- Chapter 9 proposes two novel chip-level linear weighted SIC structures that are equivalent to the successive over-relaxation iterative method. These structures are then extended to group-wise SIC detection. Convergence analysis is performed using two different methods that lead to the same result. Finally, simulation of the previous structures is performed to validate the theoretical derivations.
- Chapter 10 shows how the rich theory of iterative methods can be used for the analysis of existing interference cancellation structures in the literature. First we prove that the group-wise SIC structure is in fact equivalent to a BSOR iterative method but with a relaxation matrix instead of a relaxation factor. By using such approach, two new corollaries that result in two new conditions of convergence are derived. Finally simulations are conducted to substantiate the theoretical results.
- Chapter 11 introduces a chip-level linear group-wise PIC detector. Four different group-detection schemes are derived. The proposed structure is analyzed and conditions of convergence are determined. Finally, simulation results that corroborate the theoretical findings are obtained.
- Chapter 12 concludes this work by summarizing the most important results and contributions gained throughout this dissertation and points out possible future extensions.

#### **1.4 Thesis Contribution**

The thesis's contributions can be summarized into the following points:

- In chapter 4, a new model for the asynchronous CDMA multi-path fading channel is developed. The latter permits the derivation of new multiuser detectors.
- In chapter 5, two new iterative methods are derived, their convergence behavior is investigated and their conditions of convergence are determined. These methods will show to be useful in the identification of some existing chip-level linear SIC and group-wise SIC detectors. Moreover, they will help in deriving three new chip-level linear SIC and group-wise SIC structures for the case of an asynchronous CDMA multi-path fading channel.
- In chapter 7, three new chip-level linear weighted SIC and weighted group-wise SIC structures suitable for the case of an asynchronous CDMA multi-path fading channel are derived using the principle of under-relaxation.

- In chapter 8, two new chip-level linear weighted SIC/weighted group-wise SIC structures that can converge not only to the decorrelator detector but also to the LMMSE detector are derived. They proved to exhibit less computational complexity than their symbol-level counterparts. Moreover, conditions of convergence are determined and their performance is evaluated and verified through simulations.
- In chapter 9, four novel chip-level linear weighted SIC/weighted group-wise SIC structures that are equivalent to linear SOR/linear BSOR iterative methods are derived. Their convergence behavior is analyzed and their conditions of convergence are determined using two different methods that lead to the same result. Computational complexity of these detectors is shown to be less than that of their symbol-level counterparts.
- In chapter 10, using a matrix iterative analysis approach, the chip-level linear group-wise structure is shown to be equivalent to the linear BSOR iterative method but with a relaxation matrix rather than a relaxation factor. Establishing such connection allows the proposition of two new corollaries from which two conditions of convergence are determined.
- In chapter 11, a new chip-level linear group-wise PIC detector is proposed. Its inherent parallelism facilitates its implementation in a parallel multiprocessor structure and reduces considerably the algorithm time complexity. Four different group-detection schemes are derived and investigated in terms of convergence speed and behavior. Furthermore, and in order to ensure convergence, a chip-level linear weighted group-wise PIC detector is suggested. Conditions of convergence for this structure are determined.

## Chapter 2

### Cellular and CDMA Concepts

#### 2.1 Chapter's Contents

2.1 Chapter's Contents .....	5
2.2 Cellular Concept.....	5
2.3 Different Generations of Cellular Systems.....	9
2.3.1 First Generation Cellular Systems.....	9
2.3.2 Second Generation Cellular Systems .....	9
2.3.3 Third Generation Cellular Systems .....	9
2.4 CDMA History .....	10
2.5 Spread Spectrum Technique.....	12
2.6 Direct Sequence Spread Spectrum .....	14
2.7 Radio-Channel Access Schemes .....	15
2.7.1 Frequency Division Multiple Access .....	16
2.7.2 Time Division Multiple Access.....	16
2.7.3 Code Division Multiple Access.....	17
2.8 Spreading Codes.....	19
2.8.1 Orthogonal Codes.....	20
2.8.2 Pseudo-Random Noise (PN) Codes .....	20
2.9 Short-Code versus Long-Code CDMA Systems.....	21
2.10 Conclusion.....	22

#### 2.2 Cellular Concept

In order to understand the underlying principle behind the cellular concept, let us imagine that the frequency spectrum available for mobile communications is infinite and that regulatory authorities set no limit on the power transmitted within that frequency band. In this case, the simplest wireless system will have a centralized base station serving a large area with all the users in that area communicating directly with the base station. Such a system is unpractical for two main reasons. First, the users that

are far away from the base station have to transmit at very high power levels; this will eventually decrease the battery life of their mobile phones very fast. Second, the total bandwidth utilized in an area increases with the number of users communicating in that area, hence if a single base station is used to cover the entire geographical area and serve all the users, the total bandwidth required would be huge.

As regulatory authorities assign frequency bands for different communication applications, the number of users, in a given area, that can be accommodated without exceeding the frequency limitations is limited. Additionally, a single base station covering the entire area would require transmission at high power levels to communicate with distant users. However, this is not permitted by the regulatory authorities in order to avoid interference with other applications. Thus, in practical systems, power and bandwidth factors are constraining the service areas to be in the vicinity of the base stations.

Cellular communication consists of partitioning a large geographical area into smaller sized areas known as *cells*. The fundamental concept for such a system has emerged and evolved in 1970's as a result of extensive research in wireless communications [1]-[7]. It involves using many low-power base stations placed within cells at approximately their centers rather than using one high-power transmitter for the entire area to be covered [8]. Using this cellular concept, the allocated frequency band can be reused by cells that are separated sufficiently.

Dividing a certain geographical region into cells "*cellularization*" includes the determination of the size of different cells which is primarily dependent on the population density or subscriber density. Moreover, the size of the cell is controlled by the following factors [9]:

- Power transmitted by the base station belonging to the cell.
- Terrain within the region of the cell.
- Presence of man-made features such as buildings and other structures.

These factors also determine the shape of the cell, which is rarely regular [10]. The different cell sizes and their applications are illustrated in Table 2.1 [9].

The communication link from the base station to the mobile user is known as the *downlink (forward channel)* while that from the mobile user to the base station is known as the *uplink (reverse channel)*. In cellular systems, a user belonging to a particular cell communicates with the base station of that cell while all other base stations neglect the signal received from this user. The process in which

a user moves from one cell to another and establishes a communication link with the base station in the new cell is called *handoff* [11].

Table 2.1: Sizes of cells and associated uses

Application	Average cell diameter	Name
Sub-urban	1 – 10 km	Macro-cell
Urban	1 km	Mini-cell
Street	100 m	Micro-cell
Office	< 10 m	Pico-cell

In a cellular system, as the one shown in Figure 2.1, users typically communicate with base stations by means of *handsets*.

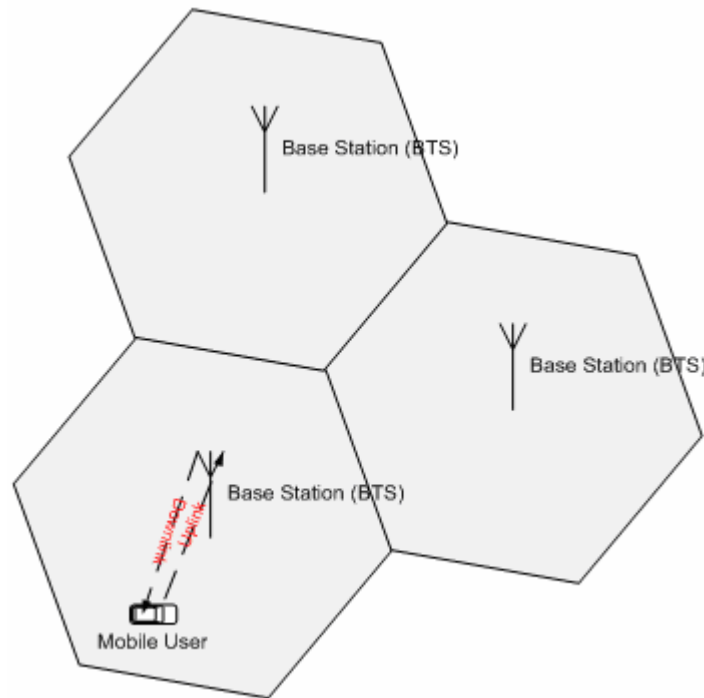


Figure 2.1: A typical cellular system.

The base stations not only offer a communication link to and from the handset, but also provide connectivity to the public switched telephone network (PSTN) through the mobile telephone switching office (MTSO) which serves as a link between the wired and wireless networks.

Use of the same frequencies for communications within different cells is known as *frequency reuse*. The *frequency reuse factor* is the rate at which the same frequency can be used in the network. It is  $1/N_{cells}$  where  $N_{cells}$  is the number of cells which cannot use the same frequency for transmission. A *cluster* is defined as a group of cells in which frequencies are not reused ( $N_{cells}$ ). For example, the number of cells in an FDMA cluster varies, with 3 and 7 as the typical values ([12] and [13]). However, in a single cell clusters such as the CDMA system, the same frequency band is reused in every cell. Frequency reuse is one of the major benefits of cellular systems as it significantly increases the capacity of the system while using only a limited number of frequencies ([3] and [12]). An illustration of the frequency reuse factor of  $1/7$  is shown in Figure 2.2.

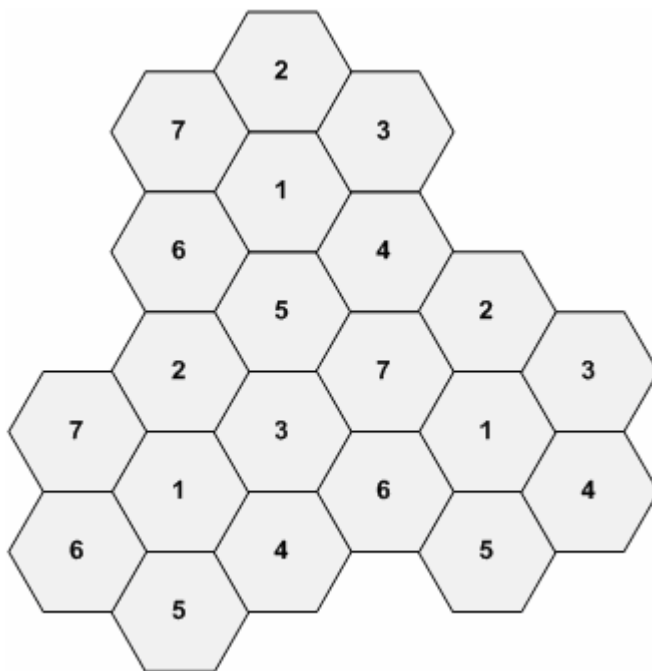


Figure 2.2: An illustration of the cellular frequency reuse concept.

## **2.3 Different Generations of Cellular Systems**

### **2.3.1 First Generation Cellular Systems**

The first generation cellular systems generally employ analog Frequency Modulation (FM) techniques. The Advanced Mobile Phone System (AMPS) was the most dominant first generation system. AMPS was developed by the Bell Telephone System. It uses FM technology for voice transmission and digital signaling for control information. Other first generation systems include [14]:

- Narrowband AMPS (NAMPS).
- Total Access Cellular System (TACS).
- Nordic Mobile Telephone System (NMT-900).

### **2.3.2 Second Generation Cellular Systems**

The rapid growth in the number of subscribers was the main reason behind the evolution towards second generation cellular systems. Second generation systems took advantage of compression and coding techniques associated with digital technology. All second generation systems employ digital modulation schemes. Multiple access techniques like Time Division Multiple Access (TDMA) and Code Division Multiple Access (CDMA) are used along with FDMA in the second generation systems. Second generation cellular systems include [12]:

- United States Digital Cellular (USDC) standards IS-54 and IS-136.
- Global System for Mobile communications (GSM).
- Pacific Digital Cellular (PDC).
- cdmaOne (IS-95).

### **2.3.3 Third Generation Cellular Systems**

Research efforts have been ongoing for more than a decade to introduce multimedia capabilities into mobile communications. Third generation cellular systems emerged to satisfy the ever-increasing need for wideband services like high speed internet access, video and high quality image transmission. The primary requirements of the next generation cellular systems are [15]:

- Voice quality comparable to Public Switched Telephone Network (PSTN).
- Support of high data rate. Table 2.2 details the data rate requirement of the 3G systems:

Table 2.2: 3G Data Rate Requirements.

Mobility Needs	Minimum Data Rate
Vehicular	144 kbps
Outdoor to indoor and pedestrian	384 kbps
Indoor Office	2 Mbps

- Support of both packet-switched and circuit-switched data services.
- More efficient usage of the available radio spectrum.
- Support of a wide variety of mobile equipments.
- Backward Compatibility with pre-existing networks and flexible introduction of new services and technology.
- An adaptive radio interface suited to the highly asymmetric nature of most Internet communications: a much greater bandwidth for the downlink than the uplink.

Third generation cellular systems include:

- WCDMA or UTRAN in Japan and Europe
- CDMA2000 in the United States

## 2.4 CDMA History

The spread spectrum technology has been originally used in the military field where it has been developed to counteract intentional jamming. In this section we highlight the milestones for CDMA evolution starting from the 1950s after the appearance of Shannon's theorem [16]. A thorough overview of spread spectrum history is provided in [17]. The CDMA era can be roughly divided into three periods, as shown in Table 2.3: the pioneer CDMA era, the narrowband CDMA era, and the wideband CDMA era [22].

In 1949, John Pierce wrote a technical memorandum where he detailed a multiplexing system in which a common medium carries coded asynchronous signals. This system can be classified as a time hopping spread spectrum multiple access system [17]. Claude Shannon and Robert Pierce introduced the basic ideas of CDMA in 1949 where they described the interference averaging effect and showed the graceful degradation of CDMA systems [18].

Table 2.3: CDMA evolution.

<p><b>Pioneer Era</b></p> <p><b>1949 John Pierce:</b> time hopping spread spectrum.</p> <p><b>1949 Claude Shannon and Robert Pierce:</b> basic ideas of CDMA.</p> <p><b>1950 De Rosa-Rogoff:</b> direct sequence spread spectrum.</p> <p><b>1956 Price and Green:</b> antimultipath “RAKE” patent.</p> <p><b>1961 Magnuski:</b> near-far problem.</p> <p><b>1970s:</b> Several developments for military field and navigation systems.</p>
<p><b>Narrowband CDMA Era</b></p> <p><b>1978 Cooper and Nettleton:</b> cellular application of spread spectrum.</p> <p><b>1980s:</b> Investigation of narrowband CDMA techniques for cellular applications.</p> <p><b>1986 Verdu:</b> Formulation of optimum multiuser detection.</p> <p><b>1993:</b> IS-95 standard.</p>
<p><b>Wideband CDMA Era</b></p> <p><b>1995 Europe:</b> FRAMES and FMA2.</p> <p><b>Japan:</b> Core-A and WCDMA.</p> <p><b>USA:</b> cdma2000.</p> <p><b>Korea:</b> TTA I and TTA II.</p> <p><b>2000s:</b> Commercialization of wideband CDMA systems.</p>

In 1950, De Rosa-Rogoff suggested a direct sequence spread spectrum system [17]. In 1956, Price and Green introduced the anti-multi-path “RAKE” receiver [17]. They showed that signals arriving over different propagation paths can be resolved by a wideband spread spectrum signal and combined by the RAKE receiver. The near-far problem (i.e., a high-power interference overwhelming a weaker spread spectrum signal) was first mentioned in 1961 by Magnuski [17]. Introducing spread spectrum techniques into the cellular world was suggested by Cooper and Nettleton in 1978 [19]. During the 1980s Qualcomm examined the possible use of DS-SS techniques in cellular systems, which finally led to the commercialization of the narrowband CDMA IS-95 standard in July 1993. Commercial operation of IS-95 systems started in 1996. Multiuser detection (MUD) attracted a lot of

attention and has been a subject of extensive research since 1986 when Verdu formulated the optimum multiuser detection for the additive white Gaussian noise (AWGN) channel [20].

During the 1990s, wideband CDMA techniques with a bandwidth of 5 MHz or more have been studied extensively throughout the world, and several trial systems have been built and tested [21]. These include FRAMES Multiple Access (FRAMES FMA2) in Europe, Core-A in Japan, the European/Japanese WCDMA scheme, cdma2000 in the United States, and the Telecommunication Technology Association I and II (TTA I and TTA II) schemes in Korea.

## 2.5 Spread Spectrum Technique

The recent fast growth in the number of subscribers and the emergence of a wide range of mobile applications has increased the need for developing more spectrally efficient schemes that can enable more users to share the same spectrum but still maintain a satisfactory quality of service. The most promising technology that offers such possibility which is known as CDMA relies on the principle of *spread spectrum* technique.

By definition, spread spectrum refers to any digital transmission technique where the data signal occupies a bandwidth much larger than the minimum bandwidth required for its transmission. Even though spread spectrum is not a Bandwidth-conserving modulation technique, it has been implemented in a wide range of applications. The main reason behind this is that it solves two key problems in communication: the unauthorized interception problem and the jamming problem [23]-[25]. Both of these problems are very critical in military communications, and this explains why this technology started and evolved within the military field.

The mitigation of the first problem is achieved by lowering the probability of unauthorized interception. In spread spectrum, this is possible due to the spreading process which lowers the power spectral density of the desired signal to a level that is below the thermal noise level of the interceptor. This means that any hostile receiver will perceive the spread spectrum signal as noise. The mitigation of this problem is shown in Figure 2.3.

The second problem is alleviated through the despreading process where all signals of undesired users, including narrow-band jamming, are spread and therefore their power spectral density within the bandwidth of the despread narrow-band desired signal is low compared to that of the desired signal. The mitigation of this problem is shown in Figure 2.4.

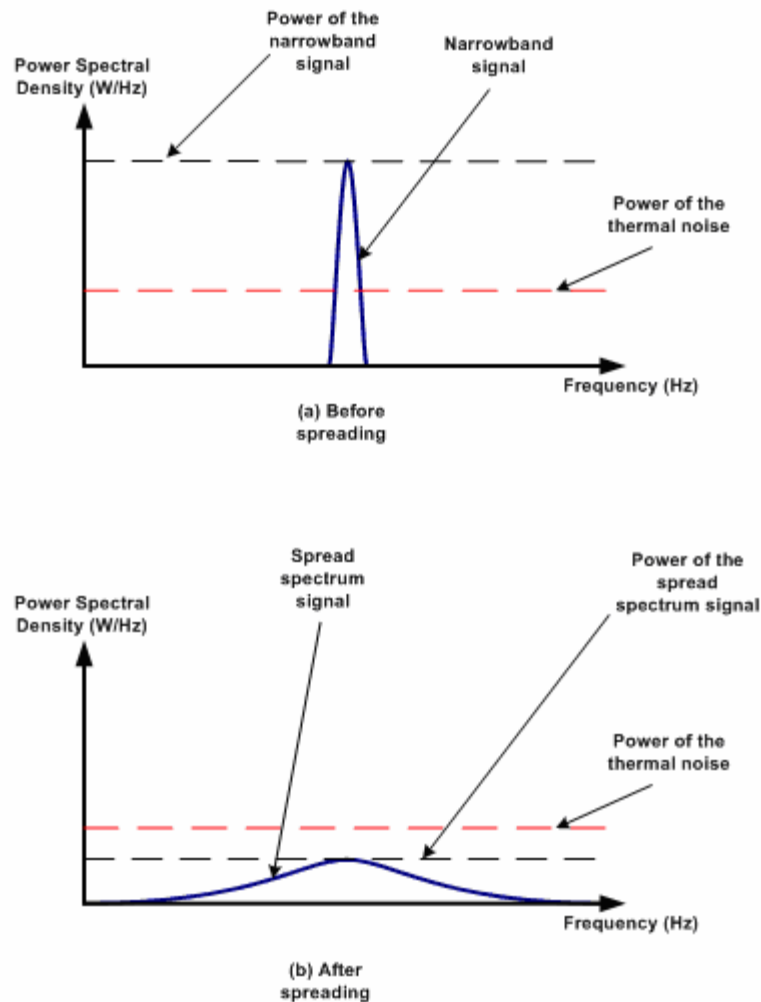


Figure 2.3: Low probability of interception capability of the spread spectrum technique.

Many types of spread spectrum technologies exist such as: *direct sequence*, *frequency hopping*, *time hopping* and *other hybrids*. Since most of the cellular standards (IS-95, UMTS, ...) use the direct sequence spread spectrum technique, we restrict our discussion to this technique only which will be detailed in the following section.

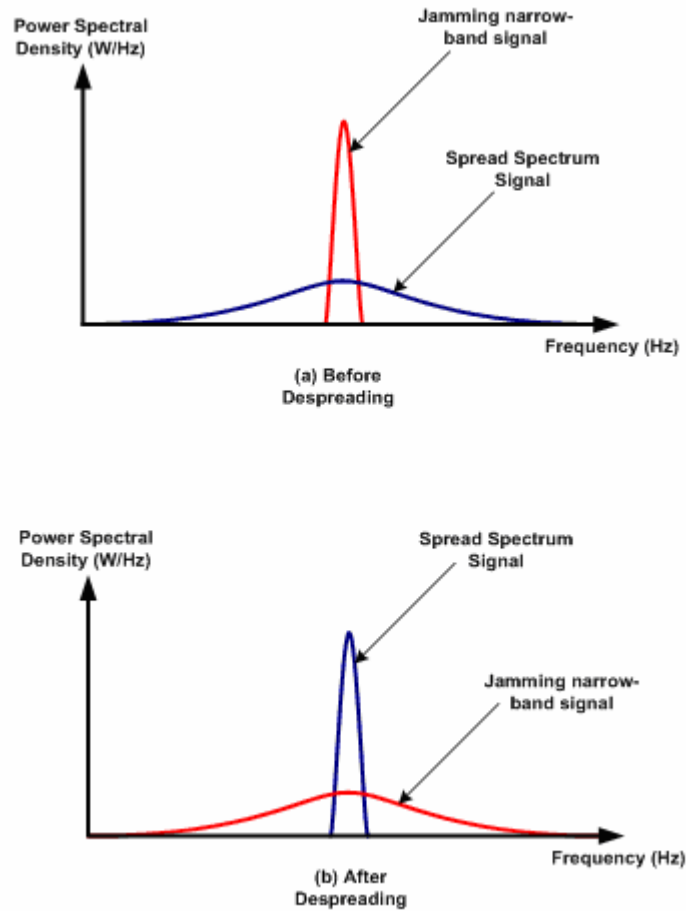


Figure 2.4: Anti-jamming capability of the spread spectrum technique.

## 2.6 Direct Sequence Spread Spectrum

In direct sequence spread spectrum, the data signal with period  $T_s$  is multiplied by a spreading code with period  $T_c$  that is very small compared to  $T_s$  [26]. This process results in the expansion of the signal's bandwidth as shown in Figure 2.5.

If we assume that the total power of the spread spectrum signal is the same as that of the original narrowband signal, then the power spectral density  $P_{ss}$  of the spread spectrum signal is expressed as

[25]:  $P_{ss} = P_s \left( \frac{B_s}{B_{ss}} \right)$ , where  $P_s$  is the power spectral density of the narrowband data signal,  $B_s$  is the

bandwidth of the narrowband data signal and  $B_{ss}$  is the bandwidth of the spread spectrum signal. The

ratio  $\frac{B_{ss}}{B_s} = \frac{T_s}{T_c}$  is known as the *processing gain* of the system [25].

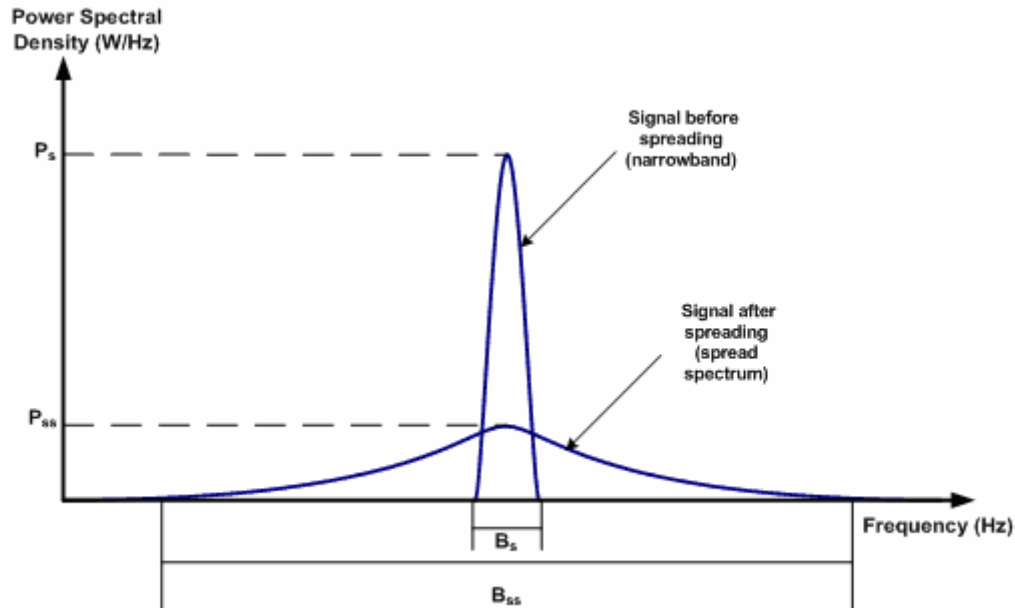


Figure 2.5: Spreading process.

For most practical systems, this parameter ranges from 10 to 30 dB which means that the bandwidth of the narrowband data signal is expanded by a factor of 10 to 1000 times and its power spectral density is reduced by the same factor [25].

## 2.7 Radio-Channel Access Schemes

Multiple access techniques are used to allow many mobile users to share simultaneously a common bandwidth. *Frequency division multiple access (FDMA)*, *time division multiple access (TDMA)* and *Code division multiple access (CDMA)* are the major access techniques used to share the available bandwidth in a mobile radio communication system. These techniques are detailed in next sections.

### 2.7.1 Frequency Division Multiple Access

Frequency division multiple access allocates individual channels (frequency bands) to individual users. As it can be seen from Figure 2.6, each user is assigned a unique frequency band on demand. During the period of the call, no other user can share the same frequency band. If an FDMA channel is not in use (for example, during pauses in telephone conversation) it stays idle and cannot be used by any other user for the purpose of increasing the system capacity. FDMA was the multiple access scheme used in most first generation standards such as AMPS (Advanced Mobile Phone System).

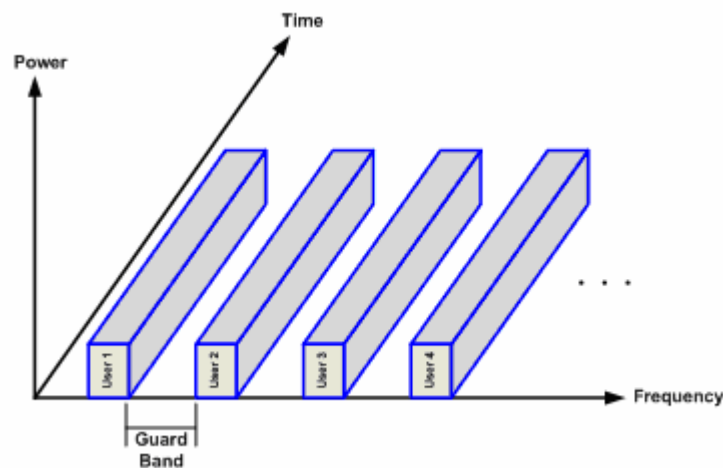


Figure 2.6: Frequency division multiple access.

### 2.7.2 Time Division Multiple Access

Time division multiple access systems, however, divide the transmission time into time slots where one user is allowed to either transmit or receive in it. As it can be seen from Figure 2.7, each user occupies cyclically repeating slots, so a channel may be thought of as a particular time slot that reoccurs periodically in every frame. Unlike in FDMA systems, which can accommodate analog frequency modulation (FM), digital data and digital modulation schemes, are used with TDMA.

TDMA shares a single carrier frequency with several users, where each user makes use of non-overlapping time slots. Analogously to FDMA, if a channel is not in use, then the corresponding time slots sit idle and cannot be used by other users. TDMA compared to FDMA needs stringent synchronization requirements and, in addition, guard slots are necessary to separate users. Generally,

the complexity of TDMA mobile systems is higher compared to that of FDMA systems. TDMA is usually combined with FDMA as in the widely used European standard GSM. Thus GSM is a hybrid TDMA/FDMA system [14].

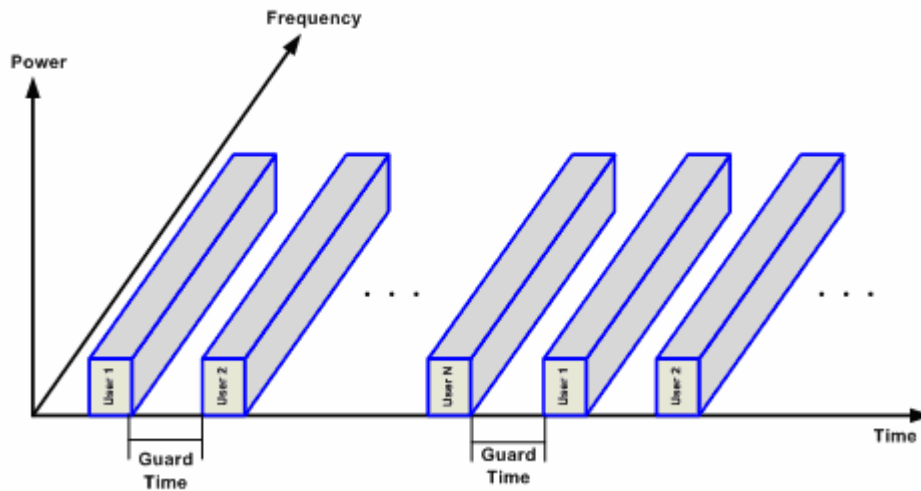


Figure 2.7: Time division multiple access.

### 2.7.3 Code Division Multiple Access

Each user of a multiple access system, based on the FDMA or the TDMA principle, is supplied with certain resources, such as frequency or time slots, or both, which are disjoint from those of any other user. Viterbi [26] pointed out that these multiple access schemes suffer from three weaknesses:

- The first weakness is that these schemes assume that all users transmit continuously. However, in a two-person conversation, the percentage of time where a speaker is active, that is, talking, ranges from 35% to 50%. In TDMA or FDMA systems, reallocation of the channel for such brief periods requires rapid circuit switching between the two users, which is practically impossible.
- The second weakness is the relatively small frequency reuse factor of FDMA and TDMA, which is proportional to the user capacity. Actual systems, such as GSM, employ a reuse factor of 1/7.
- The third weakness, which is common to all multiple access systems but it is more serious for FDMA and TDMA, is multipath fading. Multipath fading is caused by interference between two or more versions of the transmitted signal that arrive at the receiver at slightly different times. This

phenomenon is particularly severe when each channel is allocated a narrow bandwidth, as in the case of FDMA systems.

A completely different approach, realized in CDMA systems, does not attempt to allocate disjoint frequency or time resources to each user. Instead the system assigns all resources to all active users.

In *direct sequence* DS-CDMA systems, the narrowband message signal is spread by a very large-bandwidth signal called the *spreading signal*. As shown in Figure 2.8, all users in a DS-CDMA system use the same carrier frequency and transmit simultaneously. Each user has a unique spreading code, which is approximately orthogonal to the spreading codes of the rest of the users. The receiver performs a correlation operation to detect the data signal of the desired user. For detecting the data signal, the receiver requires the spreading code used by the desired user.

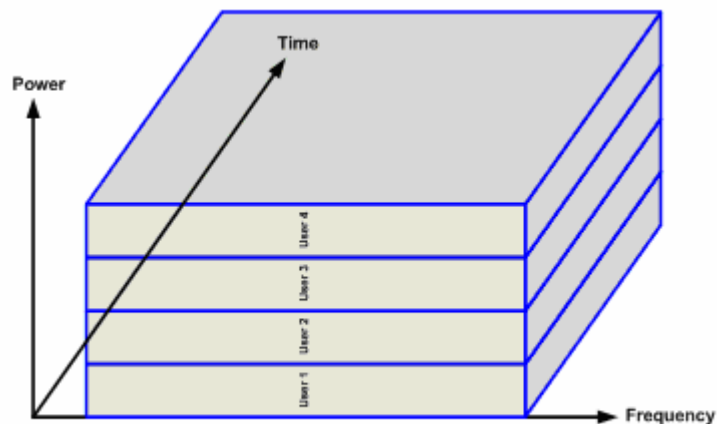


Figure 2.8: Code division multiple access.

Theoretically, CDMA systems provide a larger user capacity than FDMA and TDMA systems [27]. This is due to the fact that the CDMA system distinguishes different users by their spreading codes; the same spectrum can be used in all cells. Hence the frequency reuse factor is one.

Besides this, two other important features of CDMA systems are worth mentioning, the first is privacy and the second is its ability to combat multi-path fading. Privacy is realized by virtue of the fact that the data signal of a certain user can be recovered only if its spreading code is known. Knowledge of such codes is a difficult task and this difficulty increases proportionally to the length of

the spreading code. The ability of CDMA systems to combat multi-path fading is largely due to the fact that the CDMA signal is a wideband signal and it is larger than the *coherence bandwidth* [28] of the wireless channel. Hence, the different frequency components of the CDMA signal are affected differently by the multi-path fading channel. All multi-paths with delays larger than  $T_c$  are resolved, processed and combined in an optimal way using what is known in the literature as the Rake receiver. This is a form of diversity that can help the receiver in improving its bit error rate (BER) performance.

Despite all the advantages the CDMA system offers, its performance is limited by two major problems, namely: the *multiple access interference (MAI)* and the *near-far problem* which are interrelated and are usually treated together.

The MAI, caused by the cross-correlation between spreading codes of active users, is the dominant factor that leads to reduction of user capacity in CDMA systems. The undesirable impact of the MAI becomes more remarkable and sometimes disastrous when the number of active users becomes large or when the power level of certain users is significantly higher than that of others. In this case, weak users may lose communication because of the overwhelming MAI. This phenomenon is known as the *near-far effect* and needs what is known as *power control* [29]. Hence, unlike TDMA and FDMA systems that are bandwidth limited, CDMA systems are interference limited. Thus, increasing the capacity of the system translates directly to decreasing the amount of MAI. This process is usually referred as *interference cancellation* or *multiuser detection (MUD)* [30].

## 2.8 Spreading Codes

In all spread spectrum systems the desired signal is spread prior to transmission using one or more spreading codes. Selection of spreading codes for a certain application depends on the working environment and on the specific properties desired for the spreading codes. For single user communications in a multi-path environment, the most important thing is the ability to resolve multi-paths. To perform this successfully, the spreading codes must have excellent autocorrelation properties, ideally a delta function. However, for a multiuser system in a non-multi-path environment, the most important issue in selecting the spreading codes is the capability to minimize MAI. This can be achieved if the spreading codes are selected such that the maximum value of the cross-correlation is minimized ([30] and [31]). In practice, commercial CDMA systems are multiuser systems in multi-path environment, consequently, the selection of spreading codes for CDMA systems should take into account both the autocorrelation and cross-correlation properties. Furthermore, CDMA systems are cellular and require separation of intra-cell as well as inter-cell users. This imposes two levels of

spreading, which can be accomplished by combining two spreading codes, known as channelization codes (to distinguish between different users of the same cell) and scrambling codes (to distinguish users of different cells). Multiple spreading is described in detail in [32]. Two broad categories of spreading codes, namely orthogonal codes and pseudo-noise (PN) codes, are discussed in the subsequent subsections.

### 2.8.1 Orthogonal Codes

As their name indicates, these codes, known as Walsh-Hadamard codes [32], are mutually orthogonal; hence the cross-correlation between each synchronous pair is theoretically zero. However, if they are asynchronous, their cross-correlation is very much dependent on the particular pair of codes used; some will have a zero cross-correlation while others will have a very high correlation. In WCDMA, they are known as variable orthogonal spreading factor (OVSF) codes and they are used for channelization in both uplink and downlink channels [32].

### 2.8.2 Pseudo-Random Noise (PN) Codes

A Pseudo-random Noise (PN) code is a sequence of binary numbers, e.g.,  $\pm 1$ , which appears to be random; but is in fact perfectly deterministic. The sequence appears to be random in the sense that the binary values occur in the sequence in the same proportion they would if the sequence were being generated based on a fair "coin tossing" experiment. In such an experiment, each head could result in one binary value and a tail the other value. The PN code appears to have been generated from such an experiment. A software or hardware device designed to produce a PN code is called a PN generator ([33] and [34]).

The reason behind the use of PN codes is that if the code sequences were deterministic, then everybody could access the channel. If the code sequences were truly random on the other hand, then nobody, including the intended receiver, would be able to access the channel. Thus, using a pseudo-random sequence makes the signal look like random noise to everybody except to the transmitter and the intended receiver [31]. The most used PN codes are:

- Maximal Length codes: The maximum-length shift-register code, or  $m$ -code for short, is probably the most widely known PN code. It has a length of  $2^m - 1$  bits and is generated by using a linear feedback shift register with  $m$  taps. The  $m$ -codes have excellent autocorrelation properties but their cross-correlation properties do not follow any particular rules ([33] and [34]) and typically exhibit undesirably high values [31]. Furthermore, the number of  $m$ -codes for a given number of registers

in a linear feedback shift register is limited.  $m$ -codes are used in IS-95 for scrambling for both uplink and downlink channels [32].

- Gold codes: Gold codes tackle the problems associated with  $m$ -codes. They are derived by combining  $m$ -codes from two linear feedback shift registers ([35] and [36]). In comparison to  $m$ -codes, Gold codes provide larger sets of codes and exhibit better cross-correlation properties ([31] and [33]). Gold codes are used in WCDMA for scrambling in the downlink channel [32].
- Kasami codes: Kasami codes also solve the two undesirable properties of the  $m$ -codes: smaller sets of codes and high cross-correlation values. Kasami codes can be generated either as a small set or as a large set. The small set has better cross-correlation properties, while the large set provides more codes to choose from. Generation of Kasami codes involves a method similar to the one used to generate the Gold codes. Kasami codes are used in WCDMA for scrambling in the uplink channel [32].

## 2.9 Short-Code versus Long-Code CDMA Systems

The selection of spreading codes is critical for the system designer. The choice between a short-code and a long-code CDMA system has been subject to a long debate. However, this depends heavily on the target of the application. As such, one has clearly to set the targets and main features of the application. Nevertheless, the targets are in many cases conflicting and this may explain why the debate, which system is better, is not resolved until now. Another factor that adds more ambiguity to this issue is that many studies have ended up with conflicting results. For example, vembu and viterbi [37] state that the long-code system outperforms its counterpart the short-code system in terms of user capacity and robustness while Kärkkäinen et al [38] state that the short-code system outperforms the long-code system in terms of average BER performance (average of users).

In order to get a clear picture of the scene, it is better to emphasize on the features of both systems and discuss the benefits and shortcomings of each system. In the following we compare long-code and short-code systems:

- Historically the choice of a long-code system was motivated by the requirement for a low probability of inference of the spreading code, and hence interception of the transmitted data, since the over-riding requirement was security [39]. This prompted the desire for very long codes which could be generated easily by co-operating parties but which at the same time, were difficult for interfering, or eavesdropping parties to infer. However, the advent of the implementation of spread

spectrum techniques for multiple access communications has shifted the emphasis somewhat away from such security issues to maximizing the number of subscribers who are able to access a system simultaneously [39], while maintaining a reasonable error performance. One way of maximizing the user capacity is the use of advanced signal processing techniques such as multiuser detection. Most of the MUD schemes assume cyclostationary interference which motivated the need for periodic short-code CDMA systems.

- In a long code system, the correlation between the users changes from symbol to symbol and the MAI therefore appears to be random in time, causing the average performance for different users to be identical and determined by the average interference level [40]. Short codes, on the other hand, have cross-correlations that remain unchanged over time, and there is a fear that an unfortunate user might be trapped in an inferior performance scenario due to non time-varying cross-correlations. The capacity is therefore ruled by the *distribution* of the interference rather than solely by its mean. To overcome the shortcoming of the short-code system, the author in [41] proposed a code-hopping technique to reduce the variability of users' performance within the system.
- In terms of complexity of multiuser detectors, short-code systems are specially introduced to make MUD possible, e.g., it is set as an option in the UMTS standard [32]. Short-code systems have the property that codes are periodic with a periodicity equal to the symbol time in contrast to long codes, which essentially are random. As such, the cross-correlation matrix is fixed and doesn't have to be recomputed from one symbol period to another. It should be noted that some interference suppression and cancellation techniques are applicable to long code systems as well, but the complexity is often lower in case of short codes due to the cyclostationary interference.
- Long-codes provide a large set of codes to choose from, therefore no algorithm for code selection is needed. This is in contrast to short-codes where the set of codes is limited and hence spreading codes for different users have to be carefully selected [38].

## 2.10 Conclusion

In this chapter, we reviewed the basic concept of cellular networks and went through different generations of cellular systems. The theory behind the spread spectrum technique is provided and advantages of CDMA over other multiple access techniques are detailed. Finally, different types of spreading codes that are used in actual standards are discussed and compared.

## Chapter 3

### Wireless Fading Channels

#### 3.1 Chapter's Contents

3.1 Chapter's Contents .....	23
3.2 Introduction .....	23
3.3 Channel Model .....	27
3.4 Power-Delay Profile .....	29
3.5 Generation of Rayleigh Complex Channel Coefficients .....	33
3.6 Conclusion .....	39

#### 3.2 Introduction

Radio waves propagate from a transmitting antenna, and travel through free space undergoing absorption, reflection and scattering. They are greatly affected by the ground terrain, the atmosphere, and the objects in their path, like buildings, bridges, hills, trees, etc. These multiple physical phenomena are responsible for most of the characteristic features of the received signal.

In most of the mobile or cellular systems, the height of the mobile antenna may be smaller than the surrounding structures. Thus, the existence of a direct or *line-of-sight* path between the transmitter and the receiver is highly unlikely. In such a case, propagation is mainly due to reflection and scattering from the buildings. So, in practice, the transmitted signal arrives at the receiver via several paths with different time delays creating a *multipath* situation as in Figure 3.1.

At the receiver, these multipath waves with randomly distributed amplitudes and phases combine to give a resultant signal that fluctuates in time and space. Therefore, a receiver at one location may have a signal that is much different from the signal at another location, only a short distance away, because of the change in the phase relationship among the incoming radio waves. This causes significant fluctuations in the signal's amplitude. This phenomenon of random fluctuations in the received signal level is termed as *fading*.

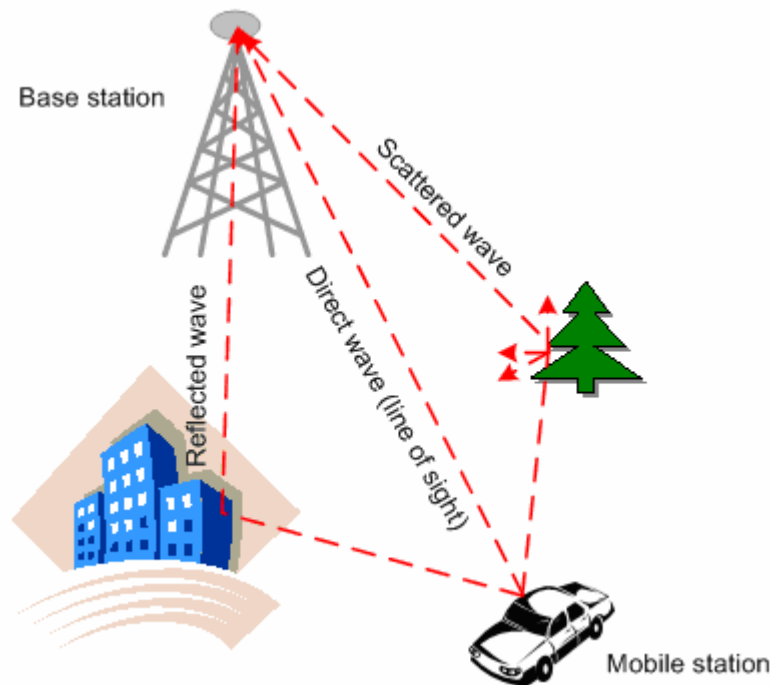


Figure 3.1: Wave propagation mechanisms

The propagation factors that affect the strength of the received signals in wireless communication systems, excellently introduced in [42], are the *path loss*, *large-scale fading* and *small-scale fading*. These are depicted in Figure 3.2 and explained briefly below:

- The path loss is basically a drop in signal power as a function of distance. When a mobile receiver moves away from the base station, i.e., when the distance increases, the signal will become weaker because of power loss in the transmission medium. For free-space propagation, the signal strength is inversely proportional to the distance squared (i.e.,  $1/d^2$ , where  $d$  is the distance between the transmitter and receiver). The path loss has the lowest rate of change of the three factors and the attenuation normally reaches 100-120 dB in the coverage area [43].
- The large-scale fading varies faster than path loss and is normally described as a log-normal distributed stochastic process around the mean of the path loss. This type of fading is introduced because of the shadowing from buildings and other structures in the environment. The large-scale fading introduces attenuations of about 6-10 dB [43].
- The small-scale fading is, as the name implies, the fastest varying mechanism. It is introduced as a consequence of the multipath propagation together with the time-varying nature of the channel.

The small-scale fading attenuates the signal with up to 40 dB, when the mobile moves as short as half a wavelength [43].

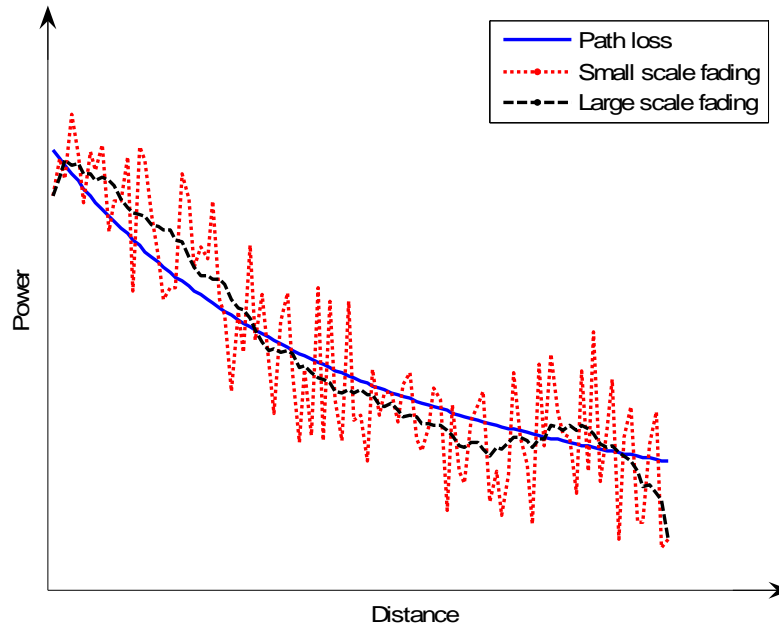


Figure 3.2: Fading mechanisms.

The path loss and large-scale fading can be mitigated by the use of power control, for example. Small-scale fading, on the other hand, introduces the need for an equalizer that is capable of removing the time-varying *intersymbol interference* (ISI) introduced by the multipath propagation. The multipath propagation arises from the fact that the transmitted signal is *reflected* from objects such as buildings or mountains and *scattered* from smaller objects such as lamp posts, for example [44]. Hence, the signal will reach the receiver from different directions, as shown in Figure 3.1. Each path may have different delay, introducing a spread in time (Delay spread) of the received signals, indicating that the channel may be characterized by an impulse response, where each impulse represents signal path with a certain delay. Depending on the maximum time difference between the first and last received signals, the *maximum excess delay*  $T_m$ , and the *symbol period*  $T_s$ , the channel may be classified as *frequency selective* or *flat*. The channel is said to be frequency selective when  $T_m > T_s$  (the mobile radio channel has a constant gain and linear phase response over a bandwidth, known as *coherence bandwidth*,

---

smaller than that of the transmitted signal), because different frequencies of the transmitted signal will experience different amount of attenuation. This leads to time dispersion of the transmitted symbols within the channel arising from these different time delays, and hence resulting in inter-symbol interference [45].

On the other hand, if  $T_s < T_m$  (the mobile radio channel has a coherence bandwidth larger than the bandwidth of the transmitted signal) then the channel is said to be flat since all frequencies of the transmitted signal would experience essentially the same amount of attenuation.

For wireless systems, the channel is time-variant because of the relative motion between the transmitter and the receiver or by movements of objects within the channel, which results in propagation changes (i.e., variations in the signal's amplitude and phase).

Another important physical mechanism that affects the signal is the *Doppler effect*. Doppler spread is introduced in the received signal spectrum, causing frequency dispersion. If the Doppler spread is significant relative to the bandwidth of the transmitted signal, the received signal is said to undergo *fast fading*. This form of fading typically occurs for very low data rates. On the other hand, if the Doppler spread of the channel is much less than the bandwidth of the baseband signal, the signal is said to undergo *slow fading*. This is the case for most 3G wideband systems [46].

If we assume that (i) the propagation of the waves takes place in the two dimensional (horizontal) plane, (ii) that there is isotropic scattering (uniformly in all directions) around the receiver, (iii) that the channel is flat, (iv) uniform distribution of signals arriving from all angles throughout the range  $[0, 2\pi]$  and that (v) the receiving antenna is omni-directional (radiates power uniformly in all directions), then it is possible to show that, when there is a great number of waves received at the antenna, a transmitted signal will be multiplied with a time-varying signal with a power spectral density often called *Jake's power spectral density*, *Clarke's power spectral density* or *the classical Doppler spectrum*. Interested readers are referred to [47] for full details regarding the derivation of Jake's PSD. It can also be shown that the signal has a complex Gaussian distribution, which implies that the magnitude of the signal will have a *Rayleigh distribution*, in the case of no line-of-sight. When a line-of-sight component is present, the distribution will be *Rician* instead. A nice presentation on this topic can be found in [28].

The final model of the channel is a time-varying impulse response, where each coefficient in the response models a certain multipath; i.e., each coefficient will have the classical Doppler spectrum and either a Rayleigh or Rician distribution.

For the Rayleigh and Rician processes, it is possible to derive a number of useful statistical properties ([28] and [48]), such as the *average fade duration (AFD)*, the *level crossing rate (LCR)* and the *autocorrelation function*.

The AFD is a measure of the average time the amplitude of the signal is below a certain threshold level. The AFD is inversely proportional to the Doppler frequency, that is, the higher the Doppler frequency, the shorter the fades will be on the average. The LCR is a measure of how often a certain amplitude level is passed by the signal. The LCR is proportional to the Doppler frequency, that is, for a higher Doppler frequency, the rate of crossing a certain level is higher. The autocorrelation function specifies the extent to which there is correlation between the channel's impulse response at time  $t_1$  and at time  $t_2$ . The time dependence goes down (i.e., less correlation) as Doppler frequency goes higher. An excellent overview on this topic and other channel modeling techniques is presented in [49].

### 3.3 Channel Model

The time-varying channel impulse response is given by the following expression [50]:

$$g(t, \tau) = \sum_{l=1}^L h_l c_l(t) \delta(\tau - \tau_l) \quad (3-1)$$

where:

$L$ : is the number of paths.

$h_l$ : is the given path amplitude satisfying the power normalization condition:  $\sum_{l=1}^L (h_l)^2 = 1$ . This

requirement allows the channel to be scaled by the transmit power in the simulation.

$\tau_l$ : is the time delay of the path relative to the first path; usually  $\tau_1 = 0$  is assumed.

$c_l(t)$ : the fading coefficient of the  $l$ -path and can be Rayleigh or Rician distributed.

$\delta(t)$ : is the delta function

A typical realization of the time-varying channel impulse response given by equation (3-1) is shown in Figure 3.3. A practical implementation of the time-varying channel in an uplink asynchronous CDMA system is shown in Figure 3.4 and 3.5. Here, the received signal is given by:

$$r(t) = \sum_{k=1}^K r_k(t - \tau^k) + n(t) \quad (3-2)$$

where:

$$r_k(t) = \sum_{l_k=1}^{L_k} h_{l_k} c_{l_k}(t - \tau_{l_k}) b_k(t - \tau_{l_k}) a_k(t - \tau_{l_k}) s_k(t - \tau_{l_k}) \quad (3-3)$$

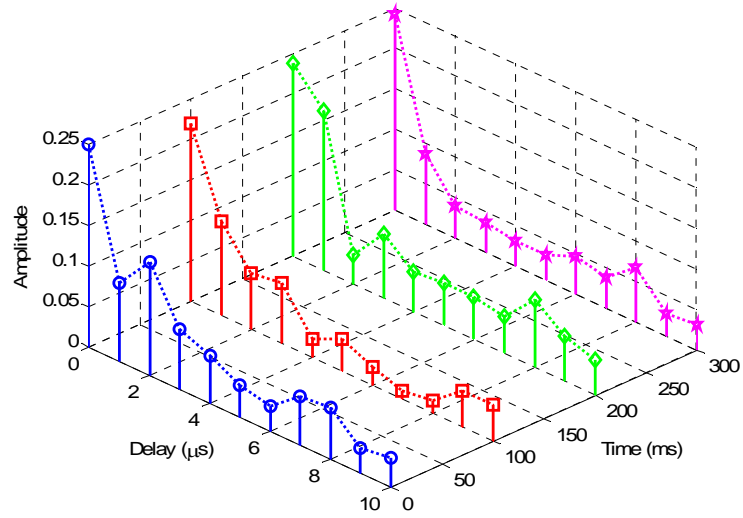


Figure 3.3: Time-varying channel impulse response.

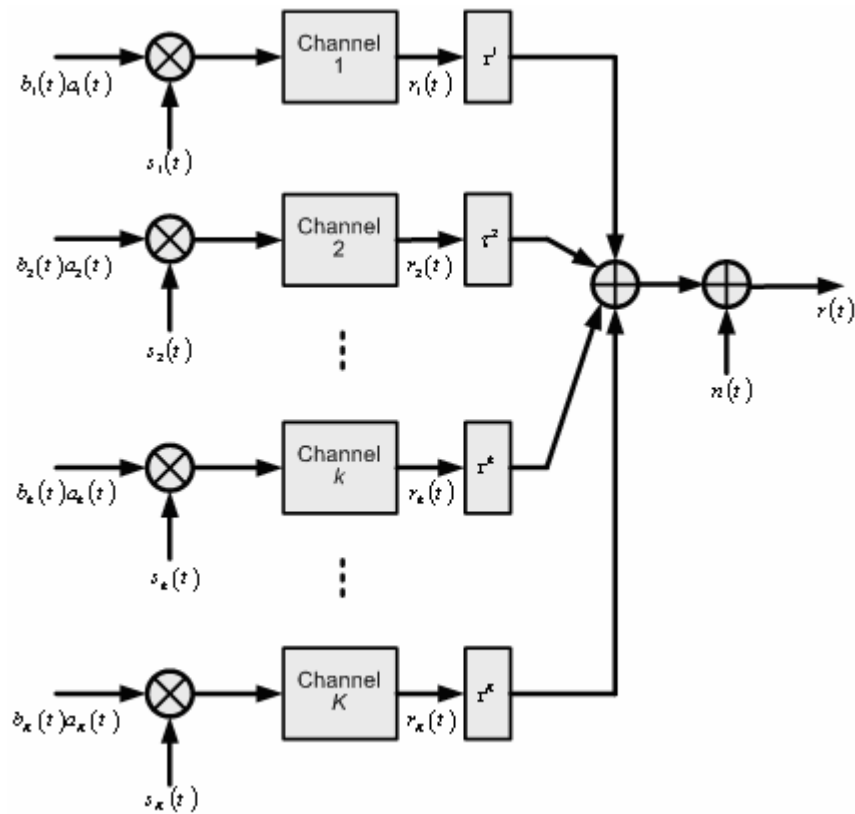


Figure 3.4: Uplink asynchronous CDMA system.

and  $n(t)$  is an AWGN noise sample at time  $t$  with variance  $\sigma^2$ , moreover,  $b_k(t)$ ,  $a_k(t)$ , and  $s_k(t)$  are the transmitted symbol value, amplitude value and spreading code value at time  $t$  of the  $k^{\text{th}}$  user, respectively.

The amplitude of each path  $h_{l_k}$  is usually obtained from the power delay profile whereas the fading coefficients  $c_{l_k}(t)$  are generated from a fading coefficients generation model. The power delay profile and the fading coefficients generation model are the subject of the next sections.

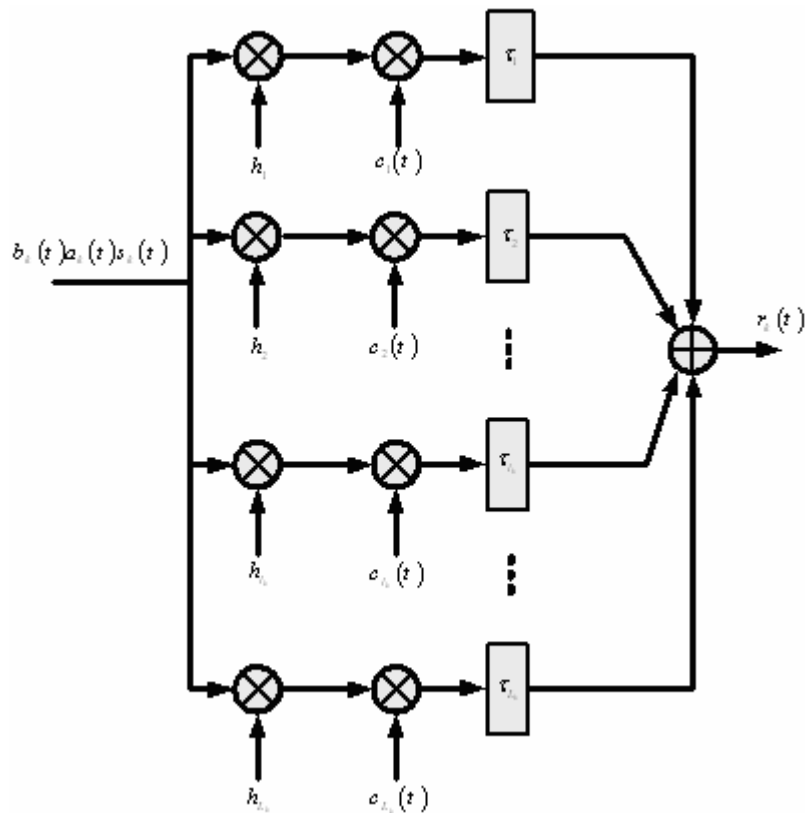


Figure 3.5: Time-varying fading channel for the  $k^{\text{th}}$  user.

### 3.4 Power-Delay Profile

Channel measurements are often summarized in terms of power-delay profiles. A Power-delay profile

$P(\tau)$  ( $\tau \geq 0$ ) can be interpreted as a density, normalized such that  $\int_0^{\infty} P(\tau) d\tau = 1$  with  $P(\tau)d\tau$  denoting the

fraction of power in taps with delays in the interval  $[\tau, \tau + d\tau]$ . The mean value and the standard deviation for this density are known as the *mean excess delay* and *rms delay spread*, respectively. If we sample this density function at the sampling rate  $F_s$  we obtain  $L$  samples that represent the number of multi-paths. If the amplitude of the  $l^{\text{th}}$  multi-path is  $h_l$  and its delay is  $\tau_l$ , then the mean excess delay is defined as:

$$\bar{\tau} = \frac{\sum_l (h_l)^2 \tau_l}{\sum_l (h_l)^2} \quad (3-4)$$

and the *rms* delay spread is given by:

$$\tau_{rms} = \sqrt{\overline{\tau_l^2} - \bar{\tau}^2} \quad (3-5)$$

where:  $\overline{\tau_l^2} = \sqrt{\frac{\sum_l h_l^2 \tau_l^2}{\sum_l h_l^2}}$ .

The power-delay profile includes the power distribution and the associated delay of a multipath channel, so that it captures the frequency selectivity of the channel. For a simulation to be useful, power-delay profiles used should be representative for the given topographical environment, such as those summarized in documents of different standard development organizations (ITU, 3GPP, 3GPP2) ([51] and [52]). These models are based on extensive measurements of the time-varying channel impulse response and are usually summarized in tables as in Table 3.1, 3.2 and 3.3 ([53] and [51]):

Table 3.1: Indoor channel power delay profile (5Km/h).

Relative Delay (ns)	Avg. Power (dB)	Avg. Power
0	0	1
50	-3	0.7079
110	-10	0.3162
170	-18	0.1259
290	-26	0.0501
310	-32	0.0251

Table 3.2: Indoor to outdoor channel power delay profile (5Km/h).

Relative Delay (ns)	Avg. Power (dB)	Avg. Power
0	0	1
110	-9.7	0.3273
190	-19.2	0.1096
410	-22.8	0.0724

Table 3.3: Vehicular A outdoor channel power delay profile (120Km/h).

Relative Delay (ns)	Avg. Power (dB)	Avg. Power
0	0	1
310	-1	0.8913
710	-9	0.3548
1090	-10	0.3162
1730	-15	0.1778
2510	-20	0.1000

The models given by multi-path channel profiles in tables 3.1, 3.2 and 3.3 should be converted to the time resolution of the simulation model (For UMTS we have the chip rate is: 3.84 *Mchips/s* therefore, the time duration of one chip is  $1/3.84 = 260.4$  ns). The ideal way to do this is to perform an interpolation with a *sinc(.)* function ( $\sin(x)/x$ ), however, this will result in a large number of additional paths which will increase the simulation time considerably. Simpler interpolation methods that give approximately the same number of paths are discussed in [54].

In our case, we implement the method known as *constant mean delay spread* due to its simplicity [54]. In this method, each ray is split into two rays, one to the left of the sample and one to the right of the sample. The power of these new rays is such that the sum is equal to the original power, and the power of each of the new rays is inversely proportional to the distance of the original ray. The power of all the rays on one sample are added and then normalized. This is graphically demonstrated in Figure 3.6.

After applying the proposed interpolation method and taking into consideration that we are using amplitudes in our simulation model instead of powers ( average amplitude =  $\sqrt{\text{average power}}$  ) we get the following equivalent amplitude delay profiles:

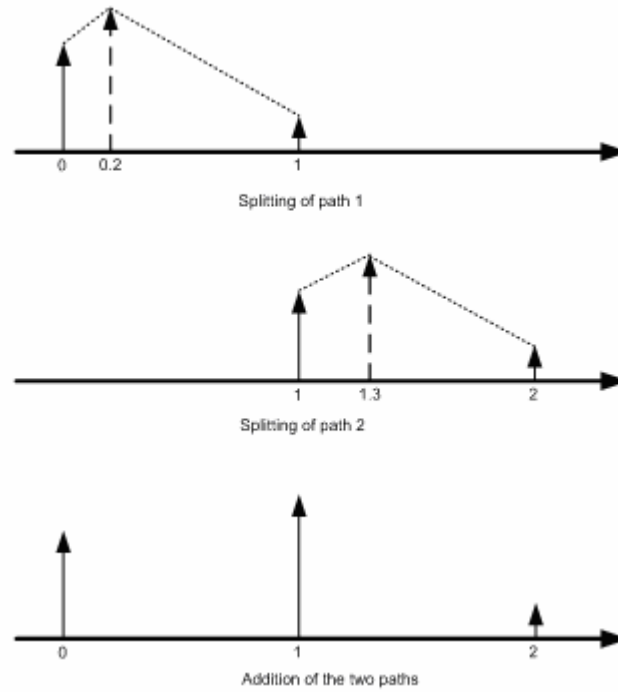


Figure 3.6: Equivalent Channel Model.

Table 3.4: Equivalent indoor channel amplitude delay profile of Table 3.1 at chip rate using the proposed interpolation method.

Relative Delay (ns)	Normalized Avg. Power	Avg. Amplitude
0	0.8082	0.8990
260.4	0.1871	0.4326
520.8	0.0047	0.0686

Table 3.5: Equivalent indoor to outdoor channel amplitude delay profile of Table 3.2 at chip rate using the proposed interpolation method.

Relative Delay (ns)	Normalized Avg. Power	Avg. Amplitude
0	0.8074	0.8986
260.4	0.1650	0.4062
520.8	0.0276	0.1661

Table 3.6: Equivalent vehicular A outdoor channel amplitude delay profile of Table 3.3 at chip rate using the proposed interpolation method.

Relative Delay (ns)	Normalized Avg. Power	Avg. Amplitude
0	0.3521	0.5934
260.4	0.2540	0.5040
520.8	0.0939	0.3064
781.2	0.1361	0.3689
1302	0.0772	0.2778
1822.8	0.0557	0.2360
2604	0.0310	0.1761

### 3.5 Generation of Rayleigh Complex Channel Coefficients

Since the introduction of the Jakes model in 1974 [55], many improved models have been developed and accessed to generate the Rayleigh complex channel coefficients with correct statistical properties [56]-[59]. Generating Rayleigh complex coefficients for the case of multiple independent fading channels was also proposed in [60]-[63].

In this dissertation, we use the improved Jakes model recently introduced in [64]. By sampling at frequency  $F_s$  (in our case, it is equal to chip-rate), the discrete form of the normalized discrete lowpass Rayleigh fading signal is given below:

$$c_l[n] = c_l^{inphase}[n] + jc_l^{quadrature}[n] \quad (3-6)$$

where:

$$c_l^{inphase}[n] = \frac{2}{\sqrt{M_o}} \sum_{m_o}^{M_o} \cos(\psi_{m_o,l}) \cos\left(\frac{\omega_d}{F_s} n \cos(\alpha_{m_o,l}) + \phi_l\right) \quad (3-7)$$

and:

$$c_l^{quadrature}[n] = \frac{2}{\sqrt{M_o}} \sum_{m_o}^{M_o} \sin(\psi_{m_o,l}) \cos\left(\frac{\omega_d}{F_s} n \cos(\alpha_{m_o,l}) + \phi_l\right) \quad (3-8)$$

with:  $\alpha_{m_o,l} = \frac{2\pi m_o - \pi + \phi_l}{4M_o}$ ,  $\omega_d = 2\pi f_d$  and  $f_d = \frac{v}{c} f_c$ .

Here,  $\varphi_l, \phi_l, \psi_{m_o, l}$  are random variables that are statistically independent and uniformly distributed over  $[-\pi, \pi]$  for all  $m_o$  and  $l$ ,  $n$  is the discrete time index,  $l$  is the  $l^{th}$  path and  $M_o$  is the number of oscillators used to approximate the complex fading signal,  $f_d$  ( $\omega_d = 2\pi f_d$ ) is the maximum Doppler frequency of the signal,  $f_c$  is the carrier frequency,  $v$  is the mobile speed,  $c$  is the speed of light and  $F_s$  is the sampling frequency. When  $M_o$  approaches infinity, the envelope

$|c_l| = \sqrt{(c_l^{inphase})^2 + (c_l^{quadrature})^2}$  is Rayleigh distributed with PDF:

$$f_{|c_l|}(c) = ce^{-\frac{c^2}{2}}, c \geq 0, \quad (3-9)$$

and the phase  $\Theta(c_l) = \arctan\left(\frac{c_l^{quadrature}}{c_l^{inphase}}\right)$  is uniformly distributed over  $[-\pi, \pi]$  with PDF:

$$f_{\Theta(c_l)}(\theta_c) = \frac{1}{2\pi}, \theta_c \in [-\pi, \pi] \quad (3-10)$$

The autocorrelation and cross-correlation functions of the inphase and quadrature components are given by:

$$R_{c_l^{inphase} c_l^{inphase}}(\tau) = J_0(\omega_d \tau) \quad (3-11)$$

$$R_{c_l^{quadrature} c_l^{quadrature}}(\tau) = J_0(\omega_d \tau) \quad (3-12)$$

$$R_{c_l^{inphase} c_l^{quadrature}}(\tau) = 0 \quad (3-13)$$

$$R_{c_l^{quadrature} c_l^{inphase}}(\tau) = 0 \quad (3-14)$$

where  $J_0$  is the zero-order Bessel function of the first kind. The width of the channel autocorrelation function is equal to the channel coherence time, denoted by  $T_{coh}$ . The coherence time satisfies  $T_{coh} \approx 1/f_d$ . The channel is said to be slowly fading if  $T_{coh} \gg T_s$  or  $f_d T_s \ll 1$ , and fast fading if  $T_{coh} < T_s$  or  $f_d T_s > 1$ . For UMTS system, the complex fading coefficients are generated at the chip rate which is 3.84Mchips/sec and Doppler shift for practical mobile speeds ranges from 0 to 200 Hz, therefore,  $f_d T_c \ll 1$  and hence the mobile channel for UMTS can be considered as a slow fading channel.

In the following, we simulate the improved Jakes model [64] and test some of its properties, where the following parameters are used:  $F_s = 1kHz, f_d = 100Hz$ . The second order statistics such as the autocorrelation and the cross-correlation of both the inphase and the quadrature components are shown

in Figure 3.7, 3.8, 3.9 and 3.10. We test two cases for  $M_o = 10$  and for  $M_o = 100$ . We note that  $M_o = 10$  is enough to approximate the theoretical models.

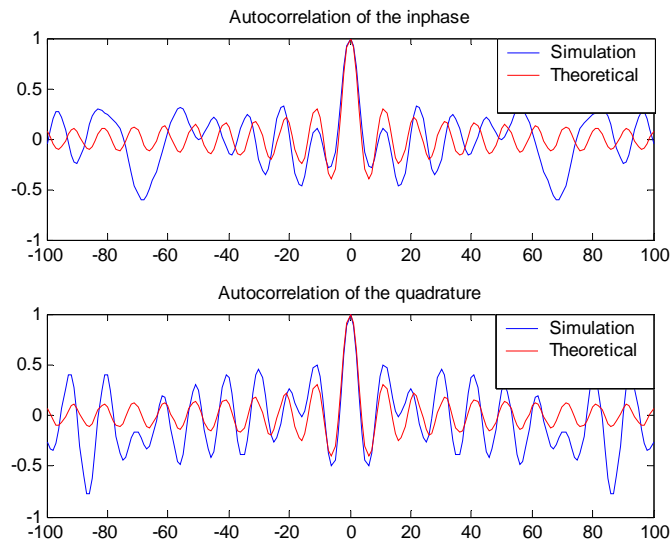


Figure 3.7: The simulated and theoretical autocorrelation of the inphase and quadrature components of the Rayleigh fading signal  $c(t)$  for  $M_o = 10$ .

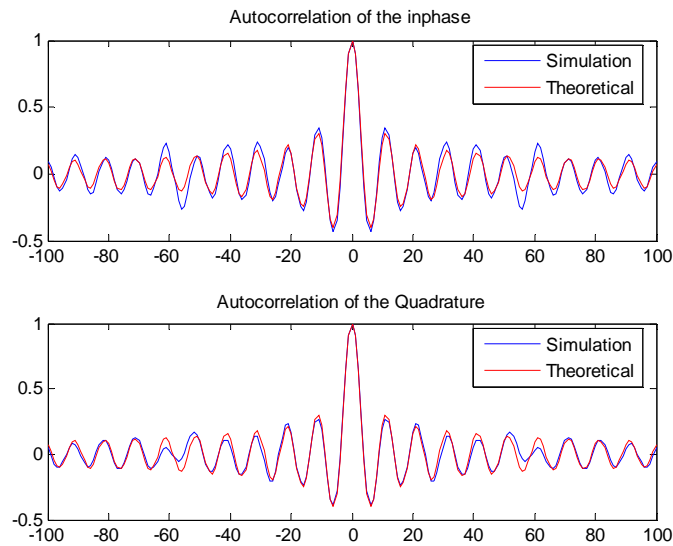


Figure 3.8: The simulated and theoretical autocorrelation of the inphase and quadrature components of the Rayleigh fading signal  $c(t)$  for  $M_o = 100$ .

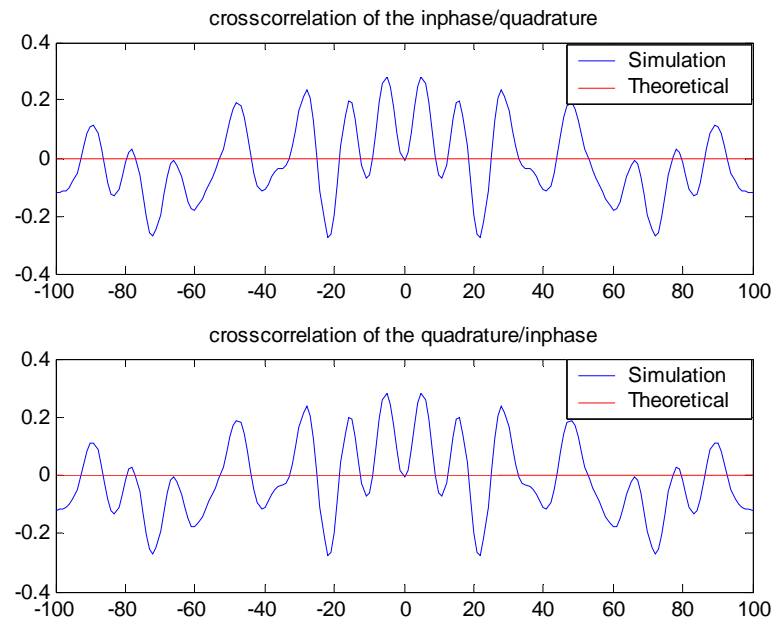


Figure 3.9: The simulated and theoretical crosscorrelation of the inphase and quadrate components of the Rayleigh fading signal  $c(t)$  for  $M_o = 10$ .

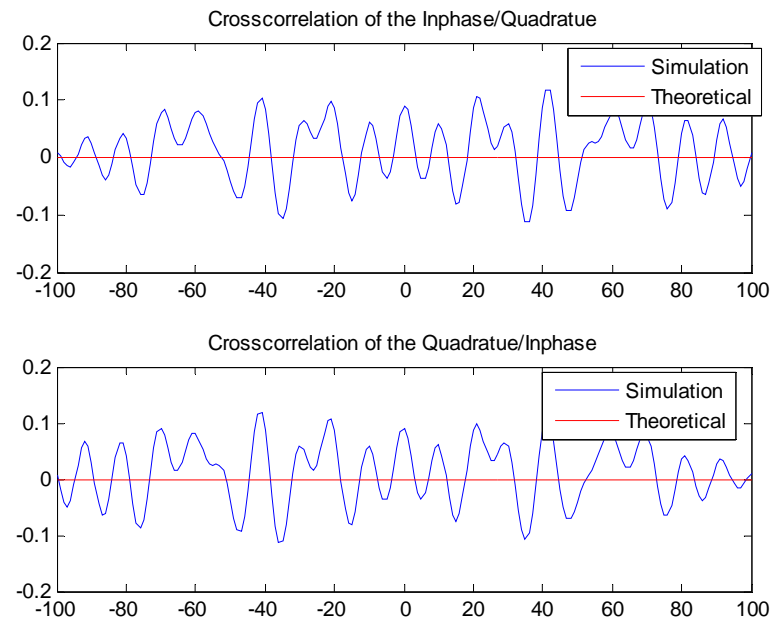


Figure 3.10: The simulated and theoretical cross-correlation of the in-phase and quadrature components of the Rayleigh fading signal  $c(t)$  for  $M_o = 100$ .

In order to check that different multi-paths generated using the improved jakes model are not correlated as it should be, we plot the simulated and theoretical cross-correlation of the in-phase components of two paths of the Rayleigh fading signal  $c(t)$  and the simulated and theoretical cross-correlation of the quadrature components of two paths of the same signal.

It is clear from Figure 3.11, that the cross-correlation between the in-phase components and the quadrature components of the two Rayleigh fading paths is very small.

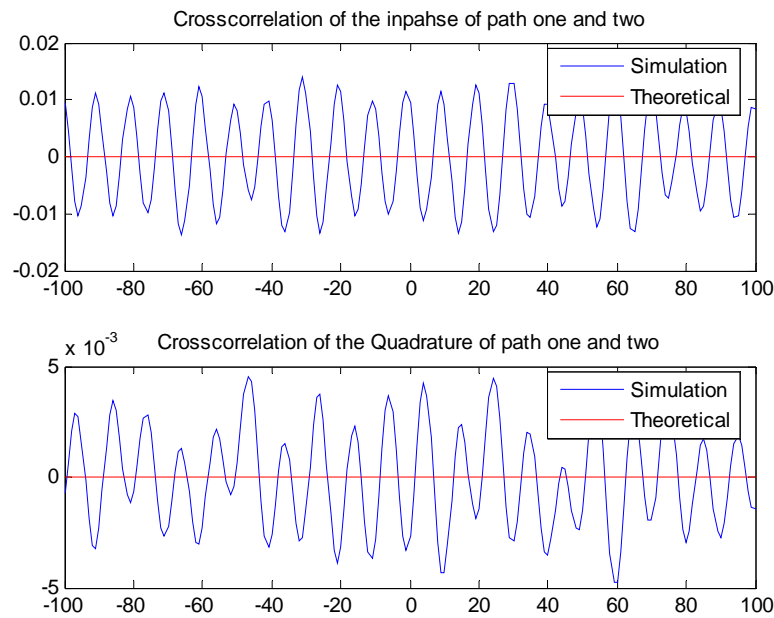


Figure 3.11: The simulated and theoretical cross-correlation of the in-phase components of two paths of the Rayleigh fading signal  $c(t)$  and simulated and theoretical cross-correlation of the quadrature components of two paths of the Rayleigh fading signal  $c(t)$  for  $M_o = 10$ .

In Figure 3.12, the probability density functions of the envelope and the phase of the signal  $c(t)$  are simulated. It is clear that the probability density function of the envelope is Rayleigh with mean one, and probability density function of the phase is uniform between  $-\pi$  and  $\pi$ .

In Figure 3.13, a realization of fast and slow fading signals which are controlled through the parameter  $f_d$  is plotted: for  $f_d = 10Hz$  (slow fading) and for  $f_d = 100Hz$  (fast fading).

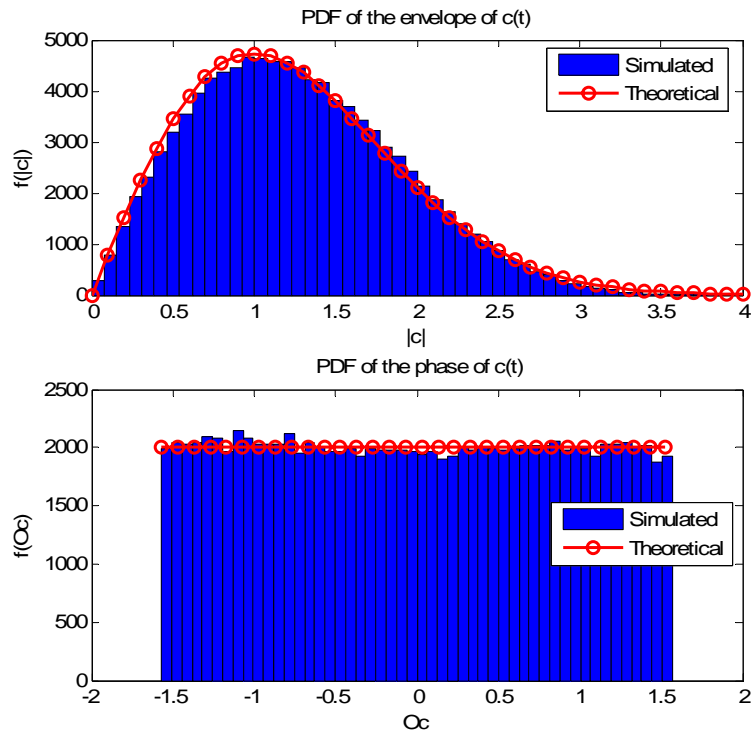


Figure 3.12: The simulated probability density function (PDF) of envelope and phase of the Rayleigh fading signal  $c(t)$ .

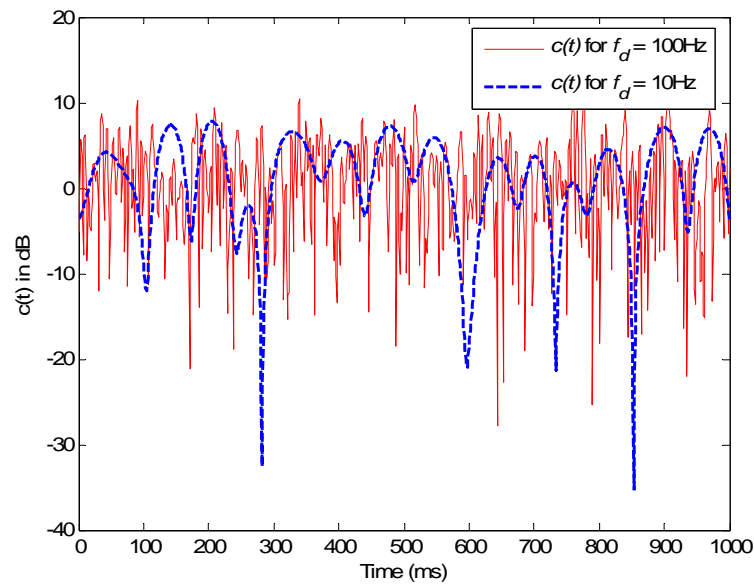


Figure 3.13: The envelope of the Rayleigh fading signal  $c(t)$ : slow versus fast fading.

### **3.6 Conclusion**

In this chapter, the multipath Rayleigh fading channel that will be used in simulation for all subsequent chapters is detailed. The channel model consists of basically two parts: the power delay profile and the complex Rayleigh fading channel coefficients. The WCDMA power delay profile and improved Jakes model were selected for implementation. Finally, different properties of the Jakes model such as the autocorrelation and cross-correlation were simulated and commented.

## Chapter 4

### CDMA Channel Model

#### 4.1 Chapter's Contents

4.1 Chapter's Contents .....	40
4.2 Introduction .....	41
4.3 Matrix Form of the Asynchronous CDMA AWGN Channel.....	42
4.3.1 Matrix of the Spreading Codes $\bar{\mathbf{S}}$ .....	43
4.3.2 Matrix of Received Amplitudes $\bar{\mathbf{A}}$ .....	44
4.3.3 Vector of BPSK Symbols $\bar{\mathbf{b}}$ .....	45
4.3.4 Determining the Matrix of Effective Spreading Codes $\bar{\mathbf{S}}_{eff}$ .....	46
4.3.5 Determining the Matrix of Effective Received Amplitudes $\bar{\mathbf{A}}_{eff}$ .....	50
4.3.6 Determining the Vector of the Effective BPSK Symbols $\bar{\mathbf{b}}^b$ .....	51
4.4 Matrix Form of the Asynchronous CDMA Multi-Path Fading Channel.....	52
4.4.1 Matrix of the Channel Coefficients $\bar{\mathbf{H}}$ .....	53
4.4.2 Matrix of the Spreading Codes $\bar{\mathbf{S}}$ .....	56
4.4.3 Matrix of the Spreading Codes $\bar{\bar{\mathbf{S}}}$ .....	58
4.4.4 Matrix of the Received Amplitudes $\bar{\mathbf{A}}$ .....	59
4.4.5 Vector of the BPSK Symbols $\bar{\mathbf{b}}$ .....	60
4.4.6 Determining the Effective Spreading Code $\bar{\bar{\mathbf{S}}}_{eff}^b$ .....	61
4.4.7 Determining the Matrix of Effective Received Amplitudes $\bar{\mathbf{A}}_{eff}$ .....	67
4.4.8 Determining the Vector of Effective BPSK Symbols $\bar{\mathbf{b}}^b$ .....	68
4.5 Conclusion.....	68

---

## 4.2 Introduction

Due to the complex nature of CDMA systems, there have been many different formulations for the CDMA uplink channel model. Several linear models have been developed starting from the simplest synchronous CDMA AWGN channel to the multiple antennas over multi-path fading channels. [65]-[67].

As the CDMA channel introduces MAI/ISI, different techniques of mitigating the effect of MAI, ISI or both result in different multiuser structures. The development of such structures depends on the CDMA channel model adopted. This is the main reason for having a variety of formulations of the CDMA channel model. Structures removing both ISI and MAI are introduced in [67]. Structures removing only MAI but not ISI are introduced in [68]. Both multiuser detector structures are based on the following model [67]:

$$\mathbf{r} = \mathbf{S}\mathbf{H}\mathbf{A}\mathbf{b} + \mathbf{n} \quad (4-1)$$

where:

**S**: is the matrix of the spreading codes.

**H**: is the matrix of the channel coefficients.

**A**: is the matrix of received amplitudes.

**b**: is the vector of BPSK symbols.

**n**: is the vector of independently, identically distributed additive white Gaussian noise with zero-mean and variance  $\sigma^2$ .

Another model proposed in [65] is given by:

$$\mathbf{r} = \mathbf{H}\mathbf{S}\mathbf{A}\mathbf{b} + \mathbf{n} \quad (4-2)$$

where **H**, **S**, **A**, **b** and **n** are the same as those defined in (4-1). The multiuser detector structures derived from this model can remove both ISI and MAI. However, if the effect of MAI is not severe, an interesting and useful structure that can be derived is a structure that will be able to remove ISI but not MAI. Furthermore, the remaining MAI can be due to either a synchronous CDMA channel or an asynchronous CDMA channel. The remaining MAI using this model is due to an asynchronous CDMA channel.

In the following, we introduce a new CDMA channel model that results in a multiuser detector structure that is able to:

- Either remove both ISI and MAI,

- Or remove ISI but not MAI where the remaining MAI is due to a synchronous CDMA channel. Hence, if the spreading codes are orthogonal then the MAI is also automatically removed.

Another advantage of the proposed CDMA channel model is its suitability for simulation, particularly in MATLAB, due its matrix formulation and the use of circular shifting operators.

In a multiuser CDMA system, there are two levels of asynchronism. In a symbol asynchronous system, symbols are not aligned but chips are and thus the delay is a multiple of the chip period. In a chip asynchronous system, chips are not aligned and thus symbols are not aligned as well. Usually in this case the chip period is sampled at a certain frequency. Hence, the delay is not a multiple of the chip period but a multiple of the sample period. In the subsequent sections, asynchronism refers to symbol asynchronism and hence all delays are multiple of the chip period.

### 4.3 Matrix Form of the Asynchronous CDMA AWGN Channel

Before starting the derivation of the matrix form of the asynchronous CDMA AWGN channel, let us define the following parameters:

$M$ : is the number of BPSK symbols.

$N$ : is the processing gain.

$K$ : is the number of active users in the system

$\tau^k$ : is the relative delay of the  $k^{th}$  user.

$k$ : is the user index.

$n$ : is the chip index.

$m$ : is the symbol index.

$T^t$ : is a circular shift operator, it shifts the rows/elements of a matrix/vector clockwise (from up to down)  $t$  rows/elements.

$\mathbf{s}_k$ : is the  $\{N-by-1\}$  spreading code of the  $k^{th}$  user.

$\mathbf{A}$ : is the  $\{K-by-K\}$  matrix of received amplitudes.

The received signal obtained at the output of the asynchronous AWGN channel is expressed in matrix form as:

$$\mathbf{r} = \overline{\mathbf{S}}\overline{\mathbf{A}}\mathbf{b} + \overline{\mathbf{n}} \quad (4-3)$$

where:

$\overline{\mathbf{S}}$ : is the  $\{(MN + \max_{1 \leq k \leq K}(\tau^k))\}-by-MK\}$  matrix of the spreading codes.

$\bar{\mathbf{A}}$ : is the  $\{MK-by-MK\}$  matrix of received amplitudes.

$\bar{\mathbf{b}}$ : is the  $\{MK-by-1\}$  vector of BPSK symbols.

$\bar{\mathbf{n}}$ : is the  $\{(NM + \max_{1 \leq k \leq K}(\tau^k)) - by - 1\}$  vector of independent, identically distributed (i.i.d) additive white Gaussian noise with zero-mean and variance  $\sigma^2$ . The matrices  $\bar{\mathbf{S}}$  and  $\bar{\mathbf{A}}$ , and vector  $\bar{\mathbf{b}}$  are derived in the following subsections.

### 4.3.1 Matrix of the Spreading Codes $\bar{\mathbf{S}}$

The following steps are required to construct the spreading matrix  $\bar{\mathbf{S}}$ :

- Define the vector  $\tilde{\mathbf{s}}_k$  of length  $\{(N + \max_{1 \leq k \leq K}(\tau^k)) - by - 1\}$  as  $\tilde{\mathbf{s}}_k = \begin{bmatrix} \mathbf{s}_k \\ \mathbf{0} \end{bmatrix}$  where  $\mathbf{0}$  is a  $\{\max_{1 \leq k \leq K}(\tau^k) - by - 1\}$  zero vector.
- Construct the matrix  $\tilde{\mathbf{S}}$  of length  $\{(N + \max_{1 \leq k \leq K}(\tau^k)) - by - K\}$  and shown in Figure 4.1 as

$$\tilde{\mathbf{S}} = \begin{bmatrix} \tilde{\mathbf{s}}_1 T^{\tau^1} & \tilde{\mathbf{s}}_2 T^{\tau^2} & \dots & \tilde{\mathbf{s}}_k T^{\tau^k} & \dots & \tilde{\mathbf{s}}_K T^{\tau^K} \end{bmatrix}.$$

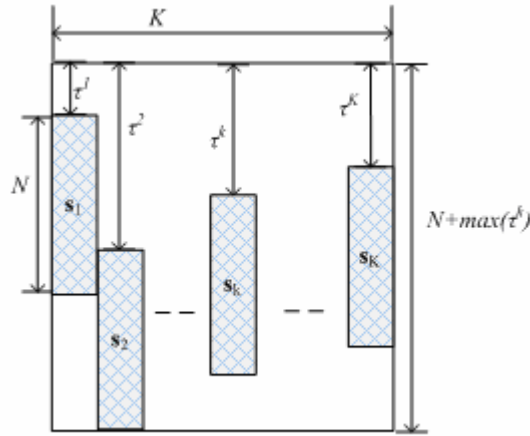


Figure 4.1: The matrix  $\tilde{\mathbf{S}}$ .

- Define  $\tilde{\tilde{\mathbf{S}}}$  of length  $\{NM + \max_{1 \leq k \leq K}(\tau^k) - by - K\}$  as  $\tilde{\tilde{\mathbf{S}}} = \begin{bmatrix} \tilde{\mathbf{S}} \\ \mathbf{0} \end{bmatrix}$ , where  $\mathbf{0}$  is a  $\{N(M-1) - by - K\}$  zero matrix.

- Finally the matrix  $\bar{\mathbf{S}}$  of length  $\{NM + \max_{1 \leq k \leq K}(\tau^k) - by - MK\}$ , shown in Figure 4.2 is obtained as:

$$\bar{\mathbf{S}} = \begin{bmatrix} \tilde{\mathbf{S}}T^0 & \tilde{\mathbf{S}}T^N & \dots & \tilde{\mathbf{S}}T^{(m-1)N} & \dots & \tilde{\mathbf{S}}T^{(M-1)N} \end{bmatrix}.$$

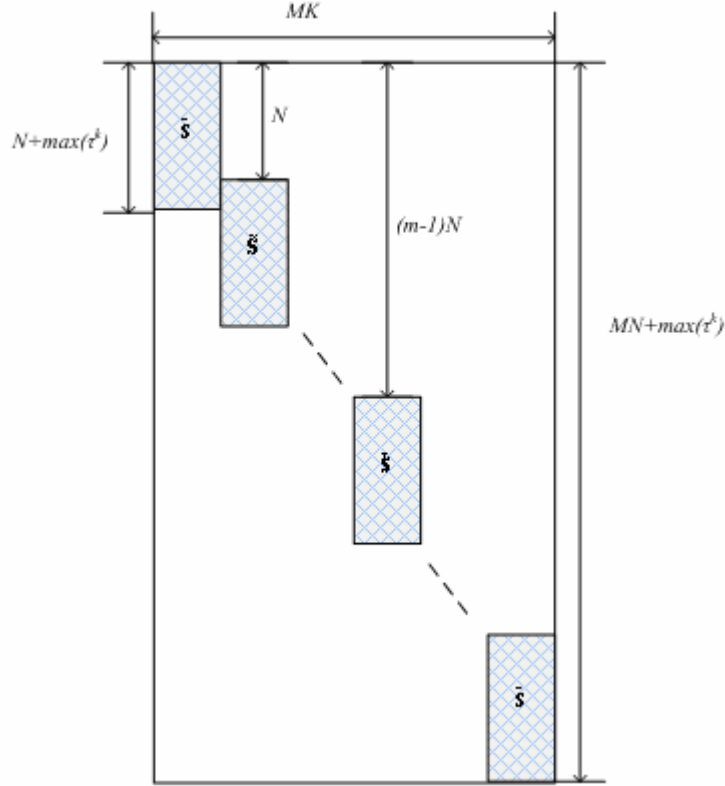


Figure 4.2: The matrix  $\bar{\mathbf{S}}$ .

### 4.3.2 Matrix of Received Amplitudes $\bar{\mathbf{A}}$

The following steps are required to construct the matrix  $\bar{\mathbf{A}}$ :

- Define the matrix  $\tilde{\mathbf{A}}$  of length  $\{MK - by - K\}$  as  $\tilde{\mathbf{A}} = \begin{bmatrix} \mathbf{A} \\ \mathbf{0} \end{bmatrix}$  where  $\mathbf{A}$  is a  $\{K - by - K\}$  matrix of the received amplitudes and  $\mathbf{0}$  is a  $\{(M-1)K - by - K\}$  zero matrix.
- Finally the matrix  $\bar{\mathbf{A}}$  of length  $\{MK - by - MK\}$  and shown in Figure 4.3 is constructed as follows:

$$\bar{\mathbf{A}} = \begin{bmatrix} \tilde{\mathbf{A}}T^0 & \tilde{\mathbf{A}}T^K & \dots & \tilde{\mathbf{A}}T^{(m-1)K} & \dots & \tilde{\mathbf{A}}T^{(M-1)K} \end{bmatrix}.$$

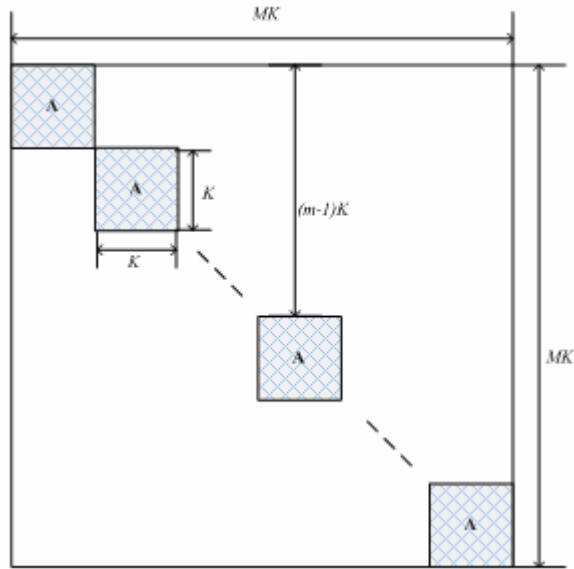


Figure 4.3: The matrix  $\bar{\mathbf{A}}$ .

### 4.3.3 Vector of BPSK Symbols $\bar{\mathbf{b}}$

The vector  $\bar{\mathbf{b}}$  of length  $\{MK-by-1\}$ , shown in Figure 4.4, is constructed as follows:

$\bar{\mathbf{b}} = [\mathbf{b}_1 \ \mathbf{b}_2 \ \cdots \ \mathbf{b}_m \ \cdots \ \mathbf{b}_M]^T$  where  $\mathbf{b}_m$  is a  $\{1-by-K\}$  vector of the  $m^{th}$  BPSK symbols of  $K$  users.

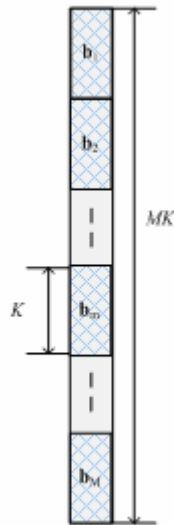


Figure 4.4: The vector  $\bar{\mathbf{b}}$ .

**4.3.4 Determining the Matrix of Effective Spreading Codes  $\bar{\mathbf{S}}_{eff}$**

Before proceeding further let us define the following symbols:

$W$ : is the number of symbols within the processing window (the length of the processing window counted in terms of BPSK symbols).

$u_g$ : is the user index within the  $g^{th}$  group.

$w$ : is the symbol index of the symbols detected within one processing window interval.

$b$ : is the block index.

$B$ : is the number of blocks in a data packet.

$PW$ : length of the processing window counted in terms of chips.

In a purely asynchronous CDMA system, the number of BPSK symbols  $M$  within one data packet is very large. Actually, each user activates and deactivates its terminal independently from each other. Thus, it is not practical to assume that the whole received signal  $\mathbf{r}$  would be processed in a receiver. Therefore, a finite sliding processing (observation) window model will be developed. The received signal will be processed using a sliding window of length  $PW$  chips and overlap  $V$  chips where  $PW$  and  $V$  are defined as:  $PW = WN + \max_{1 \leq k \leq K}(\tau^k)$  and  $V = \max_{1 \leq k \leq K}(\tau^k)$ . This is shown in Figure

4.5.

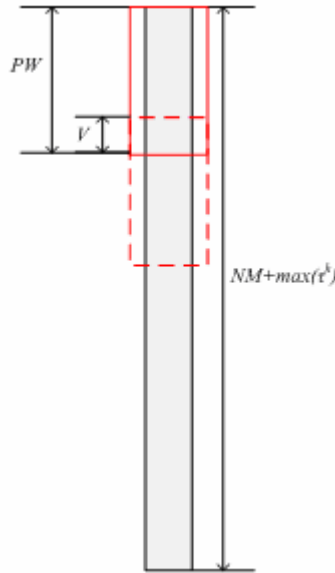


Figure 4.5: The vector  $\mathbf{r}$  and the sliding window of length  $PW$  chips and overlap  $V$  chips.

In doing so, it is better to buffer the received signal  $\mathbf{r}$  in a matrix  $\mathbf{Q} = [\mathbf{q}_1 \ \mathbf{q}_2 \ \dots \ \mathbf{q}_b \ \dots \ \mathbf{q}_B]$  of dimension  $\{PW\text{-by-}B\}$  where  $\mathbf{q}_b$  is a  $\{PW\text{-by-}1\}$  column of  $\mathbf{Q}$  as shown in Figure 4.6:

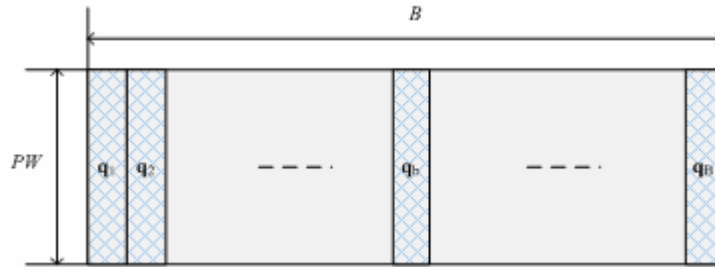


Figure 4.6: The matrix  $\mathbf{Q}$ .

The effective spreading codes are defined as:  $\bar{\mathbf{S}}_{eff} = [\tilde{\mathbf{S}}T^0 \ \tilde{\mathbf{S}}T^N \ \dots \ \tilde{\mathbf{S}}T^{(w-1)N} \ \dots \ \tilde{\mathbf{S}}T^{(W-1)N}]$

where  $\tilde{\mathbf{S}}$  is defined in Section 4.3.1. The structure of  $\bar{\mathbf{S}}_{eff}$  is shown in

Figure 4.7.

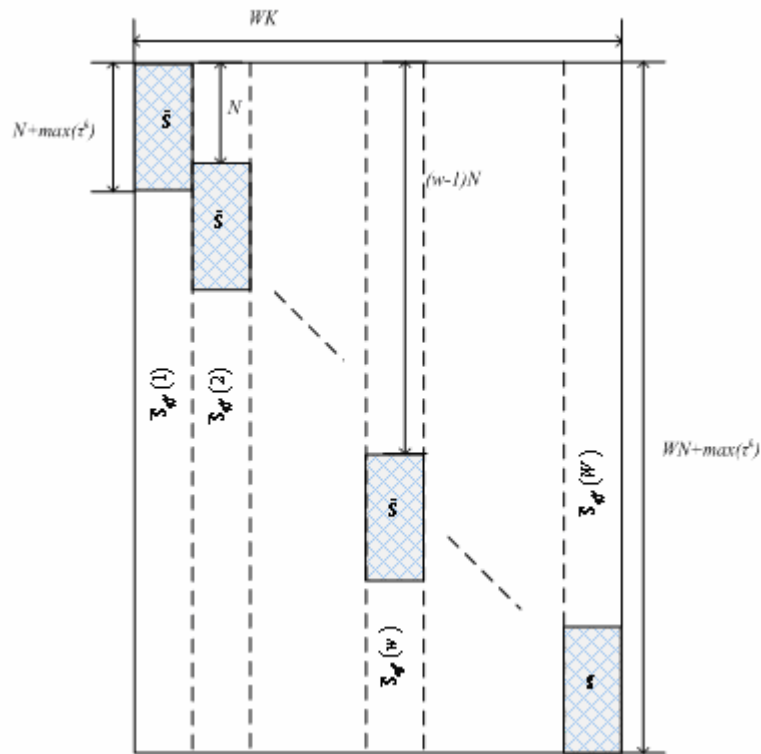


Figure 4.7: The matrix  $\bar{\mathbf{S}}_{eff}$ .

$\bar{\mathbf{S}}_{eff}$  can be decomposed as:  $\bar{\mathbf{S}}_{eff} = [\bar{\mathbf{S}}_{eff}(1) \bar{\mathbf{S}}_{eff}(2) \cdots \bar{\mathbf{S}}_{eff}(w) \cdots \bar{\mathbf{S}}_{eff}(W)]$  and  $\bar{\mathbf{S}}_{eff}(w) = [\bar{\mathbf{s}}_{eff}(w,1) \bar{\mathbf{s}}_{eff}(w,2) \cdots \bar{\mathbf{s}}_{eff}(w,k) \cdots \bar{\mathbf{s}}_{eff}(w,K)]$  where  $\bar{\mathbf{s}}_{eff}(w,k)$  is the  $w^{th}$  symbol  $k^{th}$  user effective spreading code vector. The structure of  $\bar{\mathbf{S}}_{eff}(w)$  is shown in Figure 4.8.

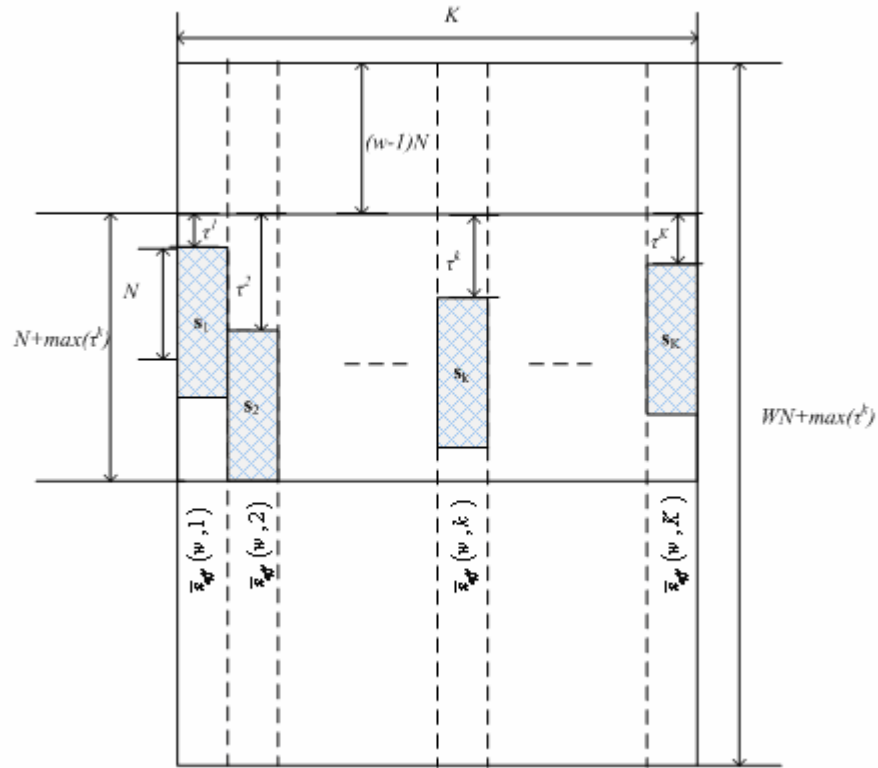
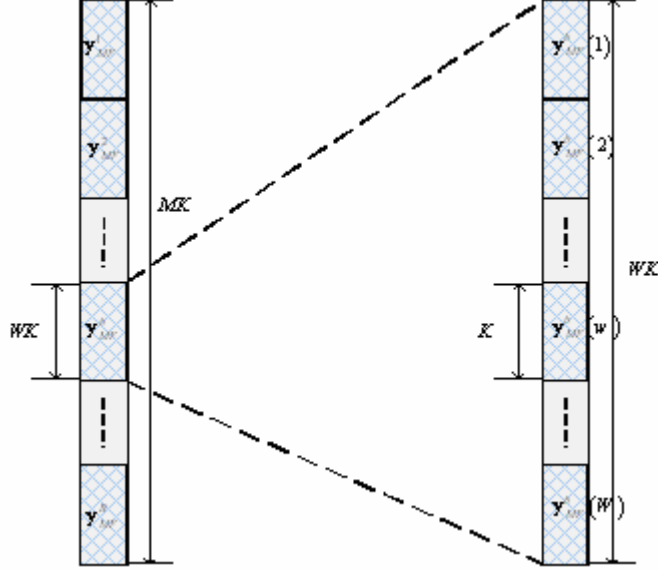


Figure 4.8: The matrix  $\bar{\mathbf{S}}_{eff}(w)$ .

The output of the bank of matched filters for the whole data packet is given by:  $\mathbf{y}_{MF} = \bar{\mathbf{S}}^T \mathbf{r}$  while the output of the bank of matched filters detector of the  $b^{th}$  block is given by:  $\mathbf{y}_{MF}^b = \bar{\mathbf{S}}_{eff}^T \mathbf{q}_b$ . This is shown in Figure 4.9:


 Figure 4.9: The vectors  $\mathbf{y}_{MF}$  (left) and  $\mathbf{y}_{MF}^b$  (right).

The cross-correlation matrix between the codes of active users for the whole data packet is given by:  $\bar{\mathbf{R}} = \bar{\mathbf{S}}^T \bar{\mathbf{S}}$ , while the cross-correlation matrix between the codes of active users for the  $b^{\text{th}}$  block is given by:  $\bar{\mathbf{R}}_{eff} = \bar{\mathbf{S}}_{eff}^T \bar{\mathbf{S}}_{eff}$ . This is shown in Figure 4.10.

In order to show the relation between  $\bar{\mathbf{R}}$  and  $\bar{\mathbf{R}}_{eff}$  let us arrange the matrix  $\tilde{\mathbf{S}}$  as:  $\tilde{\mathbf{S}} = \begin{bmatrix} \tilde{\mathbf{S}}^- \\ \tilde{\mathbf{S}}^* \\ \tilde{\mathbf{S}}^+ \end{bmatrix}$ ,

where  $\tilde{\mathbf{S}}^*$  is of length  $\{(N - \max_{1 \leq k \leq K}(\tau^k)) - by - K\}$ ,  $\tilde{\mathbf{S}}^+$  and  $\tilde{\mathbf{S}}^-$  are both of length  $\{\max_{1 \leq k \leq K}(\tau^k) - by - K\}$ . Define also  $\tilde{\mathbf{R}}^*$  as:  $\tilde{\mathbf{R}}^* = (\tilde{\mathbf{S}}^*)^T (\tilde{\mathbf{S}}^*)$ ,  $\tilde{\mathbf{R}}^+$  as  $\tilde{\mathbf{R}}^+ = (\tilde{\mathbf{S}}^+)^T (\tilde{\mathbf{S}}^-)$  and  $\tilde{\mathbf{R}}^-$  as  $\tilde{\mathbf{R}}^- = (\tilde{\mathbf{S}}^-)^T (\tilde{\mathbf{S}}^+)$ , hence  $\tilde{\mathbf{R}}^- = (\tilde{\mathbf{R}}^+)^T$ .  $\tilde{\mathbf{R}}^* = (\tilde{\mathbf{S}}^*)^T \tilde{\mathbf{S}}^*$  is the dashed matrix,  $\tilde{\mathbf{R}}^- = (\tilde{\mathbf{S}}^-)^T \tilde{\mathbf{S}}^+$  is the vertically dashed matrix and  $\tilde{\mathbf{R}}^+ = (\tilde{\mathbf{S}}^+)^T \tilde{\mathbf{S}}^-$  is the horizontally dashed matrix. It is clear that the MAI is not removed completely because of some cross-correlation elements that reside outside the sliding window. This effect is known as the finite word effect and therefore is a systematic error.

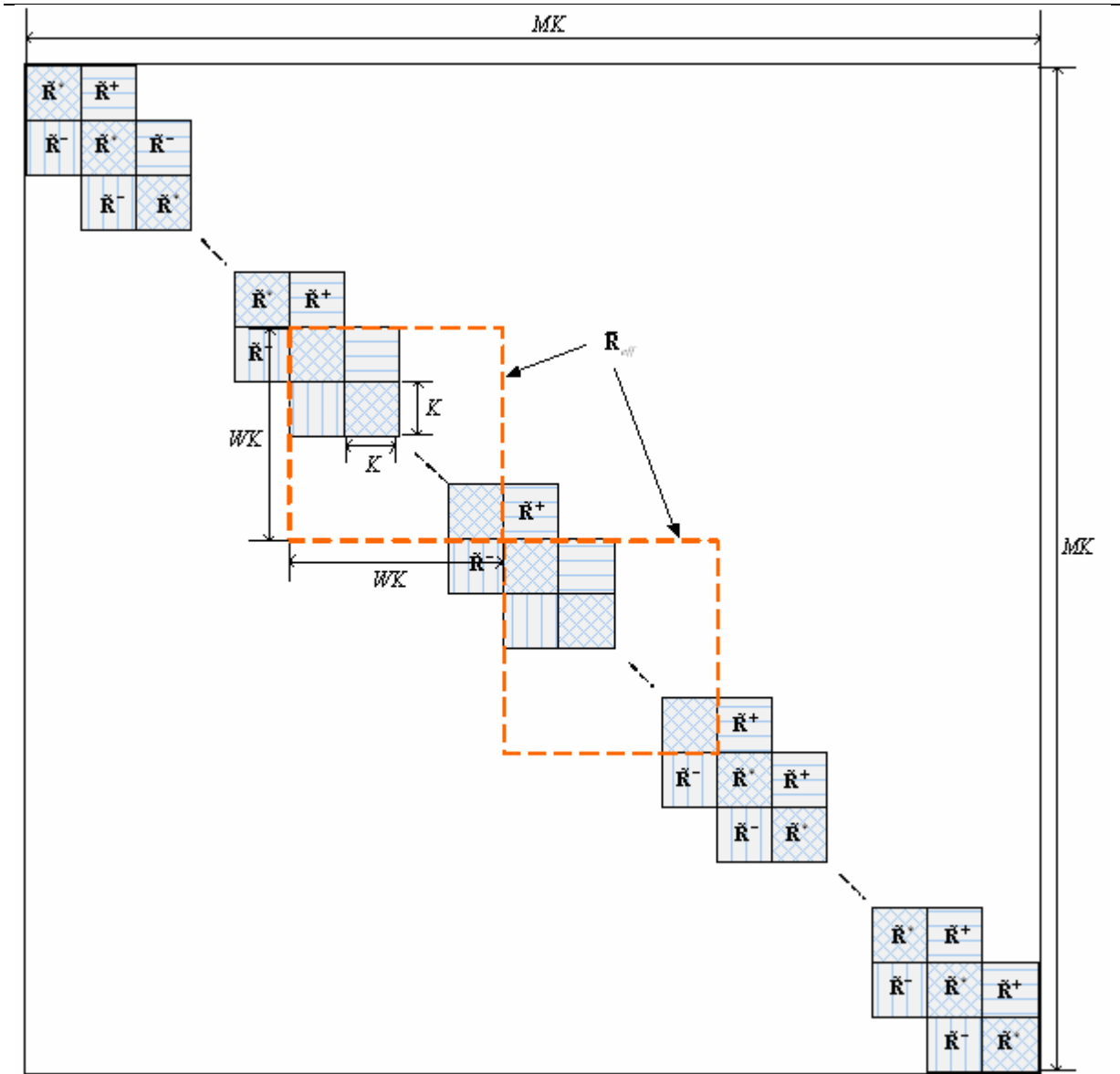


Figure 4.10: The matrices  $\bar{\mathbf{R}}$  and  $\bar{\mathbf{R}}_{eff}$  for the asynchronous CDMA AWGN channel.

### 4.3.5 Determining the Matrix of Effective Received Amplitudes $\bar{\mathbf{A}}_{eff}$

The matrix  $\bar{\mathbf{A}}_{eff}$  of length  $\{WK-by-WK\}$ , as shown in Figure 4.11, is constructed as follows:

$$\bar{\mathbf{A}}_{eff} = \left[ \tilde{\mathbf{A}}T^0 \quad \tilde{\mathbf{A}}T^K \quad \dots \quad \tilde{\mathbf{A}}T^{(w-1)K} \quad \dots \quad \tilde{\mathbf{A}}T^{(W-1)K} \right], \text{ where the matrix } \tilde{\mathbf{A}} \text{ is defined in Section}$$

4.3.2:

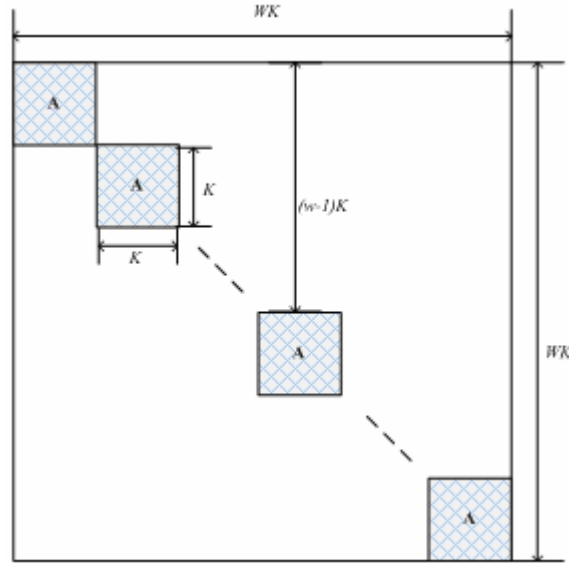


Figure 4.11: The matrix  $\bar{\mathbf{A}}_{eff}$ .

#### 4.3.6 Determining the Vector of the Effective BPSK Symbols $\bar{\mathbf{b}}^b$

The block  $b$  of BPSK symbols  $\bar{\mathbf{b}}^b$ , shown in Figure 4.12, is obtained by arranging the vector  $\bar{\mathbf{b}}$  of length  $\{MK-by-1\}$  into blocks as follows:  $\bar{\mathbf{b}} = [\bar{\mathbf{b}}^1 \ \bar{\mathbf{b}}^2 \ \dots \ \bar{\mathbf{b}}^b \ \dots \ \bar{\mathbf{b}}^B]^T$  where  $\bar{\mathbf{b}}^b = [\bar{\mathbf{b}}_1^b \ \bar{\mathbf{b}}_2^b \ \dots \ \bar{\mathbf{b}}_w^b \ \dots \ \bar{\mathbf{b}}_W^b]^T$ .  $\bar{\mathbf{b}}_w^b$  is shown in Figure 4.12 and can be decomposed by itself as follows:  $\bar{\mathbf{b}}_w^b = [\bar{\mathbf{b}}_w^b(1) \ \bar{\mathbf{b}}_w^b(2) \ \dots \ \bar{\mathbf{b}}_w^b(k) \ \dots \ \bar{\mathbf{b}}_w^b(K)]^T$ , where  $\bar{\mathbf{b}}_w^b(k)$  is the  $w^{th}$  BPSK symbol of the  $b^{th}$  block of the  $k^{th}$  user.

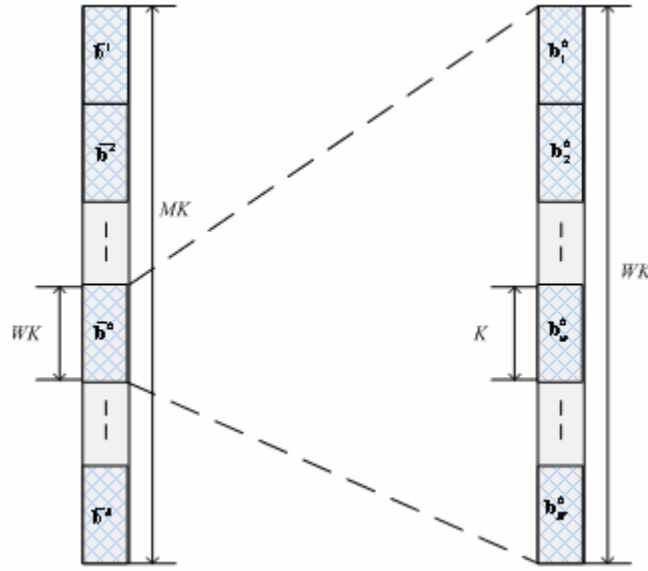


Figure 4.12: The vectors  $\bar{\mathbf{b}}^b$  and  $\bar{\mathbf{b}}_w^b$

#### 4.4 Matrix Form of the Asynchronous CDMA Multi-Path Fading Channel

Before starting the development of the matrix form of the asynchronous CDMA multi-path fading channel, let us define the following parameters:

$L_k$ : is the number of paths for the  $k^{th}$  user.

$l_k$ : is the path index for the  $k^{th}$  user.

$\tau_{l_k}$ : is the delay of the  $l^{th}$  path of the  $k^{th}$  user.

$h_{l_k}$ : is the average amplitude of the  $l^{th}$  path of the  $k^{th}$  user's channel impulse response (obtained from the power delay profile).

The received signal obtained at the output of the asynchronous multi-path fading channel is expressed in matrix form as:

$$\mathbf{r} = \bar{\mathbf{H}}\bar{\mathbf{S}}\bar{\mathbf{A}}\bar{\mathbf{b}} + \bar{\mathbf{n}} = \bar{\bar{\mathbf{S}}}\bar{\bar{\mathbf{A}}}\bar{\mathbf{b}} + \bar{\mathbf{n}} \quad (4-4)$$

where:

$\bar{\mathbf{H}}$  is  $\{(NM + \max_{1 \leq l_k \leq L_k} (\tau_{l_k}) + \max_{1 \leq k \leq K} (\tau^k)) - by - NMK\}$  matrix of the channel coefficients.

$\bar{\mathbf{S}}$  is  $\{NM \text{-by-} MK\}$  matrix of spreading codes.

$\bar{\mathbf{A}}$  is  $\{MK \text{-by-} MK\}$  matrix of the received amplitudes.

$\bar{\mathbf{b}}$  is  $\{MK \text{-by-} 1\}$  vector of BPSK symbols.

$\bar{\mathbf{n}}$  is  $\{(NM + \max_{1 \leq l_k \leq L_k} (\tau_{l_k}) + \max_{1 \leq k \leq K} (\tau^k)) \text{-by-} 1\}$  vector of independent, identically distributed additive white Gaussian noise with zero-mean and variance equals  $\sigma^2$  and  $\bar{\bar{\mathbf{S}}} = \bar{\mathbf{H}}\bar{\mathbf{S}}$ .

The matrices  $\bar{\mathbf{H}}$  and  $\bar{\mathbf{S}}$  and  $\bar{\mathbf{A}}$  and vector  $\bar{\mathbf{b}}$  are derived in the following subsections.

#### 4.4.1 Matrix of the Channel Coefficients $\bar{\mathbf{H}}$

Let us define the following:

$\mathbf{C}_k = [\mathbf{C}_k^1 \quad \mathbf{C}_k^2 \quad \cdots \quad \mathbf{C}_k^m \quad \cdots \quad \mathbf{C}_k^M]$  is the  $\{L_k \text{-by-} NM\}$  matrix of the complex channel coefficients (generated using the improved Jakes model of Section 3.4) of the  $k^{\text{th}}$  user for the data packet of length  $M$ .

$\mathbf{C}_k^m$  is  $\{L_k \text{-by-} N\}$  matrix of the complex channel coefficients of the  $k^{\text{th}}$  user for the  $m^{\text{th}}$  symbol period.

$\mathbf{C}_k$  could also be decomposed as:  $\mathbf{C}_k = \begin{bmatrix} \mathbf{c}_1 \\ \mathbf{c}_2 \\ \vdots \\ \mathbf{c}_{l_k} \\ \vdots \\ \mathbf{c}_{L_k} \end{bmatrix}$ , where  $\mathbf{c}_{l_k}$  is the  $l_k$  row of the matrix  $\mathbf{C}_k$ .

The following steps are required to construct the spreading matrix  $\bar{\mathbf{H}}$ :

- Define a new variable  $\tau_k = 0, 1, \dots, \max_{1 \leq l_k \leq L_k} (\tau_{l_k})$ .
- Define  $\tilde{\mathbf{C}}_k^m$  of length  $\{(\max_{1 \leq l_k \leq L_k} (\tau_{l_k}) + 1) \text{-by-} N\}$  where  $\tilde{\mathbf{C}}_k^m(\tau_k + 1, n)$  is given by:

$$\tilde{\mathbf{C}}_k^m(\tau_k + 1, n) = \begin{cases} \mathbf{C}_k^m(l_k, n) \times h_{l_k}, & \text{if } \tau_k = \tau_{l_k} \\ 0, & \text{elsewhere} \end{cases}$$

- Note that if  $\mathbf{C}_k^m$  is constant during one symbol period then, the elements of each row are constant, and  $\mathbf{C}_k^m$  can be reduced to the vector  $\mathbf{c}_k^m$  of length  $\{L_k \text{-by-} 1\}$ , that is:

$$\tilde{\mathbf{C}}_k^m(\tau_k + 1, n) = \begin{cases} \mathbf{c}_k^m(l_k) \times h_{l_k}, & \text{if } \tau_k = \tau_{l_k} \\ 0, & \text{elsewhere} \end{cases}$$

- Define  $\hat{\mathbf{c}}_k^m(n) = \begin{bmatrix} \tilde{\mathbf{c}}_k^m(n) \\ \mathbf{0} \end{bmatrix}$  where  $\tilde{\mathbf{c}}_k^m(n)$  is the  $n^{\text{th}}$  column of the matrix  $\tilde{\mathbf{C}}_k^m$  and  $\mathbf{0}$  is a  $\{(N-1)\text{-by-}l\}$  zero vector.
- Construct  $\mathbf{H}_k^m$  of length  $\{(N + \max_{1 \leq l_k \leq L_k}(\tau_{l_k}))\text{-by-}N\}$  as:  

$$\mathbf{H}_k^m = [\hat{\mathbf{c}}_k^m(1)T^0 \quad \hat{\mathbf{c}}_k^m(2)T^1 \quad \dots \quad \hat{\mathbf{c}}_k^m(n)T^{n-1} \quad \dots \quad \hat{\mathbf{c}}_k^m(N)T^{N-1}].$$
- Define  $\tilde{\mathbf{H}}_k^m$  of length  $\{(N + \max_{1 \leq l_k \leq L_k}(\tau_{l_k}) + \max_{1 \leq k \leq K}(\tau^k))\text{-by-}N\}$  as  $\tilde{\mathbf{H}}_k^m = \begin{bmatrix} \mathbf{H}_k^m \\ \mathbf{0} \end{bmatrix}$  where  $\mathbf{0}$  is an  $\{\max_{1 \leq k \leq K}(\tau^k)\text{-by-}N\}$  zero matrix.
- Construct the matrix  $\tilde{\mathbf{H}}^m = [\tilde{\mathbf{H}}_1^m T^{\tau^1} \quad \tilde{\mathbf{H}}_2^m T^{\tau^2} \quad \dots \quad \tilde{\mathbf{H}}_k^m T^{\tau^k} \quad \dots \quad \tilde{\mathbf{H}}_K^m T^{\tau^K}]$  of length  $\{(N + \max_{1 \leq l_k \leq L_k}(\tau_{l_k}) + \max_{1 \leq k \leq K}(\tau^k))\text{-by-}NK\}$ .
- Define  $\mathbf{H}^m$  of length  $\{(NM + \max_{1 \leq l_k \leq L_k}(\tau_{l_k}) + \max_{1 \leq k \leq K}(\tau^k))\text{-by-}NK\}$  as  $\mathbf{H}^m = \begin{bmatrix} \tilde{\mathbf{H}}^m \\ \mathbf{0} \end{bmatrix}$  where  $\mathbf{0}$  is an  $\{(M-1)N\text{-by-}NK\}$  zero matrix.
- Finally, construct the matrix  $\bar{\mathbf{H}} = [\mathbf{H}^1 T^0 \quad \mathbf{H}^2 T^N \quad \dots \quad \mathbf{H}^m T^{(m-1)N} \quad \dots \quad \mathbf{H}^M T^{(M-1)N}]$  of length  $\{(NM + \max_{1 \leq l_k \leq L_k}(\tau_{l_k}) + \max_{1 \leq k \leq K}(\tau^k))\text{-by-}NMK\}$ .

The matrices  $\bar{\mathbf{H}}$ ,  $\tilde{\mathbf{H}}^m$  and  $\mathbf{H}_k^m$  are depicted in Figure 4.13, 4.14 and 4.15, respectively.

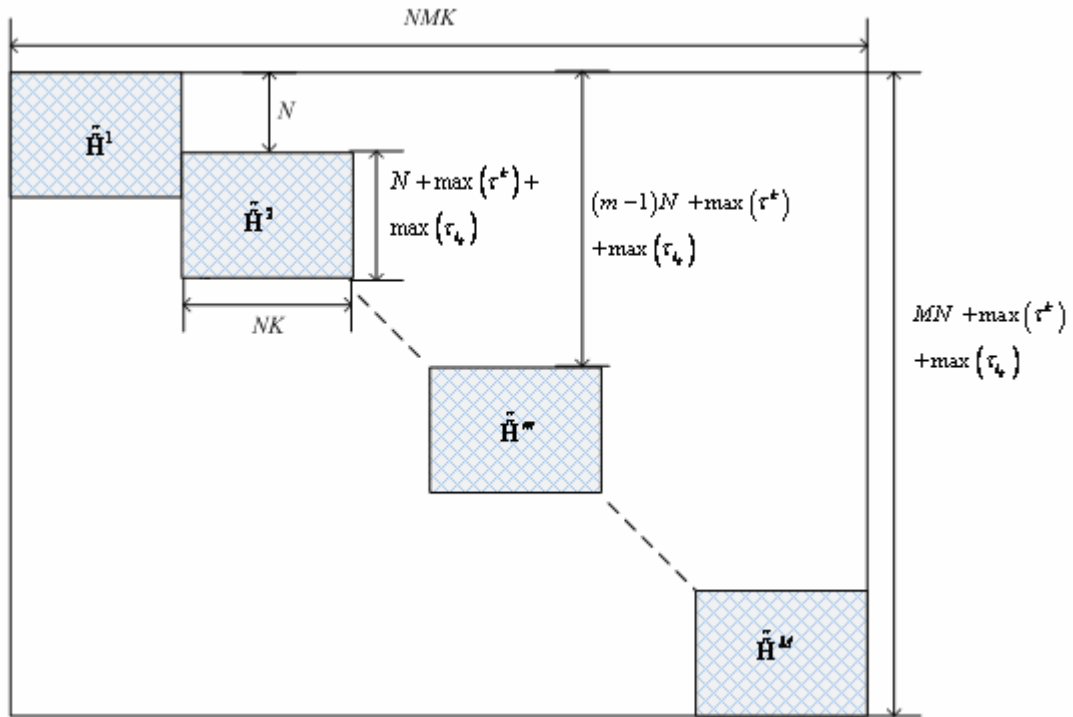


Figure 4.13: The matrix  $\tilde{\mathbf{H}}$ .

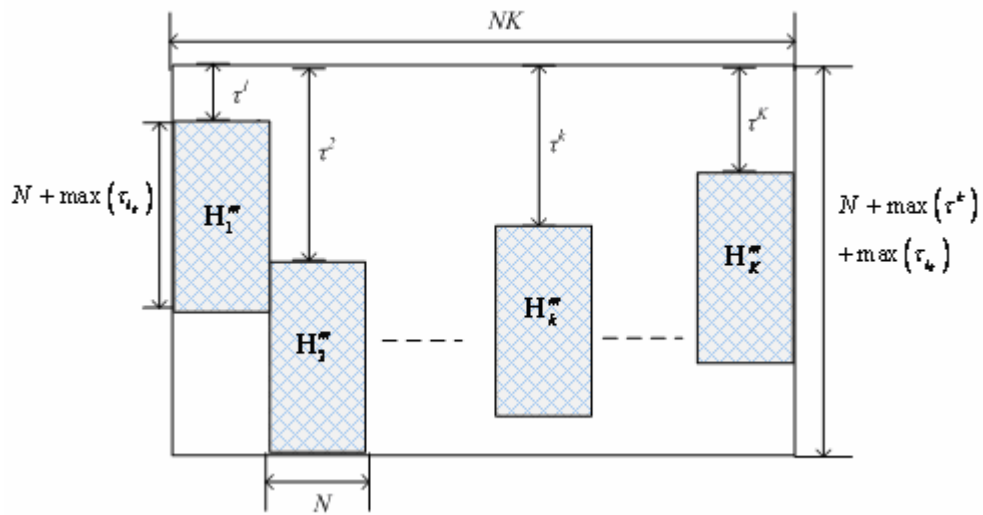
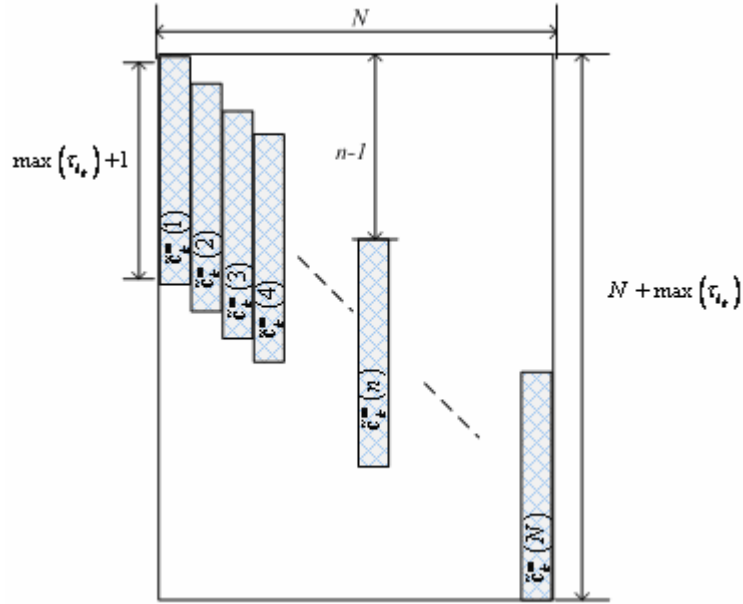


Figure 4.14: The matrix  $\tilde{\mathbf{H}}^m$ .


 Figure 4.15: The matrix  $\mathbf{H}_k^m$ .

#### 4.4.2 Matrix of the Spreading Codes $\bar{\mathbf{S}}$

The following steps are required to construct the spreading matrix  $\bar{\mathbf{S}}$ :

- First, define the vector  $\tilde{\mathbf{s}}_k$  of length  $\{NK-by-1\}$  as  $\tilde{\mathbf{s}}_k = \begin{bmatrix} \mathbf{s}_k \\ \mathbf{0} \end{bmatrix}$  where  $\mathbf{0}$  is an  $\{N(K-1)-by-1\}$  zero vector.
- Second, construct the matrix  $\tilde{\mathbf{S}} = \begin{bmatrix} \tilde{\mathbf{s}}_1 T^0 & \tilde{\mathbf{s}}_2 T^N & \dots & \tilde{\mathbf{s}}_k T^{(k-1)N} & \dots & \tilde{\mathbf{s}}_K T^{(K-1)N} \end{bmatrix}$  of length  $\{NK-by-K\}$ .
- Third, define  $\tilde{\tilde{\mathbf{S}}}$  of length  $\{NMK-by-K\}$  as  $\tilde{\tilde{\mathbf{S}}} = \begin{bmatrix} \tilde{\mathbf{S}} \\ \mathbf{0} \end{bmatrix}$  where  $\mathbf{0}$  is an  $\{N(M-1)K-by-K\}$  zero matrix.
- Finally, the matrix  $\bar{\mathbf{S}}$  of length  $\{NMK-by-MK\}$  is obtained as:
 
$$\bar{\mathbf{S}} = \begin{bmatrix} \tilde{\tilde{\mathbf{S}}} T^0 & \tilde{\tilde{\mathbf{S}}} T^{NK} & \dots & \tilde{\tilde{\mathbf{S}}} T^{(m-1)NK} & \dots & \tilde{\tilde{\mathbf{S}}} T^{(M-1)NK} \end{bmatrix}.$$

The matrices  $\bar{\mathbf{S}}$  and  $\tilde{\tilde{\mathbf{S}}}$  are depicted in Figure 4.16 and 4.17, respectively.

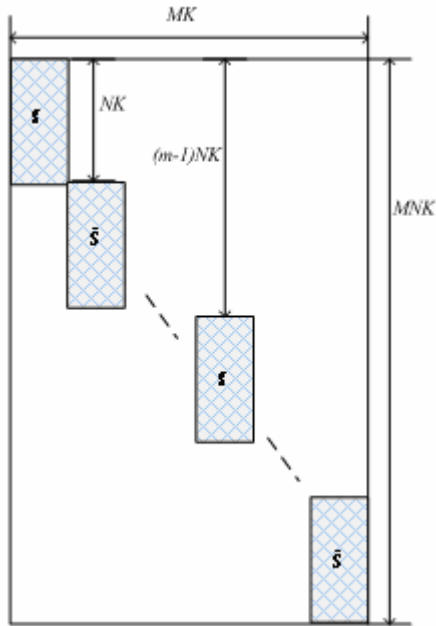


Figure 4.16: The matrix  $\bar{S}$ .

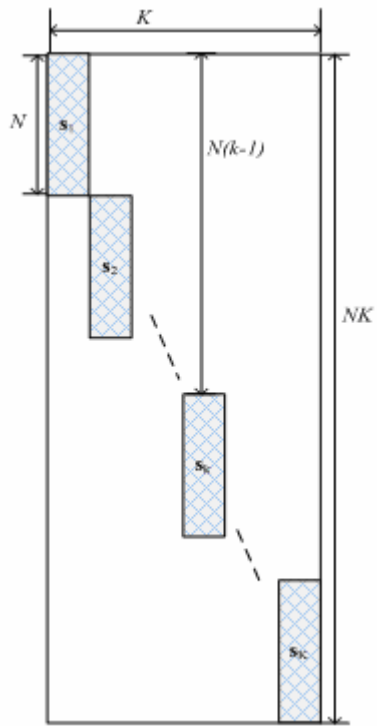


Figure 4.17: The matrix  $\tilde{S}$ .

### 4.4.3 Matrix of the Spreading Codes $\bar{\bar{\mathbf{S}}}$

The matrix  $\bar{\bar{\mathbf{S}}}$  is obtained from  $\bar{\bar{\mathbf{S}}} = \bar{\mathbf{H}}\bar{\mathbf{S}}$ . This is shown in Figure 4.18, where  $\tilde{\mathbf{S}}(m)$  is given by  $\tilde{\mathbf{S}}(m) = \tilde{\mathbf{H}}^m \tilde{\mathbf{S}}$  and it is shown in Figure 4.19. Here  $\tilde{\mathbf{s}}(m, k)$  is the non-zero part of  $k^{\text{th}}$  column of  $\tilde{\mathbf{S}}(m)$ .

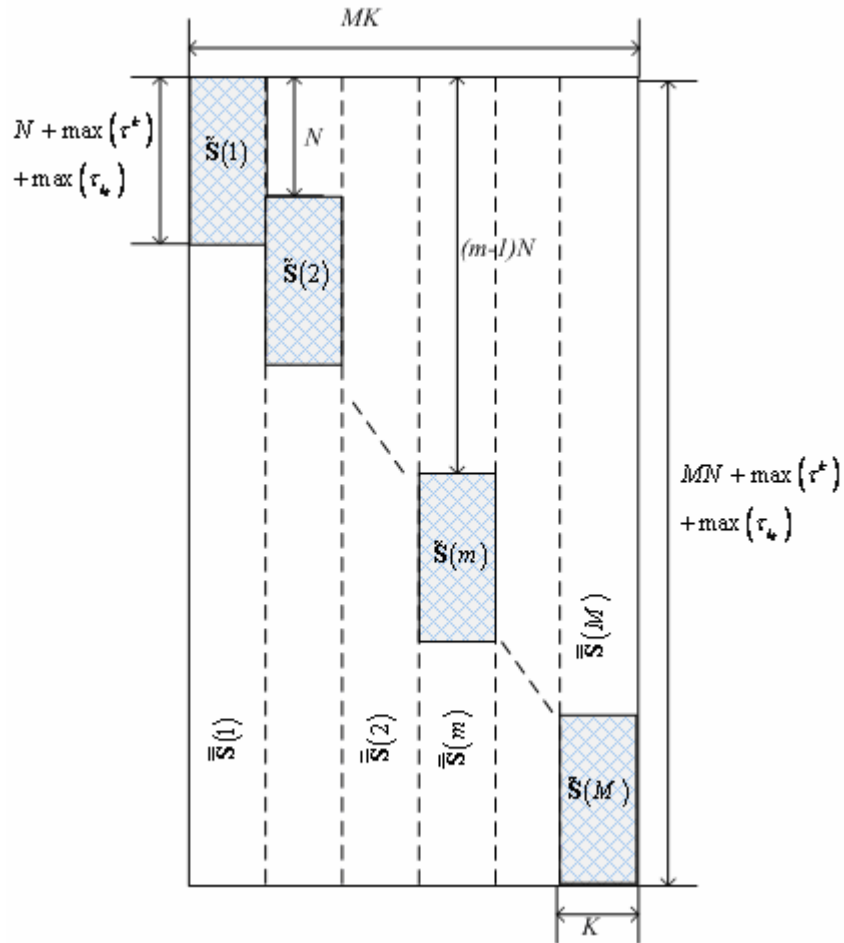


Figure 4.18: The matrix  $\bar{\bar{\mathbf{S}}}$ .



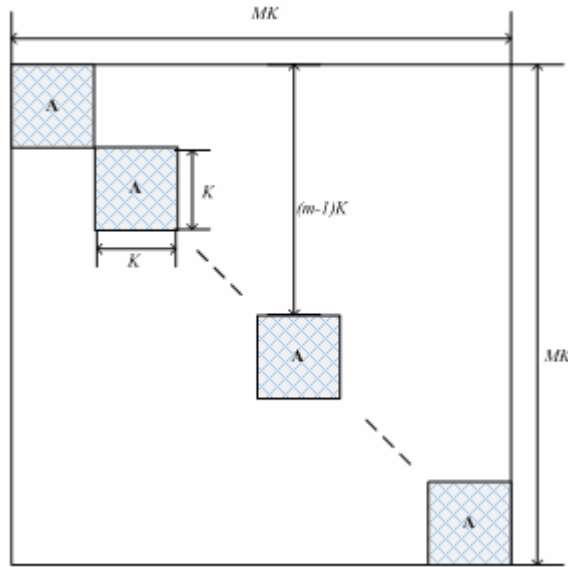


Figure 4.20: The matrix  $\bar{A}$ .

#### 4.4.5 Vector of the BPSK Symbols $\bar{\mathbf{b}}$

The vector  $\bar{\mathbf{b}}$  of length  $\{MK-by-1\}$ , as shown in Figure 4.21, is constructed as follows:

$\bar{\mathbf{b}} = [\mathbf{b}_1 \ \mathbf{b}_2 \ \cdots \ \mathbf{b}_m \ \cdots \ \mathbf{b}_M]^T$ , where  $\mathbf{b}_m$  is the  $\{1-by-K\}$  vector of the  $m^{th}$  BPSK symbols of  $K$  users.

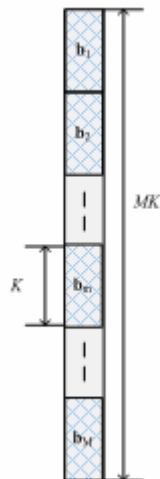


Figure 4.21: The vector  $\bar{\mathbf{b}}$ .

**4.4.6 Determining the Effective Spreading Code  $\bar{\mathbf{S}}_{eff}^b$**

As depicted in Figure 4.22, the received signal will be processed using a sliding window of length  $PW$  chips and overlap  $V$  chips of dimensions  $PW = WN + \max_{1 \leq l_k \leq L_k}(\tau_{l_k}) + \max_{1 \leq k \leq K}(\tau^k)$  and  $V = \max_{1 \leq l_k \leq L_k}(\tau_{l_k}) + \max_{1 \leq k \leq K}(\tau^k)$ , respectively. Again, the received signal  $\mathbf{r}$  is buffered in a matrix

$\mathbf{Q} = [\mathbf{q}_1 \quad \mathbf{q}_2 \quad \dots \quad \mathbf{q}_b \quad \dots \quad \mathbf{q}_B]$  of dimension  $\{PW-by-B\}$  where  $\mathbf{q}_b$  is a  $\{PW-by-1\}$  column of  $\mathbf{Q}$ .

The matrix of effective spreading codes is defined as:  $\bar{\mathbf{S}}_{eff}^b = \bar{\mathbf{H}}^b \times \bar{\mathbf{S}}_{eff}$ , where:  $\bar{\mathbf{H}}^b = \left[ \tilde{\mathbf{H}}^{1+W(b-1)T^0} \quad \tilde{\mathbf{H}}^{2+W(b-1)T^N} \quad \dots \quad \tilde{\mathbf{H}}^{w+W(b-1)T^{(w-1)N}} \quad \dots \quad \tilde{\mathbf{H}}^{W+W(b-1)T^{(W-1)N}} \right]$  and is shown in

Figure 4.23. Note taht  $\tilde{\mathbf{H}}^{w+W(b-1)}$  is the same as  $\tilde{\mathbf{H}}^m$  defined in Section 4.4.1, only  $m$  is changed with  $w+W(b-1)$  and it is shown in Figure 4.24, and  $\mathbf{H}_k^{w+W(b-1)}$  is the same as  $\mathbf{H}_k^m$  defined in 4.4.1, only  $m$  is changed with  $w+W(b-1)$  and it is shown in Figure 4.25.

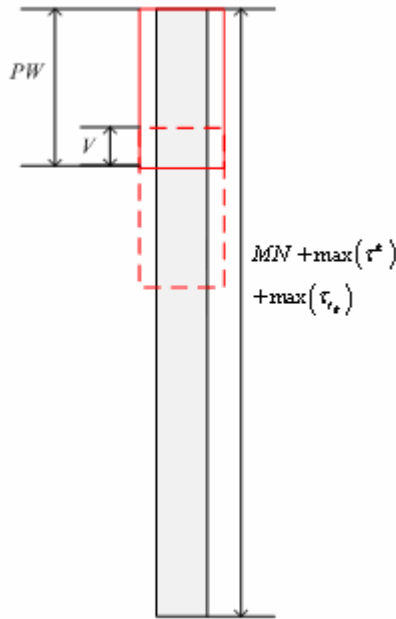


Figure 4.22: The vector  $\mathbf{r}$  and the sliding window of length  $PW$  chips and overlap  $V$  chips.

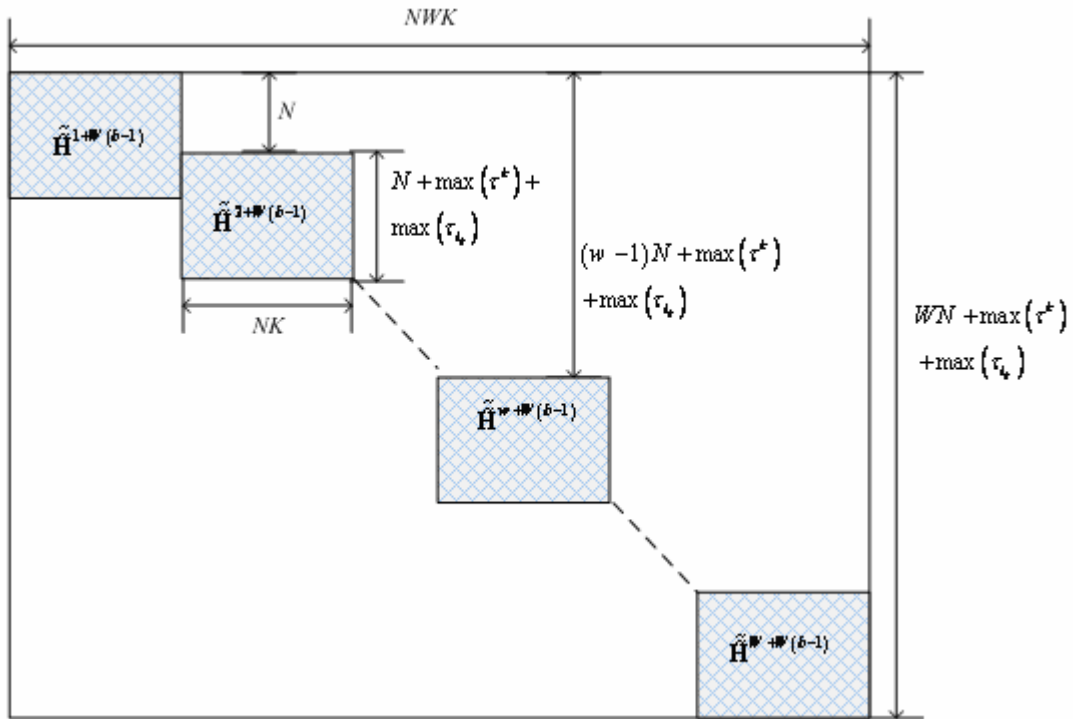


Figure 4.23: The matrix  $\tilde{\mathbf{H}}^b$ .

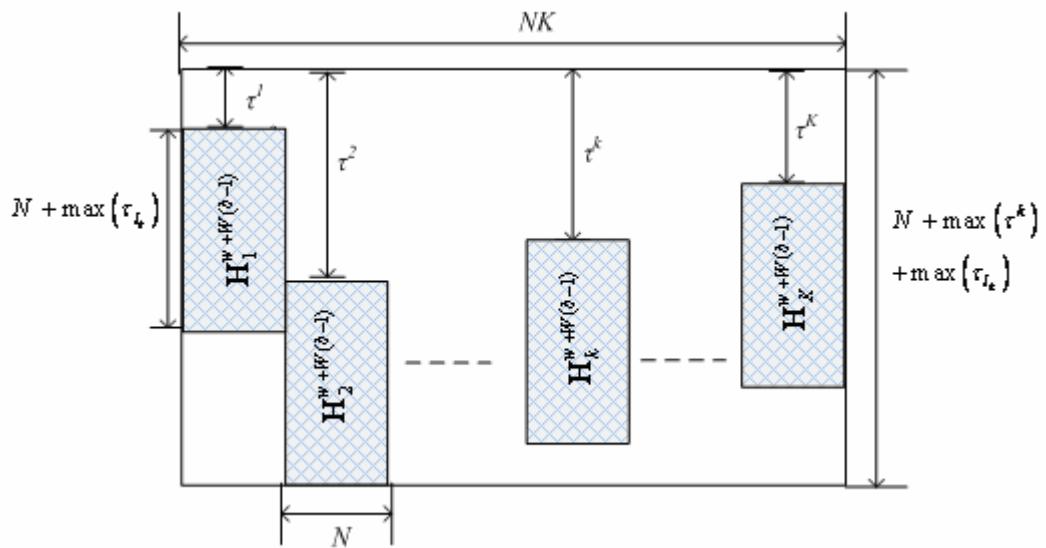
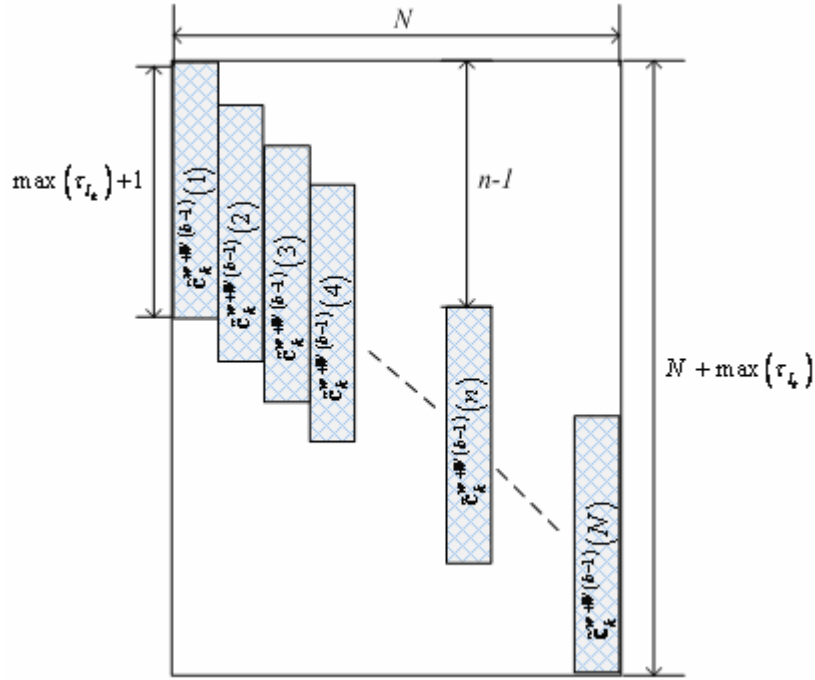


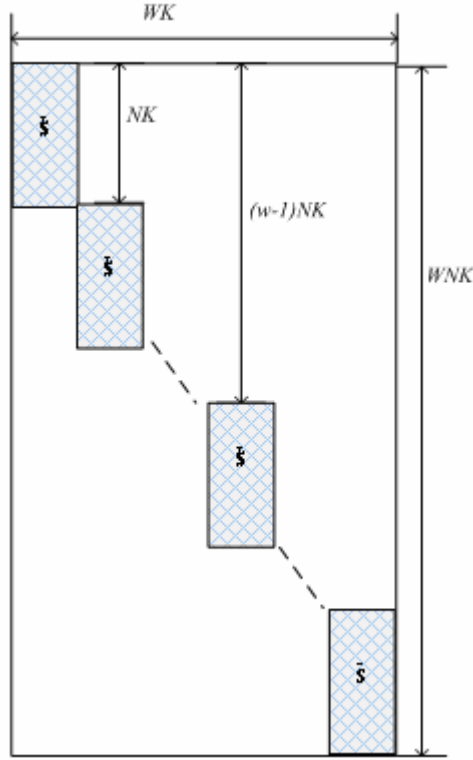
Figure 4.24: The matrix  $\tilde{\mathbf{H}}^{w+W(b-1)}$ .


 Figure 4.25: The matrix  $\mathbf{H}_k^{w+W(b-1)}$ .

Moreover,  $\tilde{\mathbf{c}}_k^{w+W(b-1)}(n)$  is the  $n^{\text{th}}$  column of the matrix  $\tilde{\mathbf{C}}_k^{w+W(b-1)}$  and  $\tilde{\mathbf{C}}_k^{w+W(b-1)}(\tau_k + 1, n)$  is given by:

$$\tilde{\mathbf{C}}_k^{w+W(b-1)}(\tau_k + 1, n) = \begin{cases} \mathbf{C}_k^{w+W(b-1)}(l_k, n) \times h_{l_k}, & \text{if } \tau_k = \tau_{l_k} \\ 0, & \text{elsewhere} \end{cases}$$

Note that  $\mathbf{C}_k^{w+W(b-1)}$  is the same as  $\mathbf{C}_k^m$  defined above, only  $m$  is changed with  $w+W(b-1)$ . On the other hand,  $\bar{\mathbf{S}}_{\text{eff}} = \begin{bmatrix} \tilde{\mathbf{S}}T^0 & \tilde{\mathbf{S}}T^N & \dots & \tilde{\mathbf{S}}T^{(w-1)N} & \dots & \tilde{\mathbf{S}}T^{(W-1)N} \end{bmatrix}$  where  $\tilde{\mathbf{S}}$  is defined in Section 4.4.2, and it shown in Figure 4.26.


 Figure 4.26: The matrix  $\bar{\mathbf{S}}_{eff}^b$ .

Hence, the matrix  $\bar{\mathbf{S}}_{eff}^b$  has the following form as shown in Figure 4.27. In this case,  $\tilde{\mathbf{S}}^b(w)$ , of length  $\{(N + \max_{1 \leq l_k \leq L_k}(\tau_{l_k}) + \max_{1 \leq k \leq K}(\tau^k)) - by - K\}$ , is given by  $\tilde{\mathbf{S}}^b(w) = \tilde{\mathbf{H}}^{w+W(b-1)} \tilde{\mathbf{S}}$ , where  $\tilde{\mathbf{S}}$  is defined in Section 4.4.2.  $\bar{\mathbf{S}}_{eff}^b$  can be decomposed as:  $\bar{\mathbf{S}}_{eff}^b = [\bar{\mathbf{S}}_{eff}^b(1) \quad \bar{\mathbf{S}}_{eff}^b(2) \quad \cdots \quad \bar{\mathbf{S}}_{eff}^b(w) \quad \cdots \quad \bar{\mathbf{S}}_{eff}^b(W)]$ , moreover  $\bar{\mathbf{S}}_{eff}^b(w)$  can be written as:  $\bar{\mathbf{S}}_{eff}^b(w) = [\bar{\mathbf{s}}_{eff}^b(w,1) \quad \bar{\mathbf{s}}_{eff}^b(w,2) \quad \cdots \quad \bar{\mathbf{s}}_{eff}^b(w,k) \quad \cdots \quad \bar{\mathbf{s}}_{eff}^b(w,K)]$ , where  $\bar{\mathbf{s}}_{eff}^b(w,k)$  is the  $(w)^{th}$  symbol  $(k)^{th}$  user effective spreading code vector and  $\tilde{\mathbf{s}}^b(w,k)$  is the non-zero part of  $k^{th}$  column of  $\tilde{\mathbf{S}}^b(w)$ . This is depicted in Figure 4.28.

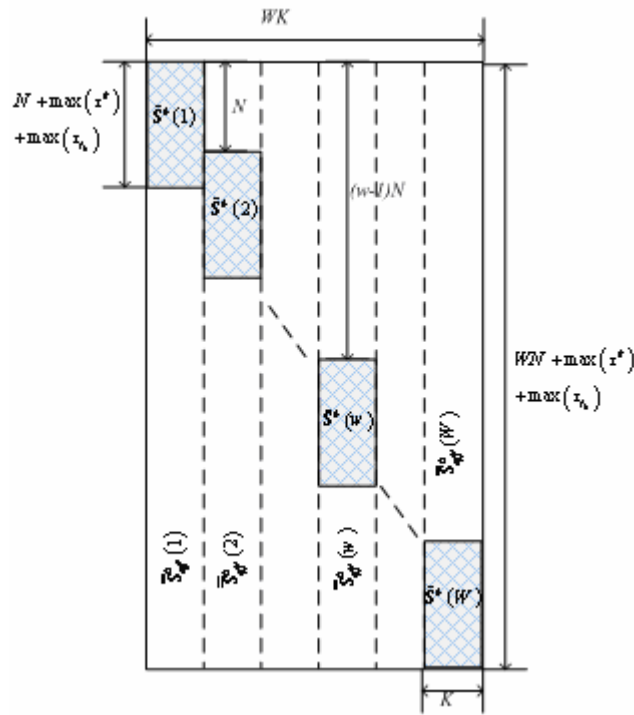


Figure 4.27: The matrix  $\bar{\mathbf{S}}_{eff}^b$ .

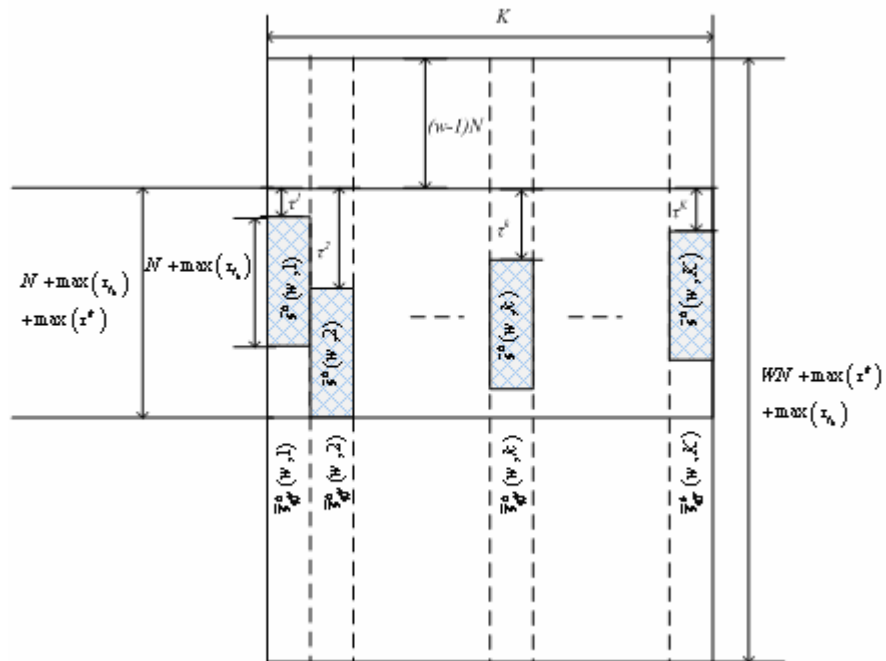


Figure 4.28: The matrix  $\bar{\mathbf{S}}_{eff}^b(w)$ .

The output of the bank of the maximum ratio combining (MRC) rake receivers for the whole data packet is given by:  $\mathbf{y}_{MRC} = \bar{\bar{\mathbf{S}}}^H \mathbf{r}$  while the output of the bank of the MRC rake receivers for the  $b^{th}$  block is given by:  $\mathbf{y}_{MRC}^b = \left(\bar{\bar{\mathbf{S}}}_{eff}^b\right)^H \mathbf{q}_b$ . This is shown in Figure 4.9.

The cross-correlation matrix between the codes of active users for the whole data packet is given by:  $\bar{\bar{\mathbf{R}}} = \bar{\bar{\mathbf{S}}}^H \bar{\bar{\mathbf{S}}}$  while the cross-correlation matrix between the codes of active users for the  $b^{th}$  block is given by:  $\bar{\bar{\mathbf{R}}}_{eff}^b = \left(\bar{\bar{\mathbf{S}}}_{eff}^b\right)^H \bar{\bar{\mathbf{S}}}_{eff}^b$ , where  $\bar{\bar{\mathbf{R}}}_{eff}^b(w) = \left(\bar{\bar{\mathbf{S}}}_{eff}^b(w)\right)^H \bar{\bar{\mathbf{S}}}_{eff}^b(w)$  is the cross-correlation matrix of the  $w^{th}$  symbol in the  $b^{th}$  block.

In order to show the relation between  $\bar{\bar{\mathbf{R}}}$  and  $\bar{\bar{\mathbf{R}}}_{eff}^b$ , let us divide the matrix  $\tilde{\mathbf{S}}(m)$  as:

$$\tilde{\mathbf{S}}(m) = \begin{bmatrix} \tilde{\mathbf{S}}^-(m) \\ \tilde{\mathbf{S}}^*(m) \\ \tilde{\mathbf{S}}^+(m) \end{bmatrix} \text{ where } \tilde{\mathbf{S}}^*(m) \text{ is of length } \{(N + \max_{1 \leq l_k \leq L_k}(\tau_{l_k}) + \max_{1 \leq k \leq K}(\tau^k)) - by - K\}, \tilde{\mathbf{S}}^+(m) \text{ and}$$

$\tilde{\mathbf{S}}^-(m)$  are both of length  $\{( \max_{1 \leq l_k \leq L_k}(\tau_{l_k}) + \max_{1 \leq k \leq K}(\tau^k) ) - by - K\}$ . Define  $\tilde{\mathbf{R}}^*(m)$  as:

$$\tilde{\mathbf{R}}^*(m) = \tilde{\mathbf{S}}^*(m)^H \tilde{\mathbf{S}}^*(m), \quad \tilde{\mathbf{R}}^-(m) \text{ as } \tilde{\mathbf{R}}^-(m) = \tilde{\mathbf{S}}^-(m)^H \tilde{\mathbf{S}}^-(m-1) \quad \text{and} \quad \tilde{\mathbf{R}}^+(m) \text{ as}$$

$$\tilde{\mathbf{R}}^+(m) = \tilde{\mathbf{S}}^+(m)^H \tilde{\mathbf{S}}^-(m+1), \text{ hence: } \tilde{\mathbf{R}}^+(m) = \tilde{\mathbf{R}}^-(m+1)^H.$$

A typical example of the matrix  $\bar{\bar{\mathbf{R}}} = \bar{\bar{\mathbf{S}}}^H \bar{\bar{\mathbf{S}}}$  for the asynchronous CDMA multi-path fading channel is depicted in Figure 4.29. It is clear that the MAI+ISI is not removed completely here as well because of some cross-correlation elements that reside outside the sliding processing window, which is known as the finite word effect.

Here  $\bar{\bar{\mathbf{R}}}_{eff}^b$  has the same structure as  $\bar{\bar{\mathbf{R}}}$ , only the subscript  $m$  is changed with  $w+W(b-1)$ . The dashed

matrix is defined as:  $\tilde{\mathbf{R}}^*(w+W(b-1)) = \tilde{\mathbf{S}}^*(w+W(b-1))^H \tilde{\mathbf{S}}^*(w+W(b-1))$ , the vertically dashed

matrix is defined as:  $\tilde{\mathbf{R}}^-(w+W(b-1)) = \tilde{\mathbf{S}}^-(w+W(b-1))^H \tilde{\mathbf{S}}^-(w+W(b-1)-1)$  and finally the

horizontally dashed matrix is defined as:

$$\tilde{\mathbf{R}}^+(w+W(b-1)) = \left(\tilde{\mathbf{S}}^+(w+W(b-1))\right)^H \left(\tilde{\mathbf{S}}^-(w+W(b-1)+1)\right), \quad \text{hence:}$$

$$\tilde{\mathbf{R}}^+(w+W(b-1)) = \tilde{\mathbf{R}}^-(w+W(b-1)+1)^H.$$

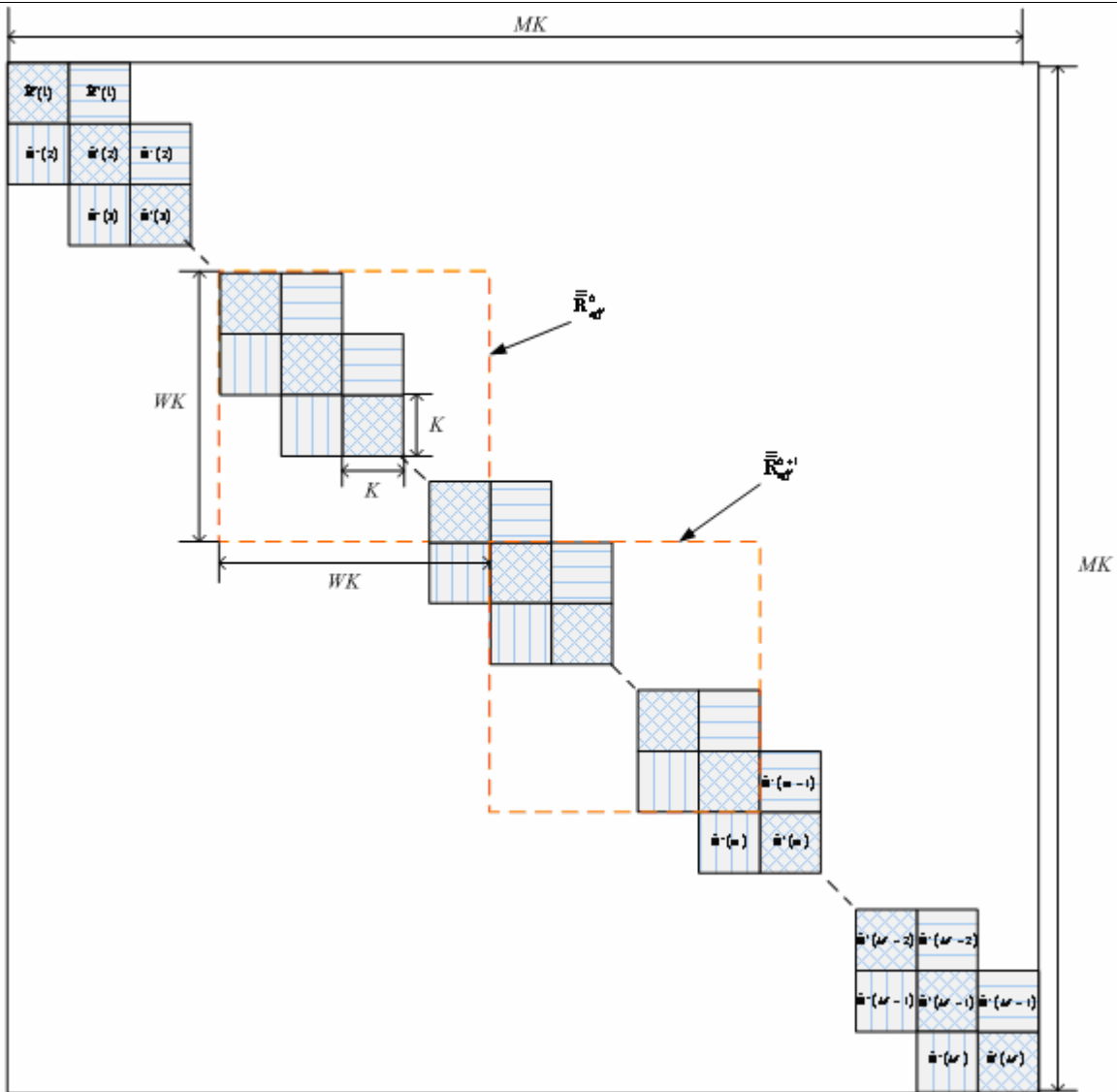


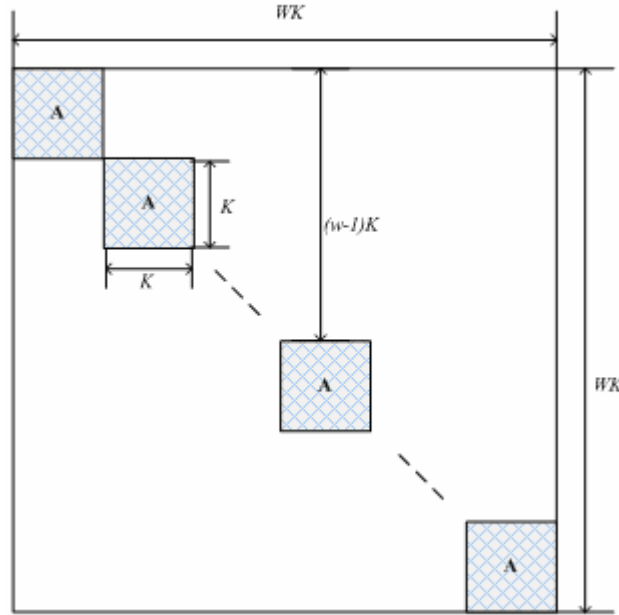
Figure 4.29: Structure of the matrix  $\bar{\mathbf{R}}$  and  $\bar{\mathbf{R}}_{eff}^b$  for the asynchronous CDMA multipath fading channel.

#### 4.4.7 Determining the Matrix of Effective Received Amplitudes $\bar{\mathbf{A}}_{eff}$

The matrix  $\bar{\mathbf{A}}_{eff}$  of length  $\{WK-by-WK\}$ , as shown in Figure 4.30, is constructed as follows:

$$\bar{\mathbf{A}}_{eff} = \begin{bmatrix} \tilde{\mathbf{A}}T^0 & \tilde{\mathbf{A}}T^K & \dots & \tilde{\mathbf{A}}T^{(w-1)K} & \dots & \tilde{\mathbf{A}}T^{(W-1)K} \end{bmatrix},$$

where the matrix  $\tilde{\mathbf{A}}$  is defined in Section 4.4.4.


 Figure 4.30: The matrix  $\bar{\mathbf{A}}$ .

#### 4.4.8 Determining the Vector of Effective BPSK Symbols $\bar{\mathbf{b}}^b$

The block  $b$  of BPSK symbols  $\bar{\mathbf{b}}^b$  is constructed by dividing the vector  $\bar{\mathbf{b}}$  of length  $\{MK-by-1\}$  into blocks as follows:  $\bar{\mathbf{b}} = [\bar{\mathbf{b}}^1 \ \bar{\mathbf{b}}^2 \ \dots \ \bar{\mathbf{b}}^b \ \dots \ \bar{\mathbf{b}}^B]^T$  where  $\bar{\mathbf{b}}^b = [\bar{\mathbf{b}}_1^b \ \bar{\mathbf{b}}_2^b \ \dots \ \bar{\mathbf{b}}_w^b \ \dots \ \bar{\mathbf{b}}_W^b]^T$ .

Furthermore,  $\bar{\mathbf{b}}_w^b$  can be decomposed as  $\bar{\mathbf{b}}_w^b = [\bar{\mathbf{b}}_w^b(1) \ \bar{\mathbf{b}}_w^b(2) \ \dots \ \bar{\mathbf{b}}_w^b(k) \ \dots \ \bar{\mathbf{b}}_w^b(K)]^T$ , where  $\bar{\mathbf{b}}_w^b(k)$  is the  $w^{\text{th}}$  BPSK symbol of the  $b^{\text{th}}$  block of the  $k^{\text{th}}$  user. This is depicted in Figure 4.12.

#### 4.5 Conclusion

In this chapter we introduced a new linear CDMA model for the uplink asynchronous CDMA multi-path fading channel. Using this model, new multiuser detection structures can be derived. Of particular interest is the one which is able to remove ISI and leave a synchronous-type of MAI. The latter can be simply removed if orthogonal codes are used.

## Chapter 5

### Iterative Methods for Matrix Inversion

#### 5.1 Chapter's Contents

5.1 Chapter's Contents .....	69
5.2 Introduction .....	70
5.3 General Concepts .....	70
5.4 Iterative Methods.....	72
5.4.1 Point Iterative Methods: .....	72
5.4.1.1 Point Richardson Iteration.....	72
5.4.1.2 Point Jacobi Iteration.....	72
5.4.1.3 Point Gauss-Seidel Iteration.....	73
5.4.1.4 Modified Point Gauss-Seidel Iteration.....	73
5.4.2 Point Iterative Relaxation Methods.....	74
5.4.2.1 Point Richardson Relaxation Iteration.....	75
5.4.2.2 Point Jacobi Relaxation Iteration.....	75
5.4.2.3 Point Successive Over-Relaxation Iteration.....	75
5.4.2.4 Modified Point Successive Over-Relaxation Iteration.....	76
5.4.3 Block Iterative Methods.....	76
5.4.3.1 Block Richardson Iteration.....	77
5.4.3.2 Block Jacobi Iteration.....	77
5.4.3.3 Block Gauss-Seidel Iteration.....	78
5.4.3.4 Modified Block Gauss-Seidel Iteration.....	78
5.4.4 Block Iterative Relaxation Methods.....	78
5.4.4.1 Block Richardson Relaxation Iteration.....	78
5.4.4.2 Block Jacobi Relaxation Iteration.....	79
5.4.4.3 Block Successive Over-Relaxation Iteration.....	79
5.4.4.4 Modified Block Successive Over-Relaxation Iteration.....	80
5.5 Convergence Issues .....	81

5.5.1 General Convergence Results .....	82
5.5.2 Convergence Results for Hermitian Positive Definite Matrices .....	82
5.5.3 Convergence Results for Strictly Diagonal Dominant Matrices .....	84
5.5.4 Convergence Results for Iterative Relaxation Methods .....	85
5.5.5 Rate of Convergence .....	90
5.6 Simulation Results.....	92
5.7 Conclusion.....	96

## 5.2 Introduction

As many scientific and engineering problems lead to the requirement to solve systems of linear equations, researchers and scientists are showing increasing interest in developing low-complexity, efficient and reliable methods for solving such systems. The latter enter at some stage in almost every engineering problem, and moreover, it often represents the dominating part of the solution to the problem. Even for nonlinear problems, their solution is usually obtained by solving a sequence of linear equations, e.g., by Newton's methods.

Two different categories of methods for solving systems of linear equations exist: *direct* methods and *iterative* methods [69]. In direct methods, such as Gaussian elimination, the system is transformed by a sequence of elementary transformations to a system of simpler form, e.g., diagonal or triangular form, which can be solved in an elementary way, e.g., forward or backward substitution. On the other hand, iterative methods refer to a wide range of techniques that compute a sequence of approximate solutions, which in the limit converges to the exact solution of the linear system.

Iterative methods date back to Gauss (1823) but have been subject to intensive development since 1950 when the computers replaced desk calculators. A thorough historical review can be found in [70]. Iterative methods are often used to solve large linear systems where direct methods exhibit high computational complexity [69].

## 5.3 General Concepts

Consider the following linear system:

$$\mathbf{Rb} = \mathbf{y} \quad (5-1)$$

where  $\mathbf{R}$  is the *coefficient matrix*,  $\mathbf{y}$  is the *right-hand side vector* and  $\mathbf{b}$  is the *vector of unknowns*. Most of the classical iterative methods such as Jacobi, Gauss–Seidel, and successive over-relaxation (SOR) are based on *splitting*  $\mathbf{R}$  into [71]:

$$\mathbf{R} = \mathbf{M} - \mathbf{N} \quad (5-2)$$

where  $\mathbf{M}$  is a nonsingular matrix known as the *splitting matrix* and it is constructed so that it is easily invertible. Then  $\mathbf{Rb} = \mathbf{y}$  is converted to the fixed-point iteration defined by the following recurrence:

$$\mathbf{b}_p = \mathbf{M}^{-1}\mathbf{N}\mathbf{b}_{p-1} + \mathbf{M}^{-1}\mathbf{y} \quad (5-3)$$

The matrix  $\mathbf{B} = \mathbf{M}^{-1}\mathbf{N}$  is known as the *iteration matrix* and it controls the convergence behavior of the iteration defined by equation (5-3). The iteration above can also be formulated as:

$$\mathbf{b}_p = \mathbf{b}_{p-1} + \mathbf{M}^{-1}\mathbf{e}_{p-1} = \mathbf{b}_{p-1} + \tilde{\mathbf{e}}_{p-1} \quad (5-4)$$

where  $\tilde{\mathbf{e}}_{p-1} = \mathbf{M}^{-1}\mathbf{e}_{p-1} = \mathbf{M}^{-1}(\mathbf{y} - \mathbf{R}\mathbf{b}_{p-1})$  is the correction term applied to the current approximate solution  $\mathbf{b}_p$  and  $\mathbf{e}_p$  is the residual vector. This form (5-4) is commonly used in correction methods [71] and [72].

Iterative methods of the form in (5-3) belong to a special class of iterative methods which are known as *stationary iterative methods* because the transition matrix is independent of the iteration index  $p$ . To study different stationary iterative methods, we begin by the following decomposition of the coefficient matrix  $\mathbf{R}$ , that is [71]:

$$\mathbf{R} = \mathbf{D} - \mathbf{L} - \mathbf{U} \quad (5-5)$$

where  $\mathbf{D}$  is the diagonal/block-diagonal of  $\mathbf{R}$ , and  $\mathbf{L}$  and  $\mathbf{U}$  are the remaining lower-left and upper-right parts of  $\mathbf{R}$ , respectively. We always assume that diagonal entries of  $\mathbf{R}$  are nonzero.

All iterative methods determine the  $i^{\text{th}}$  element of the next approximation of the solution vector  $\mathbf{b}_p$  so as to annihilate the  $i^{\text{th}}$  element of the residual vector  $(\mathbf{y} - \mathbf{R}\mathbf{b}_{p-1})$ . Basically two different approaches exist and are used to determine or update the  $i^{\text{th}}$  element of the next approximation of the solution vector ([71] and [73]). In the first approach, the  $i^{\text{th}}$  element is determined in a complete asynchronous way, that is, the determination of one element is independent of the others, while in the second approach, the  $i^{\text{th}}$  element is determined in a complete synchronous way, that is, the determination of one element depends on the calculation of the previous one in a given order. Both approaches have advantages and disadvantages. The first approach is inherently parallel which enables its implementation on a multiprocessor system, however, since it doesn't use the most recent updates

its convergence is slow. The second approach is inherently sequential, and thus cannot be implemented on a multiprocessor system; however, since it uses the most recent updates its convergence is usually faster.

## 5.4 Iterative Methods

### 5.4.1 Point Iterative Methods:

#### 5.4.1.1 Point Richardson Iteration

The point Richardson iteration is given by [74]:

$$b_{p,k} = (1 - r_{k,k})b_{p-1,k} + \sum_{\substack{j=1 \\ j \neq k}}^K r_{k,j}b_{p-1,j} + y_k \quad k = 1, \dots, K \quad (5-6)$$

This is element-wise implementation of the Richardson iteration, if all elements are grouped into vectors and matrices, then the matrix form of the Richardson iteration is given by:

$$\mathbf{b}_p = (\mathbf{I} - \mathbf{R})\mathbf{b}_{p-1} + \mathbf{y} \quad (5-7)$$

Another formulation of the equation above which is most suitable for correction methods is given by:

$$\mathbf{b}_p = \mathbf{b}_{p-1} + (\mathbf{y} - \mathbf{R}\mathbf{b}_{p-1}) \quad (5-8)$$

For all subsequent iterative methods, it can be shown easily that they are equivalent to solving a preconditioned system  $\mathbf{M}^{-1}\mathbf{R}\mathbf{b} = \mathbf{M}^{-1}\mathbf{y}$  using the Richardson iterative method. Hence, the splitting matrix  $\mathbf{M}$  can be regarded as a left preconditioning matrix applied to the system  $\mathbf{R}\mathbf{b} = \mathbf{y}$ . In general the preconditioning matrix is chosen to satisfy the following two properties [75]:

- $\mathbf{M}$  is close to  $\mathbf{R}$  in some sense, for example  $\|\mathbf{M} - \mathbf{R}\|_2$ .
- $\mathbf{M}^{-1}$  is easy to compute.

As such, and since preconditioned systems usually have faster convergence speed, it is expected that the convergence speed of iterative systems depends on the closeness of the splitting matrix to the matrix  $\mathbf{R}$ .

#### 5.4.1.2 Point Jacobi Iteration

The point Jacobi iteration is given by [71]:

$$b_{p,k} = \frac{1}{r_{k,k}} \left( y_k - \sum_{\substack{j=1 \\ j \neq k}}^K r_{k,j} b_{p-1,j} \right) \quad k = 1, \dots, K \quad (5-9)$$

This is in fact an element-wise implementation of the Jacobi iteration. The matrix form of the Jacobi iteration is given by:

$$\begin{aligned} \mathbf{b}_p &= \mathbf{D}^{-1}(\mathbf{L} + \mathbf{U})\mathbf{b}_{p-1} + \mathbf{D}^{-1}\mathbf{y} \\ &= (\mathbf{I} - \mathbf{D}^{-1}\mathbf{R})\mathbf{b}_{p-1} + \mathbf{D}^{-1}\mathbf{y} \end{aligned} \quad (5-10)$$

The equation above can be reformulated to be suitable for correction methods as:

$$\mathbf{b}_p = \mathbf{b}_{p-1} + \mathbf{D}^{-1}(\mathbf{y} - \mathbf{R}\mathbf{b}_{p-1}) \quad (5-11)$$

#### 5.4.1.3 Point Gauss-Seidel Iteration

The point Gauss-Seidel iteration is given by [71]:

$$b_{p,k} = \frac{1}{r_{k,k}} \left( y_k - \sum_{j=1}^{k-1} r_{k,j} b_{p,j} - \sum_{j=k+1}^K r_{k,j} b_{p-1,j} \right) \quad k = 1, \dots, K \quad (5-12)$$

The matrix form of the Gauss-Seidel iteration is given by:

$$\mathbf{b}_p = (\mathbf{D} - \mathbf{L})^{-1} \mathbf{U}\mathbf{b}_{p-1} + (\mathbf{D} - \mathbf{L})^{-1} \mathbf{y} \quad (5-13)$$

An alternative formulation of the equation above, which is appropriate for correction methods, is given by:

$$\mathbf{b}_p = \mathbf{b}_{p-1} + (\mathbf{D} - \mathbf{L})^{-1}(\mathbf{y} - \mathbf{R}\mathbf{b}_{p-1}) \quad (5-14)$$

#### 5.4.1.4 Modified Point Gauss-Seidel Iteration

In this section, we introduce a new iterative method which can be considered as the complement of the Richardson iterative method. The method is in fact a modified Gauss-Seidel method where the splitting matrix  $\mathbf{M} = \mathbf{D} - \mathbf{L}$  for Gauss-Seidel is replaced by:  $\mathbf{M} = \mathbf{I} - \mathbf{L}$  where  $\mathbf{I}$  is the identity matrix, the modified point Gauss-Seidel iteration is given by:

$$b_{p,k} = y_k + (1 - r_{k,k})b_{p-1,k} - \sum_{j=1}^{k-1} r_{k,j} b_{p,j} - \sum_{j=k+1}^K r_{k,j} b_{p-1,j} \quad k = 1, \dots, K \quad (5-15)$$

The matrix form of the proposed modified Gauss-Seidel iteration is given by:

$$\mathbf{b}_p = (\mathbf{I} - \mathbf{L})^{-1}(\mathbf{I} - \mathbf{D} + \mathbf{U})\mathbf{b}_{p-1} + (\mathbf{I} - \mathbf{L})^{-1} \mathbf{y} \quad (5-16)$$

A different arrangement of the equation above, that is suitable for correction methods, is given by:

$$\mathbf{b}_p = \mathbf{b}_{p-1} + (\mathbf{I} - \mathbf{L})^{-1}(\mathbf{y} - \mathbf{Rb}_{p-1}) \quad (5-17)$$

As for the Richardson method, the element-wise implementation of the proposed modified Gauss-Seidel iteration doesn't require any division, which reduces the computational complexity.

#### 5.4.2 Point Iterative Relaxation Methods

The correction term  $\mathbf{b}_p - \mathbf{b}_{p-1} = \mathbf{M}^{-1}(\mathbf{y} - \mathbf{Rb}_{p-1})$  is usually either too large and thus results in divergence or too small and thus the iteration exhibits slow convergence behavior. To overcome this problem, the correction term is modified by allowing the splitting matrix  $\mathbf{M}$  to incorporate a weighting factor which is known as the relaxation parameter or relaxation factor and it is used to control the convergence rate.

Relaxation methods are based on splitting the matrix  $\mathbf{R}$  into [74]:

$$\omega\mathbf{R} = \mathbf{M}(\omega) - \mathbf{N}(\omega) \quad (5-18)$$

$\mathbf{Rb} = \mathbf{y}$  is then converted to the fixed-point iteration defined by the following recurrence:

$$\mathbf{b}_p = \mathbf{M}(\omega)^{-1}\mathbf{N}(\omega)\mathbf{b}_{p-1} + \mathbf{M}(\omega)^{-1}\mathbf{y} \quad (5-19)$$

where the iteration matrix is given by  $\mathbf{B} = \mathbf{M}(\omega)^{-1}\mathbf{N}(\omega)$ , the iteration above can also be formulated as:

$$\mathbf{b}_p = \mathbf{b}_{p-1} + \mathbf{M}(\omega)^{-1}\mathbf{e}_{p-1} = \mathbf{b}_{p-1} + \tilde{\mathbf{e}}_{p-1} \quad (5-20)$$

where  $\tilde{\mathbf{e}}_{p-1} = \mathbf{M}(\omega)^{-1}\mathbf{e}_{p-1} = \mathbf{M}(\omega)^{-1}(\mathbf{y} - \mathbf{Rb}_{p-1})$  is the correction term applied to the current approximate solution  $\mathbf{b}_{p-1}$  and  $\mathbf{e}_{p-1}$  is the residual vector. Hence, it is clear that the correction term is controlled by the relaxation parameter  $\omega$ . The general form for the point relaxation iterative methods is given by:

$$\mathbf{b}_p = \mathbf{b}_{p-1} + \mathbf{M}(\omega)^{-1}(\mathbf{y} - \mathbf{Rb}_{p-1}) \quad (5-21)$$

where  $\omega$  is a real number. Usually, if  $\omega < 1$ , the iteration above is known as point under-relaxation iterative method, however if  $\omega > 1$ , the iteration above is known as point over-relaxation iterative method. The under-relaxation principle is often used to ensure the convergence of some non-stable iterative methods such as the point Jacobi iterative method. On the other hand the over-relaxation principle is often used to accelerate the convergence of some stable iterative methods such as the point Gauss-Seidel method.

As for the point Jacobi and point Gauss-Seidel methods, relaxed versions can be obtained and are discussed below.

#### 5.4.2.1 Point Richardson Relaxation Iteration

The point Richardson relaxation iteration is given by [71]:

$$b_{p,k} = (1 - \omega r_{k,k}) b_{p-1,k} + \omega \left( \sum_{\substack{j=1 \\ j \neq k}}^K r_{k,j} b_{p-1,j} + y_k \right) \quad k = 1, \dots, K \quad (5-22)$$

This is an element-wise implementation of the Richardson relaxation iteration, the matrix form of the Richardson relaxation iteration is given by:

$$\mathbf{b}_p = (\mathbf{I} - \omega \mathbf{R}) \mathbf{b}_{p-1} + \omega \mathbf{y} \quad (5-23)$$

For correction methods, the equation above is rearranged and given by:

$$\mathbf{b}_p = \mathbf{b}_{p-1} + \omega (\mathbf{y} - \mathbf{R} \mathbf{b}_{p-1}) \quad (5-24)$$

#### 5.4.2.2 Point Jacobi Relaxation Iteration

The point Jacobi method is known to suffer from serious convergence issues, to overcome this problem a relaxation factor is inserted and adjusted so that the convergence of the original point Jacobi method is guaranteed. The point Jacobi relaxation iteration [76] is given by:

$$b_{p,k} = \frac{\omega}{r_{k,k}} \left( y_k - \sum_{\substack{j=1 \\ j \neq k}}^K r_{k,j} b_{p-1,j} \right) + (1 - \omega) b_{p-1,k} \quad k = 1, \dots, K \quad (5-25)$$

The matrix form of the point Jacobi relaxation iteration is given by:

$$\begin{aligned} \mathbf{b}_p &= \omega \mathbf{D}^{-1} (\mathbf{L} + \mathbf{U}) \mathbf{b}_{p-1} + (1 - \omega) \mathbf{b}_{p-1} + \omega \mathbf{D}^{-1} \mathbf{y} \\ &= (\mathbf{I} - \omega \mathbf{D}^{-1} \mathbf{R}) \mathbf{b}_{p-1} + \omega \mathbf{D}^{-1} \mathbf{y} \end{aligned} \quad (5-26)$$

Another possible arrangement of the equation above, which is suitable for correction methods, is given by:

$$\mathbf{b}_p = \mathbf{b}_{p-1} + \omega \mathbf{D}^{-1} (\mathbf{y} - \mathbf{R} \mathbf{b}_{p-1}) \quad (5-27)$$

#### 5.4.2.3 Point Successive Over-Relaxation Iteration

The point successive over-relaxation iteration is given by [71]:

$$b_{p,k} = \frac{\omega}{r_{k,k}} \left( y_k - \sum_{j=1}^{k-1} r_{k,j} b_{p,j} - \sum_{j=k+1}^K r_{k,j} b_{p-1,j} \right) + (1-\omega) b_{p-1,k} \quad k = 1, \dots, K \quad (5-28)$$

The matrix form of the successive over-relaxation iteration is given by:

$$\mathbf{b}_p = (\mathbf{D} - \omega\mathbf{L})^{-1} (\omega\mathbf{U} + (1-\omega)\mathbf{D})\mathbf{b}_{p-1} + \omega(\mathbf{D} - \omega\mathbf{L})^{-1} \mathbf{y} \quad (5-29)$$

For correction methods, the equation above is reformulated as:

$$\mathbf{b}_p = \mathbf{b}_{p-1} + \left( \frac{1}{\omega} \mathbf{D} - \mathbf{L} \right)^{-1} (\mathbf{y} - \mathbf{R}\mathbf{b}_{p-1}) \quad (5-30)$$

#### 5.4.2.4 Modified Point Successive Over-Relaxation Iteration

In this section, we present a modified successive over-relaxation method where the splitting matrix

$\mathbf{M} = \frac{1}{\omega} \mathbf{D} - \mathbf{L}$  for successive over-relaxation method is replaced by:  $\mathbf{M} = \frac{1}{\omega} \mathbf{I} - \mathbf{L}$  where  $\mathbf{I}$  is the identity matrix. The point modified successive over-relaxation iteration is given by:

$$b_{p,k} = \omega y_k + (1 - \omega r_{k,k}) b_{p-1,k} - \omega \left( \sum_{j=1}^{k-1} r_{k,j} b_{p,j} - \sum_{j=k+1}^K r_{k,j} b_{p-1,j} \right) \quad k = 1, \dots, K \quad (5-31)$$

The matrix form of the proposed modified successive over-relaxation iteration is given by:

$$\mathbf{b}_p = (\mathbf{I} - \omega\mathbf{L})^{-1} ((\mathbf{I} - \omega\mathbf{D}) + \omega\mathbf{U})\mathbf{b}_{p-1} + \omega(\mathbf{I} - \omega\mathbf{L})^{-1} \mathbf{y} \quad (5-32)$$

Another possible arrangement of the equation above, which is most suitable for correction methods, is given by:

$$\mathbf{b}_p = \mathbf{b}_{p-1} + \left( \frac{1}{\omega} \mathbf{I} - \mathbf{L} \right)^{-1} (\mathbf{y} - \mathbf{R}\mathbf{b}_{p-1}) \quad (5-33)$$

As for the Richardson method, the element-wise implementation of the proposed modified successive over-relaxation iteration doesn't require any division, which reduces the computational complexity.

#### 5.4.3 Block Iterative Methods

Block or line iterative methods are generalization of point iterative methods as they update a block of elements at a time instead of individual elements. This leads to a slightly different decomposition imposed on the coefficient matrix  $\mathbf{R}$ , that is, [77]:

$$\mathbf{R} = \mathbf{D} - \mathbf{L} - \mathbf{U} \quad (5-34)$$

where  $\mathbf{D}$  is a block diagonal matrix  $\mathbf{D} = \text{diag}(\mathbf{R}_{1,1}, \mathbf{R}_{2,2}, \dots, \mathbf{R}_{G,G})$ , and  $\mathbf{L}$  and  $\mathbf{U}$  are the remaining lower-left and upper-right block triangular parts of  $\mathbf{R}$ , respectively. We assume that the submatrices  $\mathbf{R}_{1,1}, \mathbf{R}_{2,2}, \dots, \mathbf{R}_{G,G}$ , for  $g = 1, \dots, G$ , are nonsingular.

#### 5.4.3.1 Block Richardson Iteration

The block Richardson iteration is given by:

$$\mathbf{b}_{p,g} = (\mathbf{I} - \mathbf{R}_{g,g})\mathbf{b}_{p-1,g} + \sum_{\substack{j=1 \\ j \neq g}}^G \mathbf{R}_{g,j}\mathbf{b}_{p-1,j} + \mathbf{y}_g \quad g = 1, \dots, G \quad (5-35)$$

This is the block-wise version of the block Richardson iteration, if all blocks are grouped together, then the matrix form of the block Richardson iteration is given by:

$$\mathbf{b}_p = (\mathbf{I} - \mathbf{R})\mathbf{b}_{p-1} + \mathbf{y} \quad (5-36)$$

For correction methods, the equation above is rearranged as:

$$\mathbf{b}_p = \mathbf{b}_{p-1} + (\mathbf{y} - \mathbf{R}\mathbf{b}_{p-1}) \quad (5-37)$$

Note that both matrix forms of the block Richardson iteration and the point Richardson iteration are equivalent, however, the advantage of the block Richardson iteration is that if it is implemented in a parallel multiprocessor structure, blocks of variables can be assigned to different processors.

#### 5.4.3.2 Block Jacobi Iteration

The block Jacobi iteration is given by [71]:

$$\mathbf{b}_{p,g} = \mathbf{R}_{g,g}^{-1} \left( \mathbf{y}_g - \sum_{\substack{j=1 \\ j \neq g}}^G \mathbf{R}_{g,j}\mathbf{b}_{p-1,j} \right) \quad g = 1, \dots, G \quad (5-38)$$

This is the block-wise version of the block Jacobi iteration, if all blocks are grouped together, then the matrix form of the block Jacobi iteration is given by:

$$\mathbf{b}_p = \mathbf{D}^{-1}(\mathbf{L} + \mathbf{U})\mathbf{b}_{p-1} + \mathbf{D}^{-1}\mathbf{y} \quad (5-39)$$

Another possible arrangement of the equation above, which is most suitable for correction methods, is given by:

$$\mathbf{b}_p = \mathbf{b}_{p-1} + \mathbf{D}^{-1}(\mathbf{y} - \mathbf{R}\mathbf{b}_{p-1}) \quad (5-40)$$

### 5.4.3.3 Block Gauss-Seidel Iteration

The block Gauss-Seidel iteration is given by [71]:

$$\mathbf{b}_{p,g} = \mathbf{R}_{g,g}^{-1} \left( \mathbf{y}_g - \sum_{j=1}^{g-1} \mathbf{R}_{g,j} \mathbf{b}_{p,j} - \sum_{j=g+1}^G \mathbf{R}_{g,j} \mathbf{b}_{p-1,j} \right) \quad g = 1, \dots, G \quad (5-41)$$

The matrix form of the block Gauss-Seidel iteration is given by:

$$\mathbf{b}_p = (\mathbf{D} - \mathbf{L})^{-1} \mathbf{U} \mathbf{b}_{p-1} + (\mathbf{D} - \mathbf{L})^{-1} \mathbf{y} \quad (5-42)$$

For correction methods, the equation above is reformulated and given by:

$$\mathbf{b}_p = \mathbf{b}_{p-1} + (\mathbf{D} - \mathbf{L})^{-1} (\mathbf{y} - \mathbf{R} \mathbf{b}_{p-1}) \quad (5-43)$$

### 5.4.3.4 Modified Block Gauss-Seidel Iteration

In the following, we propose a modified block Gauss-Seidel method where the splitting matrix  $\mathbf{M} = \mathbf{D} - \mathbf{L}$  for Gauss-Seidel is replaced by:  $\mathbf{M} = \mathbf{I} - \mathbf{L}$  where  $\mathbf{I}$  is the identity matrix. The modified block Gauss-Seidel iteration is given by:

$$\mathbf{b}_{p,g} = \mathbf{y}_g + (\mathbf{I} - \mathbf{R}_{g,g}) \mathbf{b}_{p-1,g} - \sum_{j=1}^{g-1} \mathbf{R}_{g,j} \mathbf{b}_{p,j} - \sum_{j=g+1}^G \mathbf{R}_{g,j} \mathbf{b}_{p-1,j} \quad g = 1, \dots, G \quad (5-44)$$

The matrix form of the proposed modified block Gauss-Seidel iteration is given by:

$$\mathbf{b}_p = (\mathbf{I} - \mathbf{L})^{-1} (\mathbf{I} - \mathbf{D} + \mathbf{U}) \mathbf{b}_{p-1} + (\mathbf{I} - \mathbf{L})^{-1} \mathbf{y} \quad (5-45)$$

Another arrangement of the equation above, that is appropriate for correction methods, is given by:

$$\mathbf{b}_p = \mathbf{b}_{p-1} + (\mathbf{I} - \mathbf{L})^{-1} (\mathbf{y} - \mathbf{R} \mathbf{b}_{p-1}) \quad (5-46)$$

As for the Richardson method, the group-wise implementation of the proposed modified block Gauss-Seidel iteration doesn't require any matrix inversion, which reduces the computational complexity.

## 5.4.4 Block Iterative Relaxation Methods

As for the point iterative relaxation methods, relaxed versions of the previous block iterative methods are obtained and discussed below.

### 5.4.4.1 Block Richardson Relaxation Iteration

The block Richardson relaxation iteration is given by:

$$\mathbf{b}_{p,g} = (\mathbf{I} - \omega \mathbf{R}_{g,g}) \mathbf{b}_{p-1,g} + \omega \left( \sum_{\substack{j=1 \\ j \neq g}}^G \mathbf{R}_{g,j} \mathbf{b}_{p-1,j} + \mathbf{y}_g \right) \quad g = 1, \dots, G \quad (5-47)$$

This is in fact a block-wise implementation of the Richardson relaxation iteration, if all blocks are grouped into vectors and matrices, then the matrix form of the Richardson relaxation iteration is given by:

$$\mathbf{b}_p = (\mathbf{I} - \omega \mathbf{R}) \mathbf{b}_{p-1} + \omega \mathbf{y} \quad (5-48)$$

This equation can be rearranged to suit correction methods as:

$$\mathbf{b}_p = \mathbf{b}_{p-1} + \omega (\mathbf{y} - \mathbf{R} \mathbf{b}_{p-1}) \quad (5-49)$$

#### 5.4.4.2 Block Jacobi Relaxation Iteration

The block Jacobi method is also known to suffer from a severe convergence problem. To overcome this drawback a relaxation factor is inserted and adjusted so that the convergence of the original block Jacobi method is guaranteed. The block Jacobi relaxation is given by [71]:

$$\mathbf{b}_{p,g} = \omega \mathbf{R}_{g,g}^{-1} \left( \mathbf{y}_g - \sum_{j=1}^G \mathbf{R}_{i,j} \mathbf{b}_{p-1,j} \right) + (1 - \omega) \mathbf{b}_{p-1,g} \quad g = 1, \dots, G \quad (5-50)$$

The matrix form of the block Jacobi relaxation iteration is given by:

$$\begin{aligned} \mathbf{b}_p &= \omega \mathbf{D}^{-1} (\mathbf{L} + \mathbf{U}) \mathbf{b}_{p-1} + (1 - \omega) \mathbf{b}_{p-1} + \omega \mathbf{D}^{-1} \mathbf{y} \\ &= (\mathbf{I} - \omega \mathbf{D}^{-1} \mathbf{R}) \mathbf{b}_{p-1} + \omega \mathbf{D}^{-1} \mathbf{y} \end{aligned} \quad (5-51)$$

For correction methods, the equation above is reformulated as:

$$\mathbf{b}_p = \mathbf{b}_{p-1} + \omega \mathbf{D}^{-1} (\mathbf{y} - \mathbf{R} \mathbf{b}_{p-1}) \quad (5-52)$$

#### 5.4.4.3 Block Successive Over-Relaxation Iteration

The block successive over-relaxation iteration is given by [71]:

$$\mathbf{b}_{p,g} = \omega \mathbf{R}_{g,g}^{-1} \left( \mathbf{y}_g - \sum_{j=1}^{g-1} \mathbf{R}_{g,j} \mathbf{b}_{p,j} - \sum_{j=g+1}^G \mathbf{R}_{g,j} \mathbf{b}_{p-1,j} \right) + (1 - \omega) \mathbf{b}_{p-1,g} \quad g = 1, \dots, G \quad (5-53)$$

The matrix form of the block successive over-relaxation iteration is given by:

$$\mathbf{b}_p = (\mathbf{D} - \omega \mathbf{L})^{-1} (\omega \mathbf{U} + (1 - \omega) \mathbf{D}) \mathbf{b}_{p-1} + \omega (\mathbf{D} - \omega \mathbf{L})^{-1} \mathbf{y} \quad (5-54)$$

Another possible arrangement of the equation above, which is most suitable for correction methods, is given by:

$$\mathbf{b}_p = \mathbf{b}_{p-1} + \left( \frac{1}{\omega} \mathbf{D} - \mathbf{L} \right)^{-1} (\mathbf{y} - \mathbf{R}\mathbf{b}_{p-1}) \quad (5-55)$$

#### 5.4.4.4 Modified Block Successive Over-Relaxation Iteration

In this section, we introduce a modified block relaxation iterative method. The method is in fact a modified block successive over-relaxation method where the splitting matrix  $\mathbf{M} = \frac{1}{\omega} \mathbf{D} - \mathbf{L}$  for successive over-relaxation method is replaced by:  $\mathbf{M} = \frac{1}{\omega} \mathbf{I} - \mathbf{L}$  where  $\mathbf{I}$  is the identity matrix. The block modified block successive over-relaxation iteration is given by:

$$\mathbf{b}_{p,g} = \omega \mathbf{y}_g + (\mathbf{I} - \omega \mathbf{R}_{g,g}) \mathbf{b}_{p-1,g} - \omega \left( \sum_{j=1}^{g-1} \mathbf{R}_{g,j} \mathbf{b}_{p,j} - \sum_{j=g+1}^G \mathbf{R}_{g,j} \mathbf{b}_{p-1,j} \right) \quad g = 1, \dots, G \quad (5-56)$$

The matrix form of the proposed modified block successive over-relaxation iteration is given by:

$$\mathbf{b}_p = (\mathbf{I} - \omega \mathbf{L})^{-1} ((\mathbf{I} - \omega \mathbf{D}) + \omega \mathbf{U}) \mathbf{b}_{p-1} + \omega (\mathbf{I} - \omega \mathbf{L})^{-1} \mathbf{y} \quad (5-57)$$

For correction methods, the equation above is reformulated as:

$$\mathbf{b}_p = \mathbf{b}_{p-1} + \left( \frac{1}{\omega} \mathbf{I} - \mathbf{L} \right)^{-1} (\mathbf{y} - \mathbf{R}\mathbf{b}_{p-1}) \quad (5-58)$$

As for the Richardson method, the block-wise implementation of the proposed modified block successive over-relaxation iteration doesn't require any matrix inversion, this reduces the computational complexity.

In Table 5.1, we present the different splitting and iteration matrices for the point iterative methods discussed before. For the line or block iterative methods, the table above should be the same, however,  $\mathbf{D}$  is a block diagonal matrix  $\mathbf{D} = \text{diag}(\mathbf{R}_{1,1}, \mathbf{R}_{2,2}, \dots, \mathbf{R}_{G,G})$ , and  $\mathbf{L}$  and  $\mathbf{U}$  are the remaining lower-left and upper-right block triangular parts of  $\mathbf{R}$ , respectively.

Table 5.1: Splitting and iteration matrices of different iterative methods

Iterative method	$\mathbf{M}$	$\mathbf{N}$	$\mathbf{B}$
Point Richardson iteration	$\mathbf{I}$	$\mathbf{I} - \mathbf{R}$	$\mathbf{I} - \mathbf{R}$
Point Jacobi iteration	$\mathbf{D}$	$(\mathbf{L} + \mathbf{U})$	$\mathbf{D}^{-1}(\mathbf{L} + \mathbf{U})$
Point Gauss-Seidel iteration	$(\mathbf{D} - \mathbf{L})$	$\mathbf{U}$	$(\mathbf{D} - \mathbf{L})^{-1} \mathbf{U}$
Modified point Gauss-Seidel iteration	$(\mathbf{I} - \mathbf{L})$	$(\mathbf{I} - \mathbf{D} + \mathbf{U})$	$(\mathbf{I} - \mathbf{L})^{-1}(\mathbf{I} - \mathbf{D} + \mathbf{U})$
Point Richardson relaxation iteration	$\frac{1}{\omega} \mathbf{I}$	$\left( \frac{1}{\omega} \mathbf{I} - \mathbf{R} \right)$	$(\mathbf{I} - \omega \mathbf{R})$
Point Jacobi relaxation iteration	$\frac{1}{\omega} \mathbf{D}$	$\left( \frac{1}{\omega} \mathbf{D} - \mathbf{R} \right)$	$(\mathbf{I} - \omega \mathbf{D}^{-1} \mathbf{R})$
Point successive over-relaxation iteration	$\frac{1}{\omega} \mathbf{D} - \mathbf{L}$	$\frac{1}{\omega} ((1 - \omega) \mathbf{D} + \omega \mathbf{U})$	$(\mathbf{D} - \omega \mathbf{L})^{-1} (\omega \mathbf{U} + (1 - \omega) \mathbf{D})$
Modified point successive over-relaxation iteration	$\frac{1}{\omega} \mathbf{I} - \mathbf{L}$	$\frac{1}{\omega} ((\mathbf{I} - \omega \mathbf{D}) + \omega \mathbf{U})$	$(\mathbf{I} - \omega \mathbf{L})^{-1} ((\mathbf{I} - \omega \mathbf{D}) + \omega \mathbf{U})$

## 5.5 Convergence Issues

To study the convergence behavior of different iterative methods detailed above, we should first determine the properties and characteristics of the coefficient matrix. The coefficient matrix is a cross-correlation matrix, that is, Hermitian and positive semidefinite [45]. In the following, we assume that the cross-correlation matrix is positive definite (all eigenvalues of the cross-correlation are positive), that is, positive semidefinite and nonsingular. Non-singularity can be guaranteed in the case of the synchronous/asynchronous AWGN channel by ensuring that the spreading codes from all  $K$  users are linearly independent, that is the cross-correlation matrix is full-rank.

For the synchronous/asynchronous Rayleigh fading multipath channel the cross-correlation matrix becomes singular if the product  $KL$  is large in comparison to the processing gain of a DS-CDMA system [78]. It has been observed that the number of users and multipath components up to  $KL$

$\approx 3N$  can be tolerated in asynchronous DS-CDMA systems so that the cross-correlation matrix is still nonsingular [78]. Since  $\mathbf{R}$  is a Hermitian matrix, it must have an eigenvalue decomposition [79] as  $\mathbf{R} = \mathbf{U}\mathbf{\Lambda}\mathbf{U}^H$ , where  $\mathbf{U}$  is a unitary matrix satisfying  $\mathbf{U}\mathbf{U}^H = \mathbf{I}$  that contains the eigenvectors of  $\mathbf{R}$  while  $\mathbf{\Lambda}$  is a diagonal matrix formed by the  $K$  eigenvalues of  $\mathbf{R}$  as:  $\mathbf{\Lambda} = \text{diag}(\lambda_1, \lambda_2, \dots, \lambda_K)$ .

### 5.5.1 General Convergence Results

All the iterative methods discussed above are of the form:

$$\mathbf{b}_p = \mathbf{M}^{-1}\mathbf{N}\mathbf{b}_{p-1} + \mathbf{M}^{-1}\mathbf{y} = \mathbf{B}\mathbf{b}_{p-1} + \mathbf{f} \quad (5-59)$$

where  $\mathbf{f} = \mathbf{M}^{-1}\mathbf{y}$ . The following theorem [71] determines the condition of convergence for any stationary iterative method:

#### Theorem 5.1

*Let  $\mathbf{B}$  be a square matrix such that  $\rho(\mathbf{B}) < 1$ , then  $\mathbf{I} - \mathbf{B}$  is nonsingular and the iteration of (5-59) converges for any  $\mathbf{f}$  and  $\mathbf{b}_0$ . Conversely, if the iteration of (5-59) converges for any  $\mathbf{f}$  and  $\mathbf{b}_0$ , then  $\rho(\mathbf{B}) < 1$ .*

From this theorem, it is straightforward to deduce that the convergence of all iterative methods discussed before depends on the spectral radius of the iteration matrix  $\mathbf{B}$ . However, the calculation of the spectral radius is quit complex and thus other alternatives should be used. One alternative is to use the inequality  $\rho(\mathbf{B}) < \|\mathbf{B}\|$ , for any norm, that is [71]:

#### Corollary 5.1

*Let  $\mathbf{B}$  be a square matrix such that  $\|\mathbf{B}\| < 1$ , for some matrix norm  $\|\cdot\|$ , then  $\mathbf{I} - \mathbf{B}$  is nonsingular and the iteration of (5-59) converges for any  $\mathbf{f}$  and  $\mathbf{b}_0$ .*

Another alternative to Corollary 5.1 is to replace the norm by the trace since the trace of a matrix is also an upper bound of the spectral radius. More relaxed conditions of convergence can be obtained if properties of the cross-correlation matrix are taken into consideration. The cross-correlation matrix is hermitian, semi-definite and under most practical conditions positive definite. It is also in some cases diagonally dominant.

### 5.5.2 Convergence Results for Hermitian Positive Definite Matrices

Let us first consider the case where the cross-correlation matrix is hermitian and positive definite, that is,  $\mathbf{R} = \mathbf{D} - \mathbf{L} - \mathbf{U} = \mathbf{D} - \mathbf{E} - \mathbf{E}^H$  where  $\mathbf{E} = \mathbf{L} = \mathbf{U}^H$ , Ostrowski [80] proved that the successive over-

relaxation iterative method is convergent if and only if the coefficient matrix is positive definite and the relaxation factor is between 0 and 2. This is given by the following theorem:

**Theorem 5.2**

*Let  $\mathbf{R} = \mathbf{D} - \mathbf{E} - \mathbf{E}^H$  be a  $K$ -by- $K$  hermitian matrix, where  $\mathbf{D}$  is positive definite, and  $\mathbf{D} - \omega\mathbf{E}$  is nonsingular for  $0 < \omega < 2$ . Then, the successive over-relaxation iteration is convergent if and only if  $\mathbf{R}$  is positive definite and  $0 < \omega < 2$ .*

Since Gauss-Seidel is a special case of the successive over-relaxation iteration ( $\omega = 1$ ), then it is evident from the theorem above that the Gauss-Seidel iteration is convergent if and only if  $\mathbf{R}$  is positive definite, this is detailed in the following corollary [80]:

**Corollary 5.2**

*Let  $\mathbf{R} = \mathbf{D} - \mathbf{E} - \mathbf{E}^H$  be an  $K$ -by- $K$  hermitian matrix, where  $\mathbf{D}$  is hermitian and positive definite, and  $\mathbf{D} - \mathbf{E}$  is nonsingular. Then, the Gauss-Seidel iteration is convergent if and only if  $\mathbf{R}$  is positive definite.*

Ostrowski's theorem is also extended to both block successive over-relaxation and block Gauss-Seidel iterative methods through the following two corollaries [80]:

**Corollary 5.3**

*Let  $\mathbf{R}$  be an  $K$ -by- $K$  hermitian matrix and  $\mathbf{R} = \mathbf{D} - \mathbf{E} - \mathbf{E}^H$ , where  $\mathbf{D}$  is block diagonal matrix, and  $\mathbf{E}$  and  $\mathbf{E}^H$  are the remaining lower-left and upper-right block triangular parts of  $\mathbf{R}$ . If  $\mathbf{D}$  is positive definite, then the block successive over-relaxation method is convergent for all  $\mathbf{y}_0$  if and only if  $0 < \omega < 2$  and  $\mathbf{R}$  is positive definite.*

**Corollary 5.4**

*Let  $\mathbf{R}$  be an  $K$ -by- $K$  hermitian matrix and  $\mathbf{R} = \mathbf{D} - \mathbf{E} - \mathbf{E}^H$ , where  $\mathbf{D}$  is block diagonal matrix, and  $\mathbf{E}$  and  $\mathbf{E}^H$  are the remaining lower-left and upper-right block triangular parts of  $\mathbf{R}$ . If  $\mathbf{D}$  is positive definite, then the block Gauss-Seidel method is convergent for all  $\mathbf{y}_0$  if and only if  $\mathbf{R}$  is positive definite.*

Another theorem that is used to prove the convergence of the Gauss-Seidel and the block Gauss-Seidel iterative method is the Keller theorem [81]. This is a very important theorem, which we need later on for the subsequent chapters.

**Theorem 5.3**

Let  $\mathbf{R}$  be a hermitian matrix and let  $\mathbf{M}$  be a nonsingular matrix such that  $((\mathbf{M}+\mathbf{M}^H)-\mathbf{R})$  is positive definite. Then the iteration  $\mathbf{b}_p = \mathbf{M}^{-1} (\mathbf{M}-\mathbf{B})\mathbf{b}_{p-1} + \mathbf{M}^{-1}\mathbf{y}$  is convergent if and only if  $\mathbf{R}$  is positive semidefinite.

In order to apply Keller's theorem in our case we set the following:  $\mathbf{R} = \mathbf{D} - \mathbf{E} - \mathbf{E}^H$ ,  $\mathbf{M} = \mathbf{D} - \mathbf{E}$  which is nonsingular because  $\det(\mathbf{M}) = \det(\mathbf{D} - \mathbf{E}) = \det(\mathbf{D}) \neq 0$   $\mathbf{E}^H = \mathbf{M} - \mathbf{R}$ , hence we get:

$$\begin{aligned} \mathbf{M}+\mathbf{M}^H - \mathbf{R} &= \mathbf{M}^H + (\mathbf{M} - \mathbf{R}) \\ &= (\mathbf{D} - \mathbf{E})^H + \mathbf{E}^H \end{aligned} \tag{5-60}$$

Hence:  $\mathbf{M}+\mathbf{M}^H - \mathbf{R} = \mathbf{D}^H$ , and since the matrix  $\mathbf{D}$  is also hermitian and positive definite then the Gauss-Seidel/block Gauss-Seidel iteration matrix is convergent.

For the modified point/block Gauss-Seidel iterative methods, we obtain the necessary conditions of convergence by simply considering the modified point/block Successive over-relaxation iterative methods with the relaxation factor set to one. This is detailed in the subsequent sections.

**5.5.3 Convergence Results for Strictly Diagonal Dominant Matrices**

If we consider the case of a diagonally dominant matrix then both Jacobi and Gauss-Seidel iterative methods are convergent, this is clear from the following theorem [71]:

**Theorem 5.4**

*If  $\mathbf{R}$  is a strictly diagonally dominant, then the associated Jacobi and Gauss-Seidel iterations converges for any  $\mathbf{b}_0$ .*

For the Richardson, block Richardson, the proposed modified Gauss-Seidel and the proposed block modified Gauss-Seidel iterations more conditions need to be set in order to guarantee convergence as they are not always convergent for either hermitian positive definite or diagonally dominant matrices.

Let us start by the Richardson and block Richardson iterations, since their iteration matrix is the same then they should have the same condition of convergence. The iteration matrix of both the Richardson and block Richardson iterations is given by:  $\mathbf{B} = \mathbf{I} - \mathbf{R}$ , hence for convergence  $|\lambda_{\max}(\mathbf{I} - \mathbf{R})| < 1$  which implies that:  $0 < \lambda_{\max}(\mathbf{R}) < 2$ . If the matrix is strictly diagonal dominant then a sufficient condition is given by the following proposition:

**Proposition 5.1**

If  $\mathbf{R}$  is a strictly diagonally dominant matrix and  $\mathbf{D} \leq 1$  ( $r_{k,k} \leq 1$  for all  $k = 1, 2, \dots, K$ ), then the associated Richardson/block Richardson iteration converges for any  $\mathbf{b}_0$ .

Proof:

Using the Gershgorin circle theorem [82], which states that all eigenvalues of an arbitrary  $i$ -rowed square matrix  $\mathbf{R} = \{r_{i,j}\}$  lie within  $i$  circles. Each center of the  $i$  circles corresponds to exactly one of the  $i$ -diagonal elements of the matrix. The radius of each circle is given by summing up the magnitudes of the remaining  $i-1$  elements of each row<sup>1</sup>. We obtain the following upper bound for the largest eigenvalue:

$$\lambda_{\max}(\mathbf{R}) \leq \max_{1 \leq i \leq K} \left( \sum_{j=1}^K |r_{i,j}| \right) \quad (5-61)$$

It is clear from Gershgorin circle theorem that if we can limit the distance between the origin and the centers of these disks to be less than one then due to the diagonal dominance of the matrix  $\mathbf{R}$ , the radii of these disks are also less than one. Hence, the union of all these disks in which all eigenvalues of matrix  $\mathbf{R}$  lie should be contained within a disk centered at one and with radius one. This ensures that the maximum eigenvalue of the matrix  $\mathbf{R}$  is between 0 and 2.

**5.5.4 Convergence Results for Iterative Relaxation Methods**

For the relaxation schemes, their iteration matrix depends on the relaxation parameter and therefore their convergence behavior and region of convergence depend on the relaxation parameter as well.

For the Successive over-relaxation and block successive over-relaxation, it is clear from the Ostrowski's theorem, Corollary 5.3 and 5.4, that these two iterative methods converge if and only if  $0 < \omega < 2$ . The optimum value of the relaxation factor that results in the highest asymptotic convergence rate is the one that minimizes the spectral radius of the iteration matrix.

Unfortunately, the determination of such factor requires the calculation of the maximum eigenvalue of the iteration matrix which is prohibitively complex. A closed form of the optimum relaxation factor is obtained for a class of matrices with a special property (consistently ordered matrices) [83]. Unfortunately, the cross-correlation matrix doesn't possess this property and therefore

---

<sup>1</sup> It could also be applied column-wise but since the crosscorrelation matrix  $\mathbf{R}$  is symmetric we would obtain the same results

one has to look for an estimate of the optimum relaxation factor based on some upper bound on the maximum eigenvalue of the iteration matrix as in [84].

For the point/block Jacobi over-relaxation, the iteration matrix is given by:  $\omega \mathbf{D}^{-1}(\mathbf{L} + \mathbf{U}) + (1 - \omega)\mathbf{I} = \mathbf{I} - \omega \mathbf{D}^{-1}\mathbf{R}$  and thus this iterative method is convergent if  $|\lambda_{\max}(\mathbf{I} - \omega \mathbf{D}^{-1}\mathbf{R})| < 1$ , which implies that:  $0 < \omega < 2/\lambda_{\max}(\mathbf{D}^{-1}\mathbf{R})$ .

For the Richardson relaxation iteration, the iteration matrix is given by:  $(\mathbf{I} - \omega \mathbf{R})$  and hence this iterative method is convergent if  $|\lambda_{\max}(\mathbf{I} - \omega \mathbf{R})| < 1$  which implies that:  $0 < \omega < 2/\lambda_{\max}(\mathbf{R})$ .

Note that for the synchronous/asynchronous CDMA AWGN channel, the diagonal  $\mathbf{D}$  of the cross-correlation matrix  $\mathbf{R}$  is the identity matrix. Therefore,  $\mathbf{D}^{-1} = \mathbf{D} = \mathbf{I}$  and the Richardson and Jacobi iterations become the same. The optimal relaxation factor for the point/block Jacobi relaxation iteration is given by [85]:

$$\omega = \frac{2}{\lambda_{\max}(\mathbf{D}^{-1}\mathbf{R}) + \lambda_{\min}(\mathbf{D}^{-1}\mathbf{R})} \quad (5-62)$$

As for the Jacobi relaxation iteration, the optimal relaxation factor for the Richardson iteration is given by [71]:

$$\omega = \frac{2}{\lambda_{\max}(\mathbf{R}) + \lambda_{\min}(\mathbf{R})} \quad (5-63)$$

For the modified successive over-relaxation iteration, we use the same approach that is used to prove the Ostrowski theorem [80]. Lets first state the following propositions:

**Proposition 5.2**

*Let  $\mathbf{R}$  be a  $K$ -by- $K$  hermitian positive definite matrix and  $\mathbf{R} = \mathbf{D} - \mathbf{E} - \mathbf{E}^H$ , where  $\mathbf{D}$  is the diagonal part of  $\mathbf{R}$  and  $\mathbf{E}$  and  $\mathbf{E}^H$  are the remaining lower-left and upper-right triangular parts of  $\mathbf{R}$ . The modified successive over-relaxation method is convergent for any initial solution  $\mathbf{y}_o$  if and only if*

$$0 < \omega < \frac{2}{\max(\mathbf{D})}.$$

Proof:

The iteration matrix of the modified successive over-relaxation iterative method is given by:

$$\mathbf{H} = (\mathbf{I} - \omega \mathbf{E})^{-1}((\mathbf{I} - \omega \mathbf{D}) + \omega \mathbf{E}^H) \quad (5-64)$$

Using the determinant operator on the iteration matrix one obtains:

$$\begin{aligned}
 \det[\mathbf{H}] &= \det\left[(\mathbf{I} - \omega\mathbf{E})^{-1}((\mathbf{I} - \omega\mathbf{D}) + \omega\mathbf{E}^H)\right] \\
 &= \frac{1}{\det[\mathbf{I} - \omega\mathbf{E}]} \det[(\mathbf{I} - \omega\mathbf{D}) + \omega\mathbf{E}^H] \\
 &= \frac{1}{\det[\mathbf{I}]} \det[(\mathbf{I} - \omega\mathbf{D})] \\
 &= \det[(\mathbf{I} - \omega\mathbf{D})] \\
 &= \prod_{k=1}^K (1 - \omega r_{k,k})
 \end{aligned} \tag{5-65}$$

Since we have:  $\det[\mathbf{H}] = \prod_{k=1}^K \lambda_k(\mathbf{H}) \leq (\lambda_{\max}(\mathbf{H}))^K$  where  $\lambda_k(\mathbf{H})$ 's are the eigenvalues of  $\mathbf{H}$ . For

convergence we should have  $|\lambda_{\max}(\mathbf{H})| < 1$  and therefore  $|(\lambda_{\max}(\mathbf{H}))^K| < 1$ . Thus we get  $|\det[\mathbf{H}]| < 1$

and hence  $\left|\prod_{k=1}^K (1 - \omega r_{k,k})\right| < 1$ . If one can ensure that  $|1 - \omega r_{k,k}| < 1$  for all  $k$ , then  $\left|\prod_{k=1}^K (1 - \omega r_{k,k})\right| < 1$ .

Finally, one gets:  $\frac{2}{r_{k,k}} > \omega > 0$  for all  $k$ , which can be written as  $0 < \omega < \frac{2}{\max(\mathbf{D})}$ . As a special case,

the modified Gauss-Seidel iterative method is convergent if:  $0 < \mathbf{D} < 2$ . For the modified block successive over-relaxation iterative method we propose the following corollary:

**Corollary 5.5**

Let  $\mathbf{R}$  be an  $K$ -by- $K$  hermitian matrix and  $\mathbf{R} = \mathbf{D} - \mathbf{E} - \mathbf{E}^H$ , where  $\mathbf{D}$  is the block diagonal part of  $\mathbf{R}$ , and  $\mathbf{E}$  and  $\mathbf{E}^H$  are the remaining lower-left and upper-right block triangular parts of  $\mathbf{R}$ . The modified block successive over-relaxation iterative method is convergent for any initial solution  $\mathbf{y}_0$  if and only if  $-1 < \det[\mathbf{I} - \omega\mathbf{D}] < 1$  and  $\mathbf{R}$  is positive definite.

Proof:

The iteration matrix of the modified block successive over-relaxation iterative method is given by:

$$\mathbf{H} = (\mathbf{I} - \omega\mathbf{L})^{-1} ((\mathbf{I} - \omega\mathbf{D}) + \omega\mathbf{U}) \tag{5-66}$$

Using the determinant operator on the iteration matrix one obtains:

$$\begin{aligned}
 \det[\mathbf{H}] &= \det\left[(\mathbf{I} - \omega\mathbf{L})^{-1}((\mathbf{I} - \omega\mathbf{D}) + \omega\mathbf{U})\right] \\
 &= \frac{1}{\det[\mathbf{I} - \omega\mathbf{L}]} \det[(\mathbf{I} - \omega\mathbf{D}) + \omega\mathbf{U}] \\
 &= \frac{1}{\det[\mathbf{I}]} \det[(\mathbf{I} - \omega\mathbf{D})] \\
 &= \det[\mathbf{I} - \omega\mathbf{D}]
 \end{aligned} \tag{5-67}$$

Since we have:  $\det[\mathbf{H}] = \prod_{k=1}^K \lambda_k(\mathbf{H}) \leq (\lambda_{max}(\mathbf{H}))^K$  where  $\lambda_k(\mathbf{H})$ 's are the eigenvalues of  $\mathbf{H}$ . For convergence we should have  $|\lambda_{max}(\mathbf{H})| < 1$  and therefore  $|(\lambda_{max}(\mathbf{H}))^K| < 1$ . Thus we get  $|\det[\mathbf{H}]| < 1$  and hence  $|\det[\mathbf{I} - \omega\mathbf{D}]| < 1$ . Finally, one gets:  $-1 < \det[\mathbf{I} - \omega\mathbf{D}] < 1$  which determines the condition of convergence for the modified block successive over-relaxation iterative method.

**Corollary 5.6**

*A more restrictive condition for the modified block successive over-relaxation iterative method to converge is that  $0 < \omega < \frac{2}{\lambda_{max}(\mathbf{D})}$ .*

Proof:

The condition above can be obtained by noticing that  $\det[\mathbf{I} - \omega\mathbf{D}] = \prod_{k=1}^K \lambda_k(\mathbf{I} - \omega\mathbf{D}) \leq (\lambda_{max}(\mathbf{I} - \omega\mathbf{D}))^K$ . Thus if we can ensure that:  $|\lambda_{max}(\mathbf{I} - \omega\mathbf{D})| < 1$  then  $|\det[\mathbf{I} - \omega\mathbf{D}]| < 1$ . Finally, this results in the condition of convergence:  $0 < \omega < \frac{2}{\lambda_{max}(\mathbf{D})}$ .

Finally by setting the relaxation factor to one, we obtain the conditions of convergence for the modified block Successive over-relaxation iterative method as:  $-1 < \det[\mathbf{I} - \mathbf{D}] < 1$ . A more restrictive condition is:  $0 < \lambda_{max}(\mathbf{D}) < 2$ . All the conditions of convergence are summarized and presented in Table 5.2.

Table 5.2: Conditions of convergence for different iterative methods

Iterative method	Type of Matrix	Condition of convergence
Point Richardson iteration	$\mathbf{R}$ is strictly diagonal dominant.	$\mathbf{D} \leq 1$
Point Jacobi iteration	$\mathbf{R}$ is strictly diagonal dominant	Always convergent
Point Gauss-Seidel iteration	$\mathbf{R}$ is hermitian and positive definite.	Always convergent
Modified Point Gauss-Seidel iteration	$\mathbf{R}$ is hermitian, positive definite.	$0 < \mathbf{D} < 2$
Point Richardson relaxation iteration	Any matrix	$0 < \omega < 2/\lambda_{\max}(\mathbf{R})$
Point Jacobi relaxation iteration	Any matrix	$0 < \omega < 2/\lambda_{\max}(\mathbf{D}^{-1}\mathbf{R})$
Point successive over-relaxation iteration	$\mathbf{R}$ is hermitian, positive definite.	$0 < \omega < 2$
Modified point successive over-relaxation iteration	$\mathbf{R}$ is hermitian, positive definite.	$0 < \omega < \frac{2}{\max(\mathbf{D})}$
Block Richardson iteration	$\mathbf{R}$ is strictly diagonal dominant.	$\mathbf{D} \leq 1$
Block Jacobi iteration	$\mathbf{R}$ is strictly diagonal dominant	Always convergent
Block Gauss-Seidel iteration	$\mathbf{R}$ is hermitian and positive definite.	Always convergent
Modified block Gauss-Seidel iteration	$\mathbf{R}$ is hermitian, positive definite.	$-1 < \det[\mathbf{I} - \mathbf{D}] < 1$ or $0 < \lambda_{\max}(\mathbf{D}) < 2$
Block Richardson relaxation iteration	Any matrix	$0 < \omega < 2/\lambda_{\max}(\mathbf{R})$
Block Jacobi relaxation iteration	Any matrix	$0 < \omega < 2/\lambda_{\max}(\mathbf{D}^{-1}\mathbf{R})$
Block successive over-	$\mathbf{R}$ is hermitian, positive definite.	$0 < \omega < 2$

relaxation iteration		
Modified block successive over-relaxation iteration	$\mathbf{R}$ is hermitian, positive definite.	$ \det[\mathbf{I} - \omega\mathbf{D}]  < 1$ or $0 < \omega < \frac{2}{\lambda_{\max}(\mathbf{D})}$

The optimal relaxation factors for the relaxation methods detailed above are given in Table 5.3:

Table 5.3: Optimal relaxation factors for different iterative methods

Iterative method	Condition on the matrix	Optimal factor
Point/Block Richardson relaxation iteration	$\mathbf{R}$ is strictly diagonal dominant. $\mathbf{D} \leq 1$	$\omega = \frac{2}{\lambda_{\max}(\mathbf{R}) + \lambda_{\min}(\mathbf{R})}$
Point/Block Jacobi relaxation iteration	$\mathbf{R}$ is strictly diagonal dominant	$\omega = \frac{2}{\lambda_{\max}(\mathbf{D}^{-1}\mathbf{R}) + \lambda_{\min}(\mathbf{D}^{-1}\mathbf{R})}$
Point/Block successive over-relaxation iteration	$\mathbf{R}$ is hermitian, positive definite.	No analytical expression
Modified point/block successive over-relaxation iteration	$\mathbf{R}$ is hermitian, positive definite.	No analytical expression

### 5.5.5 Rate of Convergence

Often, we are interested not only in the conditions of convergence but also in the rate of convergence. Let's define the error between the exact solution  $\mathbf{y}^*$  and the approximate solution at iteration  $p$  to the equation  $\mathbf{Rb} = \mathbf{y}$  as  $\boldsymbol{\varepsilon}_p = \mathbf{y}^* - \mathbf{y}_p$ , we have:

$$\boldsymbol{\varepsilon}_{p+1} = \mathbf{B}\boldsymbol{\varepsilon}_p = \mathbf{B}^p \boldsymbol{\varepsilon}_0 \tag{5-68}$$

since the initial error vector is not a null vector, then the error vector at  $p+1$ ,  $\boldsymbol{\varepsilon}_{p+1}$ , converges to the null vector as the number of iterations tends to infinity only if the matrix  $\mathbf{B}^p$  converges to a null matrix as the number of iterations  $p$  tends to infinity, this is detailed in the following theory [71]:

**Theorem 5.5**

For any  $\mathbf{R} \in \mathbb{C}^{K,K}$  we have  $\lim_{p \rightarrow \infty} \mathbf{R}^p = \mathbf{0} \Leftrightarrow \rho(\mathbf{R}) < 1$ .

Taking in consideration the following inequality:  $\|\mathbf{B}^p \boldsymbol{\varepsilon}\| \leq \|\mathbf{B}^p\| \|\boldsymbol{\varepsilon}\|$ , where  $\|\cdot\|$  is any norm, hence, we can write:

$$\|\boldsymbol{\varepsilon}_{p+1}\| \leq \|\mathbf{B}^p\| \|\boldsymbol{\varepsilon}_0\| \leq \|\mathbf{B}\|^p \|\boldsymbol{\varepsilon}_0\| \quad (5-69)$$

Thus, in order to reduce the norm of the error with a factor less than one, that is,  $\frac{\|\boldsymbol{\varepsilon}_{p+1}\|}{\|\boldsymbol{\varepsilon}_0\|} \leq \delta < 1$ , we

should have  $\|\mathbf{B}^p\| \leq \delta$ . Taking the logarithm of the two sides we obtain:  $p \geq \frac{-\ln \delta}{R_p(\mathbf{B})}$  where

$$R_p(\mathbf{B}) = -\frac{1}{p} \ln \|\mathbf{B}^p\| \text{ and } R_p(\mathbf{B}) \text{ is the average convergence rate.}$$

By using the following theorem [71]:

**Theorem 5.6**

For any submultiplicative matrix norm  $\|\cdot\|$  on  $\mathbb{C}^{K,K}$  and any matrix  $\mathbf{B} \in \mathbb{C}^{K,K}$  we have:

$$\lim_{p \rightarrow \infty} \|\mathbf{B}^p\|^{\frac{1}{p}} = \rho(\mathbf{B})$$

We define the asymptotic convergence rate as [71]:

**Definition 5.1**

If the iterative method is convergent, then for any matrix norm  $\|\cdot\|$  we define the average rate of convergence as:

$$R_p(\mathbf{B}) = -\frac{1}{p} \ln \|\mathbf{B}^p\|$$

and the asymptotic rate of convergence as:

$$R_\infty(\mathbf{B}) = \lim_{p \rightarrow \infty} R_p(\mathbf{B}) = -\ln \rho(\mathbf{B})$$

Hence, for a sufficient large number of iterations the convergence rate is dominated by the largest eigenvalue of the iteration matrix.

## 5.6 Simulation Results

In the following we simulate the previously discussed iterative methods by focusing on the following points:

- Convergence speed of different point and block iterative methods.
- Region of convergence and optimal relaxation factors for different point and block relaxation iterative methods.

In the first case we simulate the convergence speed of the four point iterative methods, namely: the point Richardson iterative method, the point Jacobi iterative method, the modified point Gauss-Seidel iterative method and finally the point Gauss-Seidel iterative method. The normalized residual

defined as:  $\frac{\|\mathbf{b}_p - \mathbf{b}_{p-1}\|_2}{\|\mathbf{b}_1 - \mathbf{b}_0\|_2} = \frac{\|\mathbf{M}^{-1}(\mathbf{y} - \mathbf{Rb}_{p-1})\|_2}{\|\mathbf{M}^{-1}(\mathbf{y} - \mathbf{Rb}_0)\|_2}$  for different point iterative methods is evaluated for

increasing number of stages till it goes below a certain tolerance threshold (*tol*) which is set in our simulation to  $tol = 0.001$ . In all figures the vertical scale (normalized residual) is a logarithmic scale.

Even though, the performance of most iterative methods depends on the test matrices, their average performance is well known and usually serial (synchronous) methods are faster than parallel (asynchronous) methods.

The test matrix is a cross-correlation matrix obtained by using Gold codes of length 31 where the number of users is set to 20 users. In order to distinguish between the Richardson iteration and the Jacobi iteration which are equal if the diagonal elements of the cross-correlation matrix are ones, we set the diagonal elements of our test matrix to 0.9. Hence the test matrix is symmetric and diagonal dominant. Moreover, the diagonal part of the matrix  $\mathbf{D} = 0.9 \leq 1$ , therefore, all point iterative methods are expected to converge unconditionally including the point Richardson iteration.

Simulation results are depicted in Figure 5.1. The latter illustrates that the fastest iterative method is the Gauss-Seidel (11 iterations) followed by the Modified Gauss-Seidel (14 iterations) and then followed by Jacobi (19 iterations) and finally by the Richardson method (22 iterations). This agrees well with theory.

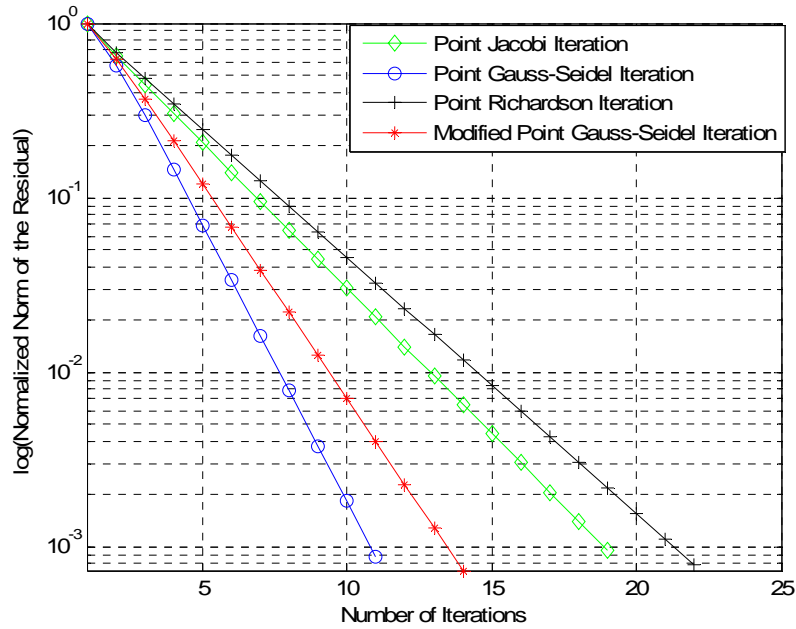


Figure 5.1: Convergence behavior of different point iterative methods.

The same test matrix is used to test the block versions of the previously discussed iterative methods, that is: the block Richardson iterative method, the block Jacobi iterative method, the modified block Gauss-Seidel iterative method and finally the block Gauss-Seidel iterative method.

Simulation results depicted in Figure 5.2 indicates that the performance of both the block Jacobi (16 iterations) and the block Gauss-Seidel (11 iterations) have improved compared to their point counterparts. This agrees well with the theory [71].

However, for the modified block Gauss-Seidel (16 iterations) it is clear that its convergence speed worsened compared to its point counterpart. This is due to the fact that the splitting matrix of the modified Gauss-Seidel iterative method is closer to  $\mathbf{R}$  than that of the modified block Gauss-Seidel iterative method.

Finally for the convergence speed of the block Richardson iteration is similar to that of the point Richardson iteration (22 iterations). This is expected because the two iterations are equivalent in the sense that they have the same iteration matrix, hence they exhibit the same convergence behavior.

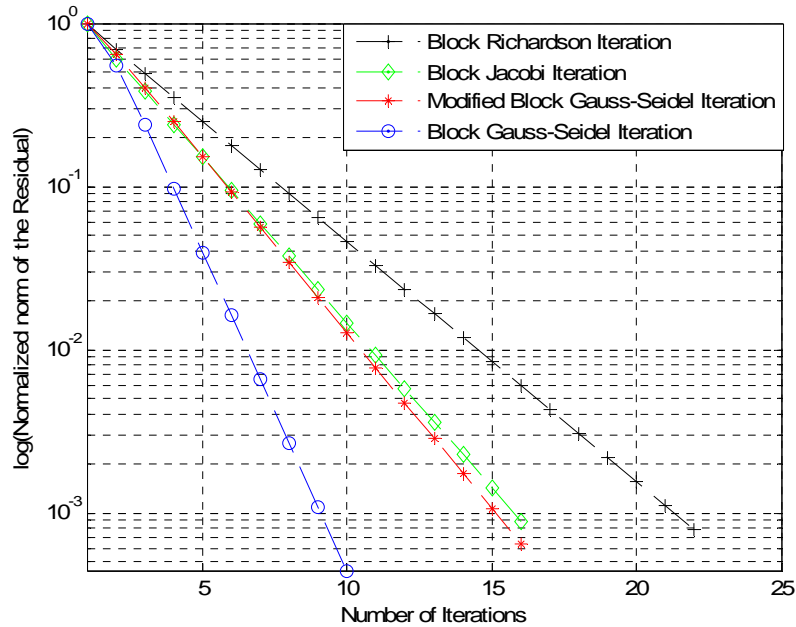


Figure 5.2: Convergence behavior of different block iterative methods.

For the point and block relaxation iterative methods we evaluate the normalized residual defined above for different values of the relaxation factor. The same test matrix above is also used here and the number of iterations is set to 5 iterations for all iterative methods. From Figure 5.2, one can notice the following:

- For the point Gauss-Seidel relaxation iterative method the minimum value of the residual is within the interval  $(0, 2)$ , which agrees well with theory (Table 5.2).
- For the modified successive over-relaxation iterative method the minimum value of the residual is within the interval  $(0, 2/\max(\mathbf{D}))$ , which agrees well with theory (Table 5.2).
- For the point Richardson relaxation iterative method, the theoretical optimum value is given in Table 5.3 and found to be in our case equal to 1.64. Hence it is very close to the value of the relaxation factor for which the residual is minimum in our simulation.
- For the point Jacobi relaxation iterative method, the theoretical optimum value is given in Table 5.3 and found to be in our case equal to 1.47. Therefore, it is very close to the value of the relaxation factor for which the residual is minimum in our simulation.

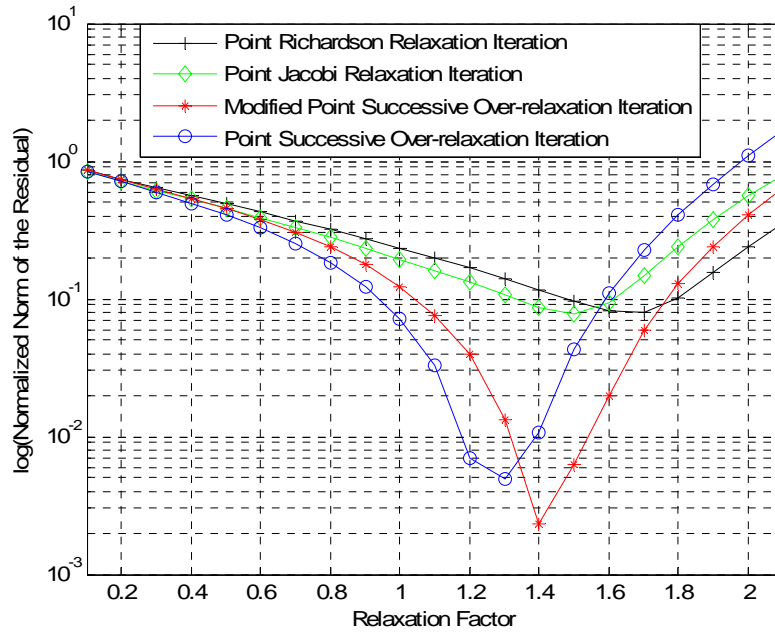


Figure 5.3: Convergence behavior of different point relaxation iterative methods versus the relaxation factor.

All the above comments for the point iterative relaxation methods are also true for the results obtained for their block counterparts as illustrated in Figure 5.4, that is:

- For the block Gauss-Seidel relaxation iterative method the minimum value of the residual is within the interval  $(0, 2)$ , which agrees well with theory (Table 5.2).
- For the modified block successive over-relaxation iterative method the minimum value of the residual is within the interval  $(0, 2/\lambda_{\max}(\mathbf{D}))$ , which agrees well with theory (Table 5.2).
- For the block Richardson relaxation iterative method, the theoretical optimum value is given in Table 5.3 and found to be in our case equal to 1.64. Hence it is very close to the value of the relaxation factor for which the residual is minimum in our simulation.
- For the block Jacobi relaxation iterative method, the theoretical optimum value is given in Table 5.3 and found to be in our case equal to 1.47. Therefore, it is very close to the value of the relaxation factor for which the residual is minimum in our simulation.

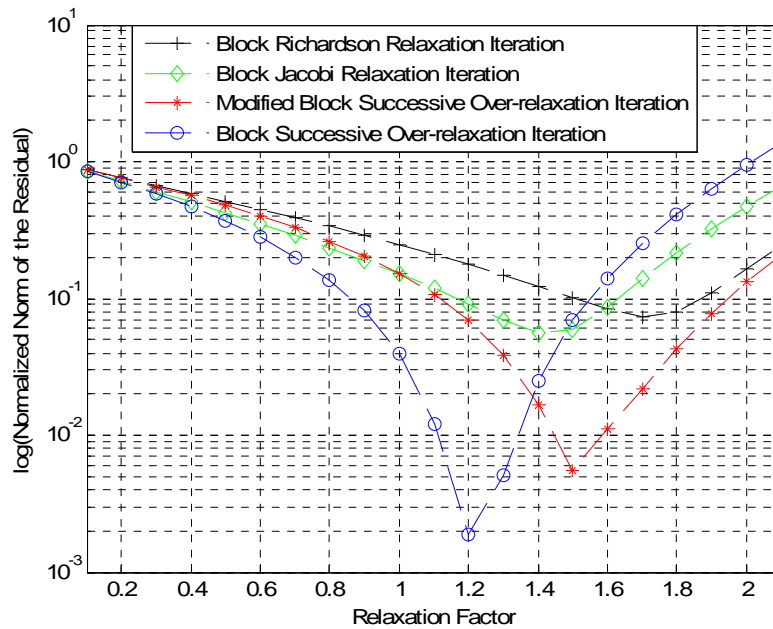


Figure 5.4: Convergence behavior of different block relaxation iterative methods versus the relaxation factor.

## 5.7 Conclusion

In this chapter, we reviewed the basic linear point and block iterative methods. Their corresponding relaxation schemes are also introduced. Two new iterative methods are introduced and studied in detail. The convergence behavior of these methods is studied and their conditions of convergence are determined. Finally, these methods are simulated and the results accessed and commented.

## Chapter 6

### Multiuser Detection in CDMA

#### 6.1 Chapter's Contents

6.1 Chapter's Contents .....	97
6.2 Introduction .....	98
6.3 Performance Metrics and Computational Complexity .....	98
6.3.1 Bit Error Rate (BER) .....	99
6.3.2 Asymptotic Multiuser Efficiency and Near-Far Resistance .....	99
6.3.3 Computational Complexity .....	100
6.4 Classification of Multiuser Detectors .....	100
6.5 Multiuser Detection Structures for Asynchronous CDMA AWGN Channel .....	102
6.5.1 The Conventional Matched Filter Detector .....	103
6.5.2 The Optimum Multiuser Detector .....	106
6.5.3 The Decorrelator Detector .....	106
6.5.4 The Linear Minimum Mean Square Error (LMMSE) Detector .....	108
6.6 Multiuser Detection Structures for Asynchronous CDMA Multipath Fading Channel .....	109
6.6.1 The Conventional Rake Receiver .....	110
6.6.2 The Optimal Multiuser Detector .....	114
6.6.3 The Decorrelator Detector .....	114
6.6.4 The Linear Minimum Mean Square Error (LMMSE) Detector .....	115
6.7 The Linear Transformation of the Received Signal .....	116
6.7.1 The Linear Transformation of the Received Signal for AWGN Channel .....	116
6.7.2 The Linear Transformation of the Received Signal for Multipath Fading Channel .....	117
6.8 The Linear Transformation of the Matched Filters/Rake Receivers' Outputs .....	117
6.8.1 The Linear Transformation of the Matched Filters' Outputs .....	118
6.8.2 The Linear Transformation of the Rake Receivers' Outputs .....	118
6.9 Computational Complexity .....	119
6.10 Simulation Results .....	120
6.11 Conclusion .....	124

## 6.2 Introduction

In CDMA, the term *Multi-User Detection* (MUD) or *Joint Detection* is any method or technique that exploits the knowledge of the spreading codes of users other than the desired user to enhance the quality of its data estimates. In general, we are not interested in the data estimates of only one user, but of all of them. As such, the detector considers the effects of all users on all other users, and attempts to improve the data estimates for all of them, thus resulting in a multiple-input multiple-output system.

In a pure flat fading synchronous channel, where all users' signals arrive synchronously at the base station, there is no need for MUD. For such systems, the best performance is obtained if orthogonal spreading codes are used along with a bank of conventional Matched Filter detectors. The performance of such systems reduces to that of the single user detector and provides an upper bound on the performance of all multi-user systems.

In practice, however, most CDMA systems are asynchronous and channels frequently exhibit dispersive multipath. Together, these factors are sufficient to destroy the orthogonality of the system and hence MAI is generated. In this situation, MUD techniques can be used to notably reduce the effect of MAI and to improve the performance so that it is closer to that of an orthogonal system.

In the ensuing, we set the following conventions in order to facilitate the study of different multiuser detectors:  $y_{MF}^b(k_{eff}) \triangleq y_{MF}^b(w, k)$ ,  $b^b(k_{eff}) \triangleq b_w^b(k)$ ,  $\bar{s}_{eff}^b(k_{eff}) \triangleq \bar{s}_{eff}^b(w, k)$  and  $\bar{s}_{eff}(k_{eff}) \triangleq \bar{s}_{eff}(w, k)$  where  $k_{eff}$  is an index that takes values from 1 to  $WK$  and it is related to  $k$  and  $w$  as follows:  $k_{eff} = (w - 1)K + k$ . If  $k_{eff}$  is provided instead, then  $w$  and  $k$  are determined from  $k_{eff}$  as follows:  $w = \left\lceil \frac{k_{eff}}{K} \right\rceil$  where  $\lceil \cdot \rceil$  is the ceiling operator and  $k = k_{eff} - (w - 1)K$ . This index will be used interchangeably with  $(k, w)$  here and in the subsequent chapters.

## 6.3 Performance Metrics and Computational Complexity

There are many criteria that can be used to quantify the performance of a multiuser detector. In this section, we list a number of important performance measures that will help in comparing different multiuser detection techniques. Mainly, we are interested in the Bit Error Rate (BER), the Asymptotic Multiuser Efficiency (AME), Near-Far Resistance (NFR), and finally the computational complexity.

### 6.3.1 Bit Error Rate (BER)

It is the figure of merit of most communication systems. It is defined as the number of incorrectly detected bits relative to the total number of detected bits. For some multiuser detectors it is possible to derive an analytical expression for the bit-error-rate, however, for many other systems this is often not straightforward and in some cases it is not possible at all (e.g. a closed form expression can not be obtained for the optimum multiuser detector that minimizes the probability of bit error). The only way to acquire a bit-error-rate for these detection schemes is through simulation.

### 6.3.2 Asymptotic Multiuser Efficiency and Near-Far Resistance

The need for other performance measures that are easier to derive is vital. One of them is the *multiuser efficiency* [30]. In this performance measure, assume that the BER of a certain multiuser detector working under a background noise of variance  $\sigma^2$  for user  $k_{eff}$  is  $P_{k_{eff}}(\sigma)$ , the effective energy  $e_{k_{eff}}(\sigma)$  is defined as the energy that is required for a single user detector to achieve  $P_{k_{eff}}(\sigma)$ , that is:

$$P_{k_{eff}}(\sigma) = Q\left(\frac{\sqrt{e_{k_{eff}}(\sigma)}}{\sigma}\right), \text{ hence: } e_{k_{eff}}(\sigma) = \sigma^2 \left(Q^{-1}(P_{k_{eff}}(\sigma))\right)^2.$$

Since the multiuser error probability is lower bounded by the single user error probability  $P_{su}(\bar{\mathbf{A}}_{eff}(k_{eff}, k_{eff}), \sigma)$  (assuming the same background noise with variance  $\sigma^2$ ), we have:

$$P_{k_{eff}}(\sigma) \geq P_{su}(\bar{\mathbf{A}}_{eff}(k_{eff}, k_{eff}), \sigma) \quad \text{thus} \quad Q\left(\frac{\sqrt{e_{k_{eff}}(\sigma)}}{\sigma}\right) \geq Q\left(\frac{\bar{\mathbf{A}}_{eff}(k_{eff}, k_{eff})}{\sigma}\right) \quad \text{and hence}$$

$\sqrt{e_{k_{eff}}(\sigma)} \leq \bar{\mathbf{A}}_{eff}(k_{eff}, k_{eff})$ . The ratio  $\frac{e_{k_{eff}}(\sigma)}{\bar{\mathbf{A}}_{eff}(k_{eff}, k_{eff})^2} \in [0, 1]$  is known as the multiuser efficiency

and it quantifies the BER performance loss due to the existence of other users' signals in the channel.

The asymptotic multiuser efficiency (AME) is defined as:  $\eta_{k_{eff}} = \lim_{\sigma \rightarrow 0} \frac{e_{k_{eff}}(\sigma)}{\bar{\mathbf{A}}_{eff}(k_{eff}, k_{eff})^2}$  and measures the slope with which  $P_{k_{eff}}(\sigma)$  goes to zero (in logarithmic scale) in the high SNR region [30].

Another definition for the AME provided by Verdu and is useful for our analysis in the subsequent chapters is given by [30]:

$$\eta_{k_{\text{eff}}} = \sup \left\{ 0 \leq r \leq 1 : \lim_{\sigma \rightarrow 0} \frac{P_{k_{\text{eff}}}(\sigma)}{Q\left(\frac{\sqrt{r} \bar{\mathbf{A}}_{\text{eff}}(k_{\text{eff}}, k_{\text{eff}})}{\sigma}\right)} < +\infty \right\} = \frac{2}{\bar{\mathbf{A}}_{\text{eff}}(k_{\text{eff}}, k_{\text{eff}})^2} \lim_{\sigma \rightarrow 0} \sigma^2 \log\left(\frac{1}{P_{k_{\text{eff}}}(\sigma)}\right)$$

which is read as: “AME is the largest value of  $r$  in  $[0,1]$  for which  $\frac{P_{k_{\text{eff}}}(\sigma)}{Q\left(\frac{\sqrt{r} \bar{\mathbf{A}}_{\text{eff}}(k_{\text{eff}}, k_{\text{eff}})}{\sigma}\right)} < +\infty$  in the

limit as  $\sigma$  vanishes to zero”.

The worst-case AME, taken over all possible interference power profiles, characterizes a detector’s robustness to the near-far problem and is known as the *near-far resistance*. The latter is given by:  $\bar{\eta}_{k_{\text{eff}}} = \inf_{\substack{\bar{\mathbf{A}}_{\text{eff}}(j,j) > 0 \\ j \neq k_{\text{eff}}}} \eta_{k_{\text{eff}}}$ .

Intuitively, near-far resistance provides an indication of the worst-case performance loss due to interference for any individual user over all possible other-user transmit power profiles.

### 6.3.3 Computational Complexity

Another criterion that is commonly used to compare multiuser detection structures is the computational complexity. This factor is of paramount importance, since it determines whether the multiuser detector can be implemented in practice or not. One way to quantify the computational load is with the notation of a *flop* where a flop stands for floating point operation [86]. Throughout this dissertation, operations such as multiply, add, subtract, divide and compare are considered as one flop. The computational load is primarily a function of the number of users,  $K$ , and the number of bits within the sliding window  $W$ .

*Algorithm execution time* is another important factor that determines the efficiency of any algorithm. It is defined as the amount of time an algorithm takes on a specific machine. Its importance resides in the fact that if the algorithm is parallelizable, then one can benefit from parallel processors or machines to reduce the algorithm’s execution time. In general the computational complexity in terms of flops is roughly equal to the algorithm’s execution time if no parallelism is considered.

## 6.4 Classification of Multiuser Detectors

A variety of multiuser detectors have been proposed in the literature [87]-[90]. Depending on the criterion selected, such as linearity, complexity..., multiuser detectors can be classified into several categories. Linear multiuser detectors are structures that perform only linear transformations to the

received signal or the matched filter/Rake receiver outputs [91]-[93]. As such, interference cancellation detectors, usually considered as nonlinear multiuser detectors, are linear if the function used to estimate the MAI to be cancelled at each stage is linear. Typical examples of such detectors are the decorrelator and LMMSE detectors. Nonlinear multiuser detectors [94], on the other side, perform nonlinear transformations to the received signal or the matched filter/Rake receiver outputs. Usually, these detectors perform better in terms of BER than their linear counterpart at the expense of increased computational complexity. Moreover, these detectors usually require estimation of channel coefficients, noise level, ..., thus if the estimation of these parameters is not accurate, due for example to fast time-varying channel conditions, then the performance of such detectors is poor.

Another classification of multiuser detectors is whether they are adaptive or fixed [89]. If the channel conditions are slowly varying, then an effective way (in terms of computational complexity) to implement the LMMSE detector is to use adaptive filters [45]. During the training period, the latter usually employ some adaptive algorithms such as the LMS, RLS, ... to adjust the filter's taps such that the adaptive filter's performance converge to the that of the LMMSE detector. Non-adaptive detectors are also known as fixed detectors [89].

Blind multiuser detection ([95] and [96]) in the context of multiuser detection usually refers to the situation where the knowledge of the spreading codes of all interferers is not available at the receiver. This situation is common at the downlink channel. Such detectors are usually adaptive and derived to optimize a certain criterion such the minimum output energy criterion ([95]-[97]) and the constant modulus criterion [98]. If all the spreading codes of all interferers are available and are also used by the receiver, then the latter are non-blind multiuser detectors.

Another classification, which is very important in the context of our work, is based on which level the multiuser detection operations are performed, at *chip-level* or *symbol-level* ([87], [89], and [99]). Chip-level multiuser detectors (known as wideband) perform all operations at chip-level and thus are computationally intensive whereas symbol-level multiuser detectors (known as narrowband) performs all operations at symbol-level and thus exhibits less computational complexity compared to the chip-level detectors. Usually, chip-level detectors act directly on the received signal while the symbol-level detectors act on the matched filter/Rake receiver outputs.

Depending on whether Rake combining is performed before or after multiuser detection most multiuser detectors can be classified as either *pre-combining* detectors or *post-combining* detectors [67] and [93]. The latter have better BER performance but restricted to slow channel conditions where the

pre-combining detector exhibits acceptable BER performance but is not sensitive to channel conditions and therefore can be implemented in fast-varying channel environments.

The last classification is whether the multiuser detector uses a deterministic approach to obtain the final outputs or not. If so, then the detector is known as a *deterministic* multiuser detector, however, if the detector incorporates some random tunable parameters then this detector is known as a *heuristic* multiuser detector ([100] and [101]). The latter is usually used to approximate the optimal multiuser detector.

### 6.5 Multiuser Detection Structures for Asynchronous CDMA AWGN Channel

The transformation  $T$ , which is applied to either the received chip-matched signal  $\mathbf{q}_b$  or to the vector of the matched filter outputs  $\mathbf{y}_{MF}^b$ , determines the type of the multi-user detector as shown in Figure 6.1 and 6.2.

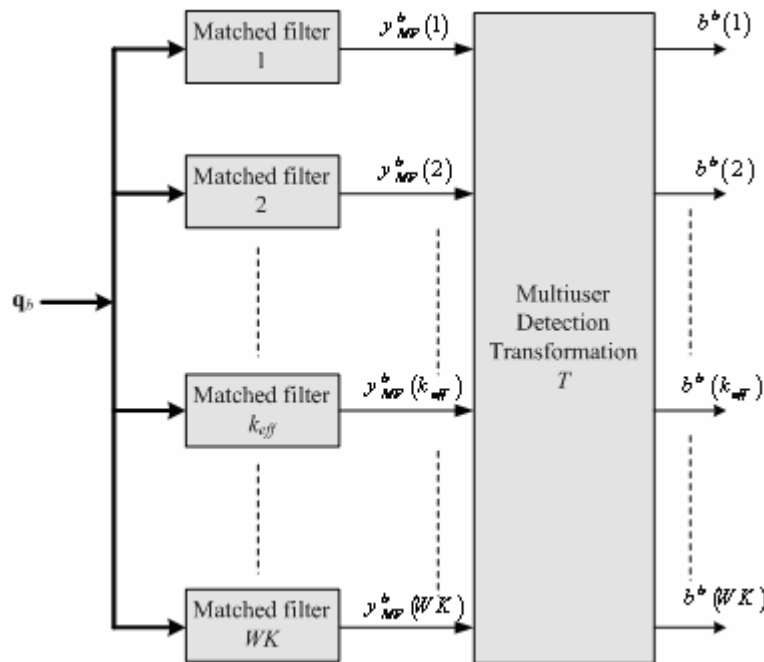


Figure 6.1: Multi-user detection Receiver acting on the vector of matched filters outputs

It is important to mention that usually, multiuser detectors acting on the vector of matched filter outputs make use of the cross-correlation coefficients and consequently the cross-correlation matrix

needs to be calculated. Finally, note that no restrictions are put on the transformation  $T$ , therefore it can be any transformation, e.g., linear or nonlinear.

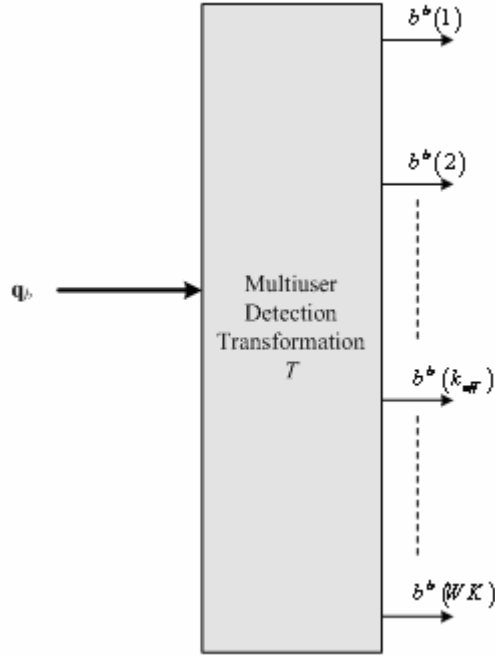


Figure 6.2: Multi-user detection acting on the received chip-matched signal.

### 6.5.1 The Conventional Matched Filter Detector

This is the simplest multiuser detector in terms of computational complexity but also the less effective in terms of performance. It consists of a bank of matched filters, where each filter is matched to the spreading code of the desired user. The conventional receiver is illustrated in Figure 6.3. For its proper operation, the conventional receiver needs the knowledge of the spreading codes, and accurate synchronization with the received signal.

The vector of the matched filters' outputs can be expressed as:

$$\mathbf{y}_{MF}^b = \bar{\mathbf{S}}_{eff}^T \mathbf{q}_b = \bar{\mathbf{S}}_{eff}^T (\bar{\mathbf{S}}_{eff} \bar{\mathbf{A}}_{eff} \bar{\mathbf{b}}^b + \bar{\mathbf{n}}_{eff}^b) = \bar{\mathbf{R}}_{eff} \bar{\mathbf{A}}_{eff} \bar{\mathbf{b}}^b + \bar{\mathbf{z}}_{eff}^b \quad (6-1)$$

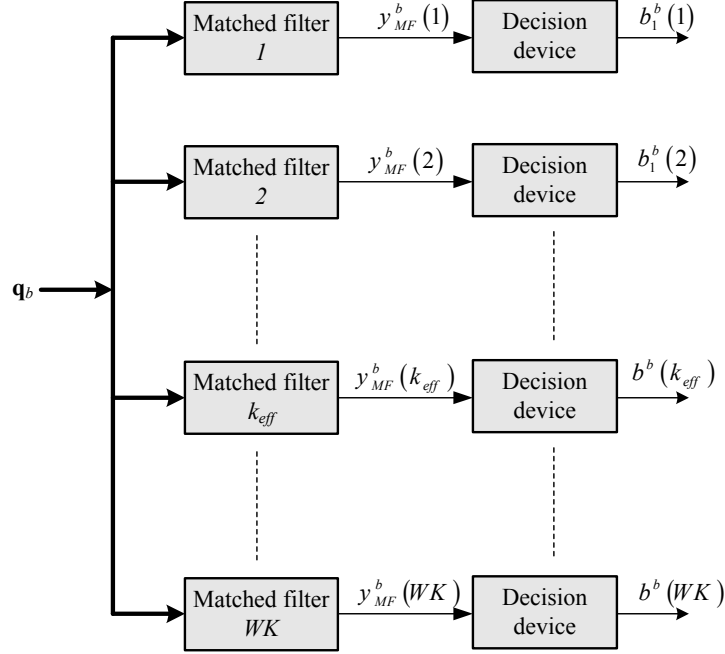


Figure 6.3: Bank of matched filter detectors

where  $\bar{\mathbf{S}}_{eff}$ ,  $\bar{\mathbf{A}}_{eff}$ ,  $\bar{\mathbf{b}}^b$  are defined in Chapter 4,  $\bar{\mathbf{n}}_{eff}^b$  is the  $b^{th}$  block of the vector  $\bar{\mathbf{n}}$  defined in Chapter 4, with dimensions  $\{(NW + \max_{1 \leq k \leq K}(\tau^k)) - by - 1\}$  and  $\bar{\mathbf{z}}_{eff}^b$  is the vector of additive colored Gaussian noise samples with a covariance matrix equal to:

$$\begin{aligned} E \left[ (\bar{\mathbf{S}}_{eff}^T \bar{\mathbf{n}}_{eff}^b) (\bar{\mathbf{S}}_{eff}^T \bar{\mathbf{n}}_{eff}^b)^T \right] &= E \left[ \bar{\mathbf{S}}_{eff}^T \bar{\mathbf{n}}_{eff}^b (\bar{\mathbf{n}}_{eff}^b)^T \bar{\mathbf{S}}_{eff} \right] \\ &= \sigma^2 \bar{\mathbf{S}}_{eff}^T \bar{\mathbf{S}}_{eff} \\ &= \sigma^2 \bar{\mathbf{R}}_{eff} \end{aligned} \quad (6-2)$$

One can see that the elements of the data vector  $\bar{\mathbf{b}}^b$  are correlated (coupled) through the cross-correlation matrix  $\bar{\mathbf{R}}_{eff}$ . To see the impact of coupling the data bits of different users let us assume for simplicity a synchronous channel and hence  $k_{eff} = k$  and  $W = 1$ . The matched filter output of the  $b^{th}$  block,  $k^{th}$  user is:

$$\begin{aligned} y_{MF}^b(k) &= \bar{\mathbf{s}}_{eff}^T(k) \mathbf{q}_b = \bar{\mathbf{s}}_{eff}^T(k) (\bar{\mathbf{S}}_{eff} \bar{\mathbf{A}}_{eff} \bar{\mathbf{b}}^b + \bar{\mathbf{n}}_{eff}^b) \\ &= \bar{\mathbf{A}}_{eff}(k, k) \bar{b}^b(k) + \underbrace{\sum_{\substack{i=1 \\ i \neq k}}^K R^*(k, i) \bar{\mathbf{A}}_{eff}(k, k) \bar{b}^b(k)}_{MAI \text{ from other users}} + \underbrace{\bar{\mathbf{s}}_{eff}^T(k) \bar{\mathbf{n}}_{eff}^b}_{\text{additive colored Gaussian Noise}} \end{aligned}$$

It is clear that the MAI resulting from the interfering users degrades the reliability of the matched filter detector output. The MAI is controlled by two factors, the cross-correlation coefficients between active users and the received amplitudes of different active users. The second factor is mainly due to the spread of users over a large area which results in a wide discrepancy in the received amplitudes of active users' signals. If strict power control is not used then weak users may lose communication because of the overwhelming MAI. This phenomenon is known as the *near-far effect*.

The conventional matched filter detector is optimum under white Gaussian noise conditions. Due to the well built structure of the MAI this assumption is not true, especially for short-code CDMA systems, and as such, the optimality of the conventional matched filter detector is lost. Moreover, its performance degrades greatly when the received powers of the interfering users are much greater than those of the desired users.

Verdu's pioneer work [30] showed that the near-far problem is not inherent to the CDMA system. In fact, it is due to the detection schemes. This reformulation of the problem launched a tremendous research, which is still active, to develop detection schemes that are able to combat shortcomings of the conventional receiver.

Before ending this section, let us go through a number of performance indicators of the conventional matched filter detector. The most important, which is the BER is given by [30]:

$$P_{k_{th}}(\sigma) = \frac{1}{2^{WK-1}} \sum_{\substack{\text{all } \mathbf{b} \\ \mathbf{b}(k_{eff})=1}} Q\left(\frac{\bar{\mathbf{s}}_{eff}^T(k_{eff}) \bar{\mathbf{R}}_{eff} \bar{\mathbf{A}}_{eff} \mathbf{b}}{\sigma}\right) \quad (6-3)$$

On the other hand, the multiuser efficiency is given by [30]:

$$\eta_{k_{eff}} = \max^2 \left\{ 0, 1 - \sum_{\substack{j=1 \\ j \neq k_{eff}}}^{WK} \frac{\bar{\mathbf{A}}_{eff}(j,j)}{\bar{\mathbf{A}}_{eff}(k_{eff},k_{eff})} |\bar{\mathbf{R}}_{eff}(j,k_{eff})| \right\} \quad (6-4)$$

It is obvious that if  $\bar{\mathbf{A}}_{eff}(k_{eff},k_{eff}) \leq \sum_{\substack{j=1 \\ j \neq k_{eff}}}^{WK} \bar{\mathbf{A}}_{eff}(j,j) |\bar{\mathbf{R}}_{eff}(j,k_{eff})|$  then  $\eta_{k_{eff}} = 0$ . Hence, the near-far

resistance of the matched filter detector is given by:

$$\bar{\eta}_{k_{eff}} = 0 \quad (6-5)$$

### 6.5.2 The Optimum Multiuser Detector

As mentioned earlier, the most important performance measure for communication systems is the BER. The multiuser detector that minimizes the BER is known as the *maximum a posteriori* (MAP) detector. It minimizes the following objective function [30]:

$$\mathbf{b}^* = \arg \min_{\mathbf{b} \in \{-1,1\}^{WK}} \left\{ -2\mathbf{b}^T \bar{\mathbf{A}}_{eff} \mathbf{y}_{MF}^b + \mathbf{b}^T \bar{\mathbf{A}}_{eff} \bar{\mathbf{R}}_{eff} \bar{\mathbf{A}}_{eff} \mathbf{b} \right\} \quad (6-6)$$

For the matched filter output  $\mathbf{y}_{MF}^b$  of each block  $b$ , the optimal detector performs an exhaustive search over all possible transmitted data sequences  $\mathbf{b}$  constrained to the set  $\{-1,1\}^{WK}$  to find the data sequence that minimizes the above objective function. This technique is the same as that used for single user systems with ISI, where the number of bits spanned by ISI is replaced in our case by the number of users. The number of possible sequences in an asynchronous CDMA system with a processing window of length  $W$  bits is  $2^{WK}$ , and hence the search space consists of  $2^{WK}$  possibilities.

It has been shown that this problem is an NP-hard [102], which means that there is no algorithm with a polynomial time complexity that can solve the above optimization problem. Therefore, the optimum detector is far too complex for practical implementation even for a moderate number of users.

The exponential complexity of the MAP detection has inspired a considerable effort over the past decade in the development of suboptimum receivers with low complexity and which are robust to the near-far problem. It is not possible to derive a closed-form analytical expression for the bit-error-rate or the multiuser efficiency of the optimum multiuser detector, however it is possible to derive a closed form expression for the near-far resistance and it is given by [30]:

$$\bar{\eta}_{k_{eff}} = \frac{1}{\bar{\mathbf{R}}_{eff}^{-1}(k_{eff}, k_{eff})} \quad (6-7)$$

### 6.5.3 The Decorrelator Detector

This approach operates to eliminate MAI in the same manner analogous to the way the zero forcing equalizer mitigates ISI. The linear transformation applied is the inverse of the effective cross-correlation matrix  $T = \mathbf{V} = \bar{\mathbf{R}}_{eff}^{-1}$ . The decorrelator detector's output is given by:

$$\mathbf{y}_{DEC}^b = \bar{\mathbf{R}}_{eff}^{-1} \mathbf{y}_{MF}^b = \bar{\mathbf{A}}_{eff} \bar{\mathbf{b}}^b + \bar{\mathbf{R}}_{eff}^{-1} \bar{\mathbf{z}}_{eff}^b \quad (6-8)$$

From an optimization point of view, the decorrelator detector is the least square solution to the maximum likelihood sequence detection if the constraint on the vector  $\mathbf{b}$  is relaxed to span all values in  $\mathbb{R}^{WK}$  [30], that is:

$$\mathbf{b}^* = \arg \min_{\mathbf{b} \in \mathbb{R}^{W_K}} \left\{ \left( \mathbf{y}_{MF}^b - \bar{\mathbf{R}}_{eff} \bar{\mathbf{A}}_{eff} \mathbf{b} \right)^T \bar{\mathbf{R}}_{eff}^{-1} \left( \mathbf{y}_{MF}^b - \bar{\mathbf{R}}_{eff} \bar{\mathbf{A}}_{eff} \mathbf{b} \right) \right\} \quad (6-9)$$

or equivalently:

$$\mathbf{b}^* = \arg \min_{\mathbf{b} \in \mathbb{R}^{W_K}} \left\{ \left\| \mathbf{q}_b - \bar{\mathbf{S}}_{eff} \bar{\mathbf{A}}_{eff} \mathbf{b} \right\|^2 \right\}$$

which reduces to:

$$\mathbf{b}^* = \arg \min_{\mathbf{b} \in \mathbb{R}^{W_K}} \left\{ -2\mathbf{b}^T \bar{\mathbf{A}}_{eff} \mathbf{y}_{MF}^b + \mathbf{b}^T \bar{\mathbf{A}}_{eff} \bar{\mathbf{R}}_{eff} \bar{\mathbf{A}}_{eff} \mathbf{b} \right\} \quad (6-10)$$

By taking the derivative of the above objective function and equating it to zero, we get:

$$2\bar{\mathbf{A}}_{eff} \bar{\mathbf{R}}_{eff} \bar{\mathbf{A}}_{eff} \mathbf{b} = 2\bar{\mathbf{A}}_{eff} \mathbf{y}_{MF}^b$$

and finally we obtain:

$$\begin{aligned} \mathbf{b}^* &= \bar{\mathbf{A}}_{eff}^{-1} \bar{\mathbf{R}}_{eff}^{-1} \mathbf{y}_{MF}^b \\ &= \bar{\mathbf{R}}_{eff}^{-1} \mathbf{y}_{MF}^b \end{aligned} \quad (6-11)$$

where the term  $\bar{\mathbf{A}}_{eff}^{-1}$  is omitted due to the fact that it is a positive scaling diagonal matrix and doesn't affect the decision statistics. The decorrelating detector eliminates MAI completely; however, the receiver considerably enhances the noise in the system. This can be verified by examining the covariance matrix of the noise vector at the output of the decorrelator detector, that is:

$$\begin{aligned} E \left[ \left( \bar{\mathbf{R}}_{eff}^{-1} \bar{\mathbf{z}}_{eff}^b \right) \left( \bar{\mathbf{R}}_{eff}^{-1} \bar{\mathbf{z}}_{eff}^b \right)^T \right] &= E \left[ \bar{\mathbf{R}}_{eff}^{-1} \bar{\mathbf{z}}_{eff}^b \left( \bar{\mathbf{z}}_{eff}^b \right)^T \bar{\mathbf{R}}_{eff}^{-1} \right] \\ &= \bar{\mathbf{R}}_{eff}^{-1} \sigma^2 \bar{\mathbf{R}}_{eff} \bar{\mathbf{R}}_{eff}^{-1} \\ &= \sigma^2 \bar{\mathbf{R}}_{eff}^{-1} \end{aligned} \quad (6-12)$$

and since the cross-correlation elements are less than one, then  $\bar{\mathbf{R}}_{eff}^{-1}(k_{eff}, k_{eff})$  is larger than 1 [103] hence the decorrelator detector enhances noise. Consequently the probability of error of the decorrelator detector of the  $k^{th}$  effective user is [30]:

$$P_{k_{eff}}(\sigma) = Q \left( \frac{\bar{\mathbf{A}}_{eff}(k_{eff}, k_{eff})}{\sigma \sqrt{\bar{\mathbf{R}}_{eff}^{-1}(k_{eff}, k_{eff})}} \right) \quad (6-13)$$

The AME of the decorrelator detector is given by [30]:

$$\eta_{k_{eff}} = \frac{1}{\bar{\mathbf{R}}_{eff}^{-1}(k_{eff}, k_{eff})} \quad (6-14)$$

which does not depend on the amplitudes of the interfering signals, and thus the near-far resistance equals the asymptotic multiuser efficiency and it is given by:

$$\bar{\eta}_{k_{eff}} = \frac{1}{\bar{\mathbf{R}}_{eff}^{-1}(k_{eff}, k_{eff})} \quad (6-15)$$

The decorrelating detector has several desirable features. It does not require the knowledge of signals' amplitudes of active users, and thus its performance is independent of the amplitudes of the interfering users. In addition, since the decorrelator detector is near-far resistant it is well suited for the near-far environment ([91], [104]).

#### 6.5.4 The Linear Minimum Mean Square Error (LMMSE) Detector

The decorrelator detector works on the principle of channel inversion and, consequently, leads to poor BER performance at low SNRs [31]. This is because the decorrelator simply eliminates MAI without taking in consideration the AWGN, which results in noise enhancement in the detector's output. Minimizing the mean square error is another approach to linear multiuser detection. The resultant detector, which is known as the LMMSE multiuser detector, performs better than the decorrelator at low and moderate SNRs because it accounts for AWGN [105].

The LMMSE transformation is given by:  $T = \mathbf{V} = (\bar{\mathbf{R}}_{eff} + \sigma^2 \bar{\mathbf{A}}_{eff}^{-2})^{-1}$ . It was shown that the LMMSE detector is the solution of the following optimization problem [30]:

$$\arg \min_{\mathbf{V} \in \mathbb{R}^{W_K \times W_K}} \left\{ \left\| \bar{\mathbf{b}}^b - \mathbf{V} \mathbf{y}_{MF}^b \right\|^2 \right\} \quad (6-16)$$

Unlike the decorrelator detector, the LMMSE detector requires the estimation of the SNR of each user, thus adding some computational complexity. If  $(\bar{\mathbf{R}}_{eff} + \sigma^2 \bar{\mathbf{A}}_{eff}^{-2})^{-1}(:, j)$  is the  $j^{th}$  column of the transformation matrix  $(\bar{\mathbf{R}}_{eff} + \sigma^2 \bar{\mathbf{A}}_{eff}^{-2})^{-1}$  (we are using matlab notation for the column of a matrix), then the bit error probability of the LMMSE detector for  $k^{th}$  effective user is given by [30]:

$$P_{k_{eff}}(\sigma) = \frac{1}{2^{W_K - 1}} \sum_{\substack{\text{all } \mathbf{b} \\ \mathbf{b}(k_{eff})=1}} \mathcal{Q} \left( \frac{\left( (\bar{\mathbf{R}}_{eff} + \sigma^2 \bar{\mathbf{A}}_{eff}^{-2})^{-1}(:, k_{eff}) \right)^T \bar{\mathbf{R}}_{eff} \bar{\mathbf{A}}_{eff} \mathbf{b}}{\sigma \sqrt{\left( (\bar{\mathbf{R}}_{eff} + \sigma^2 \bar{\mathbf{A}}_{eff}^{-2})^{-1}(:, k_{eff}) \right)^T \bar{\mathbf{R}}_{eff} (\bar{\mathbf{R}}_{eff} + \sigma^2 \bar{\mathbf{A}}_{eff}^{-2})^{-1}(:, k_{eff})}} \right) \quad (6-17)$$

For the AME and near-far resistance, since the LMMSE detector reduces to the decorrelator detector when the noise level vanishes to zero, then the LMMSE detector exhibits the same AME and near-far resistance as the decorrelator detector, that is, the AME of the LMMSE detector is given by [30]:

$$\eta_{k_{eff}} = \frac{1}{\overline{\mathbf{R}}_{eff}^{-1}(k_{eff}, k_{eff})} \quad (6-18)$$

which does not depend on the amplitudes of the interfering signals thus the near-far resistance equals the asymptotic multiuser efficiency and it is given by [30]:

$$\bar{\eta}_{k_{eff}} = \frac{1}{\overline{\mathbf{R}}_{eff}^{-1}(k_{eff}, k_{eff})} \quad (6-19)$$

Since the LMMSE detector enjoys the same interference rejection capabilities as the decorrelator detector (they have the same near-far resistance), the LMMSE detector is also suitable for near-far environments.

### 6.6 Multiuser Detection Structures for Asynchronous CDMA Multipath Fading Channel

As for the case of AWGN channel, the transformation  $T$  applied to either the received chip-matched signal  $\mathbf{q}_b$  (Figure 6.4) or to the vector of Rake receivers' outputs  $\mathbf{y}_{MRC}^b$  (Figure 6.5) can be linear, nonlinear...

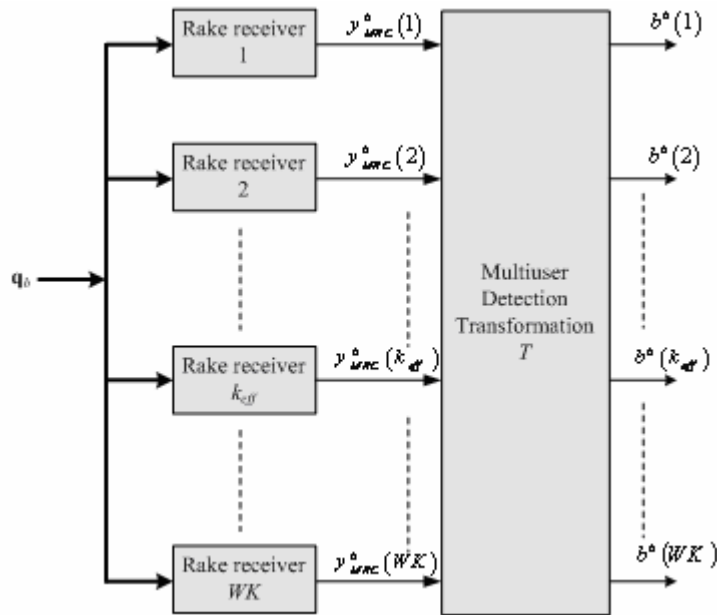


Figure 6.4: Multi-user detection Receiver acting on the vector of Rake receivers outputs.

Finally, here as well, multiuser detectors acting on the vector of matched filter outputs usually make use of the cross-correlation coefficients and consequently the cross-correlation matrix needs to be calculated.

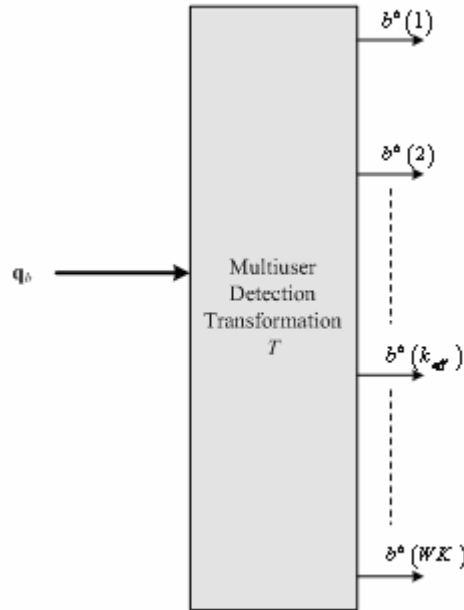


Figure 6.5: Multi-user detection acting on the received signal.

### 6.6.1 The Conventional Rake Receiver

Diversity is a powerful technique for alleviating the effects of fading environments. Diversity techniques make use of multiple, independent signal paths between the transmitter and the receiver to improve the detector's performance. Most common forms of diversity reception are spatial (using multiple antennas), temporal (data interleaving with coding), and frequency (DS or FH spread spectrum).

DS-CDMA systems are well-matched for diversity reception because for frequency selective fading, the signal bandwidth is much greater than the coherence bandwidth of the channel. As such, multi-path components with delays greater than one chip period are resolvable and independent of each other. In fact, multi-path resolution and combining is one of the major advantages of DS-CDMA system over other multi-access wireless communication systems.

The most prominent diversity combining scheme is known as the RAKE receiver and was first introduced by Price and Green in 1958 [106]. The RAKE receiver is composed of several fingers each of which consists of a matched filter detector. The matched filter detectors' outputs are weighted and combined to form a single decision statistic. In order to constructively add these components, the phase must be known. The resolution of the RAKE (i.e., its ability to resolve separate multi-paths) is dependent on the chip rate of the system. To be resolved by the Rake receiver, the multi-path components should be separated by at least one chip period. Figure 6.6 shows a generic RAKE receiver and Figure 6.7 shows a bank of Rake receivers for a multiuser environment. It is important to mention that the Rake receiver exploits frequency diversity provided by the system but it doesn't remove ISI, therefore if the latter is significant the performance of the Rake receiver degrades considerably and an equalizer should be used instead.

There are several methods for choosing the combining weights [107]: The maximal ratio combining technique (MRC) phase shifts and weights each multi-path component according to its relative SNR before coherent signal combining. This method is most appropriate in situations where phase changes of individual multi-path components vary slowly enough to be accurately estimated and tracked. In terms of implementation complexity, MRC requires a data path (finger) for each multi-path component, channel estimation blocks, and signal combining blocks. The equal gain combining (EGC) technique on the other hand, weights all multi-path components equally. Yet it is a simpler, though suboptimal combining alternative. In a selection diversity system, the receiver simply selects the strongest multi-path component, and uses it for signal detection. A major benefit of this approach is that multiple data paths are not required although additional hardware is required to distinguish the strongest path.

Unlike the simple matched filter detector in the AWGN channel, the implementation of the RAKE receiver requires channel coefficient estimation, which leads to additional computational complexity burden.

In our work, the Rake (MRC) receiver is easily implemented by despreading the received signal using the matrix of effective spreading codes developed in Chapter 4, that is:

$$\mathbf{y}_{MRC}^b = \left( \bar{\mathbf{S}}_{eff}^b \right)^H \mathbf{q}_b = \left( \bar{\mathbf{S}}_{eff}^b \right)^H \left( \bar{\mathbf{S}}_{eff}^b \bar{\mathbf{A}}_{eff} \bar{\mathbf{b}}^b + \bar{\mathbf{n}}_{eff}^b \right) = \bar{\mathbf{R}}_{eff}^b \bar{\mathbf{A}}_{eff} \bar{\mathbf{b}}^b + \bar{\mathbf{z}}_{eff}^b \quad (6-20)$$

where  $\bar{\mathbf{S}}_{eff}^b$ ,  $\bar{\mathbf{A}}_{eff}$ ,  $\bar{\mathbf{b}}^b$  are defined in Chapter 4,  $\bar{\mathbf{n}}_{eff}^b$  is the  $b^{th}$  block of the vector  $\bar{\mathbf{n}}$  defined in Chapter 4, with dimension  $\{(NW + \max_{1 \leq k \leq K} (\tau^k) + \max_{1 \leq l_k \leq L_k} (\tau_{l_k})) - by - 1\}$ .

$\bar{\mathbf{z}}_{eff}^b$  is the vector of additive colored Gaussian noise samples with covariance matrix given by:

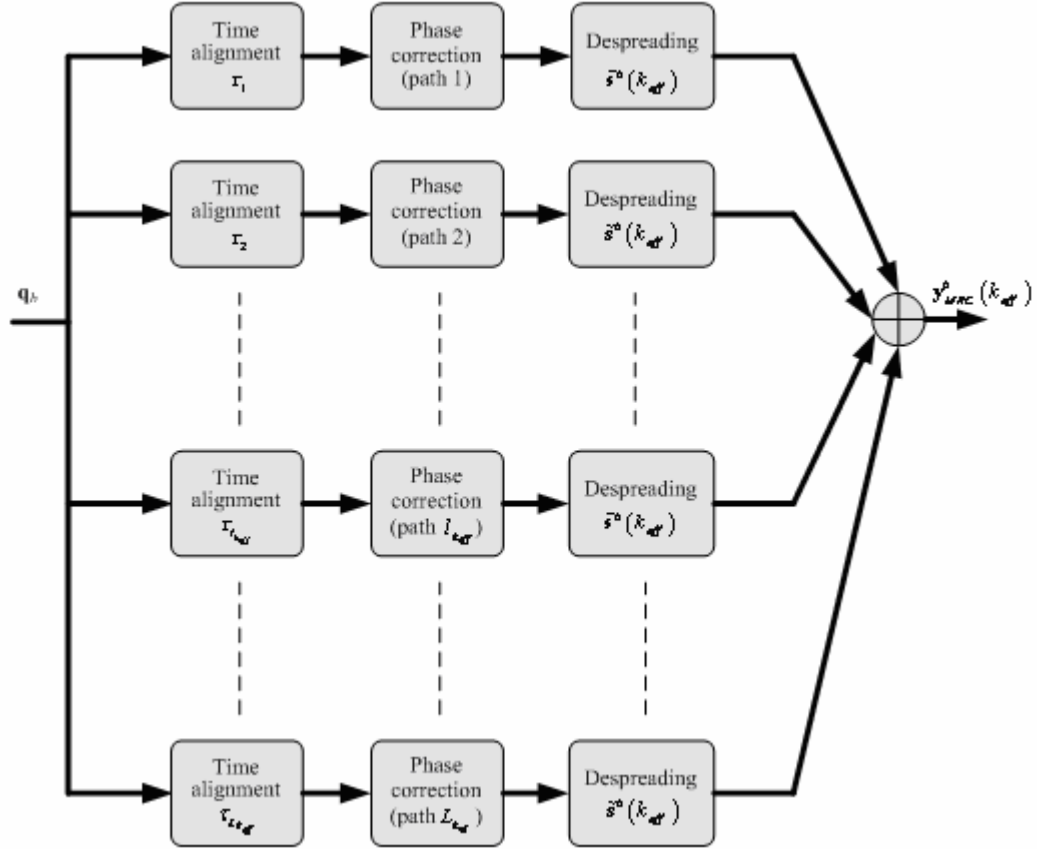


Figure 6.6: MRC Rake receiver

$$\begin{aligned}
 E \left[ \left( (\bar{\mathbf{S}}_{eff}^b)^H \bar{\mathbf{n}}_{eff}^b \right) \left( (\bar{\mathbf{S}}_{eff}^b)^H \bar{\mathbf{n}}_{eff}^b \right)^H \right] &= E \left[ (\bar{\mathbf{S}}_{eff}^b)^H \bar{\mathbf{n}}_{eff}^b (\bar{\mathbf{n}}_{eff}^b)^H \bar{\mathbf{S}}_{eff}^b \right] \\
 &= \sigma^2 (\bar{\mathbf{S}}_{eff}^b)^H \bar{\mathbf{S}}_{eff}^b \\
 &= \sigma^2 \bar{\mathbf{R}}_{eff}^b
 \end{aligned} \tag{6-21}$$

Consequently, the probability of error of the MRC Rake receiver for the  $k^{th}$  effective user conditioned on  $\bar{\mathbf{s}}_{eff}^b(k_{eff})^H \bar{\mathbf{S}}_{eff}^b$  is given by:

$$P_{k_{eff} | \bar{\mathbf{s}}_{eff}^b(k_{eff})^H \bar{\mathbf{S}}_{eff}^b}(\sigma) = \frac{1}{2^{WK-1}} \sum_{\substack{\text{all } \mathbf{b} \\ \mathbf{b}(k_{eff})=1}} Q \left( \frac{\bar{\mathbf{s}}_{eff}^b(k_{eff})^H \bar{\mathbf{S}}_{eff}^b \bar{\mathbf{A}}_{eff} \mathbf{b}}{\sigma \sqrt{\bar{\mathbf{R}}_{eff}^b(k_{eff}, k_{eff})}} \right) \quad (6-22)$$

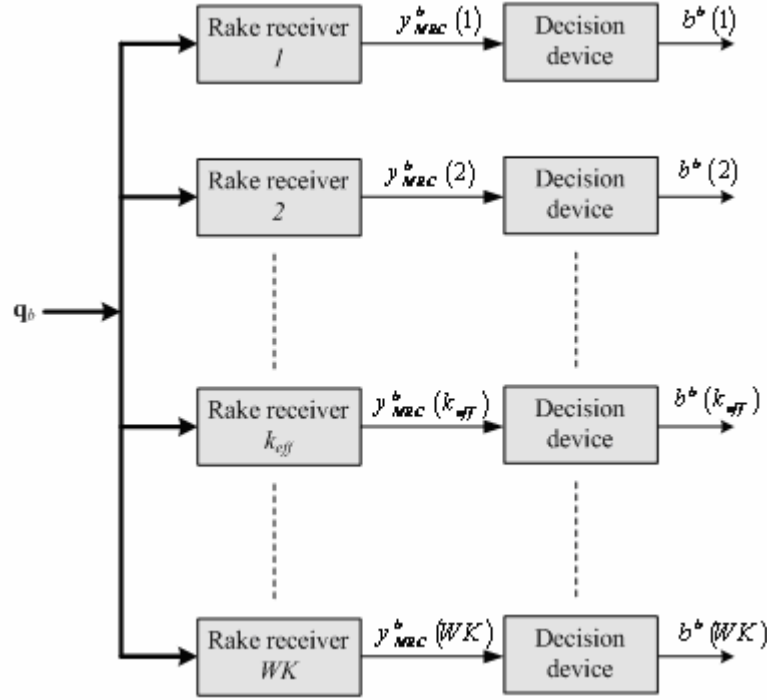


Figure 6.7: Conventional bank of Rake receivers.

Taking the expectation over possible values of the vector  $\bar{\mathbf{s}}_{eff}^b(k_{eff})^H \bar{\mathbf{S}}_{eff}^b$  results in:

$$P_{k_{eff}}(\sigma) = \int_0^\infty \int_0^\infty \dots \int_0^\infty pdf \left( \bar{\mathbf{s}}_{eff}^b(1)^H \bar{\mathbf{S}}_{eff}^b \right) \dots pdf \left( \bar{\mathbf{s}}_{eff}^b(WK)^H \bar{\mathbf{S}}_{eff}^b \right) P_{k_{eff} | \bar{\mathbf{s}}_{eff}^b(k_{eff})^H \bar{\mathbf{S}}_{eff}^b}(\sigma) \\ d \left( \bar{\mathbf{s}}_{eff}^b(1)^H \bar{\mathbf{S}}_{eff}^b \right) \dots d \left( \bar{\mathbf{s}}_{eff}^b(WK)^H \bar{\mathbf{S}}_{eff}^b \right)$$

where *pdf* stands for probability density function.

The evaluation of this  $WK$  multiple integral expression is very intensive and can be assessed only numerically. For this reason, the probability of error will be evaluated only by simulation. Since the multiuser efficiency depends on the BER in its derivation, it is also not straightforward to determine a closed form expression for the AME of the MRC Rake receiver. Hence, we refer to simulation to assess the performance of the MRC rake receiver. As for the matched filter detector, the

Rake receiver treats MAI as additive white Gaussian noise (AWGN), which is not the optimal approach since its structure is well defined through the cross-correlation matrix, and therefore can be exploited to achieve better performance results. Hence, the Rake receiver suffers from the same shortcomings of the matched filter detector, such as the near-far problem.

### 6.6.2 The Optimal Multiuser Detector

As for the AWGN channel, the optimum multiuser detector is the solution to the following objective function:

$$\mathbf{b}^* = \arg \min_{\mathbf{b} \in \{-1,1\}^{WK}} \left\{ -2\Re(\mathbf{b}^T \bar{\mathbf{A}}_{eff} \mathbf{y}_{MRC}^b) + \mathbf{b}^T \bar{\mathbf{A}}_{eff} \bar{\bar{\mathbf{R}}}_{eff}^b \bar{\mathbf{A}}_{eff} \mathbf{b} \right\} \quad (6-23)$$

where  $\mathbf{y}_{MRC}^b$  is the vector of the Rake receivers' outputs. The complexity of such detector is also of the order of  $2^{WK}$ , where  $K$  is the number of users and  $W$  is the number of bits within the sliding detection window. Hence it is an NP-hard problem [102].

As for the asynchronous CDMA AWGN channel, there is no analytical closed-form expression for the BER of the optimal multiuser detector. And since the AME relies on the derivation of the BER, it is difficult to obtain a closed form expression for the AME and hence we assess it through simulation only.

### 6.6.3 The Decorrelator Detector

The linear transformation applied is the inverse of the effective cross-correlation matrix  $T = \mathbf{V} = \left( \bar{\bar{\mathbf{R}}}_{eff}^b \right)^{-1}$ . The decorrelator's outputs are given by:

$$\mathbf{y}_{DEC}^b = \left( \bar{\bar{\mathbf{R}}}_{eff}^b \right)^{-1} \mathbf{y}_{MF}^b = \bar{\mathbf{A}}_{eff} \bar{\mathbf{b}}^b + \left( \bar{\bar{\mathbf{R}}}_{eff}^b \right)^{-1} \bar{\mathbf{z}}_{eff}^b \quad (6-24)$$

The decorrelating detector eliminates MAI+ISI within the detection window completely; nevertheless the receiver significantly enhances the noise in the system [103]. The probability of error of the decorrelator detector of the  $k^{th}$  effective user conditioned on  $\left( \bar{\bar{\mathbf{R}}}_{eff}^b \right)^{-1} (k_{eff}, k_{eff})$  is:

$$P_{k_{eff} | \left( \bar{\bar{\mathbf{R}}}_{eff}^b \right)^{-1} (k_{eff}, k_{eff})}(\sigma) = Q \left( \frac{\bar{\mathbf{A}}_{eff} (k_{eff}, k_{eff})}{\sigma \sqrt{\left( \bar{\bar{\mathbf{R}}}_{eff}^b \right)^{-1} (k_{eff}, k_{eff})}} \right) \quad (6-25)$$

Taking the expectation of the previous expression over all possible values of  $\left(\bar{\mathbf{R}}_{eff}^b\right)^{-1}(k_{eff}, k_{eff})$  yields:

$$P_{k_{eff}}(\sigma) = E \left( P_{k_{eff} | \left(\bar{\mathbf{R}}_{eff}^b\right)^{-1}(k_{eff}, k_{eff})}(\sigma) \int_0^\infty \left( \begin{array}{l} pdf \left( \left(\bar{\mathbf{R}}_{eff}^b\right)^{-1}(k_{eff}, k_{eff}) \right) P_{k_{eff} | \left(\bar{\mathbf{R}}_{eff}^b\right)^{-1}(k_{eff}, k_{eff})}(\sigma) \\ d \left(\bar{\mathbf{R}}_{eff}^b\right)^{-1}(k_{eff}, k_{eff}) \end{array} \right) \right)$$

The probability density function (pdf) of  $\left(\bar{\mathbf{R}}_{eff}^b\right)^{-1}(k_{eff}, k_{eff})$  is not straightforward to evaluate and hence we refer to simulation to evaluate the BER of the decorrelator detector.

#### 6.6.4 The Linear Minimum Mean Square Error (LMMSE) Detector

The LMMSE transformation is given by:  $T = \mathbf{V} = \left(\bar{\mathbf{R}}_{eff}^b + \sigma^2 \bar{\mathbf{A}}_{eff}^{-2}\right)^{-1}$ . Following the same approach as for the matched filter detector, the probability of bit error of the LMMSE detector for  $k^{th}$  effective user conditioned on  $\left(\left(\bar{\mathbf{R}}_{eff}^b + \sigma^2 \bar{\mathbf{A}}_{eff}^{-2}\right)^{-1}(:, k_{eff})\right)^T \bar{\mathbf{R}}_{eff}^b$  is given by:

$$P_{k_{eff} | \left(\left(\bar{\mathbf{R}}_{eff}^b + \sigma^2 \bar{\mathbf{A}}_{eff}^{-2}\right)^{-1}(:, k_{eff})\right)^T \bar{\mathbf{R}}_{eff}^b}(\sigma) = \frac{1}{2^{WK-1}} \times \sum_{\substack{all \mathbf{b} \\ \mathbf{b}(k_{eff})=1}} Q \left( \frac{\left(\left(\bar{\mathbf{R}}_{eff}^b + \sigma^2 \bar{\mathbf{A}}_{eff}^{-2}\right)^{-1}(:, k_{eff})\right)^T \bar{\mathbf{R}}_{eff}^b \bar{\mathbf{A}}_{eff} \mathbf{b}}{\sigma \sqrt{\left(\left(\bar{\mathbf{R}}_{eff}^b + \sigma^2 \bar{\mathbf{A}}_{eff}^{-2}\right)^{-1}(:, k_{eff})\right)^T \bar{\mathbf{R}}_{eff}^b \left(\bar{\mathbf{R}}_{eff}^b + \sigma^2 \bar{\mathbf{A}}_{eff}^{-2}\right)^{-1}(:, k_{eff})}} \right) \quad (6-26)$$

where:  $\left(\bar{\mathbf{R}}_{eff}^b + \sigma^2 \bar{\mathbf{A}}_{eff}^{-2}\right)^{-1}(:, j)$  is the  $j^{th}$  column of the transformation matrix  $\left(\bar{\mathbf{R}}_{eff}^b + \sigma^2 \bar{\mathbf{A}}_{eff}^{-2}\right)^{-1}$ . Taking the expectation over possible values of the vector  $\left(\left(\bar{\mathbf{R}}_{eff}^b + \sigma^2 \bar{\mathbf{A}}_{eff}^{-2}\right)^{-1}(:, k_{eff})\right)^T \bar{\mathbf{R}}_{eff}^b$  results in:

$$P_{k_{eff}}(\sigma) = \int_0^\infty \int_0^\infty \dots \int_0^\infty \left\{ \begin{aligned} & pdf \left( \left( \left( \bar{\mathbf{R}}_{eff}^b + \sigma^2 \bar{\mathbf{A}}_{eff}^{-2} \right)^{-1}(:,1) \right)^T \bar{\mathbf{R}}_{eff}^b \right) \dots \\ & pdf \left( \left( \left( \bar{\mathbf{R}}_{eff}^b + \sigma^2 \bar{\mathbf{A}}_{eff}^{-2} \right)^{-1}(:,WK) \right)^T \bar{\mathbf{R}}_{eff}^b \right) P_{k_{eff}} \left( \left( \bar{\mathbf{R}}_{eff}^b + \sigma^2 \bar{\mathbf{A}}_{eff}^{-2} \right)^{-1}(:,k_{eff}) \right)^T \bar{\mathbf{R}}_{eff}^b(\sigma) \\ & d \left( \left( \left( \bar{\mathbf{R}}_{eff}^b + \sigma^2 \bar{\mathbf{A}}_{eff}^{-2} \right)^{-1}(:,1) \right)^T \bar{\mathbf{R}}_{eff}^b \right) \dots d \left( \left( \left( \bar{\mathbf{R}}_{eff}^b + \sigma^2 \bar{\mathbf{A}}_{eff}^{-2} \right)^{-1}(:,WK) \right)^T \bar{\mathbf{R}}_{eff}^b \right) \end{aligned} \right\}.$$

The evaluation of this WK multiple integral expression is very intensive and can be assessed only numerically. For this reason, the probability of error will be evaluated only by simulation.

## 6.7 The Linear Transformation of the Received Signal

In this section we derive the BER, AME and near-far resistance of a general linear detector applied to the received signal  $\mathbf{q}_b$ .

### 6.7.1 The Linear Transformation of the Received Signal for AWGN Channel

Suppose that  $\mathbf{q}_b$  is multiplied by a linear transformation matrix  $\mathbf{V}^T$  of dimension  $\{(WN + \max_{1 \leq k \leq K} (\tau^k)) - by - WK\}$ . The output of this detector is given by:

$$\mathbf{y}_V^b = \mathbf{V}^T \mathbf{q}_b = \mathbf{V}^T \bar{\mathbf{S}}_{eff} \bar{\mathbf{A}}_{eff} \bar{\mathbf{b}}^b + \mathbf{V}^T \bar{\mathbf{n}}_{eff}^b \quad (6-27)$$

The noise vector now is an additive colored Gaussian noise with covariance matrix:

$$\begin{aligned} E \left[ (\mathbf{V}^T \bar{\mathbf{n}}_{eff}^b) (\mathbf{V}^T \bar{\mathbf{n}}_{eff}^b)^T \right] &= E \left[ \mathbf{V}^T \bar{\mathbf{n}}_{eff}^b (\bar{\mathbf{n}}_{eff}^b)^T \mathbf{V} \right] \\ &= \sigma^2 \mathbf{V}^T \mathbf{V} \end{aligned} \quad (6-28)$$

Thus the BER of the general linear detector applied to the received signal  $\mathbf{q}_b$  for the  $k^{th}$  effective user is given by:

$$P_{k_{eff}}(\sigma) = \frac{1}{2^{WK-1}} \sum_{\substack{\text{all } \mathbf{b} \\ \mathbf{b}(k_{eff})=1}} Q \left( \frac{\mathbf{V}(:,k_{eff})^T \bar{\mathbf{S}}_{eff} \bar{\mathbf{A}}_{eff} \mathbf{b}}{\sigma \sqrt{\mathbf{V}(:,k_{eff})^T \mathbf{V}(:,k_{eff})}} \right) \quad (6-29)$$

where  $\mathbf{V}(:,j)$  is the  $j^{th}$  column of the matrix  $\mathbf{V}$ . The multiuser efficiency is given by:

$$\eta_{k_{eff}} = \frac{1}{\mathbf{V}(:,k_{eff})^T \mathbf{V}(:,k_{eff})} \max^2 \left\{ \begin{aligned} & 0, \mathbf{V}(:,k_{eff})^T \bar{\mathbf{s}}_{eff}(k_{eff}) \\ & - \sum_{\substack{j=1 \\ j \neq k_{eff}}}^{WK} \frac{\bar{\mathbf{A}}_{eff}(j,j)}{\bar{\mathbf{A}}_{eff}(k_{eff},k_{eff})} \left| \mathbf{V}(:,k_{eff})^T \bar{\mathbf{s}}_{eff}(j) \right| \end{aligned} \right\} \quad (6-30)$$

where  $\mathbf{V}(:,j)$  is the  $j^{th}$  column of the matrix  $\mathbf{V}$ .

The near-far resistance of general linear detector applied to the received signal  $\mathbf{q}_b$  for the  $k^{\text{th}}$  effective user is given by:

$$\bar{\eta}_{k_{\text{eff}}} = \begin{cases} 0 & \text{if } \lim_{\sigma \rightarrow 0} \mathbf{V}^T \bar{\mathbf{S}}_{\text{eff}} \neq \mathbf{I} \\ \frac{1}{\mathbf{V}(:, k_{\text{eff}})^T \mathbf{V}(:, k_{\text{eff}})} & \text{if } \lim_{\sigma \rightarrow 0} \mathbf{V}^T \bar{\mathbf{S}}_{\text{eff}} = \mathbf{I} \end{cases} \quad (6-31)$$

The derivation of the BER and AME is detailed in Appendices A and B, respectively.

### 6.7.2 The Linear Transformation of the Received Signal for Multipath Fading Channel

Suppose that  $\mathbf{q}_b$  is multiplied by a linear transformation matrix  $\mathbf{V}^H$  of dimension  $\{(WN + \max_{1 \leq l_k \leq L_k} (\tau_{l_k}) + \max_{1 \leq k \leq K} (\tau^k)) - by - WK\}$ . The output of this detector is given by:

$$\mathbf{y}_V^b = \mathbf{V}^H \mathbf{q}_b = \mathbf{V}^H \bar{\mathbf{S}}_{\text{eff}}^b \bar{\mathbf{A}}_{\text{eff}} \bar{\mathbf{b}}^b + \mathbf{V}^H \bar{\mathbf{n}}_{\text{eff}}^b \quad (6-32)$$

The noise vector now is additive colored Gaussian noise with covariance matrix:

$$\begin{aligned} E \left[ (\mathbf{V}^H \bar{\mathbf{n}}_{\text{eff}}^b) (\mathbf{V}^H \bar{\mathbf{n}}_{\text{eff}}^b)^T \right] &= E \left[ \mathbf{V}^H \bar{\mathbf{n}}_{\text{eff}}^b (\bar{\mathbf{n}}_{\text{eff}}^b)^T \mathbf{V} \right] \\ &= \sigma^2 \mathbf{V}^H \mathbf{V} \end{aligned} \quad (6-33)$$

Hence, the BER of the  $k^{\text{th}}$  user at the  $w^{\text{th}}$  bit of the  $b^{\text{th}}$  block at the output of the transformation matrix conditioned on the vector  $\mathbf{V}(:, k_{\text{eff}})^H \bar{\mathbf{S}}_{\text{eff}}^b$  is:

$$P_{k_{\text{eff}} | \mathbf{V}(:, k_{\text{eff}})^H \bar{\mathbf{S}}_{\text{eff}}^b}(\sigma) = \frac{1}{2^{WK-1}} \sum_{\substack{\text{all } \mathbf{b} \\ \mathbf{b}(k_{\text{eff}})=1}} \mathcal{Q} \left( \frac{\mathbf{V}(:, k_{\text{eff}})^H \bar{\mathbf{S}}_{\text{eff}}^b \bar{\mathbf{A}}_{\text{eff}} \mathbf{b}}{\sigma \sqrt{\mathbf{V}(:, k_{\text{eff}})^H \mathbf{V}(:, k_{\text{eff}})}} \right) \quad (6-34)$$

Obtaining the average BER and AME requires taking the expectation over all possible values of the vector  $\mathbf{V}(:, k_{\text{eff}})^H \bar{\mathbf{S}}_{\text{eff}}^b$ . This results in a  $WK$  multiple integral expression, which is very intensive and can be evaluated only numerically. For this reason, the BER and the AME will be evaluated only by simulation.

### 6.8 The Linear Transformation of the Matched Filters/Rake Receivers' Outputs

In this section, we derive the BER, AME and near-far resistance of the general linear detector applied to the matched filters/Rake receivers' outputs  $\mathbf{y}_{MF}^b / \mathbf{y}_{MRC}^b$ .

### 6.8.1 The Linear Transformation of the Matched Filters' Outputs

Suppose that  $\mathbf{y}_{MF}^b$  is multiplied by a linear transformation matrix  $\mathbf{V}^T$  of dimension  $\{(WK\text{-by-}WK)\}$ . The output of this detector is given by:

$$\mathbf{y}_V^b = \mathbf{V}^T \mathbf{y}_{MF}^b = \mathbf{V}^T \bar{\mathbf{R}}_{eff} \bar{\mathbf{A}}_{eff} \bar{\mathbf{b}}^b + \mathbf{V}^T \bar{\mathbf{z}}_{eff}^b \quad (6-35)$$

The noise vector now is additive colored Gaussian noise with covariance matrix:

$$\begin{aligned} E \left[ (\mathbf{V} \bar{\mathbf{S}}_{eff}^T \bar{\mathbf{n}}_{eff}^b) (\mathbf{V} \bar{\mathbf{S}}_{eff}^T \bar{\mathbf{n}}_{eff}^b)^T \right] &= E \left[ \mathbf{V} \bar{\mathbf{S}}_{eff}^T \bar{\mathbf{n}}_{eff}^b (\bar{\mathbf{n}}_{eff}^b)^T \bar{\mathbf{S}}_{eff} \mathbf{V}^T \right] \\ &= \sigma^2 \mathbf{V}^T \bar{\mathbf{R}}_{eff} \mathbf{V} \end{aligned} \quad (6-36)$$

Consequently, the BER of the general linear detector applied to the bank of matched filters' outputs for the  $k^{th}$  effective user is given by:

$$P_{k_{eff}}(\sigma) = \frac{1}{2^{WK-1}} \sum_{\substack{all \mathbf{b} \\ \mathbf{b}(k_{eff})=1}} Q \left( \frac{\mathbf{V}(:,k_{eff})^T \bar{\mathbf{R}}_{eff} \bar{\mathbf{A}}_{eff} \mathbf{b}}{\sigma \sqrt{\mathbf{V}(:,k_{eff})^T \bar{\mathbf{R}}_{eff} \mathbf{V}(:,k_{eff})}} \right) \quad (6-37)$$

where  $\mathbf{V}(:,j)$  is the  $j^{th}$  column of the matrix  $\mathbf{V}$ . The multiuser efficiency is given by:

$$\eta_{k_{eff}} = \frac{1}{\mathbf{V}(:,k_{eff})^T \bar{\mathbf{R}}_{eff} \mathbf{V}(:,k_{eff})} \max^2 \left\{ \begin{array}{l} 0, \mathbf{V}(:,k_{eff})^T \bar{\mathbf{R}}_{eff}(:,k_{eff}) \\ - \sum_{\substack{j=1 \\ j \neq k_{eff}}}^{WK} \frac{\bar{\mathbf{A}}_{eff}(j,j)}{\bar{\mathbf{A}}_{eff}(k_{eff},k_{eff})} \left| \mathbf{V}(:,k_{eff})^T \bar{\mathbf{R}}_{eff}(:,j) \right| \end{array} \right\} \quad (6-38)$$

where  $\bar{\mathbf{R}}_{eff}(:,j)$  is the  $j^{th}$  column of the matrix  $\bar{\mathbf{R}}_{eff}$ . The near-far resistance of the general linear detector is given by:

$$\bar{\eta}_{k_{eff}} = \begin{cases} 0 & \text{if } \lim_{\sigma \rightarrow 0} \mathbf{V}^T \bar{\mathbf{S}}_{eff} \neq \mathbf{I} \\ \frac{1}{\mathbf{V}(:,k_{eff})^T \bar{\mathbf{R}}_{eff} \mathbf{V}(:,k_{eff})} & \text{if } \lim_{\sigma \rightarrow 0} \mathbf{V}^T \bar{\mathbf{S}}_{eff} = \mathbf{I} \end{cases} \quad (6-39)$$

The detailed derivation of the BER and AME can be found in Appendices A and B, respectively.

### 6.8.2 The Linear Transformation of the Rake Receivers' Outputs

Suppose that  $\mathbf{y}_{MRC}^b$  is multiplied by a linear transformation matrix  $\mathbf{V}^H$  of dimension  $\{(WK\text{-by-}WK)\}$ .

The output of this detector is given by:

$$\mathbf{y}_V^b = \mathbf{V}^H \mathbf{y}_{MRC}^b = \mathbf{V}^H \bar{\mathbf{R}}_{eff}^b \bar{\mathbf{A}}_{eff} \bar{\mathbf{b}}^b + \mathbf{V}^H \bar{\mathbf{z}}_{eff}^b \quad (6-40)$$

The noise vector now is additive colored Gaussian noise with covariance matrix:

$$\begin{aligned}
 E \left[ \left( \mathbf{V}^H \left( \bar{\mathbf{S}}_{eff}^b \right)^H \bar{\mathbf{n}}_{eff}^b \right) \left( \mathbf{V}^H \left( \bar{\mathbf{S}}_{eff}^b \right)^H \bar{\mathbf{n}}_{eff}^b \right)^H \right] &= E \left[ \mathbf{V}^H \left( \bar{\mathbf{S}}_{eff}^b \right)^H \bar{\mathbf{n}}_{eff}^b \left( \bar{\mathbf{n}}_{eff}^b \right)^H \bar{\mathbf{S}}_{eff}^b \mathbf{V} \right] \\
 &= \sigma^2 \mathbf{V}^H \bar{\mathbf{R}}_{eff}^b \mathbf{V}
 \end{aligned} \tag{6-41}$$

Thus, the BER of the  $k^{th}$  effective user at the output of the transformation matrix conditioned on the vector  $\mathbf{V}(:, k_{eff})^H \bar{\mathbf{R}}_{eff}^b$  is:

$$P_{k_{eff} | \mathbf{V}(:, k_{eff})^H \bar{\mathbf{R}}_{eff}^b}(\sigma) = \frac{1}{2^{WK-1}} \sum_{\substack{\text{all } \mathbf{b} \\ \mathbf{b}(k_{eff})=1}} \mathcal{Q} \left( \frac{\mathbf{V}(:, k_{eff})^H \bar{\mathbf{R}}_{eff}^b \bar{\mathbf{A}}_{eff} \mathbf{b}}{\sigma \sqrt{\mathbf{V}(:, k_{eff})^H \bar{\mathbf{R}}_{eff}^b \mathbf{V}(:, k_{eff})}} \right) \tag{6-42}$$

As for the case of the linear transformation matrix applied to the received signal, getting the average BER and AME requires taking the expectation over all possible values of the vector  $\mathbf{V}(:, k_{eff})^H \bar{\mathbf{R}}_{eff}^b$  which results in a  $WK$  multiple integral expression, which is very intensive and can be assessed only numerically. For this reason, the BER and the AME will be evaluated only by simulation.

## 6.9 Computational Complexity

In this section, we evaluate the computational complexity of the aforementioned multiuser detectors. The simplest multiuser detector which is the conventional matched filter detector consists basically of a correlation operation and it has the following computational complexity:

$$2 \left( WN + \max_{1 \leq k \leq K} (\tau^k) \right) WK \tag{6-43}$$

In a multi-path environment, a Rake receiver is the conventional multiuser detector. It consists basically of a convolution operation to obtain the effective spreading code and a correlation operation for matched filtering. The computational complexity of the Rake receiver is given by:

$$\left( (2L_k + 1)WN + (L_k + 1) \max_{1 \leq k \leq K} (\tau^k) + (L_k - 1) \max_{1 \leq k \leq K} (\tau_{l_k}) \right) WK \tag{6-44}$$

The computational complexity of the optimal multiuser detector is exponential in both the number of users and the number of bits within the sliding window. Hence we will not give any expression for its computational complexity since it is not comparable with any of the subsequent multiuser detectors.

The computational complexity of both the decorrelator detector and the LMMSE detector is due mainly to matrix inversion and the calculation of the cross-correlation matrix. All these operations cost at least (lower bound) [78]:

$$11(KW)^3 + \frac{3}{2}(KW)^2 + KW + 2\left(WN + \max_{1 \leq k \leq K}(\tau^k)\right)(WK)^2 + 2\left(WN + \max_{1 \leq k \leq K}(\tau^k)\right)WK \quad (6-45)$$

for an asynchronous CDMA AWGN channel and:

$$11(KW)^3 + \frac{3}{2}(KW)^2 + KW + 2\left(WN + \max_{1 \leq k \leq K}(\tau^k) + \max_{1 \leq l_k \leq K}(\tau_{l_k})\right)(WK)^2 + 2\left(WN + \max_{1 \leq k \leq K}(\tau^k) + \max_{1 \leq l_k \leq K}(\tau_{l_k})\right)WK \quad (6-46)$$

for an asynchronous CDMA multi-path fading channel.

### 6.10 Simulation Results

In this part, we simulate the previously discussed multiuser detectors except the optimum multiuser detector which is not included here due to its exhaustive computational complexity. All these detectors are simulated in two different scenarios; the first is a synchronous CDMA AWGN channel whereas the second is an asynchronous CDMA multipath Rayleigh fading channel. The simulation parameters are summarized in Table 6.1:

Table 6.1: Simulation parameters.

Synchronous CDMA AWGN channel			Asynchronous CDMA multipath Rayleigh fading channel
Average BER versus SNR performance	Average BER versus number of users performance	Average BER versus near-far ratio performance	Average BER versus SNR performance
$K = 20, N = 31, W = 1$ , (Gold codes), perfect power control	$SNR = 6\text{dB}, N = 31$ (Gold codes), $W = 1$ , perfect power control	$SNR = 5\text{dB}, K = 20; N = 31$ (Gold codes); $W = 1$ .	$W = 5, K = 10, N = 31$ (Gold codes), Vehicular A outdoor Channel power delay profile for WCDMA is used, $\max_{1 \leq k \leq K}(\tau^k) + \max_{1 \leq l_k \leq K}(\tau_{l_k}) \leq N$ .

In Figure 6.8, the average BER (average BER of all users) versus the SNR is depicted. As expected, the LMMSE detector achieves the best performance while the matched filter detector achieves the worst performance. The reason is that the matched filter detector performs no MAI reduction while the LMMSE reduces MAI but at the same time reduces the noise enhancement effect. The performance of the decorrelator detector is close to that of the LMMSE detector however it is slightly worse due to noise enhancement effect.

In Figure 6.9, the system capacity in terms of number of users expressed as the average BER (average BER of all users) versus the number of users is depicted. As expected, the LMMSE detector can support more users than both the matched filter detector and the decorrelator detector. The decorrelator detector in general can support more users than the matched filter detector, however, for highly loaded systems the converse is true. This is due to the fact that at high loads the noise enhancement effect becomes more severe and thus the benefit gained from interference cancellation is overwhelmed by the noise enhancement effect. Hence, in this situation leaving the interference is better than canceling it using the decorrelator detector.

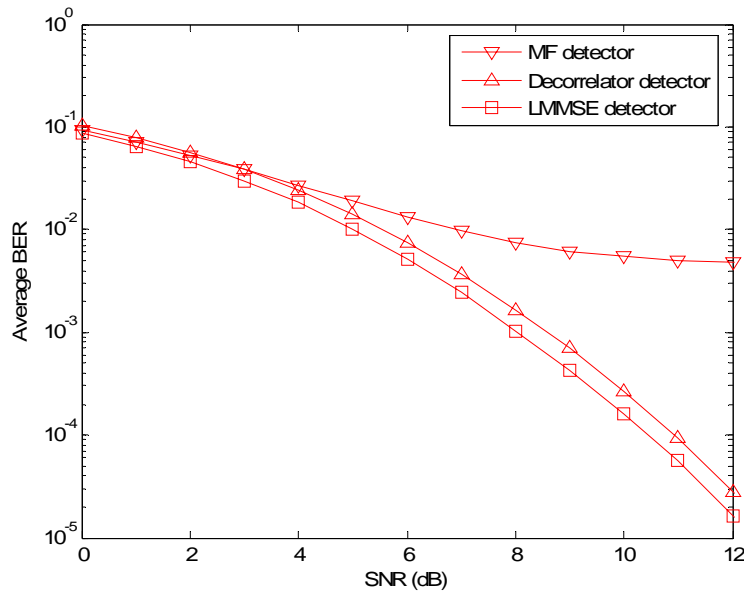


Figure 6.8: Average BER versus SNR performance of different multiuser detectors in a synchronous CDMA AWGN channel.

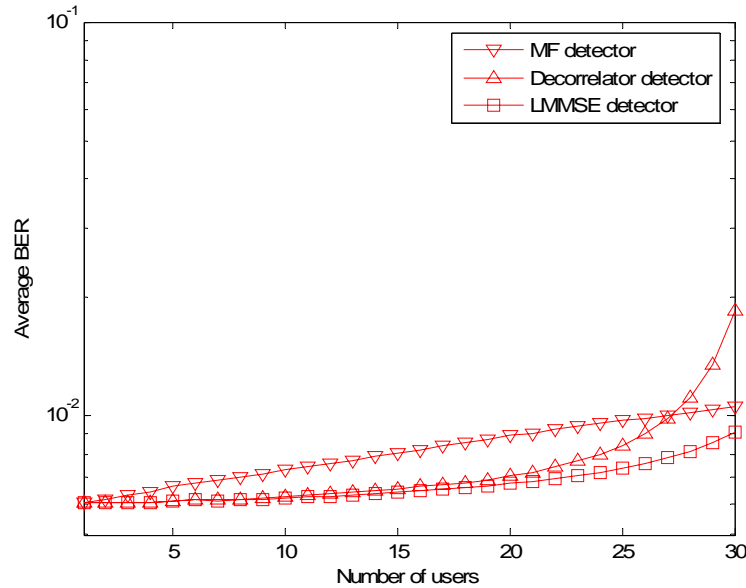


Figure 6.9: Average BER versus the number of users' performance of different multiuser detectors in a synchronous CDMA AWGN channel.

In Figure 6.10, the near-far resistance expressed as the average BER (average BER of all users) versus the near-far ratio is depicted. For the near-far ratio, we fix the amplitude of the first user and vary the amplitude of the other users from one to 3 times that of first user. From a theoretical point of view, the LMMSE detector and decorrelator detector have the same near-far resistance which is better than that of the matched filter detector. However, because the noise level here is not zero (SNR = 5dB), slightly different results are obtained. First, the LMMSE detector performs better than the decorrelator detector because it cancels interference but at the same time it does not enhance the background noise. Second, the decorrelator detector is really near-far resistant since its near-far resistance is constant and does not change with the near-far ratio. Finally, the matched filter detector performs worse than the decorrelator and the LMMSE detectors, but not for all near-far ratios. Specifically, for small near-far ratios, the matched filter detector performs better than the decorrelator detector. This is due again to the noise enhancement effect which overwhelms the gain obtained from interference cancellation. Hence, for near-far ratios under a certain threshold, it is better to leave the interference than removing it using a decorrelator detector.

In Figure 6.11, the average BER (average BER of all users) versus the SNR in an asynchronous CDMA multipath Rayleigh fading channel is depicted.

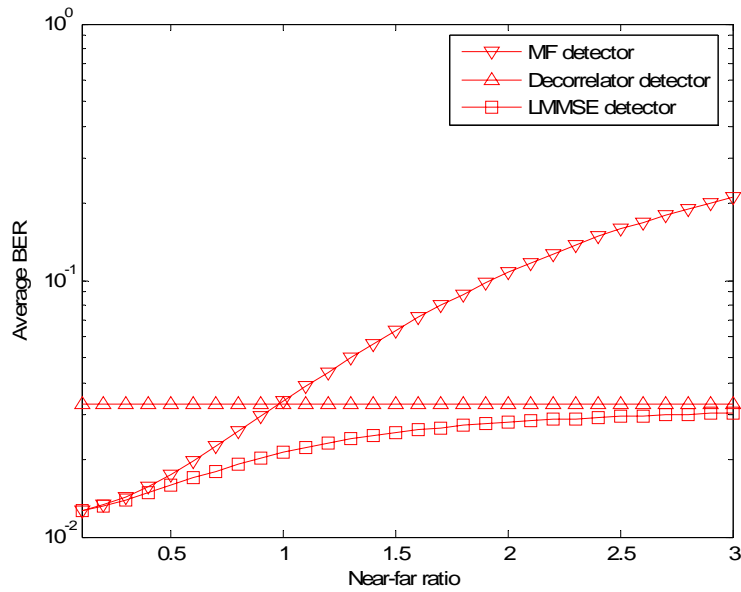


Figure 6.10: Average BER versus near-far ratio performance of different multiuser detectors in a synchronous CDMA AWGN channel.

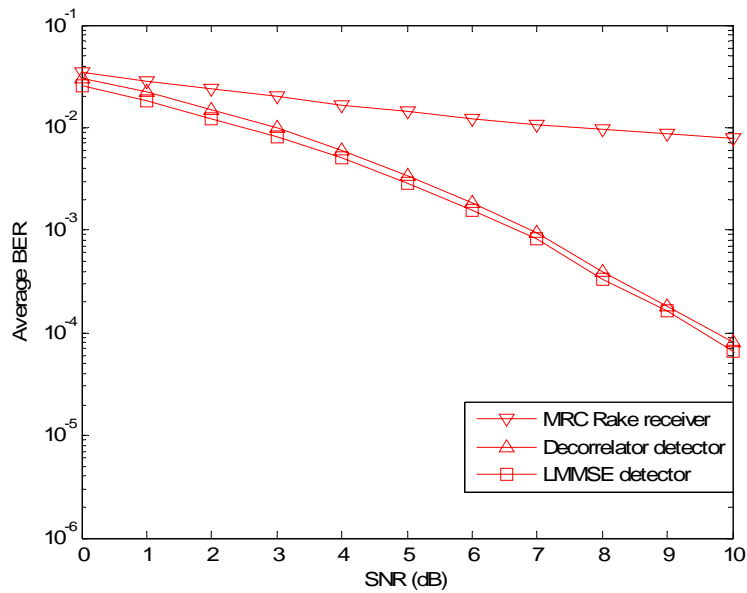


Figure 6.11: Average BER versus SNR performance of different multiuser detectors in an asynchronous CDMA multipath Rayleigh fading channel.

The vehicular A outdoor channel power delay profile for WCDMA is used and

$\max_{1 \leq k \leq K} (\tau^k) + \max_{1 \leq k \leq K} (\tau_{l_k}) \leq N$  so that ISI is negligible. The conclusion deduced for the synchronous

CDMA AWGN channel can be set here as well.

### **6.11 Conclusion**

In this chapter, we introduced the multiuser detection principle and evaluated the performance of different fundamental multiuser detection techniques for both CDMA AWGN and multipath fading channels. We detailed the basic performance metrics commonly used in this field such as the BER, the AME and the near-far resistance. Finally, simulation of the fundamental multiuser detectors is conducted for both CDMA AWGN and multipath fading channels.

# Chapter 7

## Linear Interference Cancellation Structures

### 7.1 Chapter's Contents

7.1 Chapter's Contents .....	125
7.2 Introduction .....	126
7.3 Symbol-level Linear SIC (SL-LSIC) Structure .....	127
7.4 Symbol-Level Linear SOR-SIC (SL-LSOR-SIC) Structure .....	128
7.5 Symbol-Level Linear Group-Wise SIC (SL-LGSIC) Structure .....	129
7.6 Symbol-Level Linear Block SOR Group-Wise SIC (SL-LBSOR-GSIC) Structure .....	132
7.7 Symbol-Level Linear PIC/Weighted PIC (SL-LPIC/SL-LWPIC) Structure .....	134
7.8 Chip-Level Linear SIC (CL-LSIC) Structure .....	136
7.8.1 Convergence Behavior .....	138
7.8.2 Conditions of Convergence .....	138
7.9 Reduced Complexity Chip-Level Linear SIC (RC-CL-LSIC) Structure .....	138
7.9.1 Convergence Behavior .....	141
7.9.2 Conditions of Convergence .....	141
7.10 Reduced Complexity Chip-Level Linear Group-Wise SIC (RC-CL-LGSIC) Structure .....	141
7.10.1 Group Detection Schemes .....	144
7.10.1.1 The RC-CL-LGMF-SIC Detector .....	144
7.10.1.2 The RC-CL-LGPIC-SIC Detector .....	144
7.10.1.3 The RC-CL-LGDEC-SIC Detector .....	145
7.10.1.4 The RC-CL-LGMMSE-SIC Detector .....	145
7.10.2 Convergence Behavior .....	145
7.10.3 Conditions of Convergence .....	145
7.11 Case of CDMA Multi-Path Fading Channel .....	145
7.12 Chip-Level Linear PIC/Weighted PIC (CL-LPIC/CL-LWPIC) Structure .....	149
7.12.1 Convergence Behavior .....	152
7.12.2 Conditions of Convergence .....	153

7.13 Computational Complexity .....	153
7.13.1 Computational Complexity of the SL-LSIC Structure .....	153
7.13.2 Computational Complexity of the SL-LSOR-SIC Structure .....	154
7.13.3 Computational Complexity of the SL-LGSIC Structure .....	155
7.13.4 Computational Complexity of the SL-LBSOR-GSIC Structure .....	155
7.13.5 Computational Complexity of the SL-LWPIC Detector .....	155
7.13.6 Computational Complexity of the CL-LSIC Structure .....	156
7.13.7 Computational Complexity of the RC-CL-LSIC Structure .....	156
7.13.8 Computational Complexity of the RC-CL-LGSIC Structure .....	156
7.13.9 Computational Complexity of the CL-LWPIC Detector .....	157
7.14 Simulation Results .....	157
7.15 Conclusion .....	167

## 7.2 Introduction

Linear interference cancellation (IC) structures are based on linear iterative methods and are used to approximate the decorrelator/LMMSE detector [108]. Depending on the implementation details of these methods, two different approaches exist ([87], [89] and [99]). The first approach uses the cross-correlation coefficients and it is suitable for short-code CDMA systems. This approach results in what is known as symbol-level or narrowband linear IC detectors. The second approach uses the spreading codes and it is suitable for long-code CDMA systems. This approach results in chip-level or wideband linear IC detectors. Suitability of these detectors for short-code or long-code systems is determined by the implementation complexity which is system-dependent through the frequency of computation of the cross-correlation matrix. This frequency is very low for a short-code system whereas it is very high for a long-code system.

Since we are interested in developing linear IC detectors for long-code CDMA systems, chip-level linear IC detectors are the best candidates in terms of computational complexity since they make use of the spreading codes directly and not the cross-correlation coefficients and hence the computation of the cross-correlation matrix is not necessary. This reduces considerably the total computational complexity of multiuser detectors.

In this chapter, we study different chip-level linear IC detectors detailed in the literature in terms of convergence behavior and computational complexity. These detectors are compared to their symbol-

level counterparts. Moreover, we extend some structures which are suitable for CDMA AWGN channels only to CDMA multipath fading channels.

### 7.3 Symbol-level Linear SIC (SL-LSIC) Structure

This structure is based on direct implementation of the Gauss-Seidel iterative method for the inversion of the cross-correlation matrix  $\bar{\mathbf{R}}_{eff}$ . It was implemented for the case of synchronous CDMA AWGN channel in [84] and for the asynchronous CDMA AWGN channel, in both [109] and [108]. For the case of synchronous CDMA multipath fading channel, this structure was proposed in [110].

Using the linear CDMA channel model presented in Chapter 4, we implement this structure. The basic building block for the  $k^{th}$  effective user is shown in Figure 7.1.

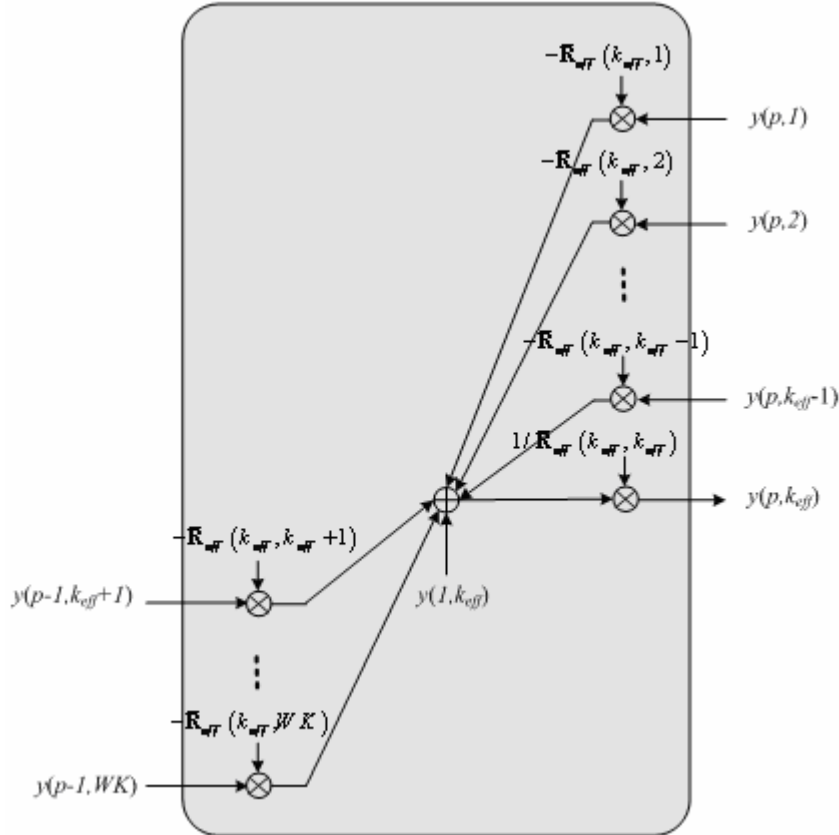


Figure 7.1: SL-LSIC unit of the  $k^{th}$  effective user

The decision variable of the  $k^{th}$  effective user is given by:

$$y(p, k_{eff}) = \frac{1}{\bar{\mathbf{R}}_{eff}(k_{eff}, k_{eff})} \left( \begin{array}{l} y(1, k_{eff}) - \sum_{j=k_{eff}+1}^{WK} \bar{\mathbf{R}}_{eff}(k_{eff}, j) y(p-1, j) \\ - \sum_{j=1}^{k_{eff}-1} \bar{\mathbf{R}}_{eff}(k_{eff}, j) y(p, j) \end{array} \right) \quad (7-1)$$

which is clearly the Gauss-Seidel iteration that is used for the inversion of the matrix  $\bar{\mathbf{R}}_{eff}$ . Hence it is an iterative implementation of the decorrelator detector.

#### 7.4 Symbol-Level Linear SOR-SIC (SL-LSOR-SIC) Structure

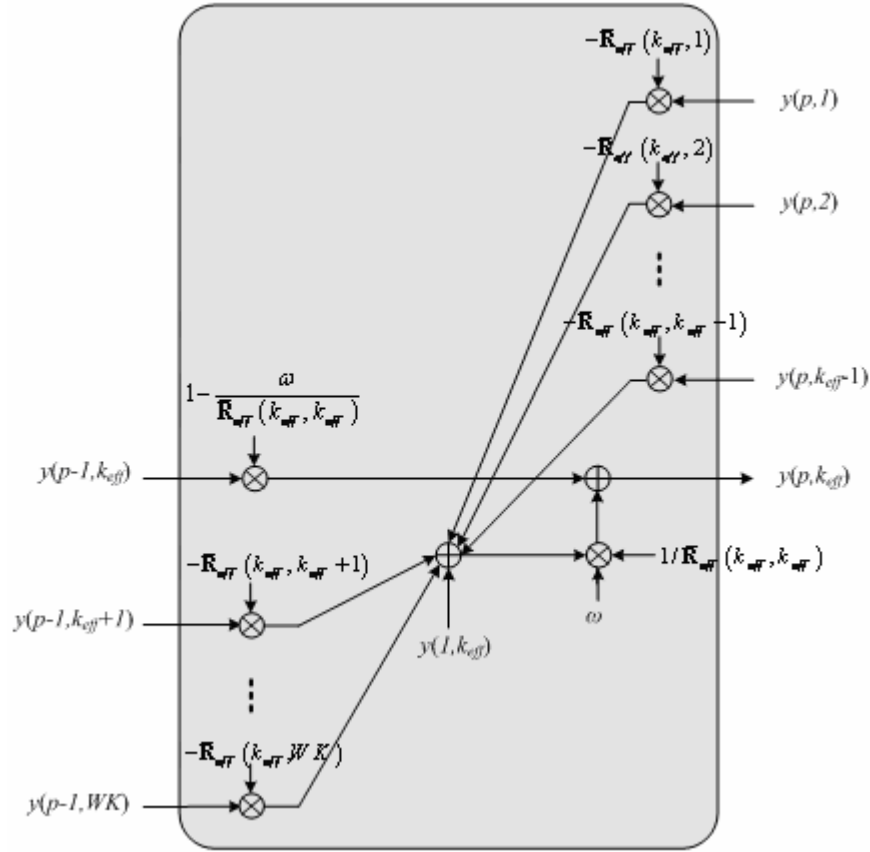
As discussed in Chapter 5, the SOR method is an enhanced variant of the SIC method based on the relaxation principle. It has been proven in [80] that the SOR method converges faster than the SIC method by an order of magnitude if an optimal weighting factor is used. The direct implementation of this iterative method was presented in [84] for the synchronous CDMA AWGN channel. Furthermore, an approximate optimal acceleration (weighting) factor was obtained and is given by [84]:

$$\omega_{opt} \approx 2 \frac{\sqrt{\lambda_{\min}(\mathbf{D}^{-1/2} \bar{\mathbf{R}}_{eff} \mathbf{D}^{-1/2}) \lambda_{\max}(\mathbf{D}^{-1/2} \bar{\mathbf{R}}_{eff} \mathbf{D}^{-1/2})} - 1}{\lambda_{\min}(\mathbf{D}^{-1/2} \bar{\mathbf{R}}_{eff} \mathbf{D}^{-1/2}) \lambda_{\max}(\mathbf{D}^{-1/2} \bar{\mathbf{R}}_{eff} \mathbf{D}^{-1/2}) - 1} \quad (7-2)$$

where  $\lambda_{\min}$  and  $\lambda_{\max}$  denote the minimum and maximum eigenvalues, respectively, and  $\mathbf{D}$  is the diagonal part of the matrix  $\bar{\mathbf{R}}_{eff}$ . Upper bounds for  $\lambda_{\max}$  and lower bounds for  $\lambda_{\min}$  can be obtained using theorems like the Gershgorin theorem [82] or the shifted matrix power method [111]. Here also we present a more general structure for the SIC based on the SOR iterative method. The latter is based on the linear asynchronous CDMA multi-path fading channel model presented in Chapter 4. The basic building block for the  $k^{th}$  effective user is shown in Figure 7.2.

The decision variable of the  $k^{th}$  effective user is given by:

$$y(p, k_{eff}) = \left( \begin{array}{l} 1 - \frac{\omega}{\bar{\mathbf{R}}_{eff}(k_{eff}, k_{eff})} \\ \frac{\omega}{\bar{\mathbf{R}}_{eff}(k_{eff}, k_{eff})} \left( \begin{array}{l} y(1, k_{eff}) - \sum_{j=k_{eff}+1}^{WK} \bar{\mathbf{R}}_{eff}(k_{eff}, j) y(p-1, j) \\ - \sum_{j=1}^{k_{eff}-1} \bar{\mathbf{R}}_{eff}(k_{eff}, j) y(p, j) \end{array} \right) \end{array} \right) \quad (7-3)$$


 Figure 7.2: SL-LSOR-SIC unit of the  $k^{\text{th}}$  effective user

which is indeed the SOR iteration used for the inversion of the matrix  $\bar{\mathbf{R}}_{\text{eff}}$ . A Symbol-level SIC that can implement iteratively the LMMSE multiuser detector was proposed in [84] for the synchronous CDMA AWGN channel and it can be obtained simply by replacing  $\bar{\mathbf{R}}_{\text{eff}}$  by  $\bar{\mathbf{R}}_{\text{eff}} + \sigma^2 \bar{\mathbf{A}}_{\text{eff}}^{-2}$ .

### 7.5 Symbol-Level Linear Group-Wise SIC (SL-LGSIC) Structure

In the symbol-level linear group-wise SIC structure, the  $K$  users are partitioned into  $G$  disjoint groups where the  $g^{\text{th}}$  group consists of  $U_g$  users such that  $K = U_1 + U_2 + \dots + U_g + \dots + U_G$ . This yields a bank of detectors; each detects the information symbols of users in each group. In a parallel group detection scheme these group-detectors operate independently in order to cancel interference, whereas in a sequential scheme, also known as group-wise successive interference cancellation (GSIC) scheme, each group-detector uses the decisions of the previous stage of group-detectors to successively cancel

the interference. These methods are based on block iterative methods such as the block Gauss-Seidel and block successive over-relaxation methods. Before detailing this structure it is of paramount importance to introduce the following indices and variables to simplify different expressions obtained during the analysis of this and all subsequent structures. Let us define a new index  $g_{eff} = 1, 2, \dots, GW$ . It is related to  $g$  and  $w$  as follows:  $g_{eff} = (w-1)G + g$ . If  $g_{eff}$  is provided then  $w$  and  $g$  are determined from  $g_{eff}$  as follows:  $w = \left\lceil \frac{g_{eff}}{G} \right\rceil$  where  $\lceil \cdot \rceil$  is the ceiling operator and  $g = g_{eff} - (w-1)G$ . Hence,  $WK = U_1 + U_2 + \dots + U_{g_{eff}} + \dots + U_{WG}$  where:  $U_{g_{eff}} = U_{(w-1)G+g}$ , however, if  $U_{g_{eff}}$  is provided then  $U_g$  is determined as:  $U_g = U_{g_{eff} - (w-1)G}$  where  $w = \left\lceil \frac{g_{eff}}{G} \right\rceil$ .

In addition, both  $k$  and  $k_{eff}$  are related to  $u_g$  and  $u_{g_{eff}}$  as:  $k = \sum_{i=1}^{g-1} U_i + u_g$  and  $k_{eff} = \sum_{i=1}^{g_{eff}-1} U_i + u_{g_{eff}}$ , respectively. However, if  $k$  and  $k_{eff}$  are given, then  $u_g$  and  $u_{g_{eff}}$  are obtained as follows:

$$g = \sup \left\{ 1 \leq i \leq G : \sum_{j=1}^i U_j < k \right\}, \quad u_g = k - \sum_{i=1}^{g-1} U_i \quad \text{and} \quad g_{eff} = \sup \left\{ 1 \leq i \leq WG : \sum_{j=1}^i U_j < k_{eff} \right\},$$

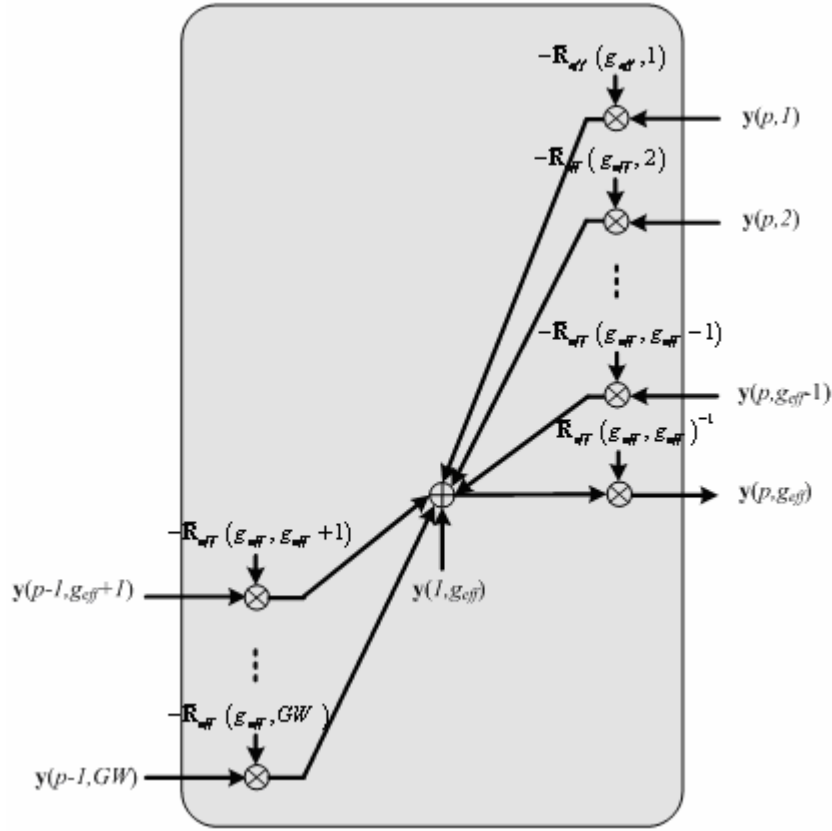
$$u_{g_{eff}} = k_{eff} - \sum_{i=1}^{g_{eff}-1} U_i, \text{ respectively.}$$

The index  $g_{eff}$  will be used interchangeably with  $(g, w)$  whenever needed in this and subsequent chapters.

The decision vector of the  $g^{th}$  effective group of users is given by:

$$\mathbf{y}(p, g_{eff}) = \bar{\mathbf{R}}_{eff}(g_{eff}, g_{eff})^{-1} \begin{pmatrix} \mathbf{y}(1, g_{eff}) - \sum_{j=g_{eff}+1}^{GW} \bar{\mathbf{R}}_{eff}(g_{eff}, j) \mathbf{y}(p-1, j) \\ - \sum_{j=1}^{g_{eff}-1} \bar{\mathbf{R}}_{eff}(g_{eff}, j) \mathbf{y}(p, j) \end{pmatrix} \quad (7-4)$$

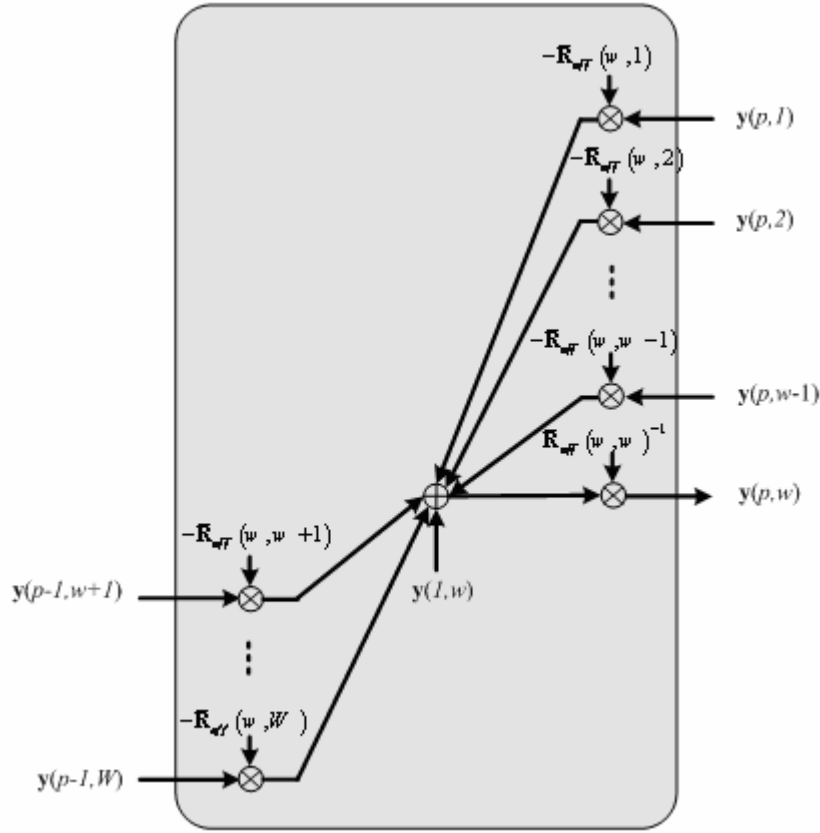
For the special case where the group size is one, that is,  $G = W$ , we obtain the symbol-level linear block-wise SIC (SL-LBSIC) detectors. In this structure, the interference due to users in one bit period is cancelled in parallel whereas the interference due to users of different bit intervals is cancelled in series. Such detectors are presented in [112] and [113]. The basic building block of the SL-LBSIC detector is shown in Figure 7.4.


 Figure 7.3: SL-LGSIC unit of the  $g^{\text{th}}$  effective group of users

where  $\bar{\mathbf{R}}_{\text{eff}}(i, j)$  is the  $i^{\text{th}}$  row,  $j^{\text{th}}$  column submatrix of the matrix  $\bar{\mathbf{R}}_{\text{eff}}$ . The decision vector of the  $w^{\text{th}}$  block of users is given by:

$$\mathbf{y}(p, w) = \bar{\mathbf{R}}_{\text{eff}}(w, w)^{-1} \begin{pmatrix} \mathbf{y}(1, w) - \sum_{j=w+1}^W \bar{\mathbf{R}}_{\text{eff}}(w, j) \mathbf{y}(p-1, j) \\ -\sum_{j=1}^{w-1} \bar{\mathbf{R}}_{\text{eff}}(w, j) \mathbf{y}(p, j) \end{pmatrix} \quad (7-5)$$

Here, the inverse of the submatrix  $\bar{\mathbf{R}}_{\text{eff}}(w, w)$  in the SL-LBSIC unit of Figure 7.4 is obtained by direct inversion, however, if the number of users is large then iterative methods can be used resulting in the *inner-outer iterative methods*, *nested iterative methods* or *two-stage block iterative methods* [114]-[116].

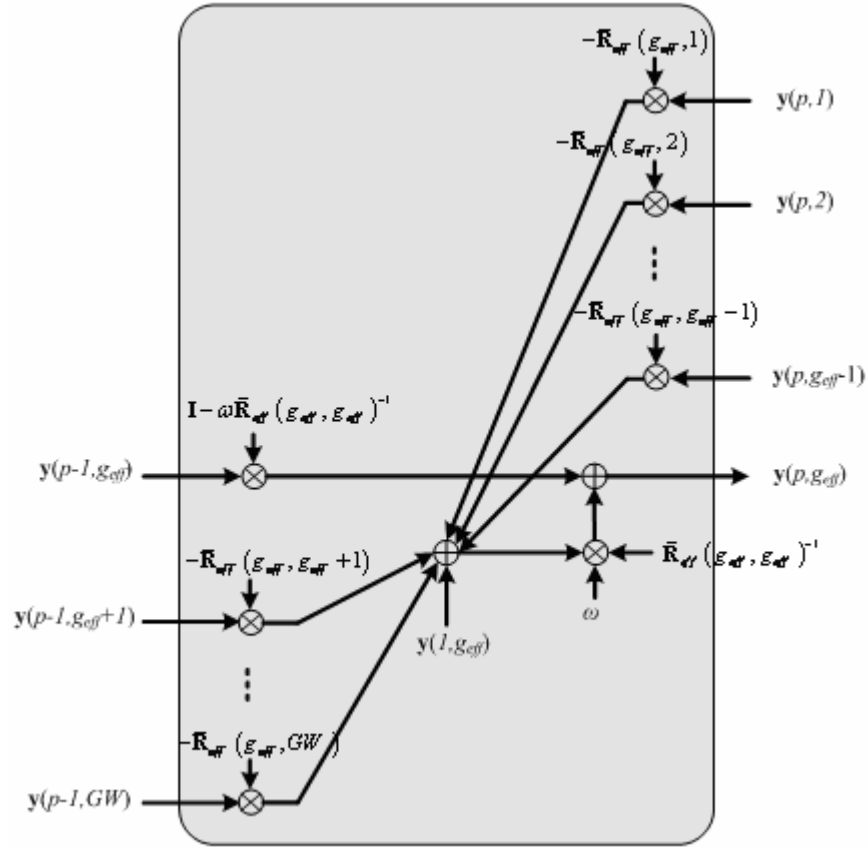

 Figure 7.4: SL-LBSIC unit of the  $w^{\text{th}}$  block of users.

## 7.6 Symbol-Level Linear Block SOR Group-Wise SIC (SL-LBSOR-GSIC)

### Structure

A symbol-level linear block SOR group-wise SIC structure can also be obtained by modifying the SOR-SIC structure to process a group of users instead of single users. The SL-LBSOR-GSIC structure is shown in Figure 7.5. The decision vector of the  $g^{\text{th}}$  effective group of users is given by:

$$\mathbf{y}(p, \mathbf{g}_{\text{eff}}) = \left( \mathbf{I} - \omega \bar{\mathbf{R}}_{\text{eff}}(\mathbf{g}_{\text{eff}}, \mathbf{g}_{\text{eff}})^{-1} \right) \mathbf{y}(p-1, \mathbf{g}_{\text{eff}}) + \omega \bar{\mathbf{R}}_{\text{eff}}(\mathbf{g}_{\text{eff}}, \mathbf{g}_{\text{eff}})^{-1} \begin{pmatrix} \mathbf{y}(1, w) - \sum_{j=\mathbf{g}_{\text{eff}}+1}^W \bar{\mathbf{R}}_{\text{eff}}(\mathbf{g}_{\text{eff}}, j) \mathbf{y}(p-1, j) \\ - \sum_{j=1}^{\mathbf{g}_{\text{eff}}-1} \bar{\mathbf{R}}_{\text{eff}}(\mathbf{g}_{\text{eff}}, j) \mathbf{y}(p, j) \end{pmatrix} \quad (7-6)$$


 Figure 7.5: SL-LBSOR-GSIC unit of the  $g^{\text{th}}$  effective group of users.

As for the SL-LGSIC detector, the SL-LBSOR-GSIC structure can be extended to obtain the symbol-level linear block-wise SOR-SIC detector by simply letting  $G = W$ . The new structure is shown in Figure 7.6.

The decision vector of the  $w^{\text{th}}$  block of users is given by:

$$\mathbf{y}(p, w) = \left( \mathbf{I} - \omega \bar{\mathbf{R}}_{\text{eff}}(w, w)^{-1} \right) \mathbf{y}(p-1, w) + \omega \bar{\mathbf{R}}_{\text{eff}}(w, w)^{-1} \begin{pmatrix} \mathbf{y}(1, w) - \sum_{j=w+1}^W \bar{\mathbf{R}}_{\text{eff}}(w, j) \mathbf{y}(p-1, j) \\ - \sum_{j=1}^{w-1} \bar{\mathbf{R}}_{\text{eff}}(w, j) \mathbf{y}(p, j) \end{pmatrix} \quad (7-7)$$

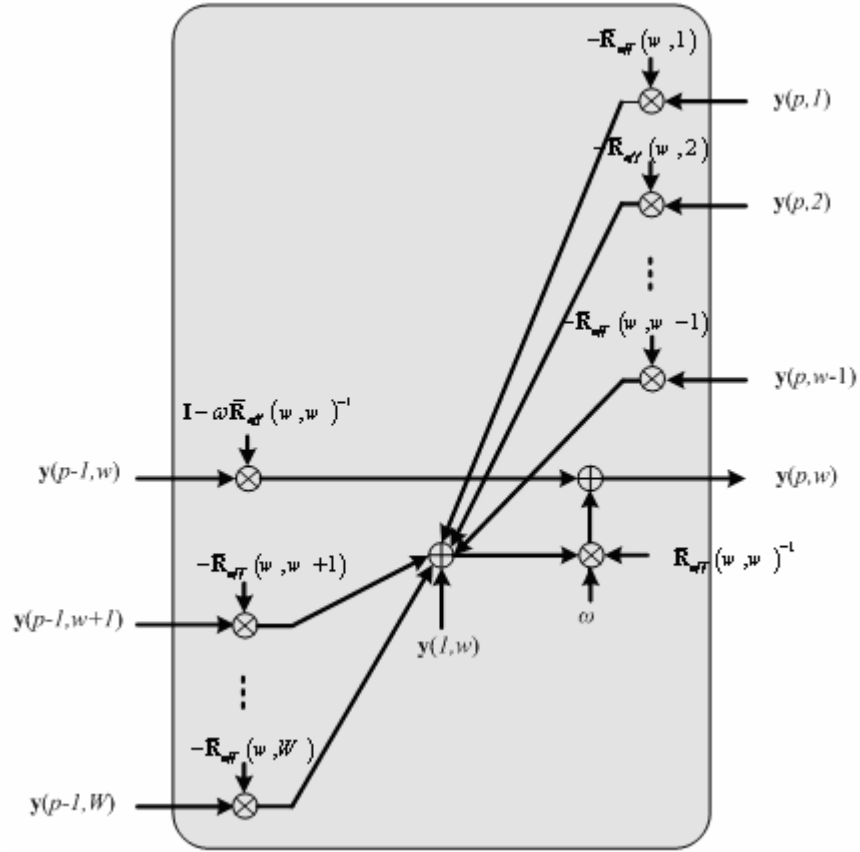


Figure 7.6: SL-LBSOR-GSIC unit of the  $w^{\text{th}}$  block of users.

All the previously detailed structures are easily extended to approximate the LMMSE detector by simply changing  $\bar{\mathbf{R}}_{\text{eff}}$  to  $\bar{\mathbf{R}}_{\text{eff}} + \sigma^2 \bar{\mathbf{A}}_{\text{eff}}^{-2}$ . As mentioned earlier, all symbol-level detectors make use of the cross-correlation coefficients and consequently the cross-correlation matrix needs to be computed. If working in a long-code CDMA system where the cross-correlation matrix is changing randomly from one symbol period to another, these detectors become computationally inefficient because the computation of the cross-correlation matrix which costs  $2NK^2$  is more intensive than the interference cancellation itself. Hence, this category is suitable for CDMA systems implementing short-codes (periodic) only.

### 7.7 Symbol-Level Linear PIC/Weighted PIC (SL-LPIC/SL-LWPIC) Structure

This structure was proposed in [84], and was shown to be a direct implementation of the linear Jacobi iterative method. Because of the well known convergence problems of the linear PIC, where it

converges for only less than 17% of the loading factor [84] ( $\lim_{K/N \rightarrow \infty} (K/N)$  with  $K/N = cst$ ), the LWPIC structure was proposed to ensure convergence. It was shown also that this scheme is equivalent to the point relaxation Jacobi iterative method. The SL-LWPIC structure is shown in Figure 7.7:

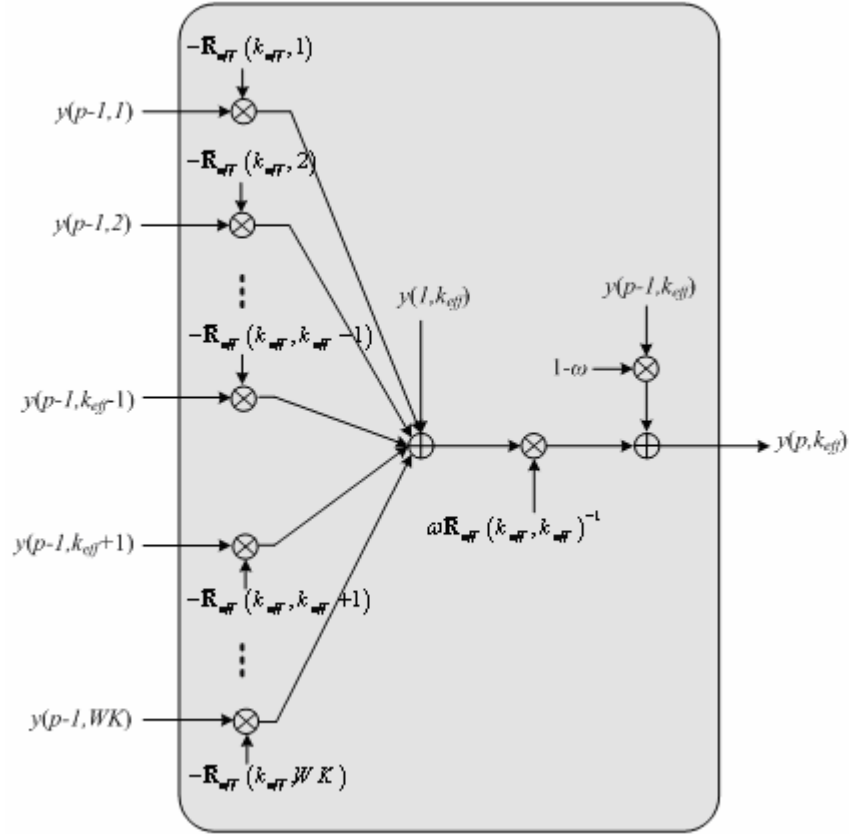


Figure 7.7: SL-LPIC/SL-LWPIC unit of the  $k^{\text{th}}$  effective user.

The decision variable of the  $k^{\text{th}}$  effective user is given by:

$$y(p, k_{\text{eff}}) = \frac{\omega}{\bar{\mathbf{R}}_{\text{eff}}(k_{\text{eff}}, k_{\text{eff}})} \left( y(1, k_{\text{eff}}) - \sum_{\substack{j=1 \\ j \neq k_{\text{eff}}}}^{WK} \bar{\mathbf{R}}_{\text{eff}}(k_{\text{eff}}, j) y(p-1, j) \right) + (1-\omega)y(p-1, k_{\text{eff}}), \quad k_{\text{eff}} = 1, \dots, WK \quad (7-8)$$

which is clearly the point Jacobi relaxation iteration that is used for the inversion of the matrix  $\bar{\mathbf{R}}_{eff}$ . Hence it is an iterative implementation of the decorrelator detector. Note that the SL-LPIC detector is obtained by setting the relaxation factor  $\omega$  to one.

## 7.8 Chip-Level Linear SIC (CL-LSIC) Structure

Unlike the SL-LSIC structure, its counterpart the CL-LSIC structure acts directly on the received chip-matched signal. Furthermore, it makes use of the spreading codes and not the cross-correlation coefficients and consequently the calculation of the cross-correlation matrix is not required. This is very suitable for long-code (aperiodic) systems where the cross-correlation matrix is changing every symbol period. This structure is well covered in the literature for both synchronous/asynchronous CDMA AWGN channel and synchronous/asynchronous CDMA multipath fading channel, for example see [117]-[120].

In this sequel, we implement the CL-LSIC structure using the linear CDMA model proposed in Chapter 4. The CL-LSIC consists of interference cancellation units (ICU) arranged in a multistage structure as illustrated in Figure 7.8. The interference cancellation unit of  $p^{th}$  stage,  $k^{th}$  effective user is shown in Figure 7.9. The composite signal  $y(p, k_{eff}) = \mathbf{e}(p, k_{eff}) + \mathbf{I}(p, k_{eff})$  at the input of the  $p^{th}$  stage,  $k^{th}$  effective user ICU, is first despreading to estimate the decision variable  $y(p, k_{eff})$ , that is:

$$y(p, k_{eff}) = \bar{\mathbf{s}}_{eff}(k_{eff})^T (\mathbf{e}(p, k_{eff}) + \mathbf{I}(p, k_{eff})).$$

The MAI  $\mathbf{I}(p, k_{eff})$  due the  $p^{th}$  stage,  $k^{th}$  effective user, is obtained by spreading the decision variable  $y(p, k_{eff})$ , that is:  $\mathbf{I}(p, k_{eff}) = \bar{\mathbf{s}}_{eff}(k_{eff}) y(p, k_{eff})$ , which in turn is subtracted out from the residual signal  $\mathbf{e}(p, k_{eff}) + \mathbf{I}(p, k_{eff})$  to get a cleaned version of the residual signal  $\mathbf{e}(p, k_{eff} + 1)$ . This process is repeated in a multistage structure as it is shown in Figure 7.8.

It was shown in [118] and [119], that the general expression for the residual signal vector and the decision variable of the  $k^{th}$  effective user's ICU unit at the  $p^{th}$  stage, respectively, can be written as:

$$\mathbf{e}(p, k_{eff}) = \mathbf{\Phi}_{k_{eff}-1} (\mathbf{\Phi}_{WK})^{p-1} \mathbf{q}_b \quad (7-9)$$

and:

$$y(p, k_{eff}) = \bar{\mathbf{s}}_{eff}(k_{eff})^T \mathbf{\Phi}_{k_{eff}-1} \sum_{i=0}^{p-1} (\mathbf{\Phi}_{WK})^i \mathbf{q}_b = \mathbf{g}_{p, k_{eff}}^T \mathbf{q}_b \quad (7-10)$$

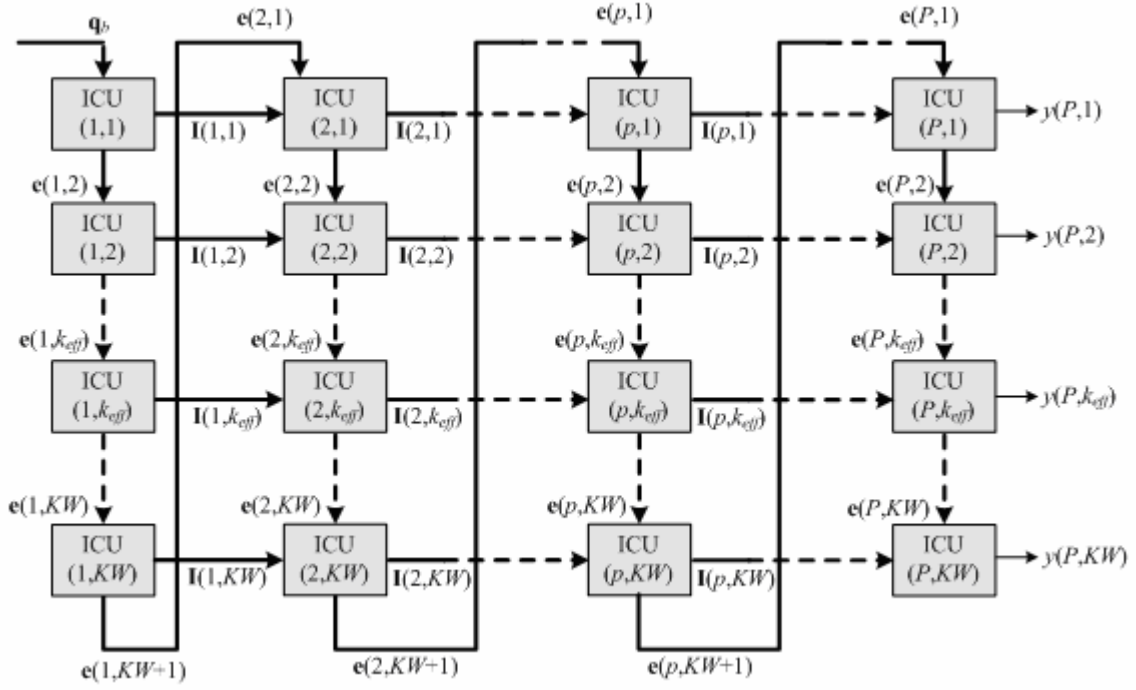


Figure 7.8: Multistage structure of the CL-LSIC detector

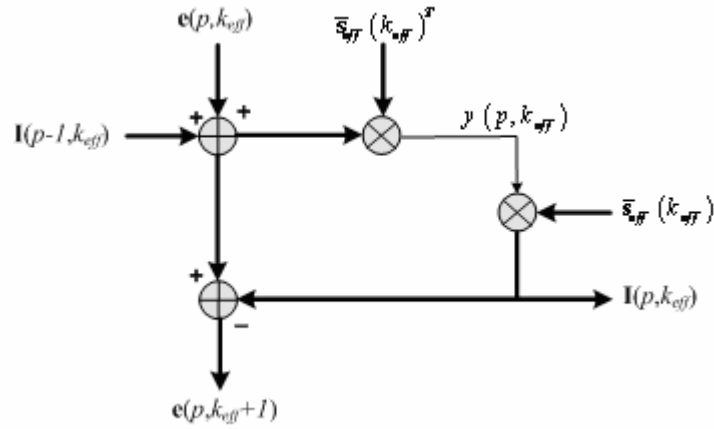


Figure 7.9:  $p^{th}$  stage,  $k^{th}$  effective user's CL-LSIC unit (ICU)

Collecting the decision variables of all users in one matrix we get:

$$\mathbf{y}(p) = \mathbf{G}_p^T \mathbf{q}_b \quad (7-11)$$

where:  $\mathbf{G}_p = [\mathbf{g}_{p,1} \ \mathbf{g}_{p,2} \ \cdots \ \mathbf{g}_{p,k_{eff}} \ \cdots \ \mathbf{g}_{p,WK}]$ . Hence, the CL-LSIC could be described as linear matrix filtering of the received chip-matched signal vector. Using the same method as for the matched filter detector, the BER of the  $k^{th}$  effective user at the  $p^{th}$  stage can be shown to be:

$$P_{p,k_{eff}}(\sigma) = \frac{1}{2^{WK-1}} \sum_{\substack{\text{all } \mathbf{b} \\ b_{k_{eff}} = 1}} Q \left( \frac{\mathbf{g}_{p,k_{eff}}^T \bar{\mathbf{S}}_{eff} \bar{\mathbf{A}}_{eff} \mathbf{b}}{\sigma \sqrt{\mathbf{g}_{p,k_{eff}}^T \mathbf{g}_{p,k_{eff}}}} \right) \quad (7-12)$$

where  $Q(\cdot)$  is the  $Q$ -function. The asymptotic multiuser efficiency for the  $k^{th}$  effective user at the  $p^{th}$  stage is given by:

$$\eta_{p,k_{eff}} = \frac{1}{\mathbf{g}_{p,k_{eff}}^T \mathbf{g}_{p,k_{eff}}} \max^2 \left( 0, \mathbf{g}_{p,k_{eff}}^T \bar{\mathbf{s}}_{eff}(k_{eff}) - \sum_{\substack{j=1 \\ j \neq k_{eff}}}^{WK} \frac{\bar{A}_{eff}(j,j)}{\bar{A}_{eff}(k_{eff},k_{eff})} |\mathbf{g}_{p,k_{eff}}^T \bar{\mathbf{s}}_{eff}(j)| \right) \quad (7-13)$$

### 7.8.1 Convergence Behavior

It was demonstrated in [118] and [119] that if the CL-LSIC detector converges, it converges to the decorrelator detector. Hence:

$$\mathbf{y}(\infty) = \bar{\mathbf{R}}_{eff}^{-1} \bar{\mathbf{S}}_{eff}^T \mathbf{q}_b \quad (7-14)$$

where  $\bar{\mathbf{R}}_{eff} = \bar{\mathbf{S}}_{eff}^T \bar{\mathbf{S}}_{eff}$  is the positive definite cross-correlation matrix (the spreading codes are linearly independent).

### 7.8.2 Conditions of Convergence

It was shown also in [118] and [119] that the CL-LSIC detector is always convergent. At intermediate stages where the residual received vector gets close to estimating the noise vector correctly, it is possible that the CL-LSIC performs better in terms of BER than at convergence.

## 7.9 Reduced Complexity Chip-Level Linear SIC (RC-CL-LSIC) Structure

A RC-CL-LSIC structure was proposed initially in [121] for the case of synchronous CDMA AWGN channel, it was extended to the case of asynchronous CDMA multipath fading channel in both [122] and [123]. In fact, the RC-CL-LSIC structure can be considered as a hybrid chip-level symbol-level SIC structure, in the sense that not all the computations are performed at chip-level since some of them are performed at symbol-level. Nevertheless, this scheme still doesn't make use of the cross-correlation coefficients and hence it is considered as a chip-level SIC detector. Because of performing some of the computations at symbol-level, this structure exhibits a reduction in computational complexity of about

33% compared to that of the conventional chip-level linear SIC structure. This will become clear later on when we discuss the computational complexity of different SIC structures.

The RC-CL-LSIC structure consists of ICU's arranged in a multistage structure as illustrated in Figure 7.10. The ICU of the  $p^{th}$  stage,  $k^{th}$  effective user is shown in Figure 7.11. The residual signal  $\mathbf{e}(p, k_{eff})$  at the input of the  $p^{th}$  stage,  $k^{th}$  effective user ICU is first despreaded to estimate the partial decision variable  $y'(p, k_{eff})$  of the  $p^{th}$  stage,  $k^{th}$  effective user, that is:  $y'(p, k_{eff}) = \bar{\mathbf{s}}_{eff}(k_{eff})^T \mathbf{e}(p, k_{eff})$ . The residual signal of the next user ( $k_{eff}+1$ ) is obtained as:  $\mathbf{e}(p, k_{eff}+1) = \mathbf{e}(p, k_{eff}) - \bar{\mathbf{s}}_{eff}(k_{eff})(y(p, k_{eff}) - y(p-1, k_{eff}))$  where:  $y(p, k_{eff}) = y'(p, k_{eff}) + y(p-1, k_{eff})$ . This process is repeated in a multistage structure as it is shown in Figure 7.10.

As shown in [121], it is easy to show that after some manipulations the general expression for the residual signal vector and the decision variable of the  $k^{th}$  effective user's ICU unit at the  $p^{th}$  stage, respectively, can be obtained as:

$$\mathbf{e}(p, k_{eff}) = \Phi_{k_{eff}-1} (\Phi_{WK})^{p-1} \mathbf{q}_b \quad (7-15)$$

and:

$$y(p, k_{eff}) = \bar{\mathbf{s}}_{eff}(k_{eff})^T \Phi_{k_{eff}-1} \sum_{i=0}^{p-1} (\Phi_{WK})^i \mathbf{q}_b = \mathbf{g}_{p, k_{eff}}^T \mathbf{q}_b \quad (7-16)$$

where:

$$\Phi_{k_{eff}} = \prod_{j=k_{eff}}^1 (\mathbf{I} - \bar{\mathbf{s}}_{eff}(j) \bar{\mathbf{s}}_{eff}(j)^T) \quad (7-17)$$

Collecting the decision variables of all users in one matrix we get:

$$\mathbf{y}(p) = \mathbf{G}_p^T \mathbf{q}_b \quad (7-18)$$

where:  $\mathbf{G}_p = [\mathbf{g}_{p,1} \quad \mathbf{g}_{p,2} \quad \cdots \quad \mathbf{g}_{p,k_{eff}} \quad \cdots \quad \mathbf{g}_{p,WK}]$ . Hence, the RC-CL-LSIC detector can be described as matrix filtering of the received chip-matched signal vector.

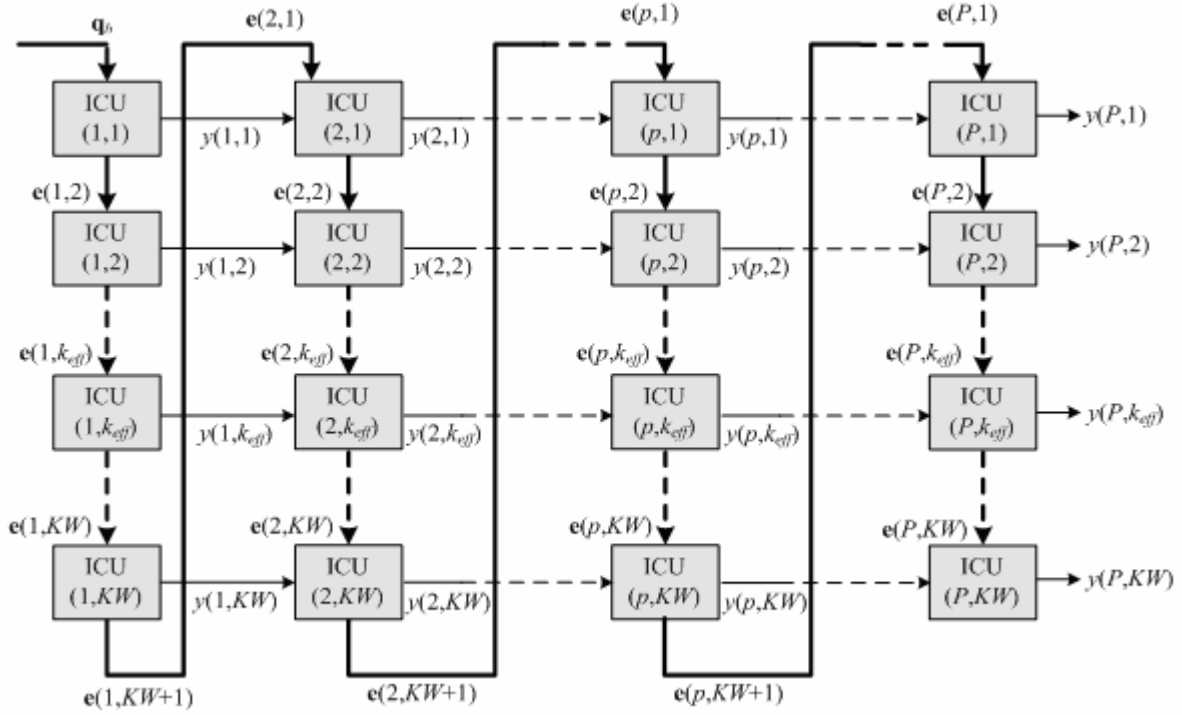


Figure 7.10: Multistage structure of the RC-CL-LSIC detector.

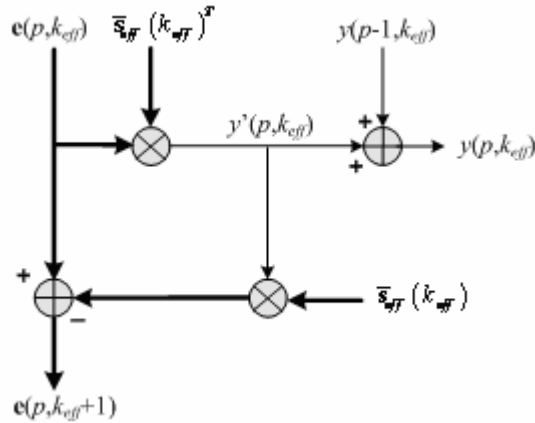


Figure 7.11:  $p^{\text{th}}$  stage,  $k^{\text{th}}$  effective user's RC-CL-LSIC unit (ICU).

Using the same method as for the conventional detector, the BER of the  $k^{\text{th}}$  effective user at the  $p^{\text{th}}$  stage can be expressed as:

$$P_{p,k_{\text{eff}}}(\sigma) = \frac{I}{2^{WK-l}} \sum_{\substack{\text{all } \mathbf{b} \\ b_{k_{\text{eff}}}=1}} Q \left( \frac{\mathbf{g}_{p,k_{\text{eff}}}^T \bar{\mathbf{S}}_{\text{eff}} \bar{\mathbf{A}}_{\text{eff}} \mathbf{b}}{\sigma \sqrt{\mathbf{g}_{p,k_{\text{eff}}}^T \mathbf{g}_{p,k_{\text{eff}}}}} \right) \quad (7-19)$$

where  $Q(\cdot)$  is the  $Q$ -function. As for the BER, the asymptotic multiuser efficiency for the  $k^{\text{th}}$  effective user at the  $p^{\text{th}}$  stage is given by:

$$\eta_{p,k_{\text{eff}}} = \frac{I}{\mathbf{g}_{p,k_{\text{eff}}}^T \mathbf{g}_{p,k_{\text{eff}}}} \max^2 \left( 0, \mathbf{g}_{p,k_{\text{eff}}}^T \bar{\mathbf{s}}_{\text{eff}}(k_{\text{eff}}) - \sum_{\substack{j=1 \\ j \neq k_{\text{eff}}}}^{WK} \frac{\bar{A}_{\text{eff}}(j,j)}{\bar{A}_{\text{eff}}(k_{\text{eff}},k_{\text{eff}})} |\mathbf{g}_{p,k_{\text{eff}}}^T \bar{\mathbf{s}}_{\text{eff}}(j)| \right) \quad (7-20)$$

### 7.9.1 Convergence Behavior

As for the case of the CL-LSIC structure, it can be shown that if the RC-CL-LSIC detector converges it converges to the decorrelator detector [121], that is,

$$\mathbf{y}(\infty) = \bar{\mathbf{R}}_{\text{eff}}^{-1} \bar{\mathbf{S}}_{\text{eff}}^T \mathbf{q}_b \quad (7-21)$$

where  $\bar{\mathbf{R}}_{\text{eff}} = \bar{\mathbf{S}}_{\text{eff}}^T \bar{\mathbf{S}}_{\text{eff}}$  is the positive definite cross-correlation matrix (the spreading codes are linearly independent).

### 7.9.2 Conditions of Convergence

As for the case of the CL-LSIC detector, it can be shown that the RC-CL-LSIC structure is always convergent for any positive definite symmetric matrix [121]. Here also and at intermediate stages where the residual received vector gets close to estimating the noise vector correctly, it is possible that the linear SIC performs better in terms of BER than at convergence.

## 7.10 Reduced Complexity Chip-Level Linear Group-Wise SIC (RC-CL-LGSIC) Structure

This scheme was first introduced in [124]. As for the SL-LGSIC detector, the users are partitioned into groups; the interference due to users within the same group is cancelled in parallel while the mutual interference between groups is cancelled in series. Additionally, this scheme reduces the detection delay with a factor of  $G/K$ .

Even though this scheme is considered as a chip-level structure, its classification in fact is dependent on the group-detection scheme. For example, if the group-detection scheme is the CL-LPIC detector or the matched filter detector, then the resultant structure is a pure chip-level linear group-wise SIC structure. However, if the group-detection scheme is the decorrelator detector or the LMMSE

detector, then the resultant structure is in reality a hybrid chip-level symbol-level linear group-wise SIC structure. The RC-CL-LGSIC detector consists of group interference cancellation units (GICU) arranged in a multistage structure as illustrated in Figure 7.12. The basic interference cancellation unit of the  $p^{th}$  stage,  $g^{th}$  effective group of users is shown in Figure 7.13. The residual signal  $\mathbf{e}(p, g_{th})$  at the input of the  $p^{th}$  stage,  $g^{th}$  effective GICU is first despreaded to estimate the partial decision variable  $\mathbf{y}'(p, g_{eff})$  of the  $p^{th}$  stage,  $g^{th}$  effective group, that is:  $\mathbf{y}'(p, g_{eff}) = \bar{\mathbf{S}}_{eff}(g_{eff})^T \mathbf{e}(p, g_{eff})$ .

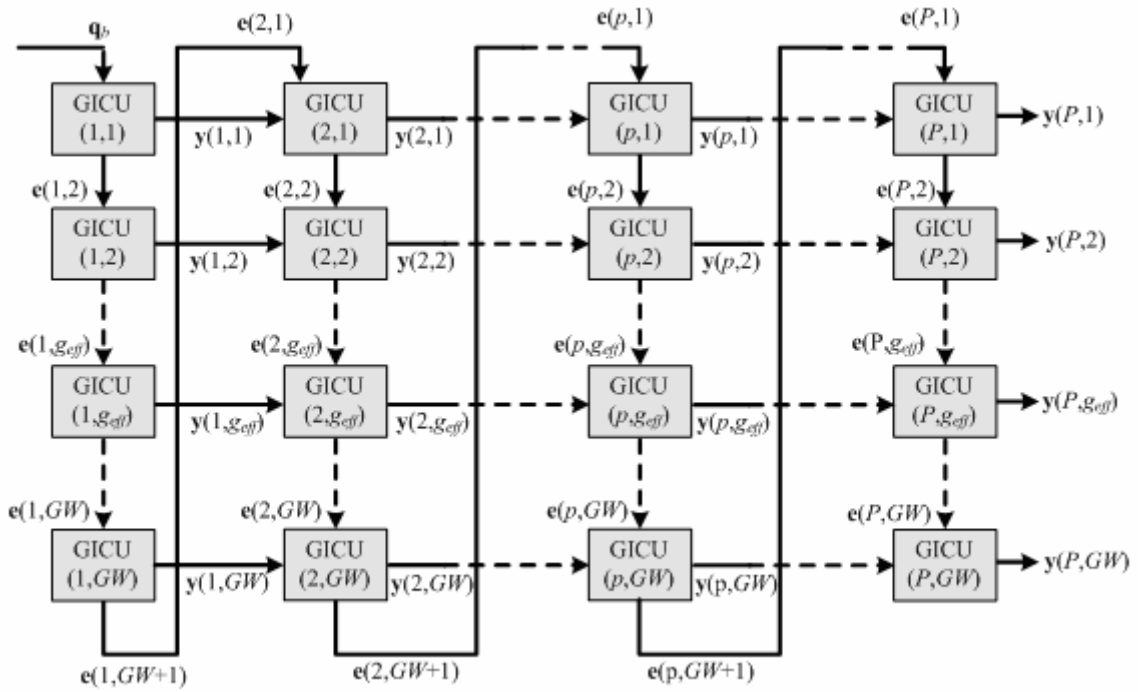
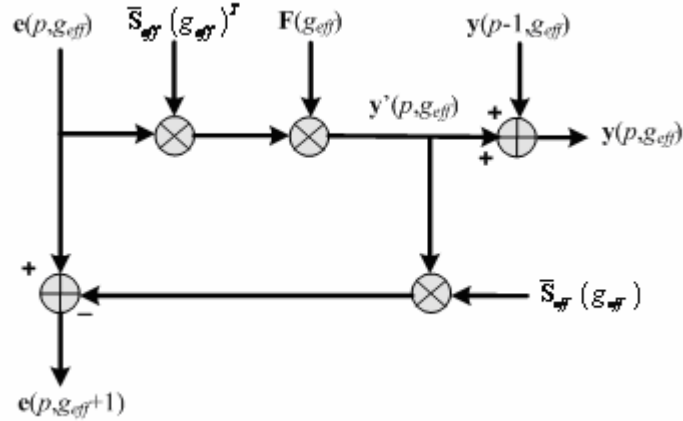


Figure 7.12: Multistage structure of the RC-CL-LGSIC detector.

The residual signal of the next group of users ( $g_{eff}+1$ ) is obtained as:

$$\mathbf{e}(p, g_{eff} + 1) = \mathbf{e}(p, g_{eff}) - \bar{\mathbf{S}}_{eff}(g_{eff})(\mathbf{y}(p, g_{eff}) - \mathbf{y}(p-1, g_{eff})) \quad \text{where:}$$

$\mathbf{y}(p, g_{eff}) = \mathbf{y}'(p, g_{eff}) + \mathbf{y}(p-1, g_{eff})$ . This process is repeated in a multistage structure as it is shown in Figure 7.12


 Figure 7.13:  $p^{\text{th}}$  stage,  $g^{\text{th}}$  effective group RC-CL-LGSIC unit (GICU).

It was demonstrated in [124] that the general expression for the residual signal vector of the  $g^{\text{th}}$  effective GICU at the  $p^{\text{th}}$  stage can be obtained as:

$$\mathbf{e}(p, g_{\text{eff}}) = \Phi_{g_{\text{eff}}-1} (\Phi_{WG})^{p-1} \mathbf{q}_b \quad (7-22)$$

and similarly, the vector of decision variables of the  $g^{\text{th}}$  effective GICU at the  $p^{\text{th}}$  stage can be expressed as:

$$\mathbf{y}(p, g_{\text{eff}}) = \mathbf{F}(g_{\text{eff}}) \bar{\mathbf{S}}_{\text{eff}}(g_{\text{eff}})^T \Phi_{g_{\text{eff}}-1} \sum_{i=0}^{p-1} (\Phi_{WG})^i \mathbf{q}_b = \mathbf{G}_{p, g_{\text{eff}}}^T \mathbf{q}_b \quad (7-23)$$

where:  $\Phi_{g_{\text{eff}}} = \prod_{j=g_{\text{eff}}}^1 (\mathbf{I} - \bar{\mathbf{S}}_{\text{eff}}(j) \mathbf{F}(j) \bar{\mathbf{S}}_{\text{eff}}(j)^T)$ .

Collecting the decision variables of all groups in one matrix we get:

$$\mathbf{y}(p) = \mathbf{G}_p^T \mathbf{q}_b$$

where

$$\mathbf{G}_p = [\mathbf{G}_{p,1} \quad \mathbf{G}_{p,2} \quad \cdots \quad \mathbf{G}_{p,g_{\text{eff}}} \quad \cdots \quad \mathbf{G}_{p,WG}].$$

and

$$\mathbf{G}_{p, g_{\text{eff}}} = [\mathbf{g}_{p, g_{\text{eff}}, 1} \quad \mathbf{g}_{p, g_{\text{eff}}, 2} \quad \cdots \quad \mathbf{g}_{p, g_{\text{eff}}, u_{g_{\text{eff}}}} \quad \cdots \quad \mathbf{g}_{p, g_{\text{eff}}, U_{g_{\text{eff}}}}].$$

The matrix  $\mathbf{G}_p$  can also be written as:  $\mathbf{G}_p = [\mathbf{g}_{p,1} \quad \mathbf{g}_{p,2} \quad \cdots \quad \mathbf{g}_{p,k_{\text{eff}}} \quad \cdots \quad \mathbf{g}_{p,WK}]$ . Therefore the RC-CL-LGSIC can be described as a matrix filtering of the received chip-matched signal vector. Using the

same method as for the matched filter detector, the BER of the  $k^{\text{th}}$  effective user at the  $p^{\text{th}}$  stage can be evaluated as:

$$P_{p,k_{\text{eff}}}(\sigma) = \frac{1}{2^{WK-1}} \sum_{\substack{\text{all } \mathbf{b} \\ b_{k_{\text{eff}}}=1}} Q \left( \frac{\mathbf{g}_{p,k_{\text{eff}}}^T \bar{\mathbf{S}}_{\text{eff}} \bar{\mathbf{A}}_{\text{eff}} \mathbf{b}}{\sigma \sqrt{\mathbf{g}_{p,k_{\text{eff}}}^T \mathbf{g}_{p,k_{\text{eff}}}}} \right) \quad (7-24)$$

where  $Q(\cdot)$  is the  $Q$ -function. On the other hand, the asymptotic multiuser efficiency for the  $k^{\text{th}}$  effective user at the  $p^{\text{th}}$  stage is given by:

$$\eta_{p,k_{\text{eff}}} = \frac{1}{\mathbf{g}_{p,k_{\text{eff}}}^T \mathbf{g}_{p,k_{\text{eff}}}} \max^2 \left( 0, \mathbf{g}_{p,k_{\text{eff}}}^T \bar{\mathbf{s}}_{\text{eff}}(k_{\text{eff}}) - \sum_{\substack{j=1 \\ j \neq k_{\text{eff}}}}^{WK} \frac{\bar{A}_{\text{eff}}(j,j)}{\bar{A}_{\text{eff}}(k_{\text{eff}},k_{\text{eff}})} \left| \mathbf{g}_{p,k_{\text{eff}}}^T \bar{\mathbf{s}}_{\text{eff}}(j) \right| \right) \quad (7-25)$$

### 7.10.1 Group Detection Schemes

Depending on the transformation matrix  $\mathbf{F}(\mathbf{g}_{\text{eff}})$ , several group detection schemes can be obtained. Four linear group detection schemes were considered in [124], namely the reduced-complexity chip-level linear group matched filter successive interference cancellation detector (RC-CL-LGMF-SIC), the reduced-complexity chip-level linear group parallel interference cancellation successive interference cancellation detector (RC-CL-LGPIC-SIC), the reduced-complexity chip-level linear group decorrelator successive interference cancellation detector (RC-CL-LGDEC-SIC) and finally the reduced-complexity chip-level linear group minimum mean square error successive interference cancellation detector (RC-CL-LGMMSE-SIC). All these group detection schemes are detailed in the next section.

#### 7.10.1.1 The RC-CL-LGMF-SIC Detector

It is the simplest scheme, and it is obtained by letting:

$$\mathbf{F}(\mathbf{g}_{\text{eff}}) = \mathbf{I} \quad (7-26)$$

where  $\mathbf{I}$  is an  $(U_{g_{\text{eff}}} - \text{by} - U_{g_{\text{eff}}})$  identity matrix. This can be seen as a generalization of the conventional SIC where more than one user is considered in each cancellation.

#### 7.10.1.2 The RC-CL-LGPIC-SIC Detector

We can generalize the concept of the RC-CL-LGMF-SIC if we let the group detector to be a linear  $N_{\text{PIC}}$ -stage PIC detector. Thus the linear transformation is given by:

$$\mathbf{F}(\mathbf{g}_{eff}) = \sum_{i=0}^{N_{PIC}} \left( \mathbf{I} - \bar{\mathbf{S}}_{eff}(\mathbf{g}_{eff})^T \bar{\mathbf{S}}_{eff}(\mathbf{g}_{eff}) \right)^i \quad (7-27)$$

### 7.10.1.3 The RC-CL-LGDEC-SIC Detector

For this detector, the linear transformation is given by:

$$\mathbf{F}(\mathbf{g}_{eff}) = \left( \bar{\mathbf{S}}_{eff}(\mathbf{g}_{eff})^T \bar{\mathbf{S}}_{eff}(\mathbf{g}_{eff}) \right)^{-1} \quad (7-28)$$

Note that if the group size is equal to one, we obtain the conventional linear RC-CL-LSIC detector.

### 7.10.1.4 The RC-CL-LGMMSE-SIC Detector

For the RC-CL-LGMMSE-SIC detector, the linear transformation is given by:

$$\mathbf{F}(\mathbf{g}_{eff}) = \left( \bar{\mathbf{S}}_{eff}(\mathbf{g}_{eff})^T \bar{\mathbf{S}}_{eff}(\mathbf{g}_{eff}) + \sigma^2 \bar{\mathbf{A}}_{eff}(\mathbf{g}_{eff}, \mathbf{g}_{eff})^{-2} \right)^{-1} \quad (7-29)$$

where  $\sigma^2$  is the variance of the AWGN. Note that when the noise level is low the linear transformation  $\mathbf{F}(\mathbf{g}_{eff})$  approaches the one for the RC-CL-LGDEC-SIC detector but, if the noise level is high  $\mathbf{F}(\mathbf{g}_{eff})$  approaches a scaled identity matrix, which corresponds to the RC-CL-LGMF-SIC detector.

## 7.10.2 Convergence Behavior

It was shown in [124] that if  $\mathbf{F}(\mathbf{g}_{eff})$  is invertible for all  $\mathbf{g}_{eff} = 1, 2, \dots, WG$ . and  $\bar{\mathbf{R}}_{eff}$  is also invertible (all spreading codes are linearly independent) than the RC-CL-LGSIC scheme converges to the decorrelator detector if it converges. Hence:

$$\mathbf{y}(\infty) = \left( \bar{\mathbf{S}}_{eff}^T \bar{\mathbf{S}}_{eff} \right)^{-1} \bar{\mathbf{S}}_{eff}^T \mathbf{q}_b \quad (7-30)$$

### 7.10.3 Conditions of Convergence

It was demonstrated in [124] that only the RC-CL-LGDEC-SIC is always convergent. For the other group detection schemes, the convergence is not always guaranteed. Nevertheless, their convergence can be ensured by inserting a weighting parameter that forces all the eigenvalues of the transition matrix to be less than one as in [125]-[127].

## 7.11 Case of CDMA Multi-Path Fading Channel

The cross-correlation matrix for the case of a CDMA multi-path fading channel is different than that of a CDMA AWGN channel because the main diagonal is not equal to the identity matrix. This causes the

previously detailed chip-level linear SIC structures to diverge. Hence, a modification to these schemes is necessary for their proper functioning in a CDMA multi-path fading channel. All the convergence analysis detailed above for the chip-level linear SIC/GSIC structure operating in a CDMA AWGN channel holds here as well. The CL-LSIC unit is modified as follows:

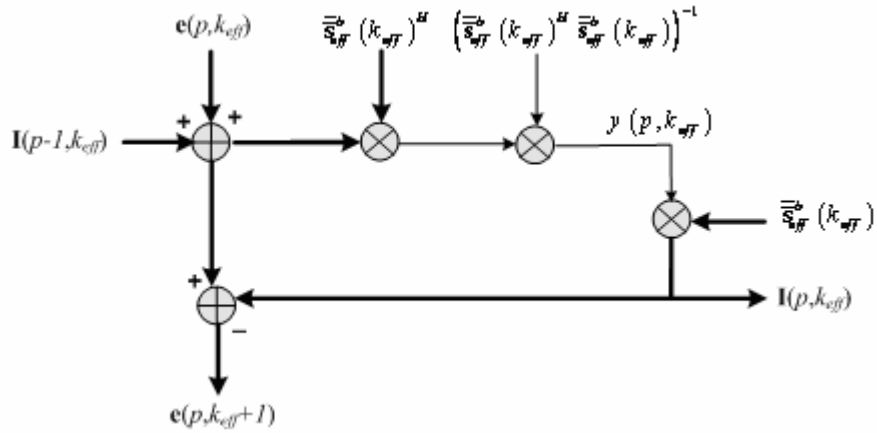


Figure 7.14: The CL-LSIC unit for the CDMA multi-path fading channel

whereas the reduced-complexity chip-level linear successive interference cancellation unit is modified as follows:

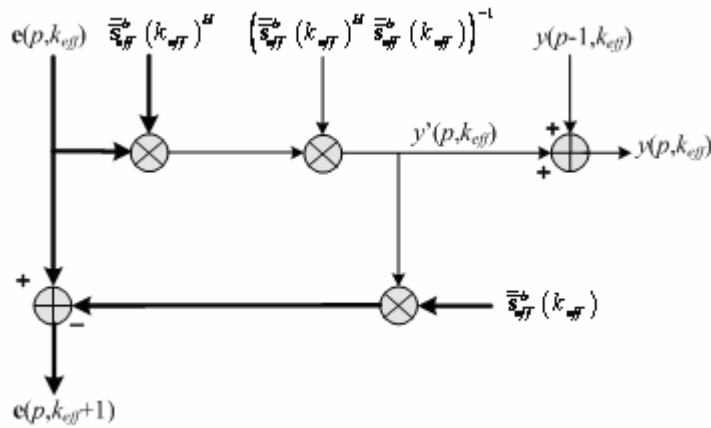


Figure 7.15: RC-CL-LSIC unit for the CDMA multi-path fading channel

Finally, the RC-CL-LGMF-SIC unit is modified as follows:

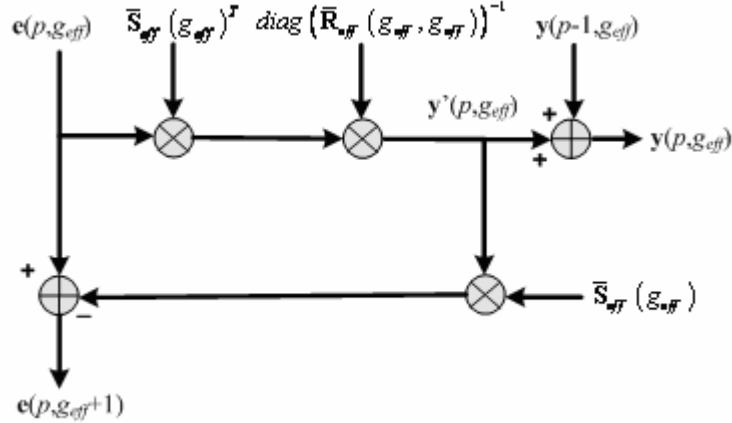


Figure 7.16: RC-CL-LGMF-SIC unit for the CDMA multi-path fading channel

The under-relaxation principle is generally used to ensure the convergence of divergent iterative methods. It was used in [125]-[127] to ensure the convergence of the divergent schemes introduced in [124]. In the following, the under-relaxation principle is used to ensure the convergence of the structures that are convergent for the CDMA AWGN channel but not for the CDMA multipath fading channel. The structures developed using this principle (Figure 7.17, 7.18 and 7.19) exhibit minor reduction in computational complexity compared to their counterparts in (Figure 7.14, 7.15 and 7.16) in the sense that these detectors avoid the inversion of the matrix  $\mathbf{D}$ .

At the  $p^{\text{th}}$  stage, the residual signal due to the  $k^{\text{th}}$  effective user of the CL-LSIC/RC-CL-LSIC detectors is derived as [117]:

$$\mathbf{e}(p, k_{\text{eff}}) = \mathbf{q}_b - \sum_{j=1}^{k_{\text{eff}}-1} \bar{\mathbf{s}}_{\text{eff}}(j) y(p, j) - \sum_{j=k_{\text{eff}}}^{WK} \bar{\mathbf{s}}_{\text{eff}}(j) y(p-1, j) \quad \text{for } k_{\text{eff}} = 1, 2, \dots, WK. \quad (7-31)$$

Hence, the decision variable is given by:

$$\begin{aligned} y(p, k_{\text{eff}}) &= \bar{\mathbf{s}}_{\text{eff}}(k_{\text{eff}})^T \mathbf{q}_b - \bar{\mathbf{s}}_{\text{eff}}(k_{\text{eff}})^T \sum_{j=1}^{k_{\text{eff}}-1} \bar{\mathbf{s}}_{\text{eff}}(j) y(p, j) \\ &\quad - \bar{\mathbf{s}}_{\text{eff}}(k_{\text{eff}})^T \sum_{j=k_{\text{eff}}+1}^{WK} \bar{\mathbf{s}}_{\text{eff}}(j) y(p-1, j) \quad \text{for } k_{\text{eff}} = 1, 2, \dots, WK. \end{aligned} \quad (7-32)$$

Also, from Figure 7.13, the residual signal due to the  $k^{\text{th}}$  effective user of the RC-CL-LGMF-SIC detector is derived as we have:

$$\mathbf{y}(p, \mathbf{g}_{\text{eff}}) = \bar{\mathbf{S}}_{\text{eff}}(\mathbf{g}_{\text{eff}})^T \mathbf{e}(p, \mathbf{g}_{\text{eff}}) + \mathbf{y}(p-1, \mathbf{g}_{\text{eff}}) \quad (7-33)$$

where  $\mathbf{e}(p, g_{eff})$  can be written in terms of the decision variables as:

$$\mathbf{e}(p, g_{eff}) = \mathbf{q}_b - \sum_{j=1}^{g_{eff}-1} \bar{\mathbf{S}}_{eff}(j) \mathbf{y}(p, j) - \sum_{j=g_{eff}}^{WG} \bar{\mathbf{S}}_{eff}(j) \mathbf{y}(p-1, j) \quad (7-34)$$

A careful look to the equations above can easily show that CL-LSIC/RC-CL-LSIC and RC-CL-LGMF-SIC detectors are equivalent to the modified point Gauss-Seidel and modified block Gauss-seidel iterative methods, respectively, detailed in Chapter 5. These methods were proven to converge if, in addition to the symmetry and positive definitiveness of the coefficient matrix, the maximum eigenvalue of the diagonal/block diagonal part of the coefficient matrix is between 0 and 2. This can be ensured by inserting a relaxation factor as for the case of modified point successive over-relaxation method and modified block successive over-relaxation method. These two methods are convergent if  $0 < \omega < \frac{2}{\lambda_{max}(\mathbf{D})}$  which can be replaced by some upper bound of the maximum eigenvalue of the matrix D, e.g. trace(D).

Therefore Figure 7.14 and 7.15 are modified by replacing  $\left(\bar{\mathbf{S}}_{eff}^b(k_{eff})^H \bar{\mathbf{S}}_{eff}^b(k_{eff})\right)^{-1}$  by  $\omega$ . However, for Figure 7.13 the group detection matrix  $\mathbf{F}(g_{eff}) = \mathbf{I}$  (for the case of RC-CL-LGMF-SIC detection scheme) is replaced by  $\mathbf{F}(g_{eff}) = \omega \mathbf{I}$ . The resulting figures are shown below:

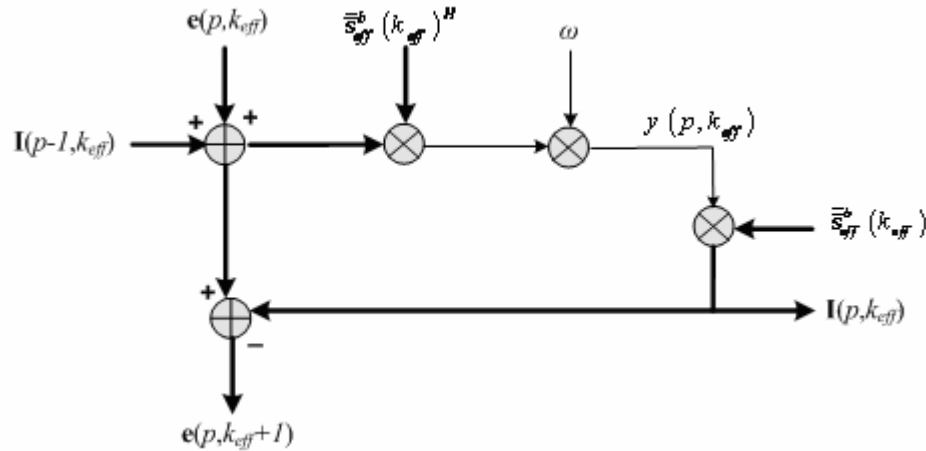


Figure 7.17: CL-LSIC unit for the CDMA multi-path fading channel using the under-relaxation principle

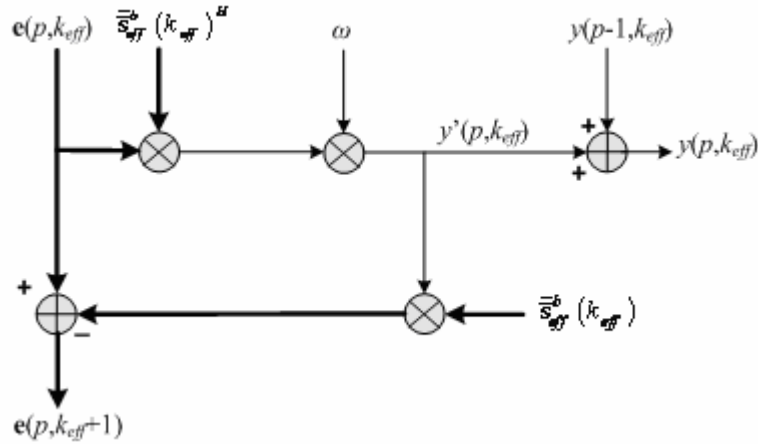


Figure 7.18: RC-CL-LSIC unit for the CDMA multi-path fading channel using the under-relaxation principle.

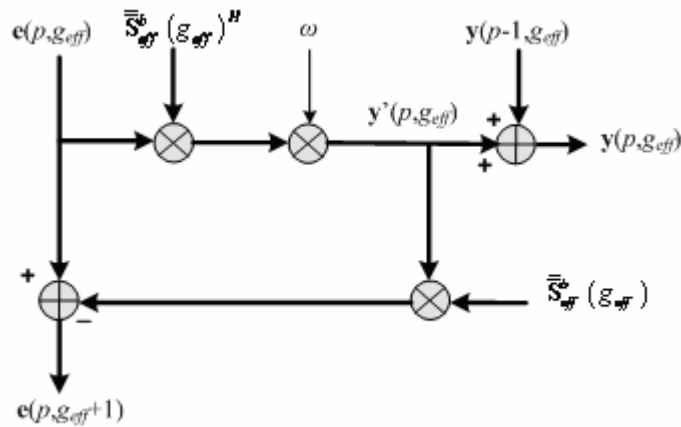


Figure 7.19: RC-CL-LGMF-SIC unit for the CDMA multi-path fading channel using the under-relaxation principle.

### 7.12 Chip-Level Linear PIC/Weighted PIC (CL-LPIC/CL-LWPIC) Structure

This scheme was proposed in [128]-[134]. It uses directly the spreading codes instead of the cross-correlation matrix coefficients in the detection process. In this section, the CL-LWPIC detector presented in [128] and extended here to the case of multipath fading scenario, consists of ICU's

arranged in a multistage structure as shown in Figure 7.20. The internal structure of each ICU is illustrated in Figure 7.21.

The vector of decision variables of the  $(p-1)^{th}$  stage,  $k^{th}$  user  $y(p-1, k_{eff})$  is first despread added to the decision variables of the other users to form the interference due to all users at the  $(p-1)^{th}$  stage, that is,  $\mathbf{I}(p-1) = \sum_{j=1}^{KW} \bar{\mathbf{s}}_{eff}(j) y(p-1, j)$ . The latter is subtracted out from the received signal  $\mathbf{q}$  to obtain a purified received signal  $(\mathbf{q} - \mathbf{I}(p-1))$  where all users exhibit less mutual interference. The decision variable of the  $p^{th}$  stage,  $k^{th}$  user  $y(p, k_{eff})$  is obtained by despreading the purified signal, multiplying the result by a weighting factor and finally adding the result to the decision variable of the previous stage, that is:

$$y(p, k_{eff}) = \frac{\omega \bar{\mathbf{s}}_{eff}(k_{eff})^T}{\bar{\mathbf{s}}_{eff}(k_{eff})^T \bar{\mathbf{s}}_{eff}(k_{eff})} (\mathbf{q} - \mathbf{I}(p-1)) + y(p-1, k_{eff}) \quad (7-35)$$

This process is repeated in a multistage structure as shown in Figure 7.20.

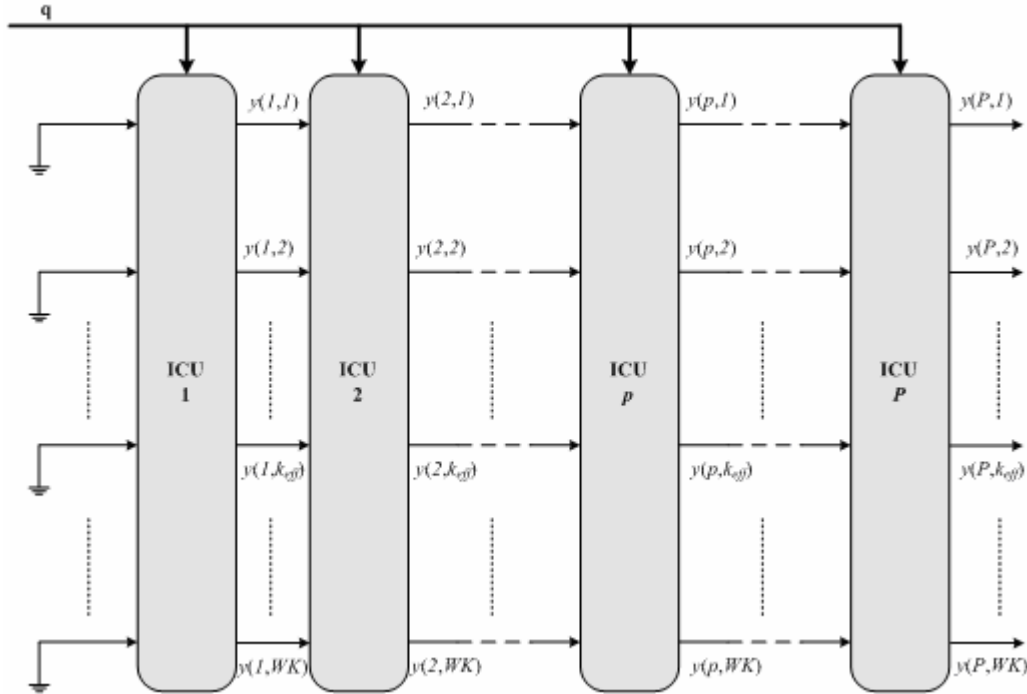


Figure 7.20: Multi-stage structure of the CL-LWPIC detector.

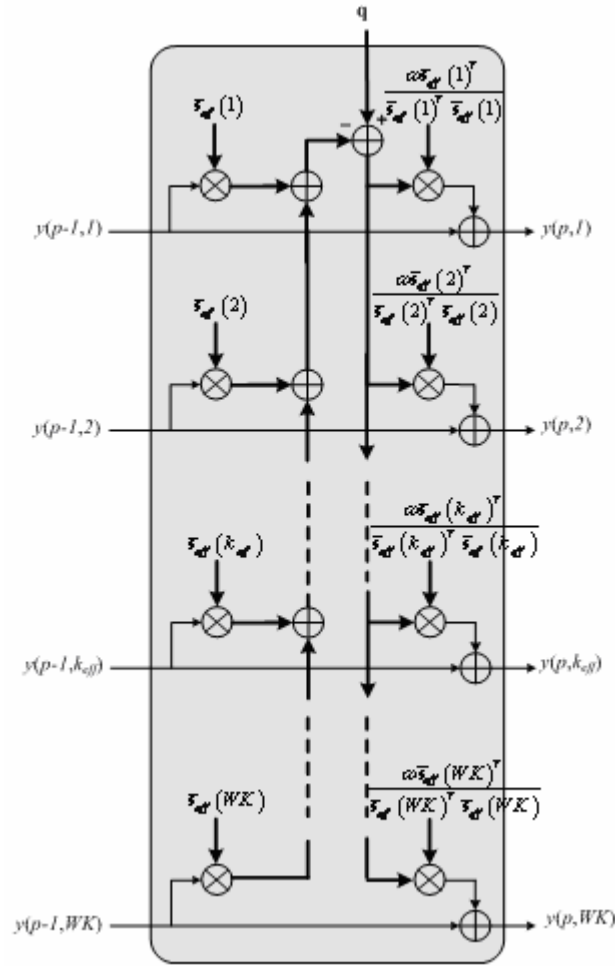


Figure 7.21: The  $p^{\text{th}}$  stage interference cancellation unit of the CL-LWPIC detector.

It was shown in [128] using an algebraic approach that the CL-LWPIC detector is equivalent to matrix filtering of the received chip-matched signal. This enables the determination of analytical expressions for the BER and AME of the proposed detector. Equation (7-35) can be written in matrix form as:

$$\mathbf{y}(p) = \omega \mathbf{D}^{-1} \bar{\mathbf{S}}_{\text{eff}}^T (\mathbf{q} - \bar{\mathbf{S}}_{\text{eff}} \mathbf{y}(p-1)) + \mathbf{y}(p-1) \quad (7-36)$$

where  $\mathbf{D}$  is the diagonal part of the cross-correlation matrix  $\bar{\mathbf{R}}_{\text{eff}} = \bar{\mathbf{S}}_{\text{eff}}^T \bar{\mathbf{S}}_{\text{eff}}$ . Taking in consideration that  $\mathbf{y}(p) = \mathbf{0}$ , it can be shown as in [128] that (7-36) is equivalent to:

$$\begin{aligned}
 y(p) &= \omega \sum_{i=1}^p (\mathbf{I} - \omega \mathbf{D}^{-1} \bar{\mathbf{S}}_{eff}^T \bar{\mathbf{S}}_{eff})^{i-1} \mathbf{D}^{-1} \bar{\mathbf{S}}_{eff}^T \mathbf{q} \\
 &= \mathbf{G}_p^T \mathbf{q}
 \end{aligned} \tag{7-37}$$

where  $\mathbf{G}_p = [\mathbf{g}_{p,1} \ \mathbf{g}_{p,2} \ \cdots \ \mathbf{g}_{p,k_{eff}} \ \cdots \ \mathbf{g}_{p,WK}]$ .

Therefore, the CL-LWPIC can be described as matrix filtering of the received chip-matched signal vector. Thus, if the spreading codes and grouping of all users are available, the decision variables of all users could be obtained without explicitly performing parallel interference cancellation.

Using the same method as for the matched filter detector, the BER of the  $k^{th}$  effective user at the  $p^{th}$  stage can be evaluated as:

$$P_{p,k_{eff}}(\sigma) = \frac{1}{2^{WK-1}} \sum_{\substack{\text{all } \mathbf{b} \\ b_{k_{eff}}=1}} Q \left( \frac{\mathbf{g}_{p,k_{eff}}^T \bar{\mathbf{S}}_{eff} \bar{\mathbf{A}}_{eff} \mathbf{b}}{\sigma \sqrt{\mathbf{g}_{p,k_{eff}}^T \mathbf{g}_{p,k_{eff}}}} \right) \tag{7-38}$$

where  $Q(\cdot)$  is the  $Q$ -function. Additionally, the AME for the  $k^{th}$  effective user at the  $p^{th}$  stage is given by:

$$\eta_{p,k_{eff}}(\sigma) = \frac{1}{\mathbf{g}_{p,k_{eff}}^T \mathbf{g}_{p,k_{eff}}} \max^2 \left( 0, \mathbf{g}_{p,k_{eff}}^T \bar{\mathbf{s}}_{eff}(k_{eff}) - \sum_{\substack{j=1 \\ j \neq k_{eff}}}^{WK} \frac{\bar{\mathbf{A}}_{eff}(j,j)}{\bar{\mathbf{A}}_{eff}(k_{eff},k_{eff})} |\mathbf{g}_{p,k_{eff}}^T \bar{\mathbf{s}}_{eff}(j)| \right) \tag{7-39}$$

Before discussing the convergence behavior of the proposed scheme let us develop the relation between the latter and the Jacobi iterative method. Equation (7-35) can be written as:

$$\begin{aligned}
 y(p, k_{eff}) &= \frac{\omega \bar{\mathbf{s}}_{eff}(k_{eff})^T}{\bar{\mathbf{s}}_{eff}(k_{eff})^T \bar{\mathbf{s}}_{eff}(k_{eff})} \mathbf{q} + (1-\omega) y(p-1, j) \\
 &\quad + \frac{\omega \bar{\mathbf{s}}_{eff}(k_{eff})^T}{\bar{\mathbf{s}}_{eff}(k_{eff})^T \bar{\mathbf{s}}_{eff}(k_{eff})} \sum_{\substack{j=1 \\ j \neq k}}^{KW} \bar{\mathbf{s}}_{eff}(j) y(p-1, j)
 \end{aligned} \tag{7-40}$$

which is exactly the linear point Jacobi relaxation iteration used for matrix inversion.

### 7.12.1 Convergence Behavior

From (7-36), it easy to show that as the number of stages tends to infinity the vector of decision variables tend to that of the decorrelator detector, that is,

$$\begin{aligned}
 \lim_{p \rightarrow \infty} \mathbf{y}(p) &= \lim_{p \rightarrow \infty} \omega \sum_{i=1}^p \left( \mathbf{I} - \omega \mathbf{D}^{-1} \bar{\mathbf{S}}_{eff}^T \bar{\mathbf{S}}_{eff} \right)^{i-1} \mathbf{D}^{-1} \bar{\mathbf{S}}_{eff}^T \mathbf{q} \\
 &= \omega \left( \omega \mathbf{D}^{-1} \bar{\mathbf{S}}_{eff}^T \bar{\mathbf{S}}_{eff} \right)^{-1} \mathbf{D}^{-1} \bar{\mathbf{S}}_{eff}^T \mathbf{q} \\
 &= \left( \bar{\mathbf{S}}_{eff}^T \bar{\mathbf{S}}_{eff} \right)^{-1} \bar{\mathbf{S}}_{eff}^T \mathbf{q}
 \end{aligned} \tag{7-41}$$

which is the decorrelator detector. Therefore, if the CL-LWPIC detector converges, it converges to the decorrelator detector.

### 7.12.2 Conditions of Convergence

The parallel interference cancellation detector is well known to suffer from severe convergence issues ([128], [129] and [134]). By observing that the iteration matrix of the proposed detector is given by:

$$\mathbf{B} = \left( \mathbf{I} - \omega \mathbf{D}^{-1} \bar{\mathbf{S}}_{eff}^T \bar{\mathbf{S}}_{eff} \right) \tag{7-42}$$

It is easy to determine the condition of convergence of the proposed scheme, that is:

$$0 < \omega < \frac{2}{\lambda_{\max} \left( \mathbf{D}^{-1} \bar{\mathbf{S}}_{eff}^T \bar{\mathbf{S}}_{eff} \right)} \tag{7-43}$$

## 7.13 Computational Complexity

In order to conduct a fair comparison between different SIC structures one has first to specify the CDMA system whether it is a short-code CDMA system or a long-code system. This is very important, since many multiuser detectors with low-computational complexity in a short-code system exhibit high-computational complexity in a long-code system and vice versa.

In all parts of this dissertation, we focus on developing linear interference cancellation structures that are suitable for long-code CDMA systems. Thus, if not stated otherwise, the CDMA system considered here is a long-code system. The computational complexity considered here is expressed in terms of number of flops per sliding window. If the computational complexity in terms of number of flops per bit is required instead, one can determine it simply by dividing the computational complexity in terms of number of flops per sliding window by the number of bits within a sliding window  $W$ .

### 7.13.1 Computational Complexity of the SL-LSIC Structure

The computational complexity of symbol-level linear interference cancellation structures consists of three steps:

- Computation of the matched filter outputs.

- Computation of the cross-correlation coefficients (because we are considering a long-code CDMA system).
- Computation of the symbol-level linear interference cancellation structure decision variables.

While the first two steps are common to all symbol-level linear interference cancellation structures, the third step distinguishes between different structures in terms of computational complexity.

The matched filter is given by:  $2\left(WN + \max_{1 \leq k \leq K}(\tau^k) + \max_{1 \leq k \leq K}(\tau_{l_k})\right)WK$  and the complexity required for the computation of the cross-correlation matrix is  $2\left(WN + \max_{1 \leq k \leq K}(\tau^k) + \max_{1 \leq k \leq K}(\tau_{l_k})\right)(WK)^2$ . The computational complexity of the SL-LSIC structure is given by:  $(3W - K - 1)WKP$ . Thus the total computational complexity of the SL-LSIC structure is given by:

$$\begin{aligned} & \left(2\left(WN + \max_{1 \leq k \leq K}(\tau^k) + \max_{1 \leq k \leq K}(\tau_{l_k})\right) - 1\right)WK + 2\left(WN + \max_{1 \leq k \leq K}(\tau^k) + \max_{1 \leq k \leq K}(\tau_{l_k})\right)(WK)^2 \\ & + (3WK - 1)WKP \end{aligned} \quad (7-44)$$

### 7.13.2 Computational Complexity of the SL-LSOR-SIC Structure

The computational complexity of the SL-LSOR-SIC structure is higher than that of the SL-LSIC structure since it comprises the estimation of the optimal relaxation factor. In view of the fact that different estimation algorithms for the relaxation factor lead to different computational complexities, it is desirable to exclude the computation of the relaxation factor when comparing different linear LSOR-SIC schemes and focus on the structure instead. However, if one wishes to compare a LSOR-SIC structure with another multiuser structure then the computation of the relaxation factor should be included.

The total computational complexity of the SL-LSOR-SIC structure (excluding the estimation of the relaxation factor) is:

$$\begin{aligned} & 2\left(WN + \max_{1 \leq k \leq K}(\tau^k) + \max_{1 \leq k \leq K}(\tau_{l_k})\right)WK + 2\left(WN + \max_{1 \leq k \leq K}(\tau^k) + \max_{1 \leq k \leq K}(\tau_{l_k})\right)(WK)^2 \\ & + (3WK + 4)WKP \end{aligned} \quad (7-45)$$

### 7.13.3 Computational Complexity of the SL-LGSIC Structure

The computational complexity of the SL-LGSIC structure is obviously higher than that of the conventional SL-LSIC structure since it acts on a group of users rather than one user. Moreover, it comprises the inversion of a set of cross-correlation sub-matrices.

Here we are assuming that the inversion of these sub-matrices is implemented using direct methods [78]. This is reasonable if the size of these sub-matrices is relatively small, that is, the number of users within each group is small. Otherwise, one has to refer to iterative methods again. The total computational complexity of the SL-LGSIC structure is:

$$\begin{aligned}
 & 2\left(WN + \max_{1 \leq k \leq K}(\tau^k) + \max_{1 \leq k \leq K}(\tau_{l_k})\right)WK + 2\left(WN + \max_{1 \leq k \leq K}(\tau^k) + \max_{1 \leq k \leq K}(\tau_{l_k})\right)(WK)^2 + (WK)^2 \\
 & -W \sum_{g=1}^G U_g^2 + PW^2 \sum_{g=1}^G U_g \sum_{j=1}^G (2U_j - 1) + W \sum_{g=1}^G \left(11U_g^3 + \frac{3}{2}U_g^2 + U_g\right) + PW \sum_{g=1}^G (U_g - 1)U_g
 \end{aligned} \tag{7-46}$$

### 7.13.4 Computational Complexity of the SL-LBSOR-GSIC Structure

The computational complexity of the SL-LBSOR-GSIC structures is obviously higher than that of the conventional SL-LSOR-SIC structure since it acts on a group of users rather than individual users. Here also, we are assuming that the number of users in each group is relatively small such that direct inversion of the corresponding sub-matrices can be performed using direct methods. As for the symbol-level linear SOR-SIC structure, the estimation of the relaxation factor is excluded from the computation complexity calculation. The total computational complexity of the symbol-level linear group-wise SOR-SIC structure is:

$$\begin{aligned}
 & 2\left(WN + \max_{1 \leq k \leq K}(\tau^k) + \max_{1 \leq k \leq K}(\tau_{l_k})\right)WK + 2\left(WN + \max_{1 \leq k \leq K}(\tau^k) + \max_{1 \leq k \leq K}(\tau_{l_k})\right)(WK)^2 \\
 & + (WK)^2 + 2W \sum_{g=1}^G U_g^2 + PW^2 \sum_{g=1}^G U_g \sum_{j=1}^G (2U_j - 1) + PW \sum_{g=1}^G U_g (2U_g - 1) \\
 & + W \sum_{g=1}^G \left(11U_g^3 + \frac{3}{2}U_g^2 + U_g\right) + PW \sum_{g=1}^G U_g^2
 \end{aligned} \tag{7-47}$$

### 7.13.5 Computational Complexity of the SL-LWPIC Detector

The computation complexity of the SL-LWPIC detector proposed in [84] and illustrated in Figure 7.7 is given as follows:

$$\begin{aligned} & \left(2\left(WN + \max_{1 \leq k \leq K}(\tau^k) + \max_{1 \leq k \leq K}(\tau_{l_k})\right) - 1\right)WK + (WK + 7)WKP \\ & + 2\left(WN + \max_{1 \leq k \leq K}(\tau^k) + \max_{1 \leq k \leq K}(\tau_{l_k})\right)(WK)^2 \end{aligned} \quad (7-48)$$

### 7.13.6 Computational Complexity of the CL-LSIC Structure

Unlike the symbol-level linear SIC structures, the chip-level linear SIC structures doesn't require the calculation of the matched filters outputs and the cross-correlation matrix, except the cross-correlation elements of the main diagonal. This represents a considerable reduction in computational complexity. Thus, the computational complexity of the CL-LSIC structure is:

$$6WKP \left( WN + \max_{1 \leq k \leq K}(\tau^k) + \max_{1 \leq k \leq K}(\tau_{l_k}) \right) + 2WK \left( WN + \max_{1 \leq k \leq K}(\tau^k) + \max_{1 \leq k \leq K}(\tau_{l_k}) \right) \quad (7-49)$$

### 7.13.7 Computational Complexity of the RC-CL-LSIC Structure

Since some computations are performed at symbol-level, this structure exhibits lower computational complexity which is given by:

$$WKP \left( 4 \left( WN + \max_{1 \leq k \leq K}(\tau^k) + \max_{1 \leq k \leq K}(\tau_{l_k}) \right) + 1 \right) + 2WK \left( WN + \max_{1 \leq k \leq K}(\tau^k) + \max_{1 \leq k \leq K}(\tau_{l_k}) \right) \quad (7-50)$$

Comparing it with that of the conventional CL-LSIC structure yields a reduction in computational complexity of about 33%.

### 7.13.8 Computational Complexity of the RC-CL-LGSIC Structure

The computational complexity of the RC-CL-LGSIC structure is clearly higher than that of the conventional reduced complexity CL-LSIC structure since it acts on a group of users rather than one user. The computational complexity of the structure is dependent on the group-detection scheme implemented. At the first look, it seems that the structure using the matched filter detector has the lowest computational complexity while the one using the decorrelator or the LMMSE detectors has the highest computational complexity. However, this maybe misleading because the structure using the decorrelator detector needs less stages than the structure using the matched filter detector to converge to the decorrelator detector's BER performance. Hence, to perform a fair comparison between the CL-LGSIC structure with different group-detection schemes, it is better to first determine the number of stages  $P$  needed for convergence for each one and then use  $P$  for the calculation of the computational complexity. For proper comparison with the SL-LGSIC structure that uses the decorrelator detector as

the group-detection scheme, we state only the computational complexity of the CL-LGSIC structure using the decorrelator detector as the group-detection scheme as well. Hence, it is given by:

$$\begin{aligned}
 & PW \left( \sum_{g=1}^G U_g (2U_g - 1) + 2 \sum_g U_g + \left( WN + \max_{1 \leq k \leq K} (\tau^k) + \max_{1 \leq l_k \leq K} (\tau_{l_k}) \right) \sum_{g=1}^G (2U_g - 1) + \right. \\
 & \left. \left( 2WN + 2 \max_{1 \leq k \leq K} (\tau^k) + 2 \max_{1 \leq l_k \leq K} (\tau_{l_k}) - 1 \right) \sum_{g=1}^G U_g \right) + \\
 & PG \left( WN + \max_{1 \leq k \leq K} (\tau^k) + \max_{1 \leq l_k \leq K} (\tau_{l_k}) \right) + W \sum_{g=1}^G \left( 11U_g^3 + \frac{3}{2}U_g^2 + U_g \right) + \\
 & 2W \left( WN + \max_{1 \leq k \leq K} (\tau^k) + \max_{1 \leq l_k \leq K} (\tau_{l_k}) \right) \sum_{g=1}^G (U_g)^2
 \end{aligned} \tag{7-51}$$

### 7.13.9 Computational Complexity of the CL-LWPIC Detector

The computation complexity of this structure is given by:

$$4PWK \left( WN + \max_{1 \leq k \leq K} (\tau^k) + \max_{1 \leq l_k \leq K} (\tau_{l_k}) \right) + (2WK + P) \left( WN + \max_{1 \leq k \leq K} (\tau^k) + \max_{1 \leq l_k \leq K} (\tau_{l_k}) \right) + WK \tag{7-52}$$

## 7.14 Simulation Results

In this section, the abovementioned multiuser detectors are simulated and the results obtained are commented. We simulate the convergence behavior of the chip-level interference cancellation detectors and compare their computational complexity to their symbol-level counterparts. Two different scenarios are considered, a synchronous CDMA AWGN channel and an asynchronous CDMA multipath Rayleigh fading channel. The simulation parameters are depicted in Table 7.1:

Table 7.1: Simulation parameters

Channel	Synchronous CDMA AWGN	Asynchronous CDMA multipath Rayleigh fading
Performance measure	Average BER versus number of stages	Average BER versus number of stages
$K$	20	10
$N$	31	31

SNR	6dB	4dB
$W$	1	5
Spreading codes	Gold	Gold
Power control	Perfect	Perfect
Power delay profile	Not applicable	Vehicular A outdoor Channel for WCDMA
Length of ISI+MAI	0	$\max_{1 \leq k \leq K}(\tau^k) + \max_{1 \leq k \leq K}(\tau_{l_k}) \leq N$

In Figure 7.22, the average BER (average of all users) is plotted versus the number of CL-LSIC/CL-LSIC stages. As it can be easily seen, the CL-LSIC converges faster than the CL-LPIC detector (4 stages for the CL-LSIC detector and 9 stages for the CL-LPIC detector) which corroborates with the theory, however, the CL-LPIC detector achieves a lower average BER level than the CL-LSIC detector. In addition, it is important to notice that lower average BER levels are achieved prior to convergence, this is more noticeable for highly loaded systems and it has also been reported in other references such as [121].

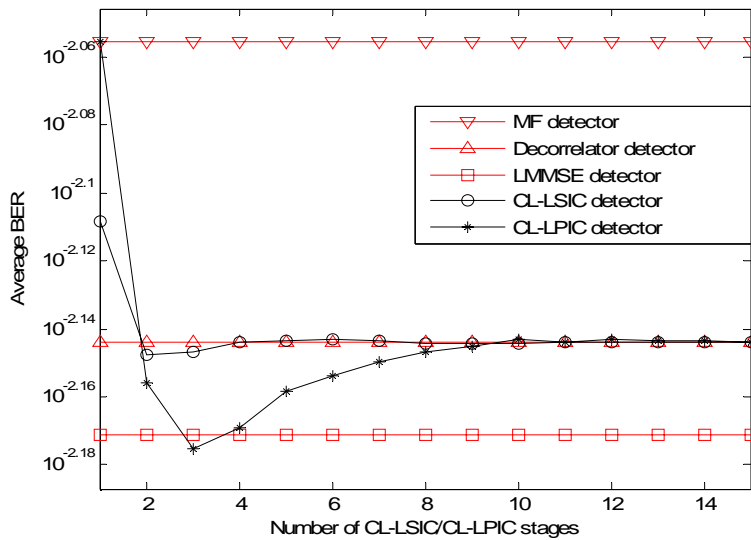


Figure 7.22: Convergence behavior of the CL-LSIC/CL-LPIC detectors.

In Figure 7.23, the average BER (average of all users) is plotted versus the number of RC-CL-LGSIC stages. Different detection schemes are considered. For the RC-CL-LGPIC-SIC detector, a 2-stage PIC detector is used. It is easy to see that the RC-CL-LGDEC-SIC converges faster than the other group-detection schemes (it needs only 4 stages whereas the RC-CL-LGPIC-SIC detector needs 6 stages, the RC-CL-LGMMSE-SIC detector needs 7 stages and the RC-CL-LGMF-SIC detector needs 9 stages). However, the linear RC-CL-LGMF-SIC detector achieves the lowest average BER level among all detection schemes. Moreover, it is important to notice that lower average BER levels are achieved prior to convergence, this is more noticeable for highly loaded systems and it has also been reported in other references such as [121].

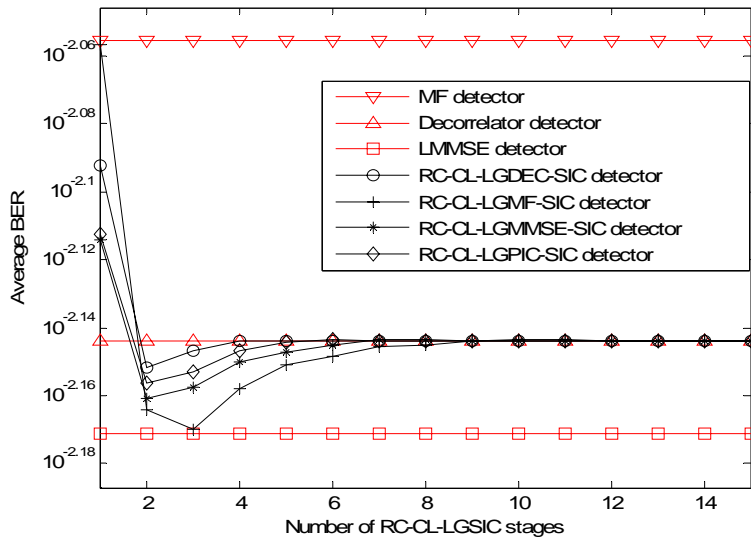


Figure 7.23: Convergence behavior of the RC-CL-LGSIC detector.

The effect of grouping is analyzed in depicted in Figure 7.24, 7.25, 7.26 and 7.27.

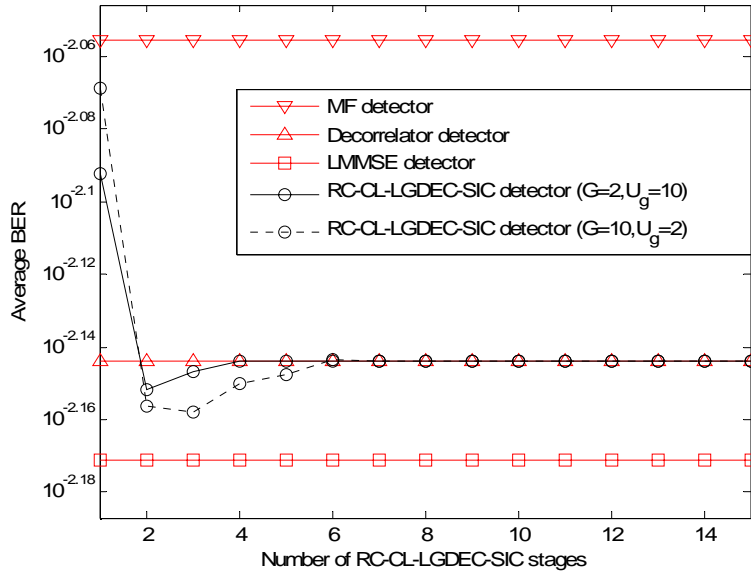


Figure 7.24: Convergence behavior of the RC-CL-LGDEC-SIC detector for  $G = 2$  and  $G = 10$ .

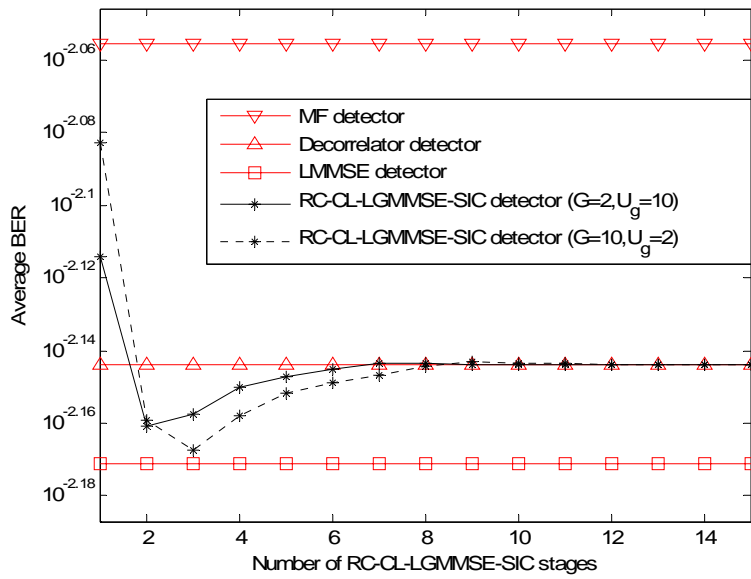


Figure 7.25: Convergence behavior of the RC-CL-LGMMSE-SIC detector for  $G = 2$  and  $G = 10$ .

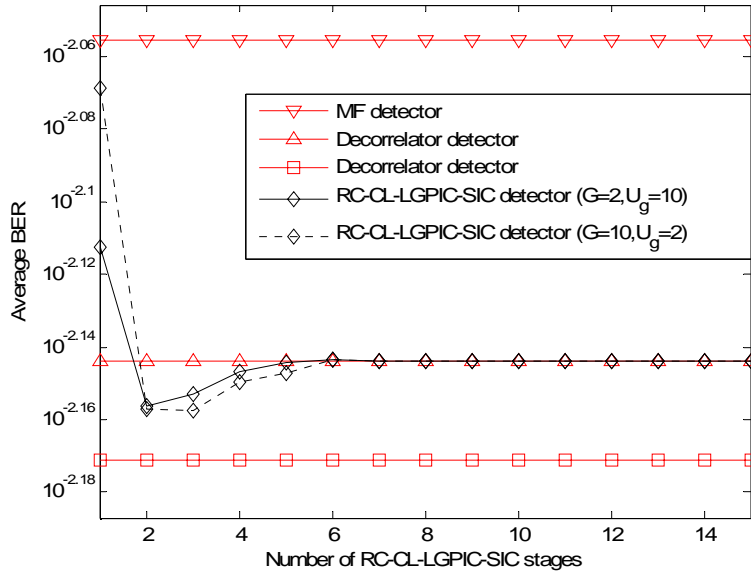


Figure 7.26: Convergence behavior of the RC-CL-LGPIC-SIC detector for  $G = 2$  and  $G = 10$ .

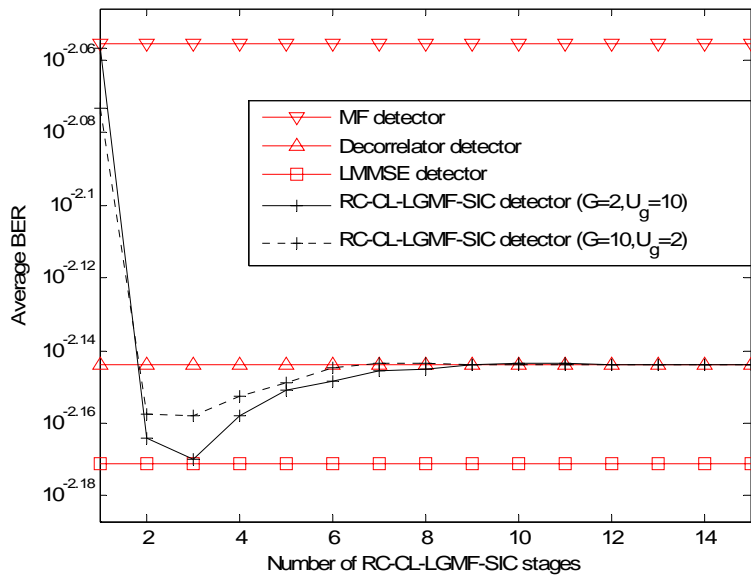


Figure 7.27: Convergence behavior of the RC-CL-LGMF-SIC detector for  $G = 2$  and  $G = 10$ .

It can be seen that the convergence speed of the linear RC-CL-LGMF-SIC detector increases with increasing number of groups whereas for the RC-CL-LGDEC-SIC, the RC-CL-LGMMSE-SIC and the

RC-CL-LGPIC-SIC detector, the opposite is true. However, the average BER difference between different groupings is small and of theoretical importance only.

To show the instability of some detectors, a set of 10 highly correlated codes are used for spreading and despreading. The six users are divided into two equally sized groups 3 users each. It can be seen from Figure 7.28, that while the RC-CL-LGDEC-SIC and the RC-CL-LGMMSE-SIC detectors are converging to the decorrelator detector's performance, the RC-CL-LGMF-SIC detector exhibits an oscillatory convergence behavior while the CL-LPIC/RC-CL-LGPIC-SIC detectors are exhibiting an oscillatory/smooth divergence behaviors, respectively. Different modes of convergence and divergence are discussed in detail in [134].

Not only high correlated spreading codes are causing divergence of some multiuser detectors, grouping is also affecting their convergence behavior. To illustrate this, we divide again the six users into two groups where the first one contains 2 users and the second one contains 4 users. From Figure 7.29, it easy to notice that not only the RC-CL-LGPIC-SIC and the CL-LPIC detectors is divergent but also the RC-CL-LGMF-SIC detector is divergent too. Thus, the grouping of users also affects the convergence/divergence behavior of different CL-LGSIC detection schemes.

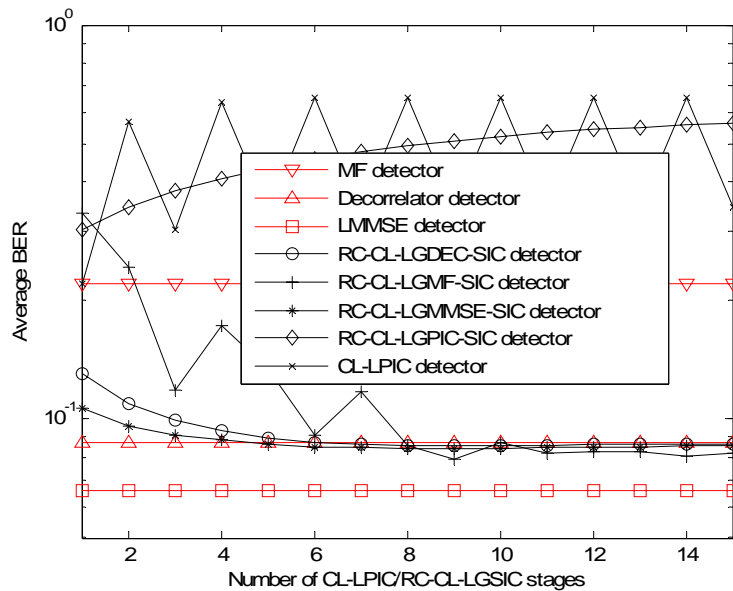


Figure 7.28: Divergence behavior of some chip-level linear interference cancellation detectors due to highly correlated codes.

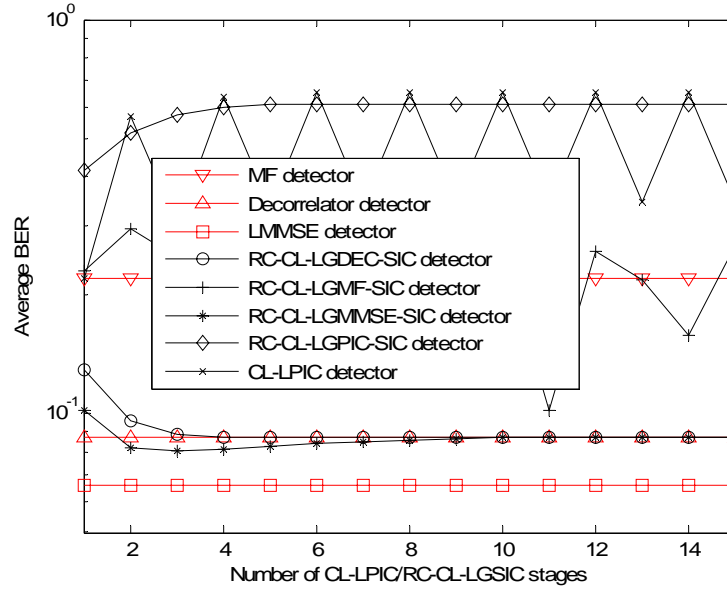


Figure 7.29: Divergence behavior of some chip-level linear interference cancellation detectors due to grouping.

In the following, we simulate the convergence behavior of the aforementioned multiuser detectors in an asynchronous CDMA multipath fading channel, the simulation parameters are depicted in Table 7.1. For the RC-CL-GSIC detector the 10 users are divided into two equally sized groups. In addition, a two-stage PIC detector is used for the RC-CL-GPIC-SIC detector. Figure 7.30 shows the convergence behavior of the CL-LPIC and the CL-LSIC detectors. It is straightforward to see that while the CL-LSIC detector converges within two stages, the CL-LPIC detector diverges. Hence, the principle of under-relaxation is used here to ensure the convergence of the CL-LPIC detector and results in the CL-LWPIC detector. The maximum eigenvalue of the matrix  $\mathbf{D}^{-1}\bar{\mathbf{R}}_{eff}$  used to determine the relaxation factor is estimated using the Gershgorin theorem [82].

The computational complexity of the CL-LSIC detector can be reduced by omitting the inversion of diagonal elements of the cross-correlation matrix by using the principle of under-relaxation as in Section 7.11. This results in the CL-LWSIC detector for which the BER performance is depicted in Figure 7.30. It is easy to see that its performance is indistinguishable from that of the conventional CL-LSIC detector. This suggests that it can be used as alternative.

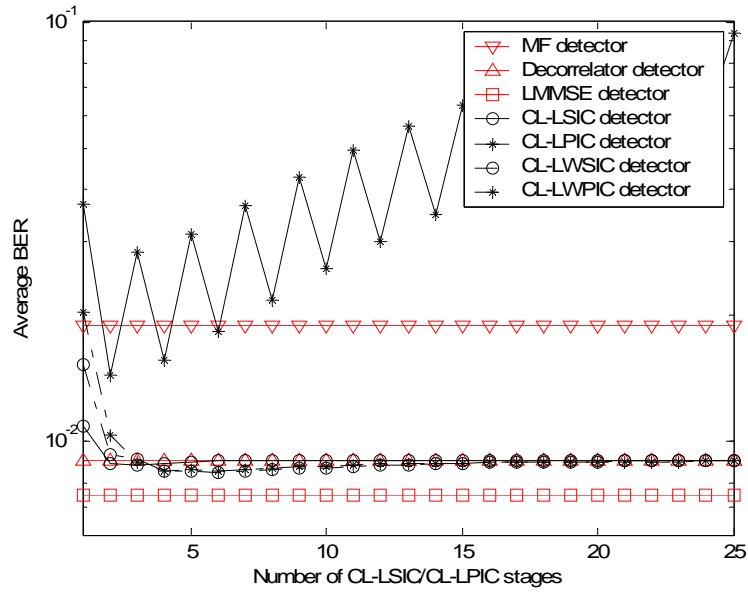


Figure 7.30: Convergence behavior of the CL-LSIC/CL-LPIC detectors.

In Figure 7.31, the convergence behavior of different RC-CL-LGSIC group-detection schemes is also evaluated and plotted.

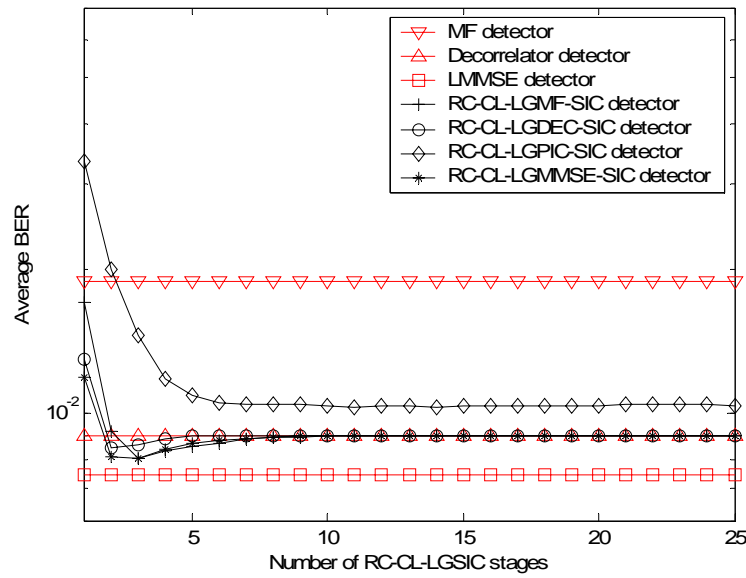


Figure 7.31: Convergence behavior of the RC-CL-LGSIC detector.

Their behavior is not far from that in a synchronous CDMA AWGN channel. Only the RC-CL-LPIC-SIC detector takes a very large number of stages to converge ( $> 25$  stages). This is due mainly to the fact that the linear PIC detector is used without a weighting factor that ensures its convergence in an asynchronous CDMA multipath fading channel. Hence, if fast convergence is required, the linear PIC detector should be replaced with a linear weighted PIC detector.

In the sequel, we simulate the computational complexity of different interference cancellation detectors. We plot the expressions developed in Section 7.13 for two cases: in the first case (a) we assume that the number of stages needed for convergence is  $P = (WK)/2$  whereas in the second case (b) we assume that the number of stages needed for convergence is  $P = (WK)/4$ . This is reasonable since from the simulations above, it can be seen that for all of the interference cancellation detectors the convergence is achieved for less than  $P = (WK)/2$ .

In Figure 7.32, the computational complexity in terms of flops per sliding window is plotted versus the number of effective users, that is,  $WK$ .

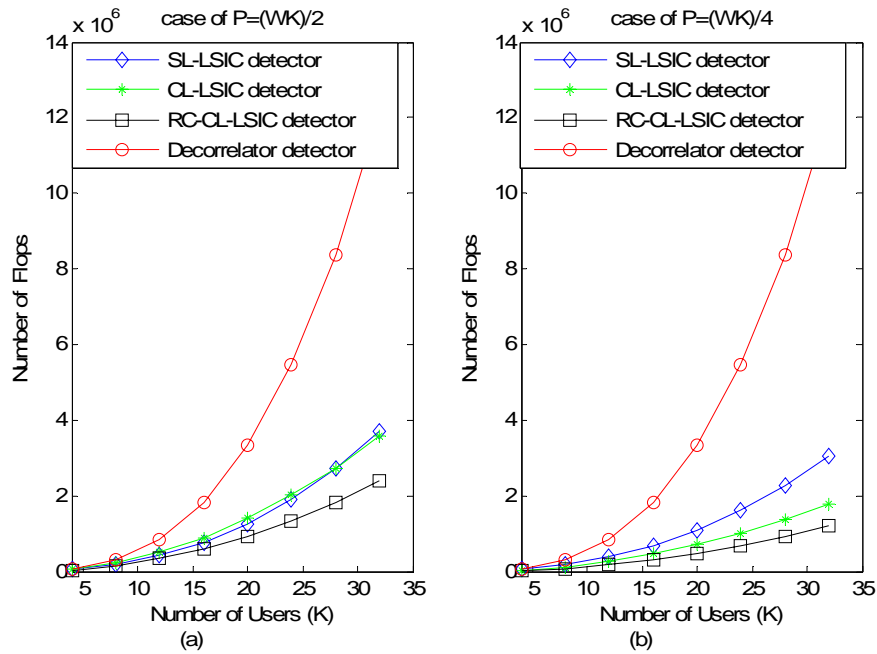


Figure 7.32: Computational complexity of different symbol-level/chip-level LSIC detectors.

It is clear that the computational complexity of the decorrelator detector is much higher than that of the IC detectors. The computational complexity of the CL-LSIC detector is comparable to that of the SL-

LSIC detector for  $P = (WK)/2$ , however, for  $P = (WK)/4$  the computational complexity of the CL-LSIC detector is less than that of the SL-LSIC detector. On the other hand, the computational complexity of the RC-CL-LSIC detector is less than that of SL-LSIC/ CL-LSIC detectors for both cases (a) and (b).

As for the symbol-level/chip-level LSIC detectors, the computational complexity of the SL-GDEC-SIC/RC-CL-GDEC-SIC detectors is depicted in Figure 7.33. It is easy to notice that the RC-CL-GDEC-SIC detector has less computational complexity than that of the SL-GDEC-SIC detector for both cases (a) and (b). Again, the computational complexity of the decorrelator detector is much higher than that of the IC detectors.

In Figure 7.34, the computational complexity of both the symbol-level and chip-level LPIC detectors is plotted versus the number of effective users  $KW$ . Here as well, it is obvious that the CL-LPIC detector exhibits less computational complexity than its symbol-level counterpart (SL-LPIC detector). Hence for most practical cases, all the chip-level linear IC detectors perform better than symbol-level linear IC detectors in terms of computational complexity.

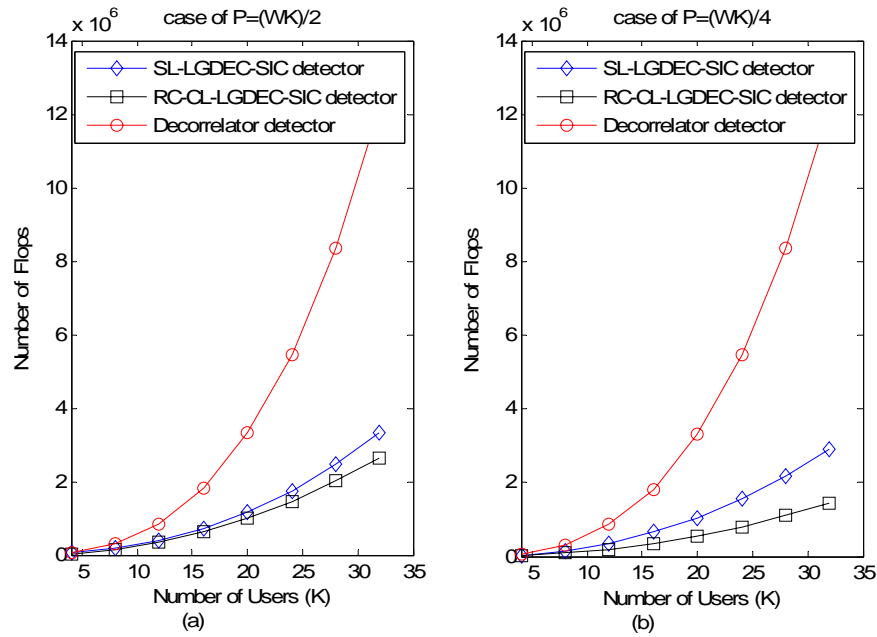


Figure 7.33: Computational complexity of the SL-LGDEC-SIC/RC-CL-LGDEC-SIC detectors.

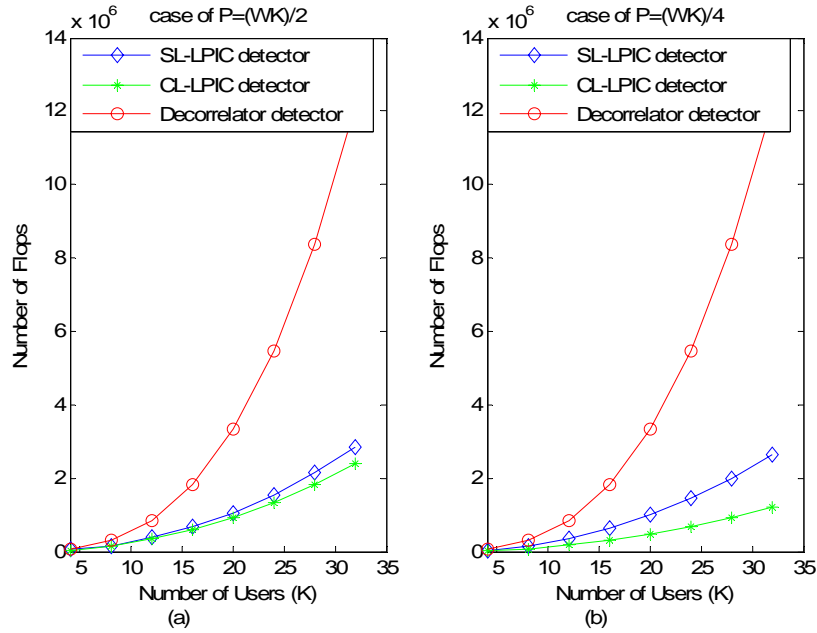


Figure 7.34: Computational complexity of different symbol-level/chip-level LPIC detectors.

## 7.15 Conclusion

In this chapter, we detailed different chip-level linear IC structures existing in the literature and their symbol-level counterparts. We studied these structures in terms of convergence behavior and computational complexity. We showed that some structures suffer from serious convergence issues such as the CL-LPIC, RC-CL-LGMF-SIC and the RC-CL-LGPIC-SIC structures. Furthermore, some structures converging for the case of the CDMA AWGN channel are diverging for the case of CDMA multipath fading channel. Hence the principle of under-relaxation is used to introduce new relaxation IC structures that exhibit relatively less computational complexity than those that do not use this principle.

## Chapter 8

### LMMSE-based Chip-level Linear SIC/GSIC Multiuser Detectors

#### 8.1 Chapter's Contents

8.1 Chapter's Contents .....	168
8.2 Introduction .....	168
8.3 The Chip-Level Linear Weighted SIC (CL-LWSIC) Structure .....	169
8.3.1 Convergence Behavior .....	170
8.3.2 Conditions of Convergence .....	171
8.3.3 Computational Complexity .....	172
8.4 The CL-LWSIC Structure for Multi-Path Fading Channels .....	173
8.5 The Chip-Level Linear Weighted Group-Wise SIC (CL-LWGSIC) Structure .....	174
8.5.1 Convergence Behavior .....	175
8.5.2 Conditions of Convergence .....	177
8.5.3 Computational Complexity .....	178
8.6 Simulation Results .....	178
8.7 Conclusion .....	184

#### 8.2 Introduction

According to our knowledge, all chip-level linear SIC structures proposed in the literature converge to the decorrelator detector. Since the Linear Minimum Mean Square (LMMSE) detector outperforms the decorrelator detector, particularly for low and medium signal-to-noise ratios, it is very important to develop a chip-level linear SIC structure that can converge not only to the decorrelator detector as in [121] and [117] but also to the LMMSE detector.

In this section, a chip-level linear weighted SIC (CL-LWSIC) multi-user detection scheme is proposed. This scheme is computationally suitable for current long-code systems because it does not rely on the computation of the cross-correlation matrix but instead makes a direct use of the spreading codes. Moreover, and as shown later, this scheme converges to the decorrelator/LMMSE detector for two distinct values of the weighting factor.

Furthermore, the CL-LWSIC structure is extended to the chip-level linear weighted group-wise SIC (CL-LWGSIC) multi-user detection structure, where group of users are processed instead of single users. This reduces significantly the detection delay of the CL-LWSIC scheme. Unlike the structure suggested in [124], that converges only to the decorrelator detector if it does at all, the CL-LWGSIC structure proposed here can converge not only to the decorrelator detector but also to the LMMSE detector.

### 8.3 The Chip-Level Linear Weighted SIC (CL-LWSIC) Structure

The proposed linear CL-LWSIC detector consists of ICU's arranged in a multistage structure of  $P$  stages as illustrated in Figure 7.8. The basic linear ICU is shown in Figure 8.1. The multiple access interference (MAI) termed  $\mathbf{I}(p, k_{eff})$  due to the  $k^{th}$  effective user at the  $p^{th}$ -stage is obtained by spreading the decision variable  $y(p, k_{eff})$ , through the operation  $\mathbf{I}(p, k_{eff}) = \bar{\mathbf{s}}_{eff}(k_{eff})y(p, k_{eff})$ , and then subtracting  $\mathbf{I}(p, k_{eff})$  from the composite signal  $(\mathbf{e}(p, k_{eff}) + \mathbf{I}(p-1, k_{eff}))$  to get a cleaned version of the residual signal for the next ICU, that is  $\mathbf{e}(p, k_{eff} + 1)$ .

Here, the decision variable  $y(p, k_{eff})$  is obtained by despreading the residual signal  $\mathbf{e}(p, k_{eff})$ , and then multiplying the result by a weighting factor,  $\mu_{k_{eff}}$ , thus obtaining  $y(p, k_{eff}) = \mu_{k_{eff}} \bar{\mathbf{s}}_{eff}(k_{eff})^T \mathbf{e}(p, k_{eff})$ . This process is repeated in a multistage structure as shown in Figure 7.8.

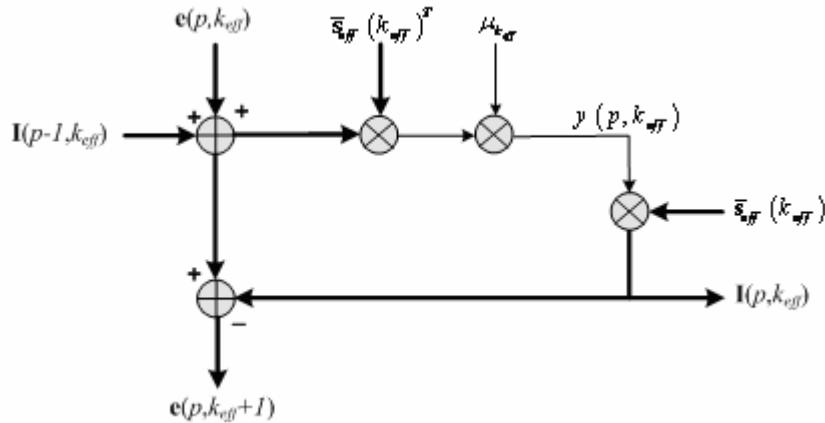


Figure 8.1:  $p^{th}$  stage,  $k^{th}$  effective user's CL-LWSIC unit (ICU)

### 8.3.1 Convergence Behavior

Let  $\mathbf{e}(1,1) = \mathbf{q}$ , at the  $p^{\text{th}}$  stage. The decision variable of the  $k^{\text{th}}$  effective user of the CL-LWSIC detector can be shown to be expressed as:

$$\begin{aligned} y(p, k_{\text{eff}}) &= \mu_{k_{\text{eff}}} \bar{\mathbf{s}}_{\text{eff}}(k_{\text{eff}})^T \mathbf{q} - \mu_{k_{\text{eff}}} \bar{\mathbf{s}}_{\text{eff}}(k_{\text{eff}})^T \sum_{j=1}^{k_{\text{eff}}-1} \bar{\mathbf{s}}_{\text{eff}}(j) y(p, j) - \\ &\mu_{k_{\text{eff}}} \bar{\mathbf{s}}_{\text{eff}}(k_{\text{eff}})^T \sum_{j=k_{\text{eff}}+1}^{WK} \bar{\mathbf{s}}_{\text{eff}}(j) y(p-1, j), \quad \text{for } k_{\text{eff}} = 1, 2, \dots, WK. \end{aligned} \quad (8-1)$$

At convergence, however, we have:  $y(p, k_{\text{eff}}) = y(p-1, k_{\text{eff}}) = y(\infty, k_{\text{eff}})$  and therefore (8-1) becomes:

$$\begin{aligned} y(\infty, k_{\text{eff}}) &= \mu_{k_{\text{eff}}} \bar{\mathbf{s}}_{\text{eff}}(k_{\text{eff}})^T \mathbf{q} - \mu_{k_{\text{eff}}} \bar{\mathbf{s}}_{\text{eff}}(k_{\text{eff}})^T \sum_{j=1}^{k_{\text{eff}}-1} \bar{\mathbf{s}}_{\text{eff}}(j) y(\infty, j) - \\ &\mu_{k_{\text{eff}}} \bar{\mathbf{s}}_{\text{eff}}(k_{\text{eff}})^T \sum_{j=k_{\text{eff}}+1}^{WK} \bar{\mathbf{s}}_{\text{eff}}(j) y(\infty, j), \quad \text{for } k_{\text{eff}} = 1, 2, \dots, WK. \end{aligned} \quad (8-2)$$

Subtracting  $\mu_{k_{\text{eff}}} \bar{\mathbf{s}}_{\text{eff}}(k_{\text{eff}})^T \bar{\mathbf{s}}_{\text{eff}}(k_{\text{eff}}) y(\infty, k_{\text{eff}})$  from both sides of (8-2) and taking into consideration the fact that  $\bar{\mathbf{s}}_{\text{eff}}(k_{\text{eff}})^T \bar{\mathbf{s}}_{\text{eff}}(k_{\text{eff}}) = 1$ , yields:

$$\begin{aligned} \frac{(1 - \mu_{k_{\text{eff}}})}{\mu_{k_{\text{eff}}}} y(\infty, k_{\text{eff}}) &= \bar{\mathbf{s}}_{\text{eff}}(k_{\text{eff}})^T \mathbf{q} - \bar{\mathbf{s}}_{\text{eff}}(k_{\text{eff}})^T \sum_{j=1}^{WK} \bar{\mathbf{s}}_{\text{eff}}(j) y(\infty, j) \\ &\text{for } k_{\text{eff}} = 1, 2, \dots, WK. \end{aligned} \quad (8-3)$$

Equation (8-3) can be written in matrix form as:

$$\mathbf{\Theta} \mathbf{y}(\infty) = \bar{\mathbf{S}}_{\text{eff}}^T \mathbf{q} - \bar{\mathbf{R}}_{\text{eff}} \mathbf{y}(\infty), \quad (8-4)$$

where  $\mathbf{\Theta} = \text{diag} \left( \frac{(1 - \mu_1)}{\mu_1}, \frac{(1 - \mu_2)}{\mu_2}, \dots, \frac{(1 - \mu_{k_{\text{eff}}})}{\mu_{k_{\text{eff}}}}, \dots, \frac{(1 - \mu_{WK})}{\mu_{WK}} \right)$  and  $\bar{\mathbf{R}}_{\text{eff}} = \bar{\mathbf{S}}_{\text{eff}}^T \bar{\mathbf{S}}_{\text{eff}}$  is the positive

definite cross-correlation matrix. Note that the spreading codes are assumed here to be linearly independent. Finally, (8-4) can be written as:

$$\mathbf{y}(\infty) = (\mathbf{\Theta} + \bar{\mathbf{R}}_{\text{eff}})^{-1} \bar{\mathbf{S}}_{\text{eff}}^T \mathbf{q} \quad (8-5)$$

Consequently, two cases of paramount importance are worth investigating:

- If  $\mu_{k_{\text{eff}}} = 1$  for all  $k_{\text{eff}} = 1, 2, \dots, WK$ , the proposed detector converges to the decorrelator detector.

- If  $\mu_{k_{eff}} = \frac{1}{1 + \sigma^2 \bar{\mathbf{A}}_{eff}^{-2}(k_{eff}, k_{eff})}$  for all  $k_{eff} = 1, 2, \dots, WK$ , the proposed detector converges to the LMMSE detector.

Depending on the choice of  $\mu_{k_{eff}}$ , the resulting CL-LWSIC detector can either converge or diverge. Hence, it is important to study the region of convergence for the proposed scheme. This is the subject of the next section.

### 8.3.2 Conditions of Convergence

Before determining the condition for convergence, let us first establish the analogy between the proposed scheme and the corresponding iterative method used to solve a set of linear equations which is known as the Gauss-Seidel iterative method [80].

The matrix  $\bar{\mathbf{R}}_{eff}$  can be decomposed into three parts, that is:  $\bar{\mathbf{R}}_{eff} = \mathbf{I} - \mathbf{L} - \mathbf{L}^T$ , where the identity matrix  $\mathbf{I}$  provides the diagonal elements of  $\bar{\mathbf{R}}_{eff}$ , and  $\mathbf{L}$  and  $\mathbf{L}^T$  are the remaining lower-left and upper-right parts of  $\bar{\mathbf{R}}_{eff}$ , respectively. Ultimately (8-1) can be written in a matrix form as follows:

$$\mathbf{D}\mathbf{y}(p) = \bar{\mathbf{S}}_{eff}^T \mathbf{q} + \mathbf{L}\mathbf{y}(p) + \mathbf{L}^T \mathbf{y}(p-1), \quad (8-6)$$

where  $\mathbf{D} = \text{diag} \left( \frac{1}{\mu_1}, \frac{1}{\mu_2}, \dots, \frac{1}{\mu_{k_{eff}}}, \dots, \frac{1}{\mu_{WK}} \right)$ . Consequently:

$$\mathbf{y}(p) = (\mathbf{D} - \mathbf{L})^{-1} \left[ \mathbf{L}^T \mathbf{y}(p-1) + \bar{\mathbf{S}}_{eff}^T \mathbf{q} \right] \quad (8-7)$$

Note that (8-7) is exactly the Gauss-Seidel iterative method for inverting the matrix  $\mathbf{D} - \mathbf{L} - \mathbf{L}^T = \bar{\mathbf{R}}_{eff} + \mathbf{\Theta}$ . For the convergence analysis of (8-7), we invoke Keller's theorem [81]. In order to apply Keller's theorem, we first set the following:

- $\mathbf{R} = \mathbf{D} - \mathbf{L} - \mathbf{L}^H = \bar{\mathbf{R}}_{eff} + \mathbf{\Theta}$ , since  $\bar{\mathbf{R}}_{eff}$  is hermitian and  $\mathbf{\Theta}$  is a diagonal matrix then  $\mathbf{R}$  is also hermitian.
- $\mathbf{M} = \mathbf{D} - \mathbf{L}$  which is nonsingular if all the elements of the diagonal matrix  $\mathbf{D}$  are nonzero and therefore  $\det(\mathbf{M}) = \det(\mathbf{D} - \mathbf{L}) = \det(\mathbf{D}) \neq 0$  and hence:  $\mu_{k_{eff}} \neq \infty$  for all  $k_{eff} = 1, 2, \dots, WK$ .
- $\mathbf{L}^H = \mathbf{M} - \mathbf{R}$  and  $\mathbf{x} = \bar{\mathbf{S}}_{eff}^T \mathbf{q}$

- $\mathbf{M} + \mathbf{M}^T - \mathbf{R} = \mathbf{M}^T + (\mathbf{M} - \mathbf{R}) = (\mathbf{D} - \mathbf{L})^T + \mathbf{L} = \mathbf{D}$ , and since  $\mathbf{D}$  is a diagonal matrix then if the diagonal elements are nonzero and positive, then  $\mathbf{D}$  is positive definite. Hence,  $\mu_{k_{eff}} > 0$  for all  $k_{eff} = 1, 2, \dots, WK$ .

We have  $\mathbf{R} = \mathbf{D} - \mathbf{L} - \mathbf{L}^H = \mathbf{R} + \mathbf{\Theta}$ , if  $\mathbf{\Theta}$  is positive semi-definite then the matrix sum  $(\mathbf{R} + \mathbf{\Theta})$  is also positive semi-definite. Since  $\mathbf{\Theta}$  is a diagonal matrix, and provided its diagonal elements are all positive, then  $\mathbf{\Theta}$  is positive semi-definite. This is equivalent to the following condition:  $0 < \mu_{k_{eff}} \leq 1$  for all  $k_{eff} = 1, 2, \dots, WK$ .

Combining the aforementioned conditions, we get:  $\{\mu_{k_{eff}} \neq \infty\} \cap \{\mu_{k_{eff}} > 0\} \cap \{0 < \mu_{k_{eff}} \leq 1\} = \{0 < \mu_{k_{eff}} \leq 1\}$  for all  $k_{eff} = 1, 2, \dots, WK$ . Therefore, if  $\{0 < \mu_{k_{eff}} \leq 1\}$  for all  $k_{eff} = 1, 2, \dots, WK$ , then the proposed scheme is guaranteed to converge.

For the two cases of interest, namely in which the proposed CL-LWSIC detector converges to either the decorrelator or the LMMSE detectors, we have  $\mu_{k_{eff}} = 1 \in (0 \ 1]$  and

$\mu_{k_{eff}} = \frac{1}{1 + \sigma^2 \bar{\mathbf{A}}_{eff}^{-2}(k_{eff}, k_{eff})} \in (0 \ 1]$  for all  $k_{eff} = 1, 2, \dots, WK$ , respectively. Hence, the proposed detector converging to the decorrelator / LMMSE detectors is always convergent.

### 8.3.3 Computational Complexity

In this section, the computational complexity of the proposed linear CL-LWSIC detector is evaluated and is given by:

$$WKP \left( 6 \left( WN + \max_{1 \leq k \leq K} (\tau^k) + \max_{1 \leq k \leq K} (\tau_{l_k}) \right) + 1 \right) + 2WK \left( WN + \max_{1 \leq k \leq K} (\tau^k) + \max_{1 \leq k \leq K} (\tau_{l_k}) \right) \quad (8-8)$$

For the sake of comparison, the computational complexity of the SL-LSIC detector proposed in [84] is evaluated and is given by:

$$\left( 2 \left( WN + \max_{1 \leq k \leq K} (\tau^k) + \max_{1 \leq k \leq K} (\tau_{l_k}) \right) - 1 \right) WK + 2 \left( WN + \max_{1 \leq k \leq K} (\tau^k) + \max_{1 \leq k \leq K} (\tau_{l_k}) \right) (WK)^2 + (3WK - 1)WKP \quad (8-9)$$

It is clear that the scheme in [84] has an additional complexity burden of  $\left( 2 \left( WN + \max_{1 \leq k \leq K} (\tau^k) + \max_{1 \leq k \leq K} (\tau_{l_k}) \right) - 1 \right) WK + 2 \left( WN + \max_{1 \leq k \leq K} (\tau^k) + \max_{1 \leq k \leq K} (\tau_{l_k}) \right) (WK)^2$  flops per sliding window, due to the computation of the cross-correlation matrix and the matched filter outputs. This is clearly illustrated in the simulation conducted in Section 8.6.

### 8.4 The CL-LWSIC Structure for Multi-Path Fading Channels

As illustrated in the previous chapter the linear CL-LWSIC detector needs to be modified to accommodate with the changes in the cross-correlation matrix (the diagonal entries are not equal to one). The modified structure is depicted in Figure 8.2.

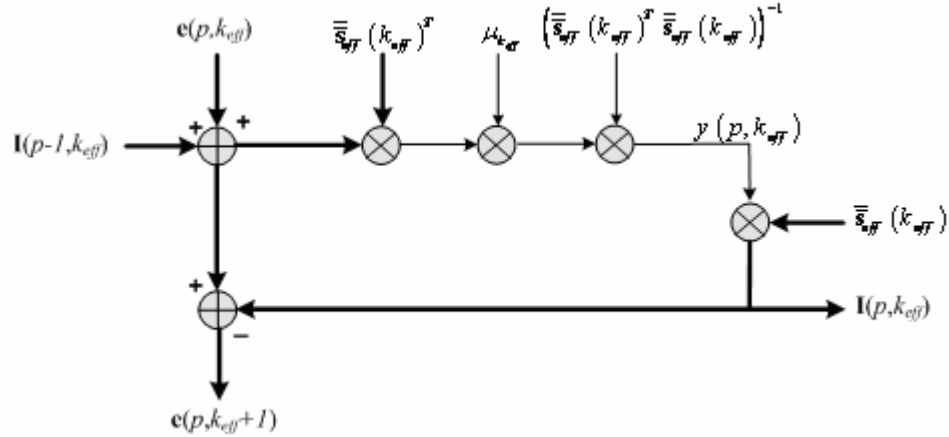


Figure 8.2:  $p^{\text{th}}$  stage,  $k^{\text{th}}$  effective user's CL-LWSIC unit (ICU) for the case of asynchronous CDMA multipath fading channel.

Following the same approach as in Section 8.3.1, it is easy to show that the vector of the decision variables at convergence is obtained as:

$$\mathbf{y}(\infty) = \left( \mathbf{\Theta} + \bar{\mathbf{R}}_{eff}^b \right)^{-1} \left( \bar{\mathbf{S}}_{eff}^b \right)^H \mathbf{q} \quad (8-10)$$

where  $\mathbf{\Theta} = \text{diag} \left( \frac{(1-\mu_1)}{\left( \bar{\mathbf{s}}_{eff}^H(1) \bar{\mathbf{s}}_{eff}(1) \right)^{-1} \mu_1}, \frac{(1-\mu_2)}{\left( \bar{\mathbf{s}}_{eff}^H(2) \bar{\mathbf{s}}_{eff}(2) \right)^{-1} \mu_2}, \dots, \frac{(1-\mu_{k_{eff}})}{\left( \bar{\mathbf{s}}_{eff}^H(k_{eff}) \bar{\mathbf{s}}_{eff}(k_{eff}) \right)^{-1} \mu_{k_{eff}}}, \dots, \frac{(1-\mu_{WK})}{\left( \bar{\mathbf{s}}_{eff}^H(WK) \bar{\mathbf{s}}_{eff}(WK) \right)^{-1} \mu_{WK}} \right)$ . Consequently, two

cases of paramount importance are worth investigating:

- If  $\mu_{k_{eff}} = 1$  for all  $k_{eff} = 1, 2, \dots, WK$ , the proposed detector converges to the decorrelator detector.

- If  $\mu_{k_{eff}} = \frac{1}{1 + \sigma^2 \left( \bar{\mathbf{s}}_{eff}^H(k_{eff}) \bar{\mathbf{s}}_{eff}(k_{eff}) \right)^{-1} \bar{\mathbf{A}}_{eff}^{-2}(k_{eff}, k_{eff})}$  for all  $k_{eff} = 1, 2, \dots, WK$ , the proposed

detector converges to the LMMSE detector.

For the conditions of convergence, and following the same approach as in Section 8.3.2, it is easy to show that the convergence of the scheme is guaranteed if  $\{0 < \mu_{k_{eff}} \leq 1\}$  for all  $k_{eff} = 1, 2, \dots, WK$ . For the two cases of interest, namely in which the proposed detector converges to either the decorrelator or the LMMSE detectors, we have  $\mu_{k_{eff}} = 1 \in (0, 1]$  and

$$\mu_{k_{eff}} = \frac{1}{1 + \sigma^2 \left( \bar{\mathbf{s}}_{eff}^H(k_{eff}) \bar{\mathbf{s}}_{eff}(k_{eff}) \right)^{-1} \bar{\mathbf{A}}_{eff}^{-2}(k_{eff}, k_{eff})} \in (0, 1] \text{ for all } k_{eff} = 1, 2, \dots, WK, \text{ respectively.}$$

Hence, the proposed detector converging to the decorrelator/LMMSE detectors is always convergent.

## 8.5 The Chip-Level Linear Weighted Group-Wise SIC (CL-LWGSIC) Structure

The proposed CL-LWGSIC detector consists of group interference cancellation units (GICU) arranged in a multistage structure of  $P$  stages as illustrated in Figure 8.3. The basic GICU is shown in Figure 8.4. The multiple access interference (MAI)  $\mathbf{I}(p, g_{eff})$  due to the  $g^{th}$  effective group of users at the  $p^{th}$  stage, is obtained by spreading the vector of decision variables  $\mathbf{y}(p, g_{eff})$  that is:

$\mathbf{I}(p, g_{eff}) = \bar{\mathbf{S}}_{eff}^T(g_{eff}) \mathbf{y}(p, g_{eff})$ , this MAI is subtracted from the composite signal  $(\mathbf{e}(p, g_{eff}) + \mathbf{I}(p-1, g_{eff}))$  to get a cleaned version of the residual signal,  $\mathbf{e}(p, g_{eff} + 1)$ , of the next

group of users. Here, the vector of decision variables  $\mathbf{y}(p, g_{eff})$  is obtained by despreading the residual signal  $\mathbf{e}(p, g_{eff})$ , and then multiplying the result by the group-detection matrix  $\mathbf{F}(g_{eff})$ , that is:

$$\mathbf{y}(p, g_{eff}) = \mathbf{F}(g_{eff}) \bar{\mathbf{S}}_{eff}^T(\mathbf{e}(p, g_{eff}) + \mathbf{I}(p-1, g_{eff})).$$

Note that for the case of a multi-path fading channel, for all derivations below one has to substitute  $\bar{\mathbf{S}}_{eff}$  by  $\bar{\bar{\mathbf{S}}}_{eff}^b$ ,  $\bar{\mathbf{R}}_{eff}$  by  $\bar{\bar{\mathbf{R}}}_{eff}^b$  and the transpose operator ( $T$ ) by the hermitian operator ( $H$ ).



$$\begin{aligned} \mathbf{y}(p, \mathbf{g}_{eff}) &= \mathbf{F}(\mathbf{g}_{eff}) \bar{\mathbf{S}}_{eff}^T(\mathbf{g}_{eff}) \mathbf{q} - \mathbf{F}(\mathbf{g}_{eff}) \sum_{j=1}^{g_{eff}-1} \bar{\mathbf{R}}_{eff}(\mathbf{g}_{eff}, j) \mathbf{y}(p, j) - \\ &\mathbf{F}(\mathbf{g}_{eff}) \sum_{j=\mathbf{g}_{eff}+1}^{WG} \bar{\mathbf{R}}_{eff}(\mathbf{g}_{eff}, j) \mathbf{y}(p-1, j) \quad \text{for } g_{eff} = 1, 2, \dots, WG \end{aligned} \quad (8-11)$$

At convergence, we have:  $\mathbf{y}(p, \mathbf{g}_{eff}) = \mathbf{y}(p-1, \mathbf{g}_{eff}) = \mathbf{y}(\infty, \mathbf{g}_{eff})$ , therefore (8-11) is equivalent to:

$$\begin{aligned} \mathbf{y}(\infty, \mathbf{g}_{eff}) &= \mathbf{F}(\mathbf{g}_{eff}) \bar{\mathbf{S}}_{eff}^T(\mathbf{g}_{eff}) \mathbf{q} - \mathbf{F}(\mathbf{g}_{eff}) \sum_{j=1}^{WG} \bar{\mathbf{R}}_{eff}(\mathbf{g}_{eff}, j) \mathbf{y}(\infty, j) \\ &+ \mathbf{F}(\mathbf{g}_{eff}) \bar{\mathbf{R}}_{eff}(\mathbf{g}_{eff}, \mathbf{g}_{eff}) \mathbf{y}(\infty, \mathbf{g}_{eff}) \quad \text{for } g_{eff} = 1, 2, \dots, WG \end{aligned} \quad (8-12)$$

Subtracting  $\mathbf{F}(\mathbf{g}_{eff}) \bar{\mathbf{R}}_{eff}(\mathbf{g}_{eff}, \mathbf{g}_{eff}) \mathbf{y}(\infty, \mathbf{g}_{eff})$  from both sides of equation (8-12) and left multiplying by  $\mathbf{F}(\mathbf{g}_{eff})^{-1}$ , one obtains:

$$\begin{aligned} \mathbf{F}(\mathbf{g}_{eff})^{-1} (\mathbf{I} - \mathbf{F}(\mathbf{g}_{eff}) \bar{\mathbf{R}}_{eff}(\mathbf{g}_{eff}, \mathbf{g}_{eff})) \mathbf{y}(\infty, \mathbf{g}_{eff}) &= \bar{\mathbf{S}}_{eff}^T(\mathbf{g}_{eff}) \mathbf{q} - \\ &\sum_{j=1}^{WG} \bar{\mathbf{R}}_{eff}(\mathbf{g}_{eff}, j) \mathbf{y}(\infty, j) \quad \text{for } g = 1, 2, \dots, G \end{aligned} \quad (8-13)$$

Equation (8-13) can be written in matrix form as:

$$\mathbf{Q} \mathbf{y}(\infty) = \bar{\mathbf{S}}_{eff}^T \mathbf{q} - \bar{\mathbf{R}}_{eff} \mathbf{y}(\infty) \quad (8-14)$$

where  $\mathbf{Q} = \text{diag} \left( \mathbf{F}(1)^{-1} (\mathbf{I} - \mathbf{F}(1) \bar{\mathbf{R}}_{eff}(1,1)), \mathbf{F}(2)^{-1} (\mathbf{I} - \mathbf{F}(2) \bar{\mathbf{R}}_{eff}(2,2)), \dots, \right. \\ \left. \mathbf{F}(\mathbf{g}_{eff})^{-1} (\mathbf{I} - \mathbf{F}(\mathbf{g}_{eff}) \bar{\mathbf{R}}_{eff}(\mathbf{g}_{eff}, \mathbf{g}_{eff})), \dots, \mathbf{F}(GW)^{-1} (\mathbf{I} - \mathbf{F}(GW) \bar{\mathbf{R}}_{eff}(GW, GW)) \right)$ .

Finally, (8-14) can be written as:

$$\mathbf{y}(\infty) = (\mathbf{Q} + \bar{\mathbf{R}}_{eff})^{-1} \bar{\mathbf{S}}_{eff}^T \mathbf{q} \quad (8-15)$$

Depending on the choice of  $\mathbf{F}(\mathbf{g}_{eff})$ , the proposed CL-LWGSIC can converge to either the decorrelator or the LMMSE detector, that is:

- If  $\mathbf{F}(\mathbf{g}_{eff}) = \bar{\mathbf{R}}_{eff}(\mathbf{g}_{eff}, \mathbf{g}_{eff})^{-1}$  for  $g_{eff} = 1, 2, \dots, WG$ , the CL-LWGSIC converges to the decorrelator detector.
- If  $\mathbf{F}(\mathbf{g}_{eff}) = (\bar{\mathbf{R}}_{eff}(\mathbf{g}_{eff}, \mathbf{g}_{eff}) + \sigma^2 \bar{\mathbf{A}}_{eff}^{-2}(\mathbf{g}_{eff}, \mathbf{g}_{eff}))^{-1}$  for  $g_{eff} = 1, 2, \dots, WG$ , the CL-LWGSIC converges to the LMMSE detector.

### 8.5.2 Conditions of Convergence

Let us first establish the analogy between the proposed scheme and the corresponding iterative method used to solve a set of linear equations, which is known as the block Gauss-Seidel iterative method [80].

The matrix  $\bar{\mathbf{R}}_{eff}$  can be decomposed into three parts:  $\bar{\mathbf{R}}_{eff} = \mathbf{D} - \mathbf{L} - \mathbf{L}^T$ , where  $\mathbf{D}$  is the block diagonal part of  $\bar{\mathbf{R}}_{eff}$ :  $\mathbf{D} = \text{diag}(\bar{\mathbf{R}}_{eff}(1,1), \bar{\mathbf{R}}_{eff}(2,2), \dots, \bar{\mathbf{R}}_{eff}(g_{eff}, g_{eff}), \dots, \bar{\mathbf{R}}_{eff}(GW, GW))$ , and  $\mathbf{L}$  and  $\mathbf{L}^T$  are the remaining lower-left and upper-right block triangular parts of  $\bar{\mathbf{R}}_{eff}$ , respectively. Equation (8-11) can be written in matrix form as:

$$\mathbf{F}^{-1}\mathbf{y}(p) = \bar{\mathbf{S}}_{eff}^T \mathbf{q} + \mathbf{L}\mathbf{y}(p) + \mathbf{L}^T \mathbf{y}(p) \quad (8-16)$$

where  $\mathbf{F} = \text{diag}(\mathbf{F}(1), \mathbf{F}(2), \dots, \mathbf{F}(g_{eff}), \dots, \mathbf{F}(GW))$ . Hence:

$$\mathbf{y}(p) = (\mathbf{F}^{-1} - \mathbf{L})^{-1} (\mathbf{L}^T \mathbf{y}(p-1) + \bar{\mathbf{S}}_{eff}^T \mathbf{q}) \quad (8-17)$$

Notice that the iteration in (8-17) is exactly the block Gauss-Seidel iteration for the inversion of the matrix  $\mathbf{F}^{-1} - \mathbf{L} - \mathbf{L}^T = \bar{\mathbf{R}}_{eff} + \mathbf{Q}$ . For the convergence of the proposed scheme, we use Keller's theorem [81]:

If we put  $\mathbf{R} = \mathbf{F}^{-1} - \mathbf{L} - \mathbf{L}^T$ ,  $\mathbf{M} = \mathbf{F}^{-1} - \mathbf{L}$  and  $\mathbf{L}^T = \mathbf{M} - \mathbf{R}$ , we get:

$$\begin{aligned} \mathbf{M} + \mathbf{M}^T - \mathbf{R} &= \mathbf{M}^T + (\mathbf{M} - \mathbf{R}) \\ &= (\mathbf{F}^{-1} - \mathbf{L})^T + \mathbf{L}^T \\ &= (\mathbf{F}^{-1})^T - \mathbf{L}^T + \mathbf{L}^T \\ &= (\mathbf{F}^{-1})^T \end{aligned} \quad (8-18)$$

Therefore, if  $\mathbf{F}(g_{eff})^{-1}$  is positive definite, for all  $g_{eff}$ , the proposed CL-LWGSIC is convergent if  $\mathbf{R}$  is positive semi-definite. We have  $\mathbf{R} = \mathbf{F}^{-1} - \mathbf{L} - \mathbf{L}^T = \mathbf{Q} + \bar{\mathbf{R}}_{eff}$ , thus if  $\mathbf{Q}$  is semi-definite, then  $\mathbf{R}$  is also semi-definite (since  $\bar{\mathbf{R}}_{eff}$  is already semi-definite). Unlike the case for the LMMSE-based linear chip-level SIC structure, it is difficult to obtain a general condition of convergence for any transformation matrix  $\mathbf{F}$ . Fortunately, for the two cases of interest, namely, the CL-LWGSIC detector converging to the decorrelator detector and the CL-LWGSIC detector converging to the LMMSE detector, we can state the following:

- If  $\mathbf{F}(\mathbf{g}_{eff}) = \bar{\mathbf{R}}_{eff}(\mathbf{g}_{eff}, \mathbf{g}_{eff})^{-1}$  (CL-LWGSIC detector converges to the decorrelator detector), then  $\mathbf{F}(\mathbf{g}_{eff})^{-1}$  is positive definite and hence  $\mathbf{R}$  is semi-definite.
- If  $\mathbf{F}(\mathbf{g}_{eff}) = (\bar{\mathbf{R}}_{eff}(\mathbf{g}_{eff}, \mathbf{g}_{eff}) + \sigma^2 \bar{\mathbf{A}}_{eff}^{-2}(\mathbf{g}_{eff}, \mathbf{g}_{eff}))^{-1}$ , (CL-LWGSIC converges to the LMMSE detector), then  $\mathbf{F}(\mathbf{g}_{eff})^{-1}$  is positive definite and hence  $\mathbf{R}$  is semi-definite (because  $\bar{\mathbf{R}}_{eff}$  is positive definite and so is  $\sigma^2 \bar{\mathbf{A}}_{eff}^{-2}(\mathbf{g}_{eff}, \mathbf{g}_{eff})$ ).

### 8.5.3 Computational Complexity

In this section, the computational complexity of the proposed CL-LWGSIC detector is evaluated and is given by:

$$\begin{aligned}
 PW & \left( \sum_{g=1}^G U_g (2U_g - 1) + \left( WN + \max_{1 \leq k \leq K}(\tau^k) + \max_{1 \leq k \leq K}(\tau_{l_k}) \right) \sum_{g=1}^G (2U_g - 1) + \right. \\
 & \left. \left( \left( WN + \max_{1 \leq k \leq K}(\tau^k) + \max_{1 \leq k \leq K}(\tau_{l_k}) \right) - 1 \right) \sum_{g=1}^G U_g \right) + \\
 & 3PG \left( WN + \max_{1 \leq k \leq K}(\tau^k) + \max_{1 \leq k \leq K}(\tau_{l_k}) \right) + W \sum_{g=1}^G \left( 11U_g^3 + \frac{3}{2}U_g^2 + U_g \right) + \\
 & 2W \left( WN + \max_{1 \leq k \leq K}(\tau^k) + \max_{1 \leq k \leq K}(\tau_{l_k}) \right) \sum_{g=1}^G (U_g)^2
 \end{aligned} \tag{8-19}$$

For the sake of comparison, we compare its complexity to its symbol-level counterpart, that is, the SL-LGSIC. The computational complexity of the latter is given by:

$$\begin{aligned}
 & 2 \left( WN + \max_{1 \leq k \leq K}(\tau^k) + \max_{1 \leq k \leq K}(\tau_{l_k}) \right) WK + 2 \left( WN + \max_{1 \leq k \leq K}(\tau^k) + \max_{1 \leq k \leq K}(\tau_{l_k}) \right) (WK)^2 + (WK)^2 \\
 & -W \sum_{g=1}^G U_g^2 + PW^2 \sum_{g=1}^G U_g \sum_{j=1}^G (2U_j - 1) + W \sum_{g=1}^G \left( 11U_g^3 + \frac{3}{2}U_g^2 + U_g \right) + PW \sum_{g=1}^G (U_g - 1)U_g
 \end{aligned} \tag{8-20}$$

### 8.6 Simulation Results

In this section the performance of the proposed structures converging to either the decorrelator detector or the LMMSE detector in terms of convergence behavior and computational complexity is evaluated.

We start by the proposed CL-LWSIC detector. First, the impact of changing the weighting factor in the region of convergence (0, 1], on the average BER (over all users) of the proposed scheme is depicted in Figure 8.5. The SNR is set to 8 dB,  $P = 4$ ,  $K = 20$ ,  $N = 31$  (Gold codes) and perfect power control is assumed. It can be seen that if  $\mu_{k_{eff}} = 1$  for all  $k_{eff} = 1, 2, \dots, WK$  (CL-LWSIC detector  $\rightarrow$

Decorrelator Detector), then the proposed scheme converges to the decorrelator detector; however, if

$$\mu_{k_{eff}} = \frac{1}{1 + \sigma^2 \bar{\mathbf{A}}_{eff}^{-2}(k_{eff}, k_{eff})} \approx 0.9 \text{ (CL-LWSIC detector} \rightarrow \text{LMMSE Detector) for all } k_{eff} = 1, 2, \dots,$$

$WK$ , then the proposed scheme converges to the LMMSE detector. Note also that for  $\mu_{k_{eff}} > 1$  for all  $k_{eff} = 1, 2, \dots, WK$ , the proposed scheme diverges which corroborates with our theoretical results detailed above.

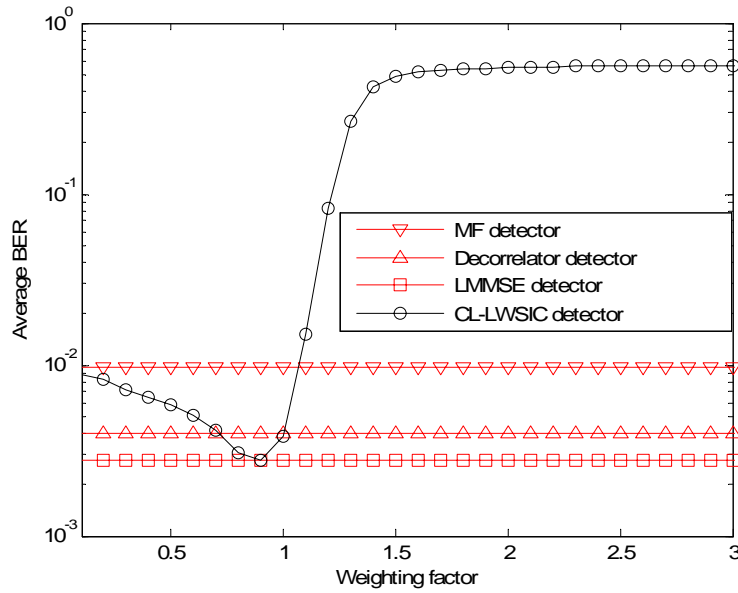


Figure 8.5: Impact of the weighting factor on the average BER of the proposed CL-LWSIC detector.

Second, the convergence behavior of the proposed scheme is evaluated by varying the number of CL-LWSIC stages between 1 and 15 and depicted in Figure 8.6. Here the SNR is set to 6 dB,  $K = 20$ ,  $N = 31$  (Gold codes) and perfect power control is assumed. It is clear that both the proposed structure converging to the LMMSE detector and the one converging to the Decorrelator detector needs less than 6 SIC stages to settle around their final average BER levels. Hence, by properly setting the weighting factors it is possible to determine the final average BER level for the proposed scheme.

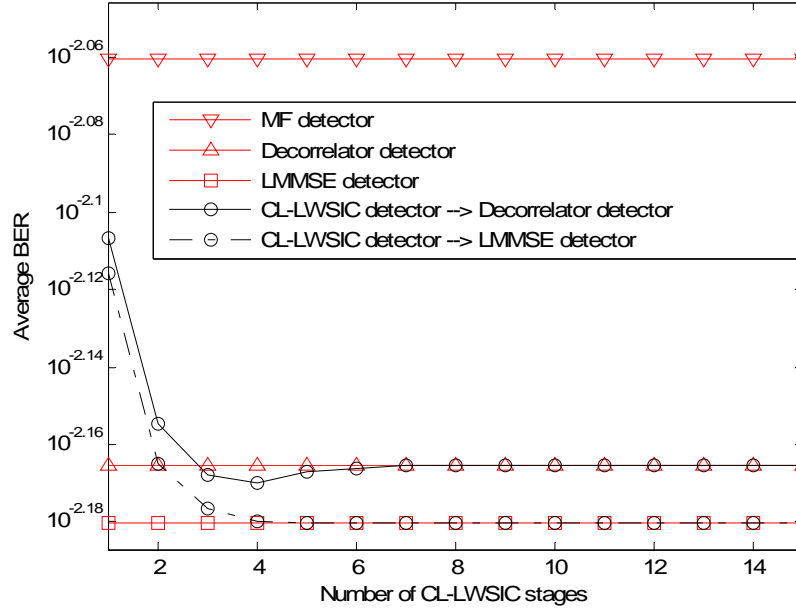


Figure 8.6: Convergence behavior of the proposed CL-LWSIC detector, converging to the Decorrelator/LMMSE detector.

The CL-LWGSIC detector is evaluated in terms of convergence behavior. We choose the matrix  $\mathbf{F}$  such that the CL-LWGSIC detector converges to the decorrelator (DEC) or the LMMSE detectors, that is:  $\mathbf{F}(g_{eff}) = \bar{\mathbf{R}}_{eff}(g_{eff}, g_{eff})^{-1}$  (CL-LWGSIC detector  $\rightarrow$  Decorrelator detector) and  $\mathbf{F}(g_{eff}) = (\bar{\mathbf{R}}_{eff}(g_{eff}, g_{eff}) + \sigma^2 \bar{\mathbf{A}}_{eff}^{-2}(g_{eff}, g_{eff}))^{-1}$  (CL-LWGSIC detector  $\rightarrow$  LMMSE detector) for  $g_{eff} = 1, 2, \dots, WG$ , respectively. The parameters used in the simulation are: SNR = 6 dB,  $K = 20$ ,  $N = 31$  (Gold codes) and perfect power control is assumed. We divide the users into two groups, 10 users each ( $U_1 = U_2 = 10$ ). From Figure 8.7, we notice that the proposed scheme can converge to the LMMSE detector within two stages whereas it needs 4 stages to converge to the decorrelator detector. In addition, the detection delay for the CL-LWSIC detector converging to the LMMSE detector is now  $PG = 4$  rather than  $PK = 40$  for the CL-LWSIC detector. This represents a significant reduction in the detection delay time.

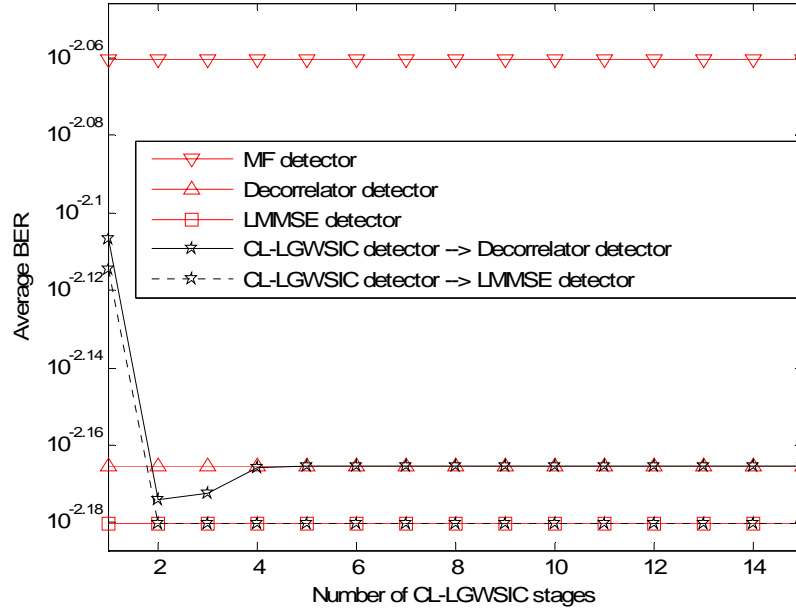


Figure 8.7: Convergence behavior of the proposed CL-LGWSIC detector, converging to the Decorrelator/LMMSE detector.

The convergence behavior of the proposed CL-LWSIC/CL-LWGSIC structures for the multi-path fading channel are simulated and depicted in Figure 8.8 and 8.9. The simulation parameters are  $W = 5$ ,  $K = 10$ ,  $N = 31$  (Gold codes),  $SNR = 6\text{dB}$ ,  $\max_{1 \leq k \leq K}(\tau^k) + \max_{1 \leq l \leq K}(\tau_{l_k}) \leq N$  and finally a Vehicular A outdoor Channel power delay profile for WCDMA is used. The 10 users are partitioned into two equally sized groups.

Simulation results confirm the results obtained for the synchronous CDMA AWGN channel and show clearly that the CL-LWSIC/CL-LGWSIC detector can be configured to converge to the either the decorrelator or the LMMSE detectors depending on the weighting factor/matrix.

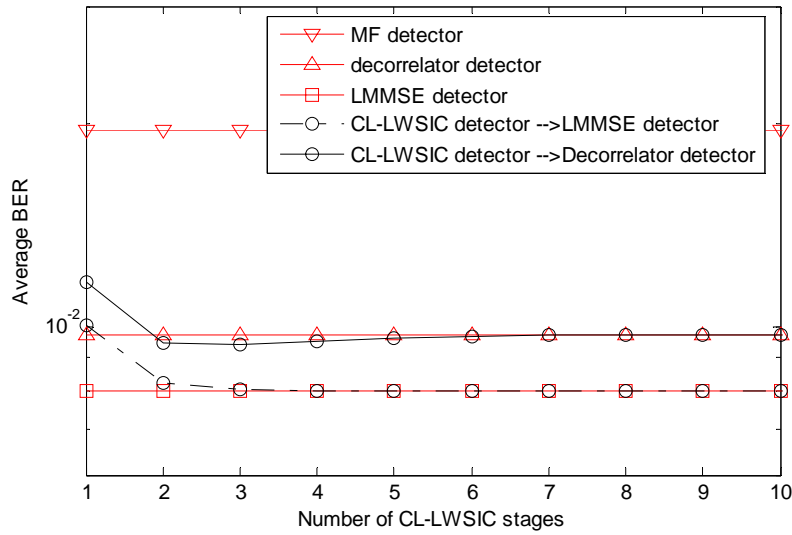


Figure 8.8: Convergence behavior of the proposed CL-LWSIC detector, converging to the Decorrelator/LMMSE detector.

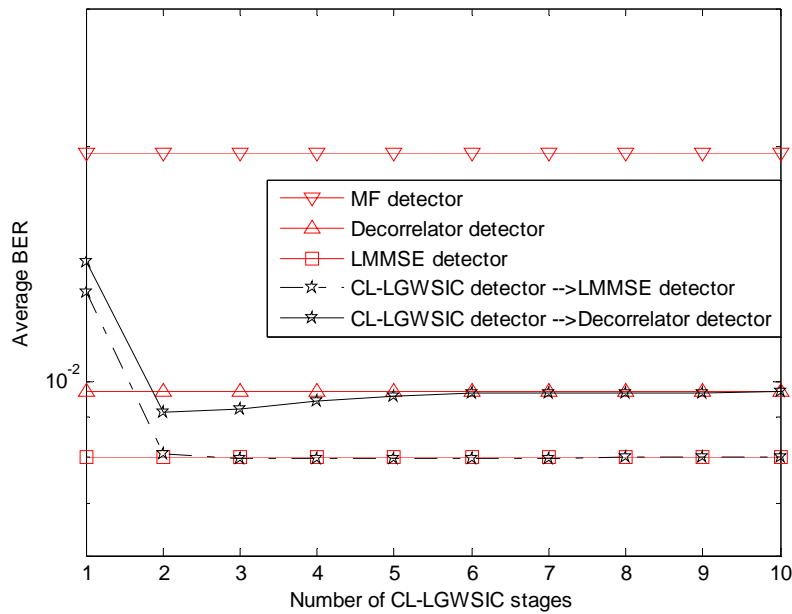


Figure 8.9: Convergence behavior of the proposed CL-LGWSIC detector, converging to the Decorrelator/LMMSE detector.

In the following, the computational complexity of the proposed CL-LWSIC detector is compared to its symbol-level counterpart (SL-LSIC). Two cases are considered; in case (a), the number of stages needed for the CL-LWSIC/SL-LSIC to converge to the decorrelator/LMMSE detectors is assumed to be  $P = (WK)/2$  whereas for case (b), the number of stages needed for the CL-LWSIC/SL-LSIC to converge to the decorrelator/LMMSE detectors is assumed to be  $P = (WK)/4$ .

It is apparent from Figure 8.10 that for  $P \leq (WK)/2$  the computational complexity of the CL-LWSIC detector is less than that of SL-LSIC detector. This condition is satisfied in most practical cases, e.g., for Figure 8.6 and 8.7 and for  $K = 20$  users, less than 4 stages are needed to achieve convergence.

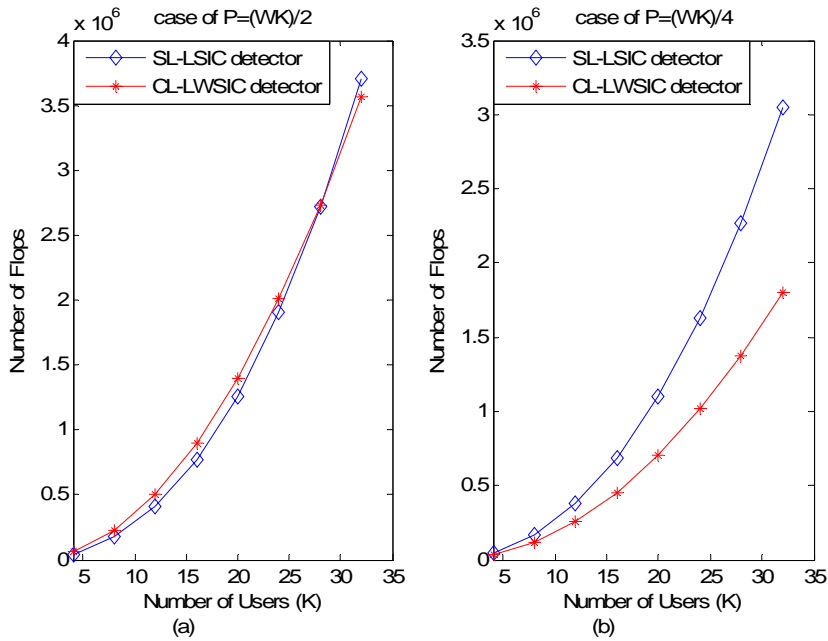


Figure 8.10: Computational complexity of the proposed CL-LWSIC structure versus that of the SL-LSIC structure.

In Figure 8.11, the computational complexity of the proposed CL-LWGSIC and that of SL-LGSIC structures is plotted versus the number of users  $K$ . It is clear that the computational complexity of the proposed structure is inferior to that of its symbol-level counterpart for both cases (a) and (b). This represents a significant reduction in computational complexity.

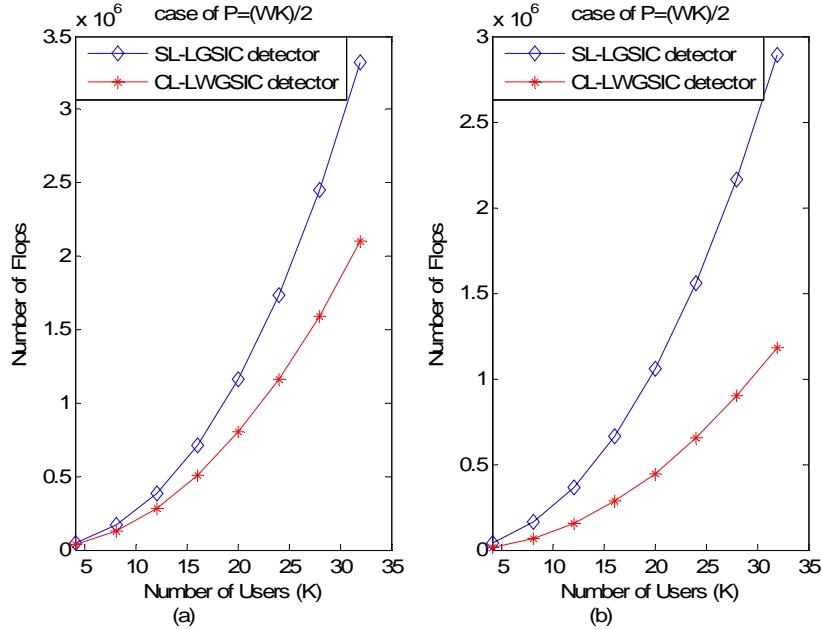


Figure 8.11: Computational complexity of the proposed CL-LWGSIC structure versus that of the SL-LGSIC structure.

## 8.7 Conclusion

In this chapter, we introduced two new chip-level structures that can converge to either the decorrelator or the LMMSE detector. The structures make use of a weighting factor/weighting matrix to determine to which average BER level the proposed structure converges to. Both convergence analysis and simulation results indicate that the proposed detectors converging to the decorrelator/LMMSE detectors are always convergent. Moreover, computational complexity analysis and simulation results shows important reduction in computational complexity compared to their symbol-level counterparts.

## Chapter 9

### Chip-level Linear SOR-SIC and BSOR-GSIC Multiuser Detectors

#### 9.1 Chapter's Contents

9.1 Chapter's Contents .....	185
9.2 Introduction .....	186
9.3 Chip-Level Linear Successive Over-Relaxation SIC (CL-LSOR-SIC) Structure.....	186
9.3.1 Matrix Algebraic Approach to the CL-LSOR-SIC Detector.....	187
9.3.2 Convergence Analysis.....	189
9.3.3 Conditions of Convergence.....	190
9.3.3.1 First Approach.....	190
9.3.3.2 Second Approach .....	191
9.3.4 Computational Complexity .....	192
9.4 Chip-Level Linear Block Successive Over-Relaxation Group-Wise SIC (CL-LBSOR-GSIC) Structure.....	193
9.4.1 Matrix Algebraic Approach to the Chip-Level Linear BSOR-GSIC Detector .....	194
9.4.2 Convergence Analysis.....	195
9.4.3 Conditions of Convergence.....	196
9.4.3.1 First Approach.....	196
9.4.3.2 Second Approach .....	197
9.4.4 Computational Complexity .....	199
9.5 Reduced-Complexity Chip-Level Linear Successive Over-Relaxation (RC-CL-LSOR-SIC) Structure.....	199
9.5.1 Convergence Behavior and Conditions of Convergence.....	200
9.5.2 Computational Complexity .....	200
9.6 Reduced-Complexity Chip-Level Linear Block Successive Over-Relaxation Group-Wise SIC (RC-CL-LBSOR-GSIC) Structure .....	201
9.6.1 Convergence Analysis and Conditions of Convergence .....	202
9.6.2 Computational Complexity .....	202

9.7 Simulation Results.....	203
9.8 Conclusion.....	209

## 9.2 Introduction

The symbol-level linear SIC detector equivalent to the SOR iterative method was implemented in [84], however, symbol-level multiuser detectors are not suitable for long-code CDMA systems because they require the recomputation of the cross-correlation matrix every symbol interval. Therefore, a chip-level linear SIC detector that uses directly the spreading codes and avoids the recomputation of the cross-correlation matrix is necessary.

First, a new chip-level linear SIC multi-user detection scheme that is equivalent to the SOR iterative (we call it chip-level linear SOR-SIC for simplicity) method is introduced. Second, the detection delay of this structure is reduced by introducing a new chip-level linear GSIC multiuser detector that is equivalent to the BSOR iterative method (we call it chip-level linear BSOR-GSIC for simplicity). Third, we show that a reduced-complexity chip-level linear SOR-SIC can be obtained by introducing a weighting factor within the linear SIC structure proposed in [121]. Fourth, and as for the chip-level linear BSOR-GSIC, a reduced-complexity chip-level linear BSOR-GSIC is introduced to reduce the detection delay of the reduced-complexity chip-level linear SOR-SIC structure. The proposed structure is obtained by proving that the scheme proposed in [124] is in fact equivalent to the block Gauss-Seidel iterative method if the group detection scheme is the decorrelator detector. Then, by inserting a weighting factor within the structure, we show that the resultant scheme is equivalent to the BSOR iterative method, which is well known to outperform the conventional block Gauss-Seidel method by an order of magnitude in terms of convergence speed.

Finally, and for all schemes converging to the decorrelator detector developed earlier, we use a matrix algebraic approach to describe the chip-level linear SOR-SIC/BSOR-GSIC schemes as linear matrix filtering. We derive closed-form expressions for the residual signal vector and the vector of the decision variables. This allows obtaining an analytical expression for both the BER and the AME. We show as well, using two different approaches that the scheme converges if the weighting factor (known also as relaxation factor) is between 0 and 2.

## 9.3 Chip-Level Linear Successive Over-Relaxation SIC (CL-LSOR-SIC) Structure

The CL-LSOR-SIC detector consists of ICU arranged in a multistage structure as illustrated in Figure 7.8. The basic interference cancellation unit is shown in Figure 9.1. The combined signal

$(\omega \mathbf{e}(p, k_{eff}) + \mathbf{I}(p-1, k_{eff}))$  at the input of the  $p^{th}$  stage,  $k^{th}$  effective user ICU is first despreaded to estimate the decision variable  $y(p, k_{eff})$ , that is,  $y(p, k_{eff}) = \bar{\mathbf{s}}_{eff}(k_{eff})^T (\omega \mathbf{e}(p, k_{eff}) + \mathbf{I}(p-1, k_{eff}))$ . The MAI  $\mathbf{I}(p, k_{eff})$  is obtained by spreading the decision variable  $y(p, k_{eff})$ , that is:  $\mathbf{I}(p, k_{eff}) = \bar{\mathbf{s}}_{eff}(k_{eff}) y(p, k_{eff})$ , the sum of the latter and the weighted residual signal  $(1-\omega)\mathbf{e}(p, k_{eff})$  is subtracted from the combined signal  $(\omega \mathbf{e}(p, k_{eff}) + \mathbf{I}(p-1, k_{eff}))$  to get a cleaner version of the residual signal  $\mathbf{e}(p, k_{eff}+1)$  for the next ICU. This process is repeated in a multistage structure as it is shown in Figure 7.8.

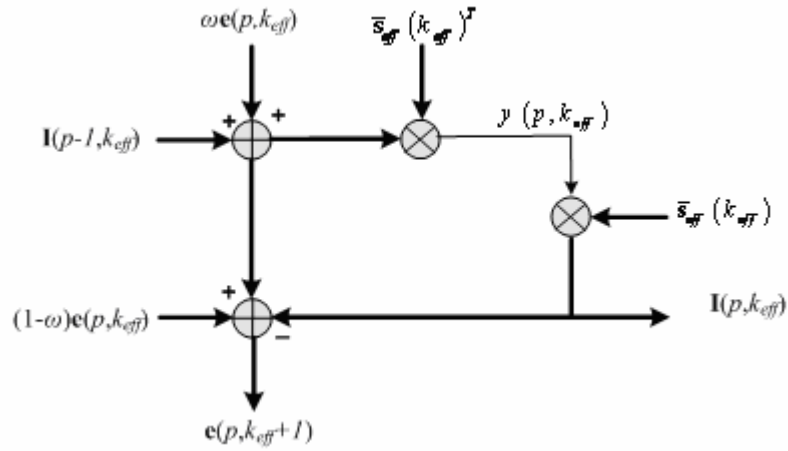


Figure 9.1: Basic interference cancellation unit (ICU).

### 9.3.1 Matrix Algebraic Approach to the CL-LSOR-SIC Detector

The residual signal at the input of the first ICU at the first stage is defined as  $\mathbf{e}(1,1) = \mathbf{q}$  and the corresponding decision variable is given by  $y(1,1) = \bar{\mathbf{s}}_{eff}(1)^T (\omega \mathbf{e}(1,1) + \mathbf{I}(0,1)) = \omega \bar{\mathbf{s}}_{eff}(1)^T \mathbf{q}$ . Moving to the input of the second ICU at the first stage, the received signal vector is obtained by estimating the MAI due to the first user and then subtracting it from the received signal that is  $\mathbf{e}(1,2) = \mathbf{e}(1,1) + \mathbf{I}(0,1) - \mathbf{I}(1,1) = (\mathbf{I} - \omega \bar{\mathbf{s}}_{eff}(1) \bar{\mathbf{s}}_{eff}(1)^T) \mathbf{q}$ . The corresponding decision variable is expressed as  $y(1,2) = \bar{\mathbf{s}}_{eff}(2)^T (\omega \mathbf{e}(1,2) + \mathbf{I}(0,2)) = \omega \bar{\mathbf{s}}_{eff}(2)^T (\mathbf{I} - \omega \bar{\mathbf{s}}_{eff}(1) \bar{\mathbf{s}}_{eff}(1)^T) \mathbf{q}$ . Proceeding in

the same way, we can express the residual signal at the output of the  $k^{\text{th}}$  effective ICU unit at the first

stage as:  $\mathbf{e}(1, k_{\text{eff}}) = \prod_{j=k_{\text{eff}}-1}^1 \left( \mathbf{I} - \omega \bar{\mathbf{s}}_{\text{eff}}(j) \bar{\mathbf{s}}_{\text{eff}}(j)^T \right) \mathbf{q} = \Phi_{k_{\text{eff}}-1} \mathbf{q}$ , where  $\prod$  indicates product of

matrices with decreasing indices, and the corresponding decision variable is given by:

$$y(1, k_{\text{eff}}) = \omega \bar{\mathbf{s}}_{\text{eff}}(k_{\text{eff}})^T \mathbf{e}(1, k_{\text{eff}}) = \omega \bar{\mathbf{s}}_{\text{eff}}(k_{\text{eff}})^T \Phi_{k_{\text{eff}}-1} \mathbf{q}.$$

The residual signal at the output of the last CL-LSOR-SIC unit at the first stage is:

$$\mathbf{e}(1, WK+1) = \prod_{j=WK}^1 \left( \mathbf{I} - \omega \bar{\mathbf{s}}_{\text{eff}}(j) \bar{\mathbf{s}}_{\text{eff}}(j)^T \right) \mathbf{q} = \Phi_{WK} \mathbf{q}.$$

This residual signal will be directed to the input of the first ICU unit at the second stage, therefore,  $\mathbf{e}(2, 1) = \mathbf{e}(1, WK+1) = \Phi_{WK} \mathbf{q}$ . Taking in

consideration that  $\bar{\mathbf{s}}_{\text{eff}}(k_{\text{eff}})^T \bar{\mathbf{s}}_{\text{eff}}(k_{\text{eff}}) = 1$ , the corresponding decision variable is expressed as:

$$\begin{aligned} y(2, 1) &= \bar{\mathbf{s}}_{\text{eff}}(1)^T (\omega \mathbf{e}(2, 1) + \mathbf{I}(1, 1)) \\ &= \omega \bar{\mathbf{s}}_{\text{eff}}(1)^T \mathbf{e}(2, 1) + \underbrace{\bar{\mathbf{s}}_{\text{eff}}(1)^T \bar{\mathbf{s}}_{\text{eff}}(1)}_{=1} y(1, 1) \\ &= \omega \bar{\mathbf{s}}_{\text{eff}}(1)^T \Phi_{WK} \mathbf{q} + \omega \bar{\mathbf{s}}_{\text{eff}}(1)^T \mathbf{q} \\ &= \omega \bar{\mathbf{s}}_{\text{eff}}(1)^T (\Phi_{WK} + \mathbf{I}) \mathbf{q} \end{aligned}$$

For the second ICU unit we have:

$$\begin{aligned} \mathbf{e}(2, 2) &= \mathbf{e}(2, 1) + \mathbf{I}(1, 1) - \mathbf{I}(2, 1) \\ &= \mathbf{e}(2, 1) + \mathbf{I}(1, 1) - \bar{\mathbf{s}}_{\text{eff}}(1) \bar{\mathbf{s}}_{\text{eff}}(1)^T (\omega \mathbf{e}(2, 1) + \mathbf{I}(1, 1)) \\ &= \mathbf{e}(2, 1) + \bar{\mathbf{s}}_{\text{eff}}(1) y(1, 1) - \omega \bar{\mathbf{s}}_{\text{eff}}(1) \bar{\mathbf{s}}_{\text{eff}}(1)^T \mathbf{e}(2, 1) - \underbrace{\bar{\mathbf{s}}_{\text{eff}}(1) \bar{\mathbf{s}}_{\text{eff}}(1)^T \bar{\mathbf{s}}_{\text{eff}}(1)}_{=1} y(1, 1) \\ &= (\mathbf{I} - \omega - \bar{\mathbf{s}}_{\text{eff}}(1) \bar{\mathbf{s}}_{\text{eff}}(1)^T) \mathbf{e}(2, 1) \\ &= (\mathbf{I} - \omega - \bar{\mathbf{s}}_{\text{eff}}(1) \bar{\mathbf{s}}_{\text{eff}}(1)^T) \Phi_{WK} \mathbf{q} \end{aligned}$$

and:

$$\begin{aligned} y(2, 2) &= \bar{\mathbf{s}}_{\text{eff}}(2)^T (\omega \mathbf{e}(2, 2) + \mathbf{I}(1, 2)) \\ &= \omega \bar{\mathbf{s}}_{\text{eff}}(2)^T \mathbf{e}(2, 2) + \underbrace{\bar{\mathbf{s}}_{\text{eff}}(2)^T \bar{\mathbf{s}}_{\text{eff}}(2)}_{=1} y(1, 2) \\ &= \omega \bar{\mathbf{s}}_{\text{eff}}(2)^T (\mathbf{I} - \omega \bar{\mathbf{s}}_{\text{eff}}(1) \bar{\mathbf{s}}_{\text{eff}}(1)^T) \Phi_{WK} \mathbf{q} + \omega \bar{\mathbf{s}}_{\text{eff}}(2)^T (\mathbf{I} - \omega \bar{\mathbf{s}}_{\text{eff}}(1) \bar{\mathbf{s}}_{\text{eff}}(1)^T) \mathbf{q} \\ &= \omega \bar{\mathbf{s}}_{\text{eff}}(2)^T (\mathbf{I} - \omega \bar{\mathbf{s}}_{\text{eff}}(1) \bar{\mathbf{s}}_{\text{eff}}(1)^T) (\Phi_{WK} + \mathbf{I}) \mathbf{q} \end{aligned}$$

Following the same procedure, we can obtain the general expression for the residual signal vector and the decision variable of the  $k^{\text{th}}$  effective ICU unit at the  $p^{\text{th}}$  stage, respectively, as:

$$\mathbf{e}(p, k_{\text{eff}}) = \Phi_{k_{\text{eff}}-1} (\Phi_{WK})^{p-1} \mathbf{q} \quad (9-1)$$

and:

$$y(p, k_{\text{eff}}) = \omega \bar{\mathbf{s}}_{\text{eff}}(k_{\text{eff}})^T \Phi_{k_{\text{eff}}-1} \sum_{i=0}^{p-1} (\Phi_{WK})^i \mathbf{q} = \mathbf{g}_{p, k_{\text{eff}}}^T \mathbf{q} \quad (9-2)$$

where:  $\Phi_{k_{\text{eff}}} = \prod_{j=k_{\text{eff}}}^1 (\mathbf{I} - \omega \bar{\mathbf{s}}_{\text{eff}}(j) \bar{\mathbf{s}}_{\text{eff}}(j)^T)$ . Collecting the decision variables of all users in one matrix

we get:

$$\mathbf{y}(p) = \mathbf{G}_p^T \mathbf{q} \quad (9-3)$$

where:  $\mathbf{G}_p = [\mathbf{g}_{p,1} \quad \mathbf{g}_{p,2} \quad \cdots \quad \mathbf{g}_{p,k_{\text{eff}}} \quad \cdots \quad \mathbf{g}_{p,WK}]$ . Hence, the CL-LSOR-SIC detector can be described as linear matrix filtering of the received chip-matched signal vector. Using the same approach as for the matched filter detector, the BER of the  $k^{\text{th}}$  effective user at the  $p^{\text{th}}$  stage can be expressed as:

$$P_{p, k_{\text{eff}}}(\sigma) = \frac{1}{2^{WK-1}} \sum_{\substack{\text{all} \\ \mathbf{b}(k_{\text{eff}})=1}} Q \left( \frac{\mathbf{g}_{p, k_{\text{eff}}}^T \bar{\mathbf{S}}_{\text{eff}} \bar{\mathbf{A}}_{\text{eff}} \mathbf{b}}{\sigma \sqrt{\mathbf{g}_{p, k_{\text{eff}}}^T \mathbf{g}_{p, k_{\text{eff}}}}} \right) \quad (9-4)$$

where  $Q(\cdot)$  is the  $Q$ -function. As for the BER, the asymptotic multiuser efficiency for the  $k^{\text{th}}$  effective user at the  $p^{\text{th}}$  stage is given by:

$$\eta_{p, k_{\text{eff}}} = \frac{1}{\mathbf{g}_{p, k_{\text{eff}}}^T \mathbf{g}_{p, k_{\text{eff}}}} \max^2 \left( 0, \mathbf{g}_{p, k_{\text{eff}}}^T \bar{\mathbf{s}}_{\text{eff}}(k_{\text{eff}}) - \sum_{\substack{j=1 \\ j \neq k_{\text{eff}}}}^{WK} \frac{\bar{A}_{\text{eff}}(j, j)}{\bar{A}_{\text{eff}}(k_{\text{eff}}, k_{\text{eff}})} |\mathbf{g}_{p, k_{\text{eff}}}^T \bar{\mathbf{s}}_{\text{eff}}(j)| \right) \quad (9-5)$$

### 9.3.2 Convergence Analysis

Let  $\mathbf{e}(1,1) = \mathbf{q}$  be the input signal to the CL-LSOR-SIC scheme. At the  $p^{\text{th}}$  stage, the decision variable of the  $k^{\text{th}}$  effective user of the CL-LSOR-SIC detector is derived as:

$$y(p, k_{\text{eff}}) = \omega \bar{\mathbf{s}}_{\text{eff}}(k_{\text{eff}})^T \mathbf{q} - \omega \bar{\mathbf{s}}_{\text{eff}}(k_{\text{eff}})^T \sum_{j=1}^{k_{\text{eff}}-1} \bar{\mathbf{s}}_{\text{eff}}(j) y(p, j) - \omega \bar{\mathbf{s}}_{\text{eff}}(k_{\text{eff}})^T \sum_{j=k_{\text{eff}}}^{WK} \bar{\mathbf{s}}_{\text{eff}}(j) y(p-1, j) + y(p-1, k_{\text{eff}}), \quad \text{for } k_{\text{eff}} = 1, 2, \dots, WK. \quad (9-6)$$

At convergence, we have:  $y(p, k_{eff}) = y(p-1, k_{eff}) = y(\infty, k_{eff})$  therefore (9-6) is equivalent to:

$$y(\infty, k_{eff}) = \omega \bar{\mathbf{s}}_{eff}^T(k_{eff}) \mathbf{q} - \omega \bar{\mathbf{s}}_{eff}^T(k_{eff}) \sum_{j=1}^{k_{eff}-1} \bar{\mathbf{s}}_{eff}(j) y(\infty, j) - \omega \bar{\mathbf{s}}_{eff}^T(k_{eff}) \sum_{j=k_{eff}}^{WK} \bar{\mathbf{s}}_{eff}(j) y(\infty, j) + y(\infty, j), \quad \text{for } k_{eff} = 1, 2, \dots, WK. \quad (9-7)$$

Equation (9-7) is equivalent to:

$$\omega \bar{\mathbf{s}}_{eff}^T(k_{eff}) \sum_{j=1}^{WK} \bar{\mathbf{s}}_{eff}(j) y(\infty, j) = \omega \bar{\mathbf{s}}_{eff}^T(k_{eff}) \mathbf{q}, \quad \text{for } k_{eff} = 1, 2, \dots, WK. \quad (9-8)$$

Equation (9-8) could be written in matrix form as:

$$\bar{\mathbf{S}}_{eff}^T \bar{\mathbf{S}}_{eff} \mathbf{y}(\infty) = \bar{\mathbf{S}}_{eff}^T \mathbf{q} \quad (9-9)$$

Finally, (9-9) could be written as:

$$\mathbf{y}(\infty) = \bar{\mathbf{R}}_{eff}^{-1} \bar{\mathbf{S}}_{eff}^T \mathbf{q} \quad (9-10)$$

Hence, if the proposed scheme converges it converges to the decorrelator detector.

### 9.3.3 Conditions of Convergence

For the conditions of convergence of the proposed scheme we propose two different approaches that lead to the same result.

#### 9.3.3.1 First Approach

This beauty of this approach is that it allows the identification of the proposed scheme as the SOR method. This permits the straightforward determination of the condition of convergence using the rich theory of the SOR iterative method.

Let's first establish the analogy between the proposed scheme and the corresponding iterative method used to solve a set of linear equations which is known basically as the SOR method. The matrix  $\bar{\mathbf{R}}_{eff}$  could be decomposed into three parts, that is:  $\bar{\mathbf{R}}_{eff} = \mathbf{I} - \mathbf{L} - \mathbf{L}^H$ , where the identity matrix  $\mathbf{I}$  is the diagonal part of  $\bar{\mathbf{R}}_{eff}$ , and  $\mathbf{L}$  and  $\mathbf{U}$  are the remaining lower-left and upper-right parts of  $\bar{\mathbf{R}}_{eff}$ , respectively. After some manipulations, equation (9-6) could be written in matrix form as:

$$\mathbf{y}(p) = \omega (\mathbf{I} - \omega \mathbf{L})^{-1} \bar{\mathbf{S}}_{eff}^T \mathbf{q} + (\mathbf{I} - \omega \mathbf{L})^{-1} ((1 - \omega) \mathbf{I} + \omega \mathbf{U}) \mathbf{y}(p-1) \quad (9-11)$$

which is exactly the SOR iteration. Note that if  $\omega = 1$ , the iteration in (9-11) reduces to the Gauss-Seidel iteration. For the convergence of (9-11), we use Kahan's theorem [135]:

**Theorem 9-1**

A necessary condition for the SOR method to converge is  $|\omega - 1| < 1$ .

Thus, for  $\omega$  real, the iteration in (9-11) converges if  $\omega \in (0, 2)$ . Nevertheless, one should set  $\omega$  within the interval (1,2) which corresponds to over-relaxation (acceleration) since the interval (0, 1) corresponds to under-relaxation (deceleration) and it is basically used to ensure convergence of the Gauss-seidel iteration if it is not convergent. The calculation of the optimum value of  $\omega$  for which the convergence is maximum, depends on the maximum eigenvalue of the iteration matrix  $(\mathbf{I} - \omega\mathbf{L})^{-1}((1 - \omega)\mathbf{I} + \omega\mathbf{U})$ , which is complex to compute. However, one can get a cheap estimate of the optimum value of  $\omega$  based on an upper bound on the maximum eigenvalue of the iteration matrix as in [84] and it is given by equation (7-2).

9.3.3.2 Second Approach

This approach was used in [121] to prove that the linear SIC detector is always convergent. Here, we adopt this approach to determine the condition of convergence for the CL-LSOR-SIC detector. We show that the condition obtained here is the same as that of the SOR iterative method. From Figure 9.1, we have:

$$\begin{aligned} y(p, k_{eff}) &= \bar{\mathbf{s}}_{eff}(k_{eff})^T (\alpha \mathbf{e}(p, k_{eff}) + \mathbf{I}(p-1, k_{eff})) \\ &= \omega \bar{\mathbf{s}}_{eff}(k_{eff})^T \mathbf{e}(p, k_{eff}) + \underbrace{\bar{\mathbf{s}}_{eff}(k_{eff})^T \bar{\mathbf{s}}_{eff}(k_{eff})}_{=1} y(p-1, k_{eff}) \\ &= \omega \bar{\mathbf{s}}_{eff}(k_{eff})^T \mathbf{e}(p, k_{eff}) + y(p-1, k_{eff}). \end{aligned} \quad (9-12)$$

For convergence we have:

$$\lim_{p \rightarrow \infty} (y(p, k_{eff}) - y(p-1, k_{eff})) = \lim_{p \rightarrow \infty} (\omega \bar{\mathbf{s}}_{eff}(k_{eff})^T \mathbf{e}(p, k_{eff})) = 0 \quad (9-13)$$

However, we can write  $\mathbf{e}(p, k_{eff})$  as:

$$\begin{aligned} \mathbf{e}(p, k_{eff}) &= \mathbf{e}(p, k_{eff}-1) - \omega \bar{\mathbf{s}}_{eff}(k_{eff}-1) \bar{\mathbf{s}}_{eff}(k_{eff}-1)^T \mathbf{e}(p, k_{eff}-1) \\ &= \mathbf{B}_{k_{eff}-1} \mathbf{e}(p, k_{eff}-1) \\ &= (\mathbf{B}_{k_{eff}-1} \mathbf{B}_{k_{eff}-2} \cdots \mathbf{B}_1 \mathbf{B}_{WK} \cdots \mathbf{B}_{k_{eff}+1} \mathbf{B}_{k_{eff}}) \mathbf{e}(p-1, k_{eff}) \\ &= \mathbf{\Omega}_{k_{eff}} \mathbf{e}(p-1, k_{eff}) \end{aligned} \quad (9-14)$$

where  $\mathbf{B}_{k_{eff}} = (\mathbf{I} - \omega \bar{\mathbf{s}}_{eff}(k_{eff}) \bar{\mathbf{s}}_{eff}(k_{eff})^T)$ . Therefore, equation (9-14) is equivalent to:

$$\lim_{p \rightarrow \infty} \mathbf{e}(p, k_{eff}) = \lim_{p \rightarrow \infty} \left( \mathbf{\Omega}_{k_{eff}} \mathbf{e}(p-1, k_{eff}) \right) = \lim_{p \rightarrow \infty} \left( \left( \mathbf{\Omega}_{k_{eff}} \right)^{p-1} \mathbf{e}(1, k_{eff}) \right) = \mathbf{0} \quad (9-15)$$

Therefore the CL-LSOR-SIC converges if:

$$\left| \lambda_{\max} \left( \mathbf{\Omega}_{k_{eff}} \right) \right| < 1 \quad (9-16)$$

Since for square matrices  $\mathbf{X}$  and  $\mathbf{Y}$  with the same dimensions, the matrices  $\mathbf{XY}$  and  $\mathbf{YX}$  have the same eigenvalues, all the  $\mathbf{\Omega}_{k_{eff}}$ ,  $1 \leq k_{eff} \leq WK$  have the same eigenvalues. Thus we consider the case where  $k_{eff} = WK$ .

Consequently, the CL-LSOR-SIC converges if:

$$\left| \lambda_{\max} \left( \mathbf{\Omega}_{WK} \right) \right| < 1 \quad (9-17)$$

In the following, we consider the following lemma [124]:

**Lemma 9-1**

$$\left| \lambda_{\max} \left( \mathbf{\Omega}_{WK} \right) \right| \leq \prod_{k_{eff}=1}^{WK} \left| \lambda_{\max} \left( \mathbf{B}_{k_{eff}} \right) \right|$$

Thus, if  $\left| \lambda_{\max} \left( \mathbf{B}_k \right) \right|$ ,  $1 \leq k \leq K$  is less than one, then the condition in equation (9-17) is satisfied and the CL-LSOR-SIC is guaranteed to converge. We have:

$$\max_{1 \leq k_{eff} \leq WK} \left( \left| \lambda_{\max} \left( \mathbf{B}_{k_{eff}} \right) \right| \right) < 1$$

thus

$$\max_{1 \leq k_{eff} \leq WK} \left( \left| \lambda_{\max} \left( \mathbf{I} - \omega \bar{\mathbf{s}}_{eff}(k_{eff}) \bar{\mathbf{s}}_{eff}(k_{eff})^T \right) \right| \right) < 1$$

Consequently

$$\max_{1 \leq k_{eff} \leq WK} \left( \left| 1 - \omega \lambda_{\max} \left( \bar{\mathbf{s}}_{eff}(k_{eff}) \bar{\mathbf{s}}_{eff}(k_{eff})^T \right) \right| \right) < 1$$

but since  $\lambda \left( \bar{\mathbf{s}}_{eff}(k_{eff}) \bar{\mathbf{s}}_{eff}(k_{eff})^T \right) = \lambda \left( \bar{\mathbf{s}}_{eff}(k_{eff})^T \bar{\mathbf{s}}_{eff}(k_{eff}) \right) = 1$  for  $1 \leq k_{eff} \leq WK$ , we get  $|1 - \omega| < 1$  and hence  $0 < \omega < 2$ , which is the same condition as for the SOR iterative method.

**9.3.4 Computational Complexity**

The number of floating point operations (flops) per processing window required by the proposed CL-LSOR-SIC detector is:

$$8WKP \left( WN + \max_{1 \leq k \leq K} (\tau^k) + \max_{1 \leq k \leq K} (\tau_{l_k}) \right) + 2WK \left( WN + \max_{1 \leq k \leq K} (\tau^k) + \max_{1 \leq k \leq K} (\tau_{l_k}) \right) \quad (9-18)$$

while the SL-LSOR-SIC detector proposed in [84] requires:

$$2 \left( WN + \max_{1 \leq k \leq K} (\tau^k) + \max_{1 \leq k \leq K} (\tau_{l_k}) \right) WK + 2 \left( WN + \max_{1 \leq k \leq K} (\tau^k) + \max_{1 \leq k \leq K} (\tau_{l_k}) \right) (WK)^2 + (3WK + 4)WKP \quad (9-19)$$

and the decorrelator detectors requires at least (lower bound) [78]:

$$11(KW)^3 + \frac{3}{2}(KW)^2 + KW + 2 \left( WN + \max_{1 \leq k \leq K} (\tau^k) + \max_{1 \leq k \leq K} (\tau_{l_k}) \right) (WK)^2 + 2 \left( WN + \max_{1 \leq k \leq K} (\tau^k) + \max_{1 \leq k \leq K} (\tau_{l_k}) \right) WK \quad (9-20)$$

#### 9.4 Chip-Level Linear Block Successive Over-Relaxation Group-Wise SIC (CL-LBSOR-GSIC) Structure

The proposed CL-LBSOR-GSIC detector consists of group interference cancellation units (GICU) arranged in a multistage structure of  $P$  stages as illustrated in Figure 8.3. The basic linear GICU is shown in Figure 9.2. In the ensuing, the following notations are used:  $\mathbf{e}(p, \mathbf{g}_{eff})$  is the residual signal of the  $p^{th}$  stage,  $g^{th}$  group of users GICU,  $\mathbf{I}(p, \mathbf{g}_{eff})$  is the MAI due the  $p^{th}$  stage,  $g^{th}$  group GICU and finally  $\mathbf{y}(p, \mathbf{g}_{eff})$  is the vector of decision variables of the  $p^{th}$  stage,  $g^{th}$  group GICU.

The combined signal  $(\omega \mathbf{e}(p, \mathbf{g}_{eff}) + \mathbf{I}(p-1, \mathbf{g}_{eff}))$  at the input of the  $p^{th}$  stage,  $g^{th}$  group GICU is first despreading to estimate the vector of decision variables  $\mathbf{y}(p, \mathbf{g}_{eff})$ , that is,  $\mathbf{y}(p, \mathbf{g}_{eff}) = \bar{\mathbf{R}}_{eff}(\mathbf{g}_{eff}, \mathbf{g}_{eff})^{-1} \bar{\mathbf{S}}_{eff}(\mathbf{g}_{eff})^T (\omega \mathbf{e}(p, \mathbf{g}_{eff}) + \mathbf{I}(p-1, \mathbf{g}_{eff}))$ . The MAI  $\mathbf{I}(p, \mathbf{g}_{eff})$  is obtained by spreading the vector of decision variables  $\mathbf{y}(p, \mathbf{g}_{eff})$ , that is:  $\mathbf{I}(p, \mathbf{g}_{eff}) = \bar{\mathbf{S}}_{eff}(\mathbf{g}_{eff}) \mathbf{y}(p, \mathbf{g}_{eff})$ , the sum of the latter and the weighted residual signal  $(1-\omega) \mathbf{e}(p, \mathbf{g}_{eff})$  is subtracted from the combined signal  $(\omega \mathbf{e}(p, \mathbf{g}_{eff}) + \mathbf{I}(p-1, \mathbf{g}_{eff}))$  to get a cleaned version of the residual signal  $\mathbf{e}(p, \mathbf{g}_{eff} + 1)$  for the next group of users, that is  $g+1$ .

This process is repeated in a multistage structure as it is shown in Figure 8.3; more insight is given in the next section where a matrix-algebraic approach is used to describe the CL-LBSOR-GSIC detector.

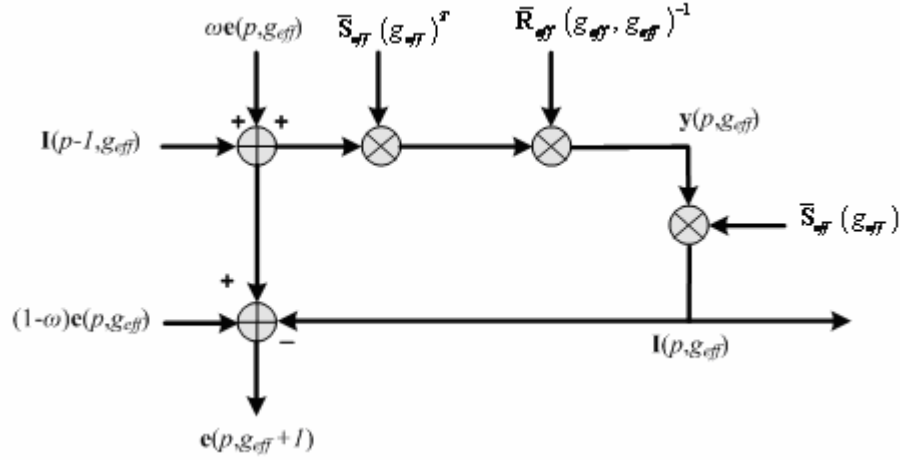


Figure 9.2: Basic group interference cancellation unit (GICU)

#### 9.4.1 Matrix Algebraic Approach to the Chip-Level Linear BSOR-GSIC Detector

Following the same procedure used for the CL-LBSOR-GSIC detector, we can obtain the general expression for the residual signal vector of the  $g^{th}$  effective GICU at the  $p^{th}$  stage as:

$$\mathbf{e}(p, g_{eff}) = \Phi_{g_{eff}-1} (\Phi_{WG})^{p-1} \mathbf{q}_b \quad (9-21)$$

and similarly, the vector of decision variables of the  $g^{th}$  effective GICU at the  $p^{th}$  stage can be expressed as:

$$\mathbf{y}(p, g_{eff}) = \omega \bar{\mathbf{R}}_{eff}(g_{eff}, g_{eff})^{-1} \bar{\mathbf{S}}_{eff}(g_{eff})^T \Phi_{g_{eff}-1} \sum_{i=0}^{p-1} (\Phi_{WG})^i \mathbf{q} = \mathbf{G}_{p, g_{eff}}^T \mathbf{q} \quad (9-22)$$

where:  $\Phi_{g_{eff}} = \prod_{j=g_{eff}}^1 (\mathbf{I} - \omega \bar{\mathbf{S}}_{eff}(j) \bar{\mathbf{R}}_{eff}(j, j)^{-1} \bar{\mathbf{S}}_{eff}(j)^T)$ .

Collecting the decision variables of all groups in one matrix we get:

$$\mathbf{y}(p) = \mathbf{G}_p^T \mathbf{q} .$$

where

$$\mathbf{G}_p = [\mathbf{G}_{p,1} \quad \mathbf{G}_{p,2} \quad \cdots \quad \mathbf{G}_{p,g_{eff}} \quad \cdots \quad \mathbf{G}_{p,WG}] .$$

and

$$\mathbf{G}_{p, g_{eff}} = [\mathbf{g}_{p, g_{eff}, 1} \quad \mathbf{g}_{p, g_{eff}, 2} \quad \cdots \quad \mathbf{g}_{p, g_{eff}, M_{g_{eff}}} \quad \cdots \quad \mathbf{g}_{p, g_{eff}, U_{g_{eff}}}] .$$

The matrix  $\mathbf{G}_p$  can also be written as:  $\mathbf{G}_p = [\mathbf{g}_{p,1} \ \mathbf{g}_{p,2} \ \cdots \ \mathbf{g}_{p,k_{eff}} \ \cdots \ \mathbf{g}_{p,WK}]$ . Therefore the CL-LBSOR-GSIC structure can be described as matrix filtering of the received chip-matched signal vector. Using the same method as for the matched filter detector, the BER of the  $k^{th}$  effective user at the  $p^{th}$  stage can be evaluated as:

$$P_{p,k_{eff}}(\sigma) = \frac{1}{2^{WK-1}} \sum_{\substack{\text{all } \mathbf{b} \\ \mathbf{b}(k_{eff})=1}} Q \left( \frac{\mathbf{g}_{p,k_{eff}}^T \bar{\mathbf{S}}_{eff} \bar{\mathbf{A}}_{eff} \mathbf{b}}{\sigma \sqrt{\mathbf{g}_{p,k_{eff}}^T \mathbf{g}_{p,k_{eff}}}} \right) \quad (9-23)$$

where  $Q(\cdot)$  is the  $Q$ -function. The asymptotic multiuser efficiency for the  $k^{th}$  effective user of the  $g^{th}$  effective group at the  $p^{th}$  stage is given by:

$$\eta(p, k_{eff}) = \frac{1}{\mathbf{g}_{p,k_{eff}}^T \mathbf{g}_{p,k_{eff}}} \max^2 \left( 0, \mathbf{g}_{p,k_{eff}}^T \bar{\mathbf{S}}_{eff}(k_{eff}) - \sum_{\substack{j=1 \\ j \neq k_{eff}}}^{WK} \frac{\bar{A}_{eff}(j, j)}{\bar{A}_{eff}(k_{eff}, k_{eff})} |\mathbf{g}_{p,k_{eff}}^T \bar{\mathbf{S}}_{eff}(j)| \right) \quad (9-24)$$

#### 9.4.2 Convergence Analysis

Let  $\mathbf{e}(1,1) = \mathbf{q}$ , at the  $p^{th}$  stage. The vector of decision variables of the  $g^{th}$  effective group of users of the CL-LBSOR-GSIC detector is derived as:

$$\begin{aligned} \mathbf{y}(p, \mathbf{g}_{eff}) &= \omega \bar{\mathbf{R}}_{eff}(\mathbf{g}_{eff}, \mathbf{g}_{eff})^{-1} \bar{\mathbf{S}}_{eff}(\mathbf{g}_{eff})^T \mathbf{q} - \omega \bar{\mathbf{R}}_{eff}(\mathbf{g}_{eff}, \mathbf{g}_{eff})^{-1} \bar{\mathbf{S}}_{eff}(\mathbf{g}_{eff})^T \\ &\sum_{j=1}^{g_{eff}-1} \bar{\mathbf{S}}_{eff}(j) \mathbf{y}(p, j) - \omega \bar{\mathbf{R}}_{eff}(\mathbf{g}_{eff}, \mathbf{g}_{eff})^{-1} \bar{\mathbf{S}}_{eff}(\mathbf{g}_{eff})^T \sum_{j=g_{eff}}^{WG-1} \bar{\mathbf{S}}_{eff}(j) \mathbf{y}(p-1, j) \\ &+ \mathbf{y}(p-1, \mathbf{g}_{eff}), \quad \text{for } \mathbf{g}_{eff} = 1, 2, \dots, WG. \end{aligned} \quad (9-25)$$

At convergence we have:  $\mathbf{y}(p, \mathbf{g}_{eff}) = \mathbf{y}(p-1, \mathbf{g}_{eff}) = \mathbf{y}(\infty, \mathbf{g}_{eff})$  therefore (9-25) is equivalent to:

$$\begin{aligned} \mathbf{y}(\infty, \mathbf{g}_{eff}) &= \omega \bar{\mathbf{R}}_{eff}(\mathbf{g}_{eff}, \mathbf{g}_{eff})^{-1} \bar{\mathbf{S}}_{eff}(\mathbf{g}_{eff})^T \mathbf{q} - \omega \bar{\mathbf{R}}_{eff}(\mathbf{g}_{eff}, \mathbf{g}_{eff})^{-1} \bar{\mathbf{S}}_{eff}(\mathbf{g}_{eff})^T \\ &\sum_{j=1}^{g_{eff}-1} \bar{\mathbf{S}}_{eff}(j) \mathbf{y}(\infty, j) - \omega \bar{\mathbf{R}}_{eff}(\mathbf{g}_{eff}, \mathbf{g}_{eff})^{-1} \bar{\mathbf{S}}_{eff}(\mathbf{g}_{eff})^T \sum_{j=g_{eff}}^{WG-1} \bar{\mathbf{S}}_{eff}(j) \mathbf{y}(\infty, j) \\ &+ \mathbf{y}(\infty, \mathbf{g}_{eff}), \quad \text{for } \mathbf{g}_{eff} = 1, 2, \dots, WG. \end{aligned} \quad (9-26)$$

Equation (9-26) is equivalent to:

$$\begin{aligned} \omega \bar{\mathbf{R}}_{eff}(\mathbf{g}_{eff}, \mathbf{g}_{eff})^{-1} \bar{\mathbf{S}}_{eff}(\mathbf{g}_{eff})^T \sum_{j=1}^{WG-1} \bar{\mathbf{S}}_{eff}(j) \mathbf{y}(\infty, j) &= \omega \bar{\mathbf{R}}_{eff}(\mathbf{g}_{eff}, \mathbf{g}_{eff})^{-1} \bar{\mathbf{S}}_{eff}(\mathbf{g}_{eff})^T \mathbf{q} \\ \text{for } \mathbf{g}_{eff} &= 1, 2, \dots, WG. \end{aligned} \quad (9-27)$$

Since  $\bar{\mathbf{R}}_{eff}(\mathbf{g}_{eff}, \mathbf{g}_{eff})$  is nonsingular, equation (9-27) could be written in matrix form as:

$$\bar{\mathbf{S}}_{eff}^T \bar{\mathbf{S}}_{eff} \mathbf{y}(\infty) = \bar{\mathbf{S}}_{eff}^T \mathbf{q} \quad (9-28)$$

Finally, (9-28) could be written as:

$$\mathbf{y}(\infty) = \bar{\mathbf{R}}_{eff}^{-1} \bar{\mathbf{S}}_{eff}^T \mathbf{q} \quad (9-29)$$

The expression above looks exactly like that of the decorrelator detector, therefore, if the proposed scheme converges, it converges to the decorrelator detector.

### 9.4.3 Conditions of Convergence

For the conditions of convergence of the proposed scheme, we propose two different approaches that lead to the same result. These two approaches are detailed in the ensuing analysis.

#### 9.4.3.1 First Approach

This approach allows the identification of the proposed scheme as the BSOR iterative method; this facilitates the determination of the condition of convergence. Let's first establish the equivalence between the proposed scheme and the corresponding iterative method used to solve a set of linear equations which is known as the BSOR method.

The matrix  $\bar{\mathbf{R}}_{eff}$  could be decomposed into three parts, that is,  $\bar{\mathbf{R}}_{eff} = \mathbf{D} - \mathbf{L} - \mathbf{L}^T$  where  $\mathbf{D}$  is the block diagonal part of the matrix  $\bar{\mathbf{R}}_{eff}$ , that is:  $\mathbf{D} = \text{diag}(\bar{\mathbf{R}}_{eff}(1,1), \bar{\mathbf{R}}_{eff}(2,2), \dots, \bar{\mathbf{R}}_{eff}(g_{eff}, g_{eff}), \dots, \bar{\mathbf{R}}_{eff}(WG, WG))$ , and  $\mathbf{L}$  and  $\mathbf{L}^T$  are the remaining lower-left and upper-right block triangular parts of  $\bar{\mathbf{R}}_{eff}$ , respectively. After some manipulations, equation (9-25) could be written in matrix form as:

$$\mathbf{y}(p) = \omega(\mathbf{D} - \omega\mathbf{L})^{-1} \bar{\mathbf{S}}_{eff}^T \mathbf{q} + (\mathbf{D} - \omega\mathbf{L})^{-1} ((1 - \omega)\mathbf{D} + \omega\mathbf{U})\mathbf{y}(p-1) \quad (9-30)$$

which is exactly the BSOR iteration. Note that if  $\omega = 1$  (this is the case for the scheme proposed in [124] where the group detection scheme is the decorrelator detector), the iteration in (9-30) reduces to the block Gauss-Seidel iteration. For the convergence of (9-30), we use the following corollary [80]:

#### Corollary 9-1

*Let  $\mathbf{R}$  be an  $K$ -by- $K$  hermitian matrix and  $\mathbf{R} = \mathbf{D} - \mathbf{L} - \mathbf{L}^H$ , where  $\mathbf{D}$  is block diagonal matrix, and  $\mathbf{L}$  and  $\mathbf{L}^T$  are the remaining lower-left and upper-right block triangular parts of  $\mathbf{R}$ . If  $\mathbf{D}$  is positive definite, then the block successive over-relaxation method is convergent for all  $\mathbf{y}(0)$  if and only if  $0 < \omega < 2$  and  $\mathbf{R}$  is positive definite.*

Thus, for  $\omega$  real, the iteration in (9-30) converges if  $\omega \in (0, 2)$ . Nevertheless, one should set  $\omega$  within the interval (1, 2) which corresponds to over-relaxation (acceleration) since the interval (0, 1) corresponds to under-relaxation (deceleration) and it is basically used to ensure convergence of the block Gauss-seidel iteration if it is not convergent. The calculation of the optimum value of  $\omega$  for which the convergence is maximum, depends on the maximum eigenvalue of the iteration matrix  $(\mathbf{D} - \omega\mathbf{L})^{-1}((1-\omega)\mathbf{D} + \omega\mathbf{L}^T)$ , which is complex to compute. However, one can get a cheap fairly-accurate estimate of the optimum value of  $\omega$  based on some upper bound on the maximum eigenvalue of the iteration matrix as in [84] and it is given by equation (7-2).

#### 9.4.3.2 Second Approach

Here, the approach used in [124] is adopted to determine the condition of convergence for the proposed scheme. As it can be seen from Figure 9.2, we have:

$$\begin{aligned}
 \mathbf{y}(p, \mathbf{g}_{eff}) &= \bar{\mathbf{R}}_{eff}(\mathbf{g}_{eff}, \mathbf{g}_{eff})^{-1} \bar{\mathbf{S}}_{eff}(\mathbf{g}_{eff})^T (\omega \mathbf{e}(p, \mathbf{g}_{eff}) + \mathbf{I}(p-1, \mathbf{g}_{eff})) \\
 &= \omega \bar{\mathbf{R}}_{eff}(\mathbf{g}_{eff}, \mathbf{g}_{eff})^{-1} \bar{\mathbf{S}}_{eff}(\mathbf{g}_{eff})^T \mathbf{e}(p, \mathbf{g}_{eff}) \\
 &\quad + \underbrace{\bar{\mathbf{R}}_{eff}(\mathbf{g}_{eff}, \mathbf{g}_{eff})^{-1} \bar{\mathbf{S}}_{eff}(\mathbf{g}_{eff})^T \bar{\mathbf{S}}_{eff}(\mathbf{g}_{eff})}_{=\mathbf{I}} \mathbf{y}(p-1, \mathbf{g}_{eff}) \\
 &= \omega \bar{\mathbf{R}}_{eff}(\mathbf{g}_{eff}, \mathbf{g}_{eff})^{-1} \bar{\mathbf{S}}_{eff}(\mathbf{g}_{eff})^T \mathbf{e}(p, \mathbf{g}_{eff}) + \mathbf{y}(p-1, \mathbf{g}_{eff})
 \end{aligned} \tag{9-31}$$

At convergence, we have:

$$\begin{aligned}
 \lim_{p \rightarrow \infty} (\mathbf{y}(p, \mathbf{g}_{eff}) - \mathbf{y}(p-1, \mathbf{g}_{eff})) &= \lim_{p \rightarrow \infty} (\bar{\mathbf{R}}_{eff}(\mathbf{g}_{eff}, \mathbf{g}_{eff})^{-1} \bar{\mathbf{S}}_{eff}(\mathbf{g}_{eff})^T \mathbf{e}(p, \mathbf{g}_{eff})) \\
 &= \mathbf{0}
 \end{aligned} \tag{9-32}$$

However, we can write  $\mathbf{e}(p, \mathbf{g}_{eff})$  as:

$$\begin{aligned}
 \mathbf{e}(p, \mathbf{g}_{eff}) &= \mathbf{e}(p, \mathbf{g}_{eff}-1) - \omega \bar{\mathbf{S}}_{eff}(\mathbf{g}_{eff}-1) \bar{\mathbf{R}}_{eff}(\mathbf{g}_{eff}-1, \mathbf{g}_{eff}-1)^{-1} \\
 &\quad \bar{\mathbf{S}}_{eff}(\mathbf{g}_{eff}-1)^T \mathbf{e}(p, \mathbf{g}_{eff}-1) \\
 &= \mathbf{B}_{\mathbf{g}_{eff}-1} \mathbf{e}(p, \mathbf{g}_{eff}-1) \\
 &= (\mathbf{B}_{\mathbf{g}_{eff}-1} \mathbf{B}_{\mathbf{g}_{eff}-2} \cdots \mathbf{B}_1 \mathbf{B}_{WG} \cdots \mathbf{B}_{\mathbf{g}_{eff}+1} \mathbf{B}_{\mathbf{g}_{eff}}) \mathbf{e}(p-1, \mathbf{g}_{eff}) \\
 &= \mathbf{\Omega}_{\mathbf{g}_{eff}} \mathbf{e}(p-1, \mathbf{g}_{eff})
 \end{aligned} \tag{9-33}$$

where  $\mathbf{B}_{\mathbf{g}_{eff}} = (\mathbf{I} - \omega \bar{\mathbf{S}}_{eff}(\mathbf{g}_{eff}) \bar{\mathbf{R}}_{eff}(\mathbf{g}_{eff}, \mathbf{g}_{eff})^{-1} \bar{\mathbf{S}}_{eff}(\mathbf{g}_{eff})^T)$ . Therefore, equation (9-32) is equivalent to:

$$\lim_{p \rightarrow \infty} \mathbf{e}(p, \mathbf{g}_{eff}) = \lim_{p \rightarrow \infty} \left( \mathbf{\Omega}_{g_{eff}} \mathbf{e}(p-1, \mathbf{g}_{eff}) \right) = \lim_{p \rightarrow \infty} \left( \left( \mathbf{\Omega}_{g_{eff}} \right)^{p-1} \mathbf{e}(1, \mathbf{g}_{eff}) \right) = \mathbf{0} \quad (9-34)$$

Therefore the CL-LBSOR-GSIC converges if:

$$\left| \lambda_{\max} \left( \mathbf{\Omega}_{g_{eff}} \right) \right| < 1 \quad (9-35)$$

Since for square matrices  $\mathbf{X}$  and  $\mathbf{Y}$  with the same dimensions, the matrices  $\mathbf{XY}$  and  $\mathbf{YX}$  have the same eigenvalues, then all the  $\mathbf{\Omega}_{g_{eff}}$ 's,  $1 \leq g_{eff} \leq WG$  have the same eigenvalues. Thus we consider the case where  $g_{eff} = WG$ . Consequently, the CL-LBSOR-GSIC converges if:

$$\left| \lambda_{\max} \left( \mathbf{\Omega}_{WG} \right) \right| < 1 \quad (9-36)$$

In the ensuing, we state the following lemma [124]:

**Lemma 9-2**

$$\left| \lambda_{\max} \left( \mathbf{\Omega}_{WG} \right) \right| \leq \prod_{g_{eff}=1}^{WG} \left| \lambda_{\max} \left( \mathbf{B}_{g_{eff}} \right) \right|$$

Thus, if  $\left| \lambda_{\max} \left( \mathbf{B}_{g_{eff}} \right) \right|$ ,  $1 \leq g_{eff} \leq WG$ , is less than one, then the condition in equation (9-36) is satisfied and the CL-LBSOR-GSIC detector is guaranteed to converge. That is:

$$\max_{1 \leq g_{eff} \leq WG} \left( \left| \lambda_{\max} \left( \mathbf{B}_{g_{eff}} \right) \right| \right) < 1$$

thus:

$$\max_{1 \leq g_{eff} \leq WG} \left( \left| \lambda_{\max} \left( \mathbf{I} - \omega \bar{\mathbf{S}}_{eff} \left( \mathbf{g}_{eff} \right) \bar{\mathbf{R}}_{eff} \left( \mathbf{g}_{eff}, \mathbf{g}_{eff} \right)^{-1} \bar{\mathbf{S}}_{eff} \left( \mathbf{g}_{eff} \right)^T \right) \right| \right) < 1$$

consequently:  $\max_{1 \leq g_{eff} \leq WG} \left( \left| 1 - \omega \lambda_{\max} \left( \bar{\mathbf{S}}_{eff} \left( \mathbf{g}_{eff} \right) \bar{\mathbf{R}}_{eff} \left( \mathbf{g}_{eff}, \mathbf{g}_{eff} \right)^{-1} \bar{\mathbf{S}}_{eff} \left( \mathbf{g}_{eff} \right)^T \right) \right| \right) < 1.$

Hence:

$$0 < \omega < \frac{2}{\lambda_{\max} \left( \bar{\mathbf{S}}_{eff} \left( \mathbf{g}_{eff} \right) \bar{\mathbf{R}}_{eff} \left( \mathbf{g}_{eff}, \mathbf{g}_{eff} \right)^{-1} \bar{\mathbf{S}}_{eff} \left( \mathbf{g}_{eff} \right)^T \right)}. \text{ Since } \bar{\mathbf{S}}_{eff} \left( \mathbf{g}_{eff} \right) \bar{\mathbf{R}}_{eff} \left( \mathbf{g}_{eff}, \mathbf{g}_{eff} \right)^{-1} \bar{\mathbf{S}}_{eff} \left( \mathbf{g}_{eff} \right)^T \text{ is}$$

a projection matrix then  $\left| \lambda_{\max} \left( \bar{\mathbf{S}}_{eff} \left( \mathbf{g}_{eff} \right) \bar{\mathbf{R}}_{eff} \left( \mathbf{g}_{eff}, \mathbf{g}_{eff} \right)^{-1} \bar{\mathbf{S}}_{eff} \left( \mathbf{g}_{eff} \right)^T \right) \right| = 1$  and consequently  $0 < \omega < 2$ ,

which is identical to that of the BSOR method.

#### 9.4.4 Computational Complexity

In this section, the computational complexity of the proposed scheme is addressed. First, the computational complexity of the proposed detector requires:

$$\begin{aligned}
 & PW \left[ \sum_{g=1}^G U_g (2U_g - 1) + \left( WN + \max_{1 \leq k \leq K} (\tau^k) + \max_{1 \leq l \leq K} (\tau_{l_k}) \right) \sum_{g=1}^G (2U_g - 1) + \right. \\
 & \left. \left( 2 \left( WN + \max_{1 \leq k \leq K} (\tau^k) + \max_{1 \leq l \leq K} (\tau_{l_k}) \right) - 1 \right) \sum_{g=1}^G U_g \right] + \\
 & 6PG \left( WN + \max_{1 \leq k \leq K} (\tau^k) + \max_{1 \leq l \leq K} (\tau_{l_k}) \right) + W \sum_{g=1}^G \left( 11U_g^3 + \frac{3}{2}U_g^2 + U_g \right) + \\
 & 2W \left( WN + \max_{1 \leq k \leq K} (\tau^k) + \max_{1 \leq l \leq K} (\tau_{l_k}) \right) \sum_{g=1}^G (U_g)^2
 \end{aligned} \tag{9-37}$$

Second, the computational complexity of the SL-LBSOR-GSIC detector is:

$$\begin{aligned}
 & 2 \left( WN + \max_{1 \leq k \leq K} (\tau^k) + \max_{1 \leq l \leq K} (\tau_{l_k}) \right) WK + 2 \left( WN + \max_{1 \leq k \leq K} (\tau^k) + \max_{1 \leq l \leq K} (\tau_{l_k}) \right) (WK)^2 + \\
 & (WK)^2 + 2W \sum_{g=1}^G U_g^2 + PW^2 \sum_{g=1}^G U_g \sum_{j=1}^G (2U_j - 1) + PW \sum_{g=1}^G U_g (2U_g - 1) + \\
 & W \sum_{g=1}^G \left( 11U_g^3 + \frac{3}{2}U_g^2 + U_g \right) + PW \sum_{g=1}^G U_g^2
 \end{aligned} \tag{9-38}$$

Finally the decorrelator detector needs at least (lower bound) [78]:

$$\begin{aligned}
 & 11(KW)^3 + \frac{3}{2}(KW)^2 + KW + 2 \left( WN + \max_{1 \leq k \leq K} (\tau^k) + \max_{1 \leq l \leq K} (\tau_{l_k}) \right) (WK)^2 \\
 & + 2 \left( WN + \max_{1 \leq k \leq K} (\tau^k) + \max_{1 \leq l \leq K} (\tau_{l_k}) \right) WK
 \end{aligned} \tag{9-39}$$

#### 9.5 Reduced-Complexity Chip-Level Linear Successive Over-Relaxation (RC-CL-LSOR-SIC) Structure

The RC-CL-LSOR-SIC detector consists of interference cancellation units (ICU) arranged in a multistage structure of  $P$  stages as illustrated in Figure 7.10. The basic linear ICU is shown in Figure 9.3. The partial decision variable of the  $k^{\text{th}}$  effective user at the  $p^{\text{th}}$ -stage  $y'(p, k_{\text{eff}})$  is obtained by spreading the residual signal  $\mathbf{e}(p, k_{\text{eff}})$  and multiplying it with the relaxation factor  $\omega$  that is,  $y'(p, k_{\text{eff}}) = \omega \bar{\mathbf{s}}_{\text{eff}}(k_{\text{eff}})^T \mathbf{e}(p, k_{\text{eff}})$ . The decision variable  $y(p, k_{\text{eff}})$  is obtained by adding the partial decision variable  $y'(p, k_{\text{eff}})$  to the decision variable of the previous stage  $y(p-1, k_{\text{eff}})$ , that

is,  $y(p, k_{eff}) = y'(p, k_{eff}) + y(p-1, k_{eff})$ . The residual signal for the next ICU is obtained by spreading the partial decision variable and subtracting it from the residual signal, that is,  $e(p, k_{eff} + 1) = e(p, k_{eff}) - \bar{s}_{eff}(k_{eff}) y'(p, k_{eff})$ . This process is repeated in a multistage structure as it is shown in Figure 7.10.

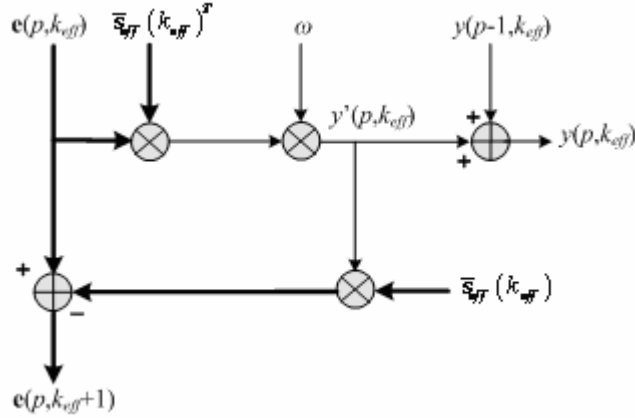


Figure 9.3:  $p^{th}$  stage,  $k^{th}$  effective user RC-CL-LSOR-SIC's ICU.

Following the same procedure as in [121], we can obtain similar expressions to those of (9-1) and (9-2) for the residual signal vector and the decision variable of the  $k^{th}$  effective user's ICU unit at the  $p^{th}$  stage, respectively.

Hence, the RC-CL-LSOR-SIC detector can be described as matrix filtering of the received chip-matched signal vector. Using the same method as for the CL-LSOR-SIC detector, one can obtain the same BER and AME expressions as those in (9-4) and (9-5), respectively.

### 9.5.1 Convergence Behavior and Conditions of Convergence

Following the same procedure as in Section 9.3.2 and 9.3.3, it is easy to show that if the structure converges it converges to the decorrelator detector. Moreover, the structure converges to the decorrelator detector if  $\omega \in (0, 2)$ .

### 9.5.2 Computational Complexity

The number of flops required by the proposed RC-CL-LSOR-SIC detector is:

$$WK P \left( 4 \left( WN + \max_{1 \leq k \leq K} (\tau^k) + \max_{1 \leq k \leq K} (\tau_{l_k}) \right) + 2 \right) + 2WK \left( WN + \max_{1 \leq k \leq K} (\tau^k) + \max_{1 \leq k \leq K} (\tau_{l_k}) \right) \quad (9-40)$$

while the SL-LSOR-SIC detector proposed in [84] requires:

$$2 \left( WN + \max_{1 \leq k \leq K} (\tau^k) + \max_{1 \leq k \leq K} (\tau_{l_k}) \right) WK + 2 \left( WN + \max_{1 \leq k \leq K} (\tau^k) + \max_{1 \leq k \leq K} (\tau_{l_k}) \right) (WK)^2 + (3WK + 4)WK P \quad (9-41)$$

and the decorrelator detectors requires at least (lower bound) [78]:

$$11(KW)^3 + \frac{3}{2}(KW)^2 + KW + 2 \left( WN + \max_{1 \leq k \leq K} (\tau^k) + \max_{1 \leq k \leq K} (\tau_{l_k}) \right) (WK)^2 + 2 \left( WN + \max_{1 \leq k \leq K} (\tau^k) + \max_{1 \leq k \leq K} (\tau_{l_k}) \right) WK \quad (9-42)$$

These expressions are plotted and compared in Section 9.7.

## 9.6 Reduced-Complexity Chip-Level Linear Block Successive Over-Relaxation Group-Wise SIC (RC-CL-LBSOR-GSIC) Structure

The proposed RC-CL-LBSOR-GSIC detector consists of group interference cancellation units (GICU) arranged in a multistage structure of  $P$  stages as illustrated in Figure 7.12. The basic linear GICU is shown in Figure 9.4. The residual signal  $\mathbf{e}(p, \mathbf{g}_{eff})$  at the input of the  $p^{th}$ -stage,  $g^{th}$  effective group GICU is first despreaded, multiplied by a transformation matrix  $\bar{\mathbf{R}}(\mathbf{g}_{eff}, \mathbf{g}_{eff})^{-1}$  and then by a relaxation factor  $\omega$  to estimate the vector of the partial decision variables  $\mathbf{y}'(p, \mathbf{g}_{eff})$  of users of the  $g^{th}$  effective group at the  $p^{th}$ -stage that is  $\mathbf{y}'(p, \mathbf{g}_{eff}) = \omega \bar{\mathbf{R}}(\mathbf{g}_{eff}, \mathbf{g}_{eff})^{-1} \bar{\mathbf{S}}_{eff}(\mathbf{g}_{eff})^T \mathbf{e}(p, \mathbf{g}_{eff})$ . The vector of the decision variables of the users of the  $g^{th}$  effective group at the  $p^{th}$ -stage is obtained by summing up the vector of decision variables of the previous stage  $\mathbf{y}(p-1, \mathbf{g}_{eff})$  and the vector of partial decision variables of the current stage  $\mathbf{y}'(p, \mathbf{g}_{eff})$ , that is,  $\mathbf{y}(p, \mathbf{g}_{eff}) = \mathbf{y}'(p, \mathbf{g}_{eff}) + \mathbf{y}(p-1, \mathbf{g}_{eff})$ .

The residual signal for the next GICU is obtained by spreading the vector of the partial decision variables  $\mathbf{y}'(p, \mathbf{g}_{eff})$  and subtracting it from the residual signal of the current GICU  $\mathbf{e}(p, \mathbf{g}_{eff})$ , that is,  $\mathbf{e}(p, \mathbf{g}_{eff} + 1) = \mathbf{e}(p, \mathbf{g}_{eff}) - \bar{\mathbf{S}}_{eff}(\mathbf{g}_{eff}) \mathbf{y}'(p, \mathbf{g}_{eff})$ .

Following the same procedure as in Section 9.4.1, we can obtain similar expressions to those of (9-21) and (9-22) for the residual signal vector and the vector of decision variables of the  $g^{th}$  effective group's ICU unit at the  $p^{th}$  stage, respectively.

Hence, the RC-CL-LBSOR-GSIC can be described as matrix filtering of the received chip-matched signal vector. Using the same approach as for the CL-LBSOR-GSIC detector, one can obtain the same BER and AME expressions as those in (9-23) and (9-24), respectively.

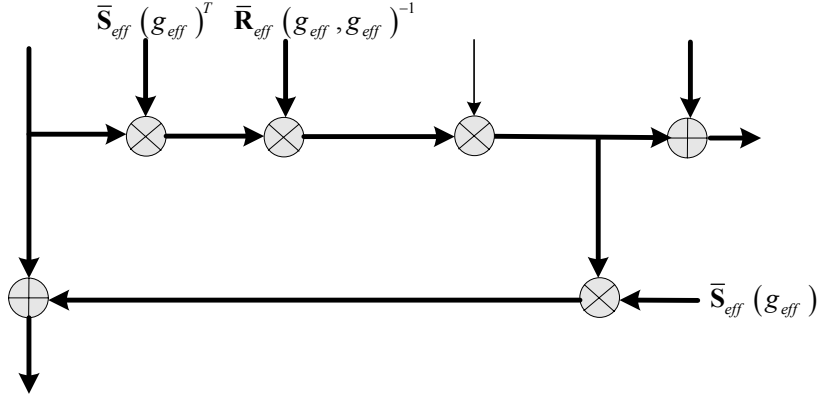


Figure 9.4:  $p^{th}$  stage,  $g^{th}$  effective user CL-LBSOR-GSIC's GICU

### 9.6.1 Convergence Analysis and Conditions of Convergence

Following the same procedure as in Section 9.4.2 and 9.4.3, it is easy to show that if the structure converges it converges to the decorrelator detector. Moreover, the structure converges to the decorrelator detector if  $\omega \in (0, 2)$ .

### 9.6.2 Computational Complexity

The computational complexity of the proposed detector requires:

$$PW \left( \sum_{g=1}^G U_g (2U_g - 1) + 3 \sum_g U_g + \left( WN + \max_{1 \leq k \leq K} (\tau^k) + \max_{1 \leq k \leq K} (\tau_{l_k}) \right) \sum_{g=1}^G (2U_g - 1) + \left( 2 \left( WN + \max_{1 \leq k \leq K} (\tau^k) + \max_{1 \leq k \leq K} (\tau_{l_k}) \right) - 1 \right) \sum_{g=1}^G U_g + G \left( WN + \max_{1 \leq k \leq K} (\tau^k) + \max_{1 \leq k \leq K} (\tau_{l_k}) \right) \right) + \quad (9-43)$$

$$+ W \sum_{g=1}^G \left( 11U_g^3 + \frac{3}{2}U_g^2 + U_g \right) + 2W \left( WN + \max_{1 \leq k \leq K} (\tau^k) + \max_{1 \leq k \leq K} (\tau_{l_k}) \right) \sum_{g=1}^G (U_g)^2$$

where the computational complexity of the SL-LBSOR-GSIC detector is:

$$2\left(WN + \max_{1 \leq k \leq K}(\tau^k) + \max_{1 \leq k \leq K}(\tau_{l_k})\right)WK + 2\left(WN + \max_{1 \leq k \leq K}(\tau^k) + \max_{1 \leq k \leq K}(\tau_{l_k})\right)(WK)^2 + (WK)^2$$

$$-W \sum_{g=1}^G U_g^2 + PW^2 \sum_{g=1}^G U_g \sum_{j=1}^G (2U_j - 1) + W \sum_{g=1}^G \left(11U_g^3 + \frac{3}{2}U_g^2 + U_g\right) + PW \sum_{g=1}^G (U_g - 1)U_g \quad (9-44)$$

Finally, the decorrelator detector needs at least (lower bound) [78]:

$$11(KW)^3 + \frac{3}{2}(KW)^2 + KW + 2\left(WN + \max_{1 \leq k \leq K}(\tau^k) + \max_{1 \leq k \leq K}(\tau_{l_k})\right)(WK)^2$$

$$+ 2\left(WN + \max_{1 \leq k \leq K}(\tau^k) + \max_{1 \leq k \leq K}(\tau_{l_k})\right)WK \quad (9-45)$$

These expressions are plotted and compared in Section 9.7.

### 9.7 Simulation Results

In this section, we simulate the proposed schemes in two different scenarios; in the first one a synchronous CDMA AWGN channel is considered while in the second one an asynchronous CDMA multi-path fading channel is considered. The average BER (average of all users) is evaluated versus the value of the relaxation factor and depicted in Figure 9.5.

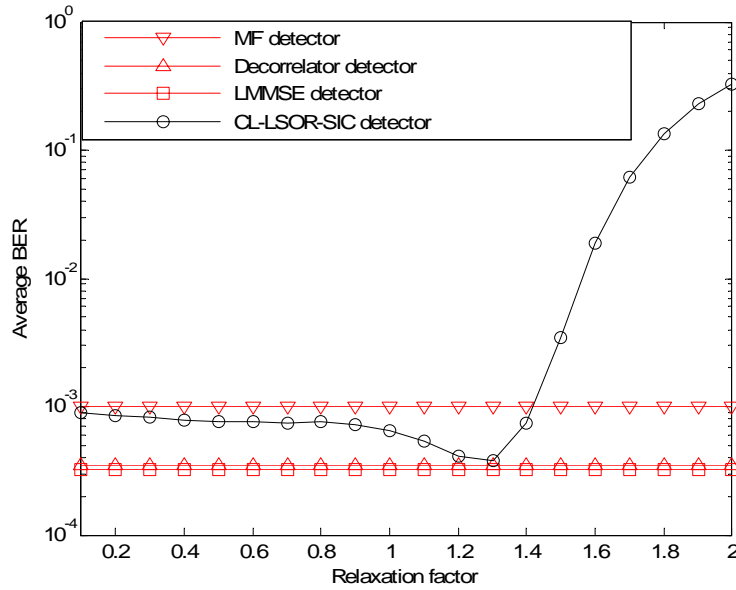


Figure 9.5: Average BER performance versus the relaxation factor of the proposed CL-LSOR-SIC detector for the case of a synchronous CDMA AWGN channel.

The aim of doing so is first to confirm that the CL-LSOR-SIC and CL-LBSOR-GSIC detectors converges if the relaxation factor is within the interval (0,2) as predicted by theory and second to verify that the minimum average BER is within the interval [1,2), which corresponds to over-relaxation. The SNR is set to 9dB,  $K = 24$ ,  $N = 31$  (Gold codes),  $P = 2$  and perfect power control is assumed.

It is clear from Figure 9.5 that the average BER of the proposed CL-LSOR-SIC detector achieves its minimum value for a relaxation factor of 1.3, which is within the interval [1,2) (over-relaxation). Hence, this confirms the theoretical findings concerning the CL-LSOR-SIC detector.

The convergence speed is now investigated by plotting the average BER versus the number of CL-LSOR-SIC stages for different relaxation factor values. The number of the CL-LSOR-SIC stages is varied between 1 and 15 and the average BER performance of the proposed detector is evaluated for  $\omega = 1, 1.1, 1.3, 1.5$  and  $1.8$ . The simulation results are plotted in Figure 9.6.

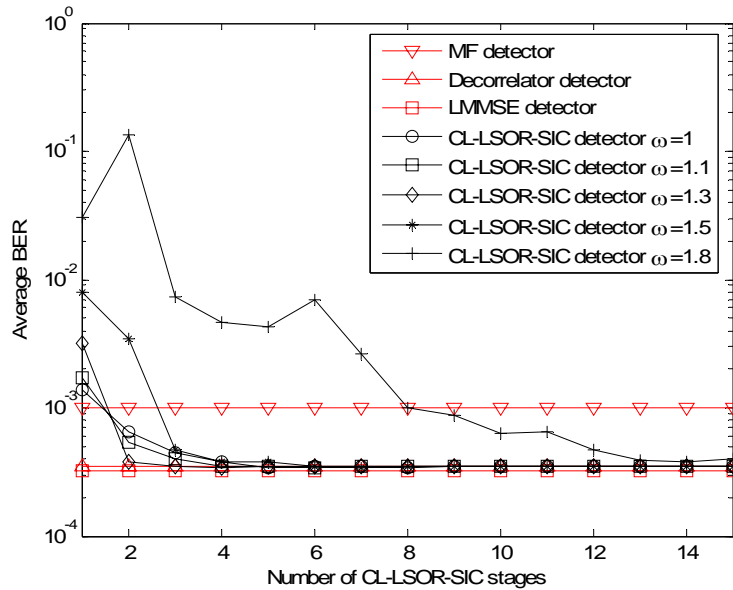


Figure 9.6: Convergence behavior of the proposed CL-LSOR-SIC detector for different relaxation factor values for the case of a synchronous CDMA AWGN channel.

It is clear that the CL-LSOR-SIC detector with  $\omega = 1.3$  results in the fastest convergence speed (2 stages are enough to converge to the decorrelator's detector average BER performance). One can

notice also that for  $\omega = 1.8$  the average BER performance of the proposed detector exhibits an oscillating behavior which is expected because we are close to the region of divergence  $(2, +\infty)$ .

As for the CL-LSOR-SIC detector, the performance of the CL-LBSOR-GSIC detector is now investigated. First, for the same simulation parameters of Figure 9.5, the average BER level is plotted versus the relaxation factor value and depicted in Figure 9.7. Here as well, it is evident that the minimum achievable average BER is for a relaxation factor of around 1.1 which is within  $[1,2)$  (over-relaxation). Note that the average BER performance is different from one grouping to another, this is mainly because the iteration matrix  $(\mathbf{D} - \omega\mathbf{L})^{-1}((1 - \omega)\mathbf{D} + \omega\mathbf{U})$ , on which the convergence behavior relies on, depends on grouping through the block diagonal matrix  $\mathbf{D}$ .

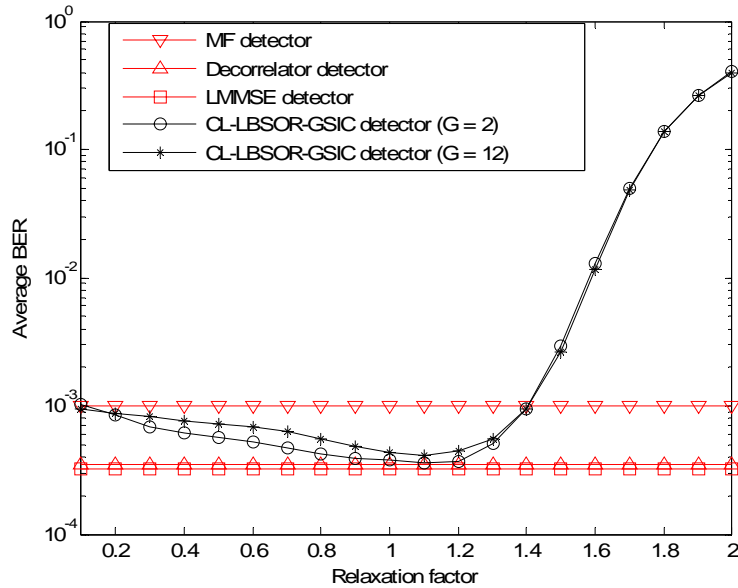


Figure 9.7: Average BER performance versus the relaxation factor of the proposed CL-LBSOR-GSIC detector for the case of a synchronous CDMA AWGN channel.

Next, the convergence speed is now investigated by plotting the average BER versus the number of CL-LBSOR-GSIC stages for different relaxation factor values. Simulation results are depicted in Figure 9.8. It is obvious that the CL-LBSOR-GSIC detector with  $\omega = 1.1$  results in the fastest convergence speed (2 stages are enough to converge to the decorrelator's detector average BER performance). However, its performance is indistinguishable from that of the CL-LGDEC-SIC detector

( $\omega = 1$ ). Hence, the over-relaxation didn't add much to the convergence speed of the proposed detector. One can notice also that for  $\omega = 1.8$  the average BER performance of the proposed detector exhibits an oscillating behavior which is expected because we are close to the region of divergence ( $2, +\infty$ ).

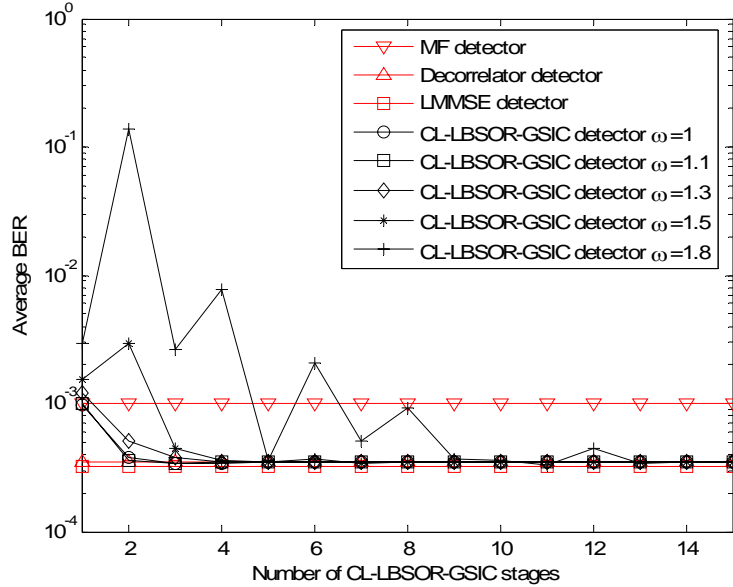


Figure 9.8: Convergence behavior of the proposed CL-LBSOR-GSIC detector for different relaxation factor values for the case of a synchronous CDMA AWGN channel.

In the following, we assess the average BER performance of the proposed CL-LSOR-SIC/CL-LBSOR-GSIC detectors versus the relaxation factor for the case of an asynchronous CDMA multipath fading channel. We use the following simulation parameters:  $W = 5$ ,  $K = 20$ ,  $N = 31$  (Gold codes), SNR = 4dB, vehicular A outdoor channel power delay profile for WCDMA is used and  $\max_{1 \leq k \leq K} (\tau^k) + \max_{1 \leq k \leq K} (\tau_{l_k}) \leq N$ . For the CL-LBSOR-GSIC detector, the users are divided into two equally sized groups, that is,  $U_1 = U_2 = 10$ .

As expected the region of convergence of both detectors is between 0 and 2. However, the unexpected, is that the minimum achievable average BER is attained for a relaxation factor between 0 and 1 (under-relaxation) where it was expected that the minimum achievable average BER should be attained for a relaxation factor between 1 and 2 (over-relaxation). It is difficult to justify this since there is no closed form expression for the optimum relaxation factor in our case. However, a careful inspection of equation (7-2) shows that the relaxation factor is dependent on the diagonal/block

diagonal  $\mathbf{D}$  of the cross-correlation matrix. And since the matrix  $\mathbf{D}$  is not the same for the case of CDMA AWGN and CDMA multipath fading channels, this may cause the discrepancy noted above. Nevertheless, more investigation and studies need to be carried out to justify the results above.

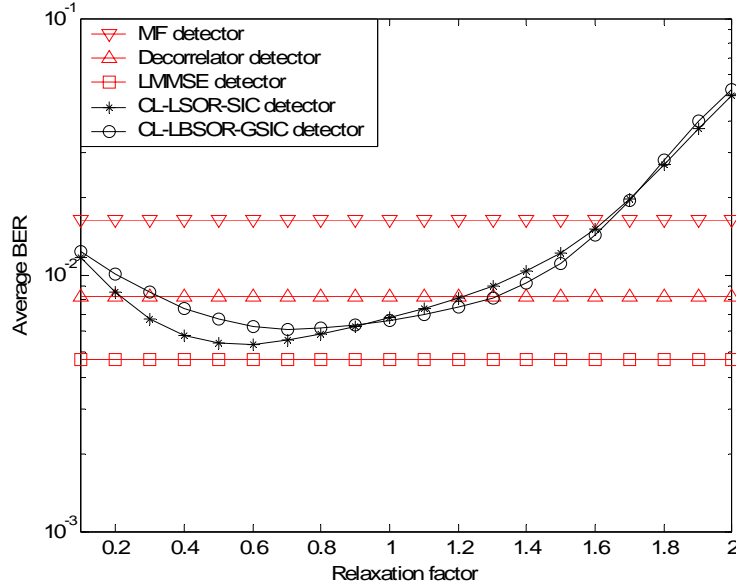


Figure 9.9: Average BER performance versus the relaxation factor of the proposed CL-LSOR-SIC/CL-LBSOR-GSIC detectors for the case of an asynchronous CDMA multipath fading channel.

In the following, we simulate the computational complexity of the four proposed chip-level schemes that are equivalent to the SOR/BSOR iterative methods. As depicted in Figure 9.10, two cases are considered; in case (a), the number of stages needed for the SL-LSOR-SIC/CL-LSOR-SIC/RC-CL-LSOR-SIC detectors to converge to the decorrelator detector is assumed to be  $P = (WK)/2$  whereas for case (b), the number of stages needed for the SL-LSOR-SIC/CL-LSOR-SIC/RC-CL-LSOR-SIC detectors to converge to the decorrelator detector is assumed to be  $P = (WK)/4$ .

It is easy to notice that the CL-LSOR-SIC detector exhibits less computational complexity than the SL-LSOR-SIC detector only for case (b), however, the RC-CL-LSOR-SIC detector exhibits less computational complexity for both cases (a) and (b). This represents a significant reduction in computational complexity.

As for the SL-LSOR-SIC/CL-LSOR-SIC/RC-CL-LSOR-SIC detectors, the computational complexity of the SL-LBSOR-GSIC/CL-LBSOR-GSIC/RC-CL-LBSOR-GSIC detectors is simulated and depicted in Figure 9.11. Again, two cases (a) and (b) are considered. The number of groups is fixed to four groups.

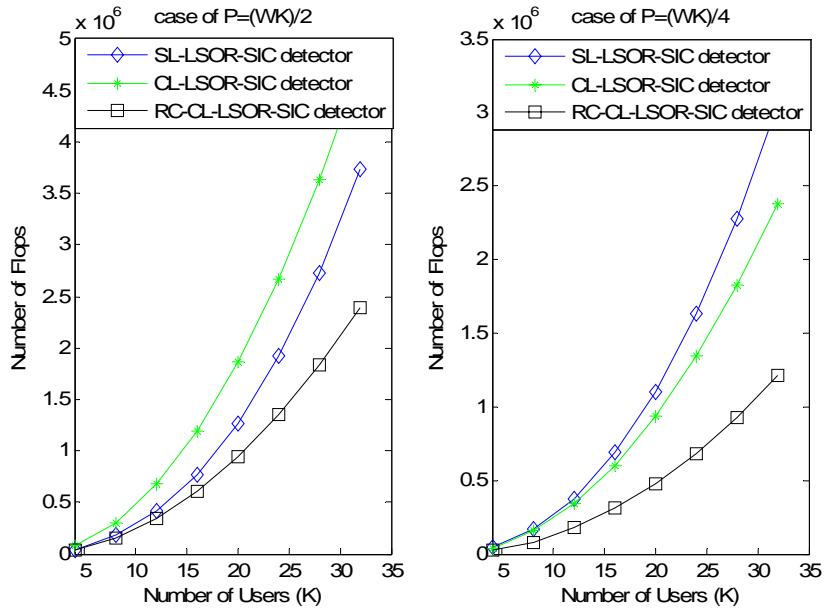


Figure 9.10: Computational complexity of the proposed CL-LSOR-SIC/RC-CL-LSOR-SIC structures versus that of the SL-LSOR-SIC structure.

Surprisingly, the proposed RC-CL-LBSOR-GSIC structure doesn't introduce any reduction in computational complexity compared to the CL-LBSOR-GSIC structure. However, both structures exhibit less computational complexity than the SL-LBSOR-GSIC scheme for both cases (a) and (b). Hence, both chip-level group-wise structures presented in this chapter have less computational complexity than their symbol-level counterparts.

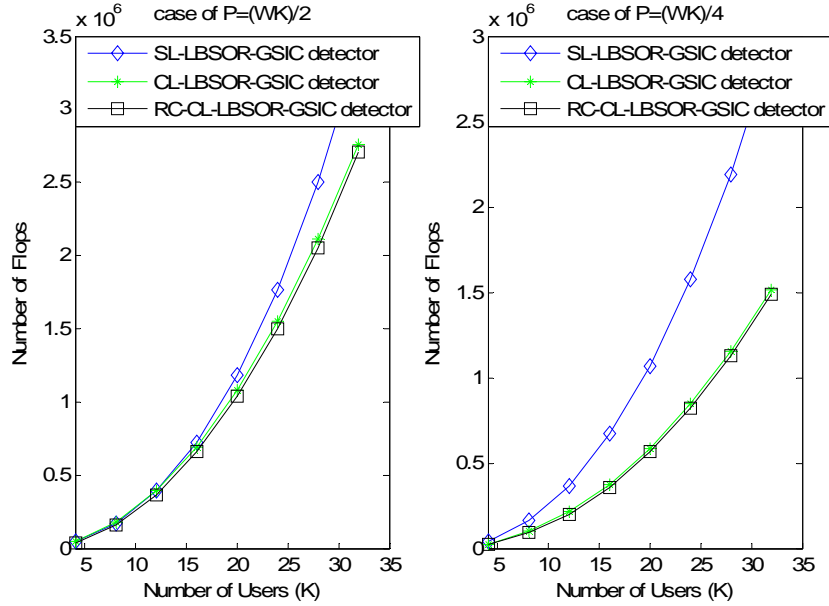


Figure 9.11: Computational complexity of the proposed CL-LBSOR-GSIC/RC-CL-LBSOR-GSIC structures versus that of the SL-LBSOR-GSIC structure.

## 9.8 Conclusion

In this chapter, we proposed four SIC/GSIC structures that are equivalent to the SOR/BSOR iterative methods, respectively. We studied the convergence behavior of the proposed schemes using two different approaches that lead to the same result. We determined the conditions of convergence and we proved that these structures converge if the relaxation factor is within the interval (0,2). Simulation results indicated that an important reduction in computational complexity can be gained by using the proposed chip-level structures compared to their symbol-level counterparts.

## **Chapter 10**

### **Analysis of the Reduced-Complexity Chip-level Linear GSIC Multi-user Detector Using a Matrix Iterative Approach**

#### **10.1 Chapter's Contents**

10.1 Chapter's Contents .....	210
10.2 Introduction .....	210
10.3 Convergence Behavior and Conditions of Convergence.....	211
10.4 Simulation Results.....	215
10.5 Conclusion.....	216

#### **10.2 Introduction**

In order to reduce the long detection delay time of the linear SIC, the linear group-wise successive interference cancellation (GSIC) detector was proposed [124]. The authors in [124] suggested a chip-level linear GSIC detection scheme and showed that if the proposed structure converges it converges to the decorrelator detector. Four group detection schemes were identified in [124], namely: the RC-CL-LGDEC-SIC detector, the RC-CL-LGMMSE-SIC detector, the RC-CL-LGPIC-SIC detector and finally the RC-CL-LGMF-SIC detector. It has been shown that only the RC-CL-LGDEC-SIC detector is always stable, while there is no guarantee of convergence for the other detectors. It was shown in [136] that the RC-CL-LGMF-SIC is in fact a hybrid SIC/PIC detector that can extract both advantages of the SIC and PIC detectors. In [124], it was illustrated through simulations that the RC-CL-LGMF-SIC detector is not always stable especially for small number of groups. For this reason and in order to overcome this drawback, a weighted RC-CL-LGMF-SIC (RC-CL-LGWMF-SIC) detector was proposed and a condition of convergence was derived. In [127], a more relaxed condition of convergence for the RC-CL-LGWMF-SIC detector was derived.

In this work, we show, by using a matrix iterative analysis approach, that the RC-CL-LGSIC scheme proposed in [124] is in fact equivalent to a modified block successive over-relaxation iterative method where the relaxation factor is a matrix instead of a scalar. Up to our knowledge, no proof for

the convergence of such scheme exists in the literature and thus we propose two new corollaries that extend the work of Kahan [80] to the case where the relaxation factor is a matrix instead of a scalar. By using the new corollaries we derive two new conditions of convergence for the RC-CL-LGSIC detector and we show as well that the conditions of convergence obtained in [124] and [127] can also be obtained by using our approach.

### 10.3 Convergence Behavior and Conditions of Convergence

It was shown in Section 7.10.2 that if the RC-CL-LGSIC detector converges, it converges to the decorrelator detector. In this section we propose a new approach that is based on matrix iterative analysis and allows us to identify the RC-CL-LGSIC scheme as a BSOR iterative method but with a relaxation matrix rather than a relaxation scalar. This facilitates the determination of the conditions of convergence.

Recall that the vector of decision variables of the  $g^{th}$  effective group of users at the  $p^{th}$  stage of the RC-CL-LGSIC detector is derived as:

$$\begin{aligned} \mathbf{y}(p, g_{eff}) &= \mathbf{F}(g_{eff}) \bar{\mathbf{S}}_{eff}(g_{eff})^T \mathbf{q} \\ &- \mathbf{F}(g_{eff}) \bar{\mathbf{S}}_{eff}(g_{eff})^T \left( \sum_{j=1}^{g_{eff}-1} \bar{\mathbf{S}}_{eff}(j) \mathbf{y}(p, j) + \sum_{j=g_{eff}}^{WG} \bar{\mathbf{S}}_{eff}(j) \mathbf{y}(p-1, j) \right) \\ &+ \mathbf{y}(p-1, g_{eff}) \quad \text{for } g_{eff} = 1, 2, \dots, WG \end{aligned} \quad (10-1)$$

In the ensuing analysis, we establish the analogy between the proposed scheme and the corresponding iterative method used to solve a set of linear equations which is known as the BSOR method. The cross-correlation matrix  $\bar{\mathbf{R}}_{eff}$  can be decomposed into three parts, that is:  $\bar{\mathbf{R}}_{eff} = \mathbf{D} - \mathbf{L} - \mathbf{L}^T$ , where  $\mathbf{D}$  is block diagonal matrix, that is  $\mathbf{D} = \text{diag}(\bar{\mathbf{R}}_{eff}(1,1), \bar{\mathbf{R}}_{eff}(2,2), \dots, \bar{\mathbf{R}}_{eff}(g_{eff}, g_{eff}), \dots, \bar{\mathbf{R}}_{eff}(WG, WG))$ ,  $\mathbf{L}$  and  $\mathbf{L}^H$  are the remaining lower-left and upper-right block triangular parts of  $\bar{\mathbf{R}}_{eff}$ , respectively. After some manipulations, equation (9-30) can be setup into the following matrix form:

$$\mathbf{y}(p) = [\mathbf{D} - \mathbf{DFL}]^{-1} \left[ \mathbf{DF} \bar{\mathbf{S}}_{eff}(g_{eff})^T \mathbf{q} + (\mathbf{D}(\mathbf{I} - \mathbf{DF}) + \mathbf{DFL}^T) \mathbf{y}(p-1) \right] \quad (10-2)$$

where

$$\mathbf{y}(p) = [\mathbf{y}(p,1) \quad \mathbf{y}(p,2) \quad \dots \quad \mathbf{y}(p, g_{eff}) \quad \dots \quad \mathbf{y}(p, WG)]^T \quad (10-3)$$

and:

$$\mathbf{F} = \text{diag} [\mathbf{F}(1), \mathbf{F}(2), \dots, \mathbf{F}(g_{eff}), \dots, \mathbf{F}(WG)] \quad (10-4)$$

On the other hand, the matrix form of the BSOR iteration is given by [80]:

$$\mathbf{y}(p) = [\mathbf{D} - \omega \mathbf{L}]^{-1} \left[ \omega \bar{\mathbf{S}}_{eff} (\mathbf{g}_{eff})^T \mathbf{q} + (\mathbf{D}(1 - \omega) + \omega \mathbf{L}^T) \mathbf{y}(p-1) \right] \quad (10-5)$$

where  $\omega$  is a relaxation parameter. By comparing (10-2) to (10-5), one can immediately deduce that (10-2) is exactly the same as (10-5) except that instead of the relaxation scalar,  $\omega$ , we have a relaxation matrix  $\mathbf{DF}$ .

All the theory we have at hand, regarding the conditions of convergence, deals with the conventional BSOR iterative method where the relaxation factor is a scalar. Up to our knowledge no theorem deals with the case we have in this work. Therefore, in order to determine the conditions of convergence of the linear GSIC detector, an extension of Kahan's theorem [80] to the case where the relaxation factor is a matrix is necessary.

**Corollary 10-1**

*Let  $\mathbf{R}$  be a  $K$ -by- $K$  hermitian matrix and  $\mathbf{R} = \mathbf{D} - \mathbf{L} - \mathbf{U}$ , where  $\mathbf{D}$  is block diagonal matrix, and  $\mathbf{L}$  and  $\mathbf{U}$  are the remaining lower-left and upper-right block triangular parts of  $\mathbf{R}$ . If  $\mathbf{D}$  is positive definite, then the block successive over-relaxation method with a relaxation matrix  $\mathbf{\Omega}$  is convergent for any initial solution  $\mathbf{y}(0)$  if and only if  $-1 < \det[\mathbf{I} - \mathbf{\Omega}] < 1$  and  $\mathbf{R}$  is positive definite.*

Proof:

The iteration matrix of the BSOR iterative method in case of a relaxation matrix is given by:

$$\mathbf{B} = [\mathbf{D} - \mathbf{\Omega} \mathbf{L}]^{-1} [\mathbf{D}(\mathbf{I} - \mathbf{\Omega}) + \mathbf{\Omega} \mathbf{L}^T] \quad (10-6)$$

where:

$$\mathbf{\Omega} = \text{diag} \left( \mathbf{F}(1) \bar{\mathbf{R}}_{eff} (1,1), \mathbf{F}(2) \bar{\mathbf{R}}_{eff} (2,2), \dots, \mathbf{F}(g_{eff}) \bar{\mathbf{R}}_{eff} (g_{eff}, g_{eff}), \dots, \mathbf{F}(WG) \bar{\mathbf{R}}_{eff} (WG, WG) \right) \quad (10-7)$$

Taking the determinant of both sides of (10-6), one obtains:

$$\begin{aligned}
 \det[\mathbf{B}] &= \det\left[(\mathbf{D} - \mathbf{\Omega L})^{-1} (\mathbf{D}(\mathbf{I} - \mathbf{\Omega}) + \mathbf{\Omega L}^T)\right] \\
 &= \frac{1}{\det[\mathbf{D} - \mathbf{\Omega L}]} \det[\mathbf{D}(\mathbf{I} - \mathbf{\Omega}) + \mathbf{\Omega L}^T] \\
 &= \frac{1}{\det[\mathbf{D}]} \det[\mathbf{D}(\mathbf{I} - \mathbf{\Omega})] \\
 &= \det[\mathbf{I} - \mathbf{\Omega}]
 \end{aligned} \tag{10-8}$$

Since we have  $\det[\mathbf{B}] = \prod_{k_{eff}=1}^{WK} \lambda_{k_{eff}}(\mathbf{B}) \leq [\lambda_{max}(\mathbf{B})]^{WK}$  where  $\lambda_{k_{eff}}(\mathbf{B})$ 's are the eigenvalues of  $\mathbf{B}$ . For convergence we should have  $|\lambda_{max}(\mathbf{B})| < 1$  and consequently  $|\lambda_{max}(\mathbf{B})|^{WK} < 1$ . Thus we get  $|\det[\mathbf{B}]| < 1$  and hence  $|\det[\mathbf{I} - \mathbf{\Omega}]| < 1$ . Finally, one gets:  $-1 < \det[\mathbf{I} - \mathbf{\Omega}] < 1$  which determines the condition of convergence for the BSOR iterative method with a relaxation matrix  $\mathbf{\Omega}$ .

#### Corollary 10-2

*A more restrictive condition for the BSOR iterative method with a relaxation matrix  $\mathbf{\Omega}$  to converge is that  $0 < \lambda_{max}(\mathbf{\Omega}) < 2$ .*

Proof:

The condition above can be obtained by noticing that  $\det[\mathbf{I} - \mathbf{\Omega}] = \prod_{k_{eff}=1}^{WK} \lambda_{k_{eff}}(\mathbf{I} - \mathbf{\Omega}) \leq [\lambda_{max}(\mathbf{I} - \mathbf{\Omega})]^{WK}$ .

Thus if we can ensure that:  $|\lambda_{max}(\mathbf{I} - \mathbf{\Omega})| < 1$  then  $|\det[\mathbf{I} - \mathbf{\Omega}]| < 1$ . Finally, this results in the condition of convergence  $0 < \lambda_{max}(\mathbf{\Omega}) < 2$ .

Two special cases can be distinguished:

- In case of the RC-CL-LGDEC-SIC detector we have  $\mathbf{F} = \mathbf{D}^{-1}$ , which results in  $\mathbf{\Omega} = \mathbf{I}$ . Therefore we get  $|\det[\mathbf{I} - \mathbf{\Omega}]| = |\det[\mathbf{I} - \mathbf{I}]| = |\det[\mathbf{0}]| = 0 < 1$  which is always true. Hence, the RC-CL-LGDEC-SIC (which is equivalent to the block Gauss-Seidel iterative method) detector is always convergent. This agrees with the condition reported in [124] that was obtained using a different approach than the one developed here.
- In case of the RC-CL-LGMF-SIC detector we have  $\mathbf{F} = \mathbf{I}$  which results in  $\mathbf{\Omega} = \mathbf{D}$  and thus from corollary 1 we get  $|\det[\mathbf{I} - \mathbf{\Omega}]| = |\det[\mathbf{I} - \mathbf{D}]| < 1$ . Since  $(\mathbf{I} - \mathbf{D})$  is block diagonal, then the above

condition can be expressed as:

$$-1 < \det[\mathbf{I} - \bar{\mathbf{R}}_{eff}(1,1)] \times \det[\mathbf{I} - \bar{\mathbf{R}}_{eff}(2,2)] \times \cdots \times \det[\mathbf{I} - \bar{\mathbf{R}}_{eff}(\mathbf{g}_{eff}, \mathbf{g}_{eff})] \times \cdots \times \det[\mathbf{I} - \bar{\mathbf{R}}_{eff}(WG, WG)] < 1$$

that  $\det[\mathbf{I} - \bar{\mathbf{R}}_{eff}(\mathbf{g}_{eff}, \mathbf{g}_{eff})] = \prod_{u_{g_{eff}}=1}^{U_{g_{eff}}} \lambda_{u_{g_{eff}}}[\mathbf{I} - \bar{\mathbf{R}}_{eff}(\mathbf{g}_{eff}, \mathbf{g}_{eff})] \leq [\lambda_{max}(\mathbf{I} - \bar{\mathbf{R}}_{eff}(\mathbf{g}_{eff}, \mathbf{g}_{eff}))]^{U_{g_{eff}}}$ ,

thus, if we can ensure that  $\left| \max_{1 \leq g_{eff} \leq WG} [\lambda_{max}(\mathbf{I} - \bar{\mathbf{R}}_{eff}(\mathbf{g}_{eff}, \mathbf{g}_{eff}))] \right| < 1$ , then  $|\det[\mathbf{I} - \mathbf{D}]| < 1$ .

Ultimately, for the RC-CL-LGMF-SIC detector to converge, the following condition of convergence  $0 < \max_{1 \leq g_{eff} \leq WG} [\lambda_{max}(\bar{\mathbf{R}}_{eff}(\mathbf{g}_{eff}, \mathbf{g}_{eff}))] < 2$  is required.

It can be seen from the condition obtained from the second corollary, that only the RC-CL-LGDEC-SIC detector is always convergent because  $\lambda_{max}(\mathbf{\Omega}) = 1$ . However for the other group detectors, the condition may be violated and as an example: the RC-CL-LGMF-SIC detector may diverge if

$$\max_{1 \leq g_{eff} \leq WG} (\lambda_{max}(\bar{\mathbf{R}}_{eff}(\mathbf{g}_{eff}, \mathbf{g}_{eff}))) > 2.$$

For this reason, and as suggested in [125] for the RC-CL-LGMF-SIC detector, we use a weighting factor  $\omega$  to stabilize the detectors that are not guaranteed to converge. Following the same procedure as we did before, it easy to show that one obtains the following condition of convergence:

$$0 < \omega < \frac{2}{\lambda_{max}(\mathbf{\Omega})}.$$

Again two special cases are worth exploring:

- In case of the RC-CL-LGDEC-SIC detector we have  $\mathbf{F} = \mathbf{D}^{-1}$ , which results in  $\mathbf{\Omega} = \mathbf{I}$ . Therefore we get  $0 < \omega < 2$  which is the same condition as for the conventional BSOR iterative method [80].
- In case of the RC-CL-LGMF-SIC detector we have  $\mathbf{F} = \mathbf{I}$ , which results in  $\mathbf{\Omega} = \mathbf{D}$  and thus we obtain the following condition of convergence  $0 < \omega < \frac{2}{\max_{1 \leq g_{eff} \leq WG} [\lambda_{max}(\bar{\mathbf{R}}_{eff}(\mathbf{g}_{eff}, \mathbf{g}_{eff}))]}$ . Note that

this is the same condition of convergence that the authors in [127] obtained by using a different approach than the one devised here.

Finally, Table 10.1 summarizes the conditions of convergence for different group detection schemes.

Table 10.1: Conditions of convergence for different group detection schemes.

RC-CL-LGSIC Detector	$\mathbf{F}(\mathbf{g}_{eff})$	1 <sup>st</sup> Condition of convergence	2 <sup>nd</sup> Condition of convergence
RC-CL-LGMF-SIC detector	$\mathbf{I}$	$ \det[\mathbf{I} - \mathbf{D}]  < 1$	$0 < \max_{1 \leq g_{eff} \leq WG} (\lambda_{max}(\bar{\mathbf{R}}_{eff}(\mathbf{g}_{eff}, \mathbf{g}_{eff}))) < 2$
RC-CL-LGDEC-SIC detector	$\bar{\mathbf{R}}_{eff}(\mathbf{g}_{eff}, \mathbf{g}_{eff})^{-1}$	Always Converging	Always Converging
RC-CL-LGWMF-SIC detector	$\omega \mathbf{I}$	$ \det[\mathbf{I} - \omega \mathbf{D}]  < 1$	$0 < \omega < \frac{2}{\max_{1 \leq g_{eff} \leq WG} (\lambda_{max}(\bar{\mathbf{R}}_{eff}(\mathbf{g}_{eff}, \mathbf{g}_{eff})))}$
RC-CL-LGWDEC-SIC detector	$\omega \bar{\mathbf{R}}_{eff}(\mathbf{g}_{eff}, \mathbf{g}_{eff})^{-1}$	$0 < \omega < 2$	$0 < \omega < 2$

## 10.4 Simulation Results

In the following, we simulate the convergence behavior of the RC-CL-LGSIC multiuser detector in an AWGN channel. For all simulations conducted here, Gold codes are used and thus the cross-correlation between users is equal. This removes any effect of certain grouping or order of cancellation. As in the case of the conventional BSOR iterative method where the relaxation factor is varied between 0 and 2, the determinant of the relaxation matrix is varied by changing the weighting factor  $\omega$  between 0 and 2 to illustrate its impact on the average BER (average of all users' BER) of the RC-CL-LGSIC detectors (RC-CL-LGMF-SIC and RC-CL-LGDEC-SIC) as shown in Figure 10.1. Here the SNR is set to 10 dB,  $M = 3$ ,  $K = 24$ ,  $N = 31$ ,  $G = 2$  (equal size groups) and perfect power control is assumed. As can be seen for Figure 10.1, the average BER is minimum for a determinant of the relaxation matrix between 1 and 2. Also, as it can be seen from this Figure 10.1, the RC-CL-LGMF-SIC and RC-CL-LGDEC-SIC detectors achieve the minimum average BER for a relaxation factor of 1.1 and 1.2, respectively. This agrees well with the conventional BSOR theory, which states that the optimal relaxation factor that results in maximum convergence speed of the BSOR iterative method is between 1 and 2 [80].

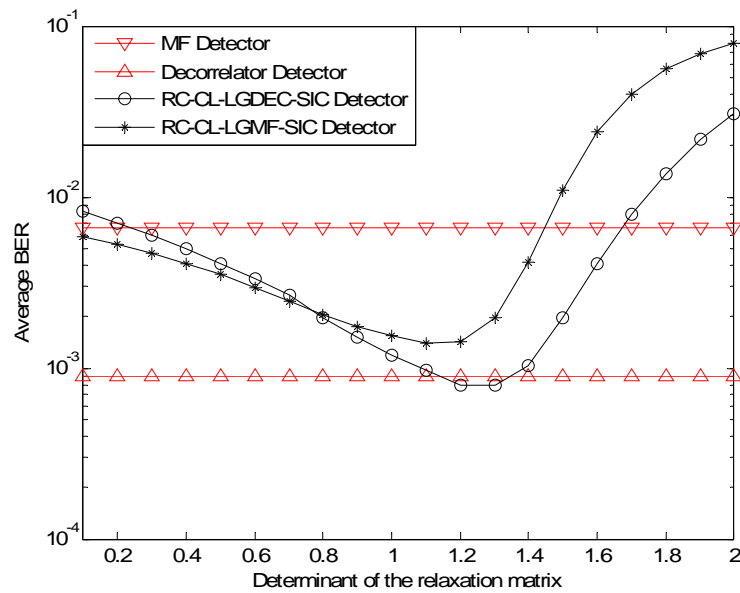


Figure 10.1: Convergence behavior of the RC-CL-LGSIC detector versus the determinant of the relaxation matrix.

### 10.5 Conclusion

In this chapter, we used a matrix iterative analysis approach to identify the RC-CL-LGSIC detector proposed in [124] as a linear BSOR iterative method but with a relaxation matrix instead of a relaxation factor. This approach allowed us to determine two new conditions of convergence. Finally, simulation results were in excellent agreement with our theoretical findings.

## Chapter 11

### Chip-level Linear GPIC Detectors

#### 11.1 Chapter's Contents

11.1 Chapter's Contents .....	217
11.2 Introduction .....	217
11.3 Structure of the Chip-Level Linear Group-Wise Parallel Interference Cancellation (CL-LGPIC) Detector .....	218
11.4 Algebraic Approach to the CL-LGPIC Detector.....	220
11.4.1 The CL-LGMF-PIC Detector.....	221
11.4.2 The CL-LGDEC-PIC Detector.....	222
11.4.3 The CL-LGMMSE-PIC Detector.....	222
11.4.4 The CL-LGPIC-PIC Detector .....	222
11.5 Convergence Behavior and Conditions of Convergence.....	222
11.6 The Chip-Level Linear Weighted Group-Wise PIC (CL-LWGPIC) Detector.....	223
11.7 The CL-LGPIC Detector for the Case of an Asynchronous CDMA Multi-Path Fading Channel .....	224
11.7.1 The CL-LGMF-PIC Detector.....	224
11.7.2 The CL-LGPIC-PIC Detector .....	225
11.8 Computational Complexity .....	225
11.9 Simulation Results.....	226
11.10 Conclusion.....	233

#### 11.2 Introduction

Chip-level linear group-wise successive interference cancellation schemes have been studied extensively in the literature ([124]-[127] and [137]-[139]). Surprisingly, their counterparts, the chip-level linear group-wise parallel interference cancellation schemes were not investigated till now, despite their apparent advantages such as parallelism. Hence if a parallel multiprocessor architecture is available, the algorithm execution time can be greatly reduced. In this chapter, a new chip-level linear

group-wise parallel interference cancellation (CL-LGPIC) detector is proposed. Four different group-detection schemes are derived, namely, the chip-level linear group matched filter PIC (CL-LGMF-PIC) detector, the chip-level linear group decorrelator PIC (CL-LGDEC-PIC) detector, the chip-level linear group minimum mean square error PIC (CL-LGMMSE-PIC) detector and the chip-level linear group parallel interference cancellation PIC (CL-LGPIC-PIC) detector. The convergence behavior of the proposed scheme is analyzed and conditions of convergence are derived. As for the CL-LPIC detector, the convergence of the proposed structure is ensured by the use of a weighting factor (relaxation factor). Finally, the computational complexity of the proposed detector is compared to that of its symbol-level counterpart. Simulation results conducted are in excellent agreement with the theory.

### 11.3 Structure of the Chip-Level Linear Group-Wise Parallel Interference Cancellation (CL-LGPIC) Detector

The CL-LGPIC detector consists of interference cancellation units arranged in a multistage structure as shown in Figure 11.1.

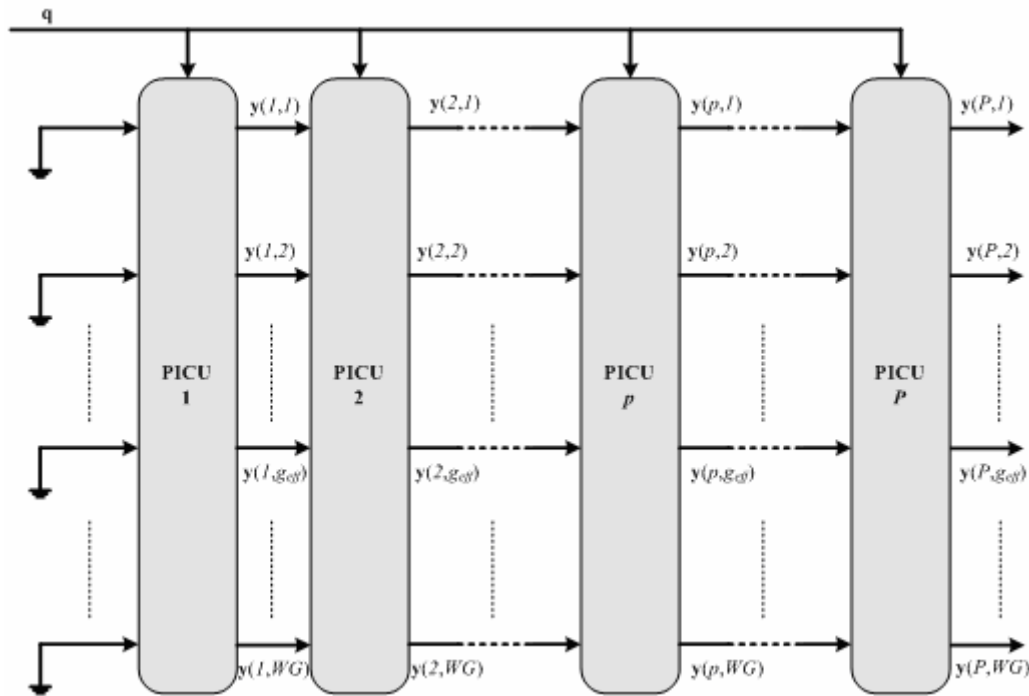


Figure 11.1: Multi-stage structure of the CL-LGPIC detector.

The internal structure of each interference cancellation unit is illustrated in Figure 11.2.

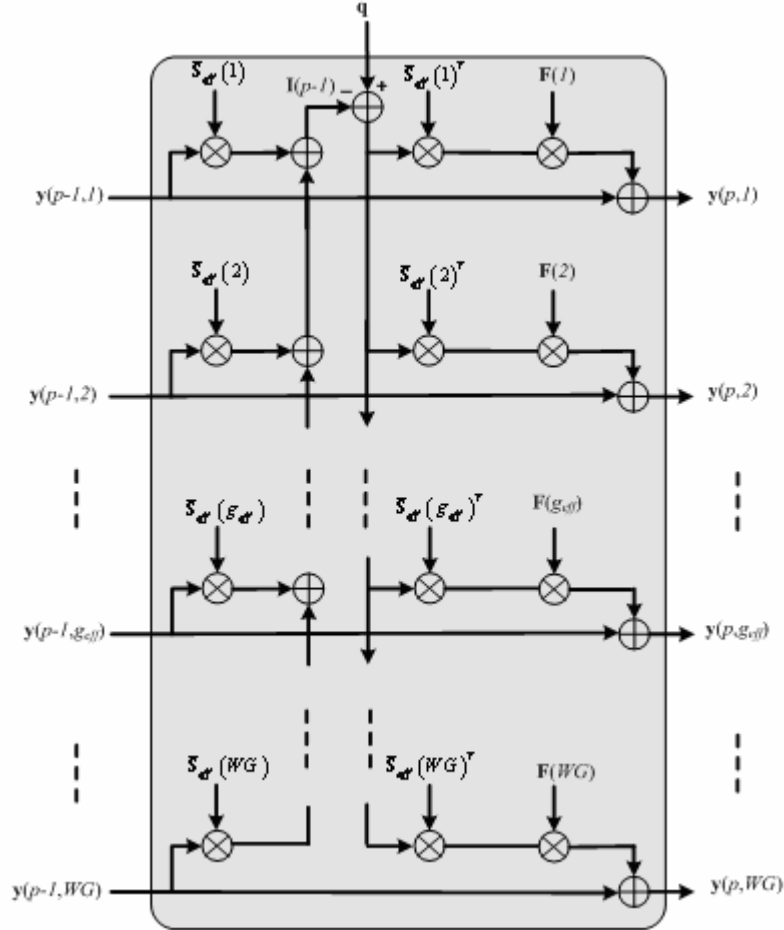


Figure 11.2: The  $p^{\text{th}}$  stage interference cancellation unit of the CL-LGPIC detector.

The vector of decision variables of the  $(p-1)^{\text{th}}$  stage,  $g^{\text{th}}$  group  $\mathbf{y}(p-1, g_{\text{eff}})$  is first despread added to the vectors of decision variables of the other groups to form the interference due to all users at the  $(p-1)^{\text{th}}$  stage, that is,  $\mathbf{I}(p-1) = \sum_{j=1}^{GW} \bar{\mathbf{S}}_{\text{eff}}(j) \mathbf{y}(p-1, j)$ . The latter is subtracted from the received signal  $\mathbf{q}$

to obtain a purified received signal  $[\mathbf{q} - \mathbf{I}(p)]$  where all users exhibit less mutual interference. The vector of decision variables of the  $p^{\text{th}}$  stage,  $g^{\text{th}}$  group  $\mathbf{y}(p, g_{\text{eff}})$  is obtained by despreading the purified signal, multiplying the result by a transformation matrix and finally adding the result to the vector of decision variables of the previous stage, that is:

$$\mathbf{y}(p, \mathbf{g}_{eff}) = \mathbf{F}(\mathbf{g}_{eff}) \bar{\mathbf{S}}_{eff}(\mathbf{g}_{eff})^T (\mathbf{q} - \mathbf{I}(p-1)) + \mathbf{y}(p-1, \mathbf{g}_{eff}) \quad (11-1)$$

This process is repeated in a multistage structure as shown in Figure 11.1

Note that the structure for the CDMA multipath fading channel is the same as the one shown here except  $\bar{\mathbf{S}}_{eff}(\mathbf{g}_{eff})$  should be replaced by  $\bar{\mathbf{S}}_{eff}^b(\mathbf{g}_{eff})$  and the transpose operator ( $^T$ ) should be replaced by the hermitian operator ( $^H$ ).

#### 11.4 Algebraic Approach to the CL-LGPIC Detector

In this section, we show using an algebraic approach that the CL-LGPIC detector is equivalent to matrix filtering of the received chip-matched signal. This enables the determination of analytical expressions for the BER and AME of the proposed detector.

The vector of decision variables at the  $p^{th}$  stage,  $\mathbf{g}^{th}$  group  $\mathbf{y}(p, \mathbf{g}_{eff})$  in equation (11-1) can be written in matrix form as:

$$\mathbf{y}(p) = \mathbf{F} \bar{\mathbf{S}}_{eff}^T (\mathbf{q} - \bar{\mathbf{S}}_{eff} \mathbf{y}(p-1)) + \mathbf{y}(p-1) \quad (11-2)$$

where  $\mathbf{F} = \text{diag} [\mathbf{F}(1), \mathbf{F}(2), \dots, \mathbf{F}(\mathbf{g}_{eff}), \dots, \mathbf{F}(WG)]$ . Hence (7-36) is equivalent to:

$$\begin{aligned} \mathbf{y}(p) &= \mathbf{F} \bar{\mathbf{S}}_{eff}^T \mathbf{q} - \mathbf{F} \bar{\mathbf{S}}_{eff}^T \bar{\mathbf{S}}_{eff} \mathbf{y}(p-1) + \mathbf{y}(p-1) \\ &= \mathbf{F} \bar{\mathbf{S}}_{eff}^T \mathbf{q} - (\mathbf{I} - \mathbf{F} \bar{\mathbf{S}}_{eff}^T \bar{\mathbf{S}}_{eff}) \mathbf{y}(p-1) \\ &= \mathbf{F} \bar{\mathbf{S}}_{eff}^T \mathbf{q} - (\mathbf{I} - \mathbf{F} \bar{\mathbf{S}}_{eff}^T \bar{\mathbf{S}}_{eff}) (\mathbf{F} \bar{\mathbf{S}}_{eff}^T \mathbf{q} - (\mathbf{I} - \mathbf{F} \bar{\mathbf{S}}_{eff}^T \bar{\mathbf{S}}_{eff}) \mathbf{y}(p-2)) \\ &= \mathbf{F} \bar{\mathbf{S}}_{eff}^T \mathbf{q} - (\mathbf{I} - \mathbf{F} \bar{\mathbf{S}}_{eff}^T \bar{\mathbf{S}}_{eff}) \mathbf{F} \bar{\mathbf{S}}_{eff}^T \mathbf{q} + (\mathbf{I} - \mathbf{F} \bar{\mathbf{S}}_{eff}^T \bar{\mathbf{S}}_{eff})^2 \mathbf{y}(p-2) \\ &= \mathbf{F} \bar{\mathbf{S}}_{eff}^T \mathbf{q} - (\mathbf{I} - \mathbf{F} \bar{\mathbf{S}}_{eff}^T \bar{\mathbf{S}}_{eff}) \mathbf{F} \bar{\mathbf{S}}_{eff}^T \mathbf{q} \\ &\quad + (\mathbf{I} - \mathbf{F} \bar{\mathbf{S}}_{eff}^T \bar{\mathbf{S}}_{eff})^2 (\mathbf{F} \bar{\mathbf{S}}_{eff}^T \mathbf{q} - (\mathbf{I} - \mathbf{F} \bar{\mathbf{S}}_{eff}^T \bar{\mathbf{S}}_{eff}) \mathbf{y}(p-3)) \\ &= \mathbf{F} \bar{\mathbf{S}}_{eff}^T \mathbf{q} - (\mathbf{I} - \mathbf{F} \bar{\mathbf{S}}_{eff}^T \bar{\mathbf{S}}_{eff}) \mathbf{F} \bar{\mathbf{S}}_{eff}^T \mathbf{q} \\ &\quad + (\mathbf{I} - \mathbf{F} \bar{\mathbf{S}}_{eff}^T \bar{\mathbf{S}}_{eff})^2 \mathbf{F} \bar{\mathbf{S}}_{eff}^T \mathbf{q} + (\mathbf{I} - \mathbf{F} \bar{\mathbf{S}}_{eff}^T \bar{\mathbf{S}}_{eff})^3 \mathbf{y}(p-3) \end{aligned} \quad (11-3)$$

Proceeding in the same way and taking in consideration that  $\mathbf{y}(p) = \mathbf{0}$ , we obtain:

$$\begin{aligned} \mathbf{y}(p) &= \sum_{i=1}^p (\mathbf{I} - \mathbf{F} \bar{\mathbf{S}}_{eff}^T \bar{\mathbf{S}}_{eff})^{i-1} \mathbf{F} \bar{\mathbf{S}}_{eff}^T \mathbf{q} \\ &= \mathbf{G}_p^T \mathbf{q} \end{aligned} \quad (11-4)$$

where  $\mathbf{G}_p = [\mathbf{G}_{p,1} \quad \mathbf{G}_{p,2} \quad \dots \quad \mathbf{G}_{p,\mathbf{g}_{eff}} \quad \dots \quad \mathbf{G}_{p,WG}]$ ,

and  $\mathbf{G}_{p, g_{eff}} = \begin{bmatrix} \mathbf{g}_{p, g_{eff}, 1} & \mathbf{g}_{p, g_{eff}, 2} & \cdots & \mathbf{g}_{p, g_{eff}, \mu_{g_{eff}}} & \cdots & \mathbf{g}_{p, g_{eff}, U_{g_{eff}}} \end{bmatrix}$ . The matrix  $\mathbf{G}_p$  can also be written as:

$\mathbf{G}_p = \begin{bmatrix} \mathbf{g}_{p, 1} & \mathbf{g}_{p, 2} & \cdots & \mathbf{g}_{p, k_{eff}} & \cdots & \mathbf{g}_{p, WK} \end{bmatrix}$ . Therefore, the CL-LGPIC can be described as a matrix filtering of the received chip-matched signal vector. Thus, if the spreading codes and grouping of all users are available, the decision variables of all users could be obtained without explicitly performing parallel interference cancellation.

Using the same method as for the matched filter detector, the BER of the  $k^{th}$  effective user at the  $p^{th}$  stage can be shown to be:

$$P_{p, k_{eff}}(\sigma) = \frac{1}{2^{WK-1}} \sum_{\substack{\text{all } \mathbf{b} \\ \mathbf{b}(k_{eff})=1}} Q \left( \frac{\mathbf{g}_{p, k_{eff}}^T \bar{\mathbf{S}}_{eff} \bar{\mathbf{A}}_{eff} \mathbf{b}}{\sigma \sqrt{\mathbf{g}_{p, k_{eff}}^T \mathbf{g}_{p, k_{eff}}}} \right) \quad (11-5)$$

where  $Q(\cdot)$  is the  $Q$ -function. Moreover, the asymptotic multiuser efficiency for the  $k^{th}$  effective user at the  $p^{th}$  stage can be shown to be given by:

$$\eta_{p, k_{eff}} = \frac{I}{\mathbf{g}_{p, k_{eff}}^T \mathbf{g}_{p, k_{eff}}} \max^2 \left( 0, \mathbf{g}_{p, k_{eff}}^T \bar{\mathbf{s}}_{eff}(k_{eff}) - \sum_{\substack{j=1 \\ j \neq k_{eff}}}^{WK} \frac{\bar{A}_{eff}(j, j)}{\bar{A}_{eff}(k_{eff}, k_{eff})} |\mathbf{g}_{p, k_{eff}}^T \bar{\mathbf{s}}_{eff}(j)| \right) \quad (11-6)$$

Before discussing the convergence behavior of the proposed scheme let us develop the relation between the latter and the Jacobi/block Jacobi iterative method. Equation (11-1) can be shown to be setup into:

$$\begin{aligned} \mathbf{y}(p, \mathbf{g}_{eff}) &= \mathbf{F}(\mathbf{g}_{eff}) \bar{\mathbf{S}}_{eff}(\mathbf{g}_{eff})^T \mathbf{q} + \left( \mathbf{I} - \mathbf{F}(\mathbf{g}_{eff}) \bar{\mathbf{S}}_{eff}(\mathbf{g}_{eff})^T \bar{\mathbf{S}}_{eff}(\mathbf{g}_{eff}) \right) \mathbf{y}(p-1, j) \\ &+ \mathbf{F}(\mathbf{g}_{eff}) \bar{\mathbf{S}}_{eff}(\mathbf{g}_{eff})^T \sum_{\substack{j=1 \\ j \neq g}}^{GW} \bar{\mathbf{S}}_{eff}(j) \mathbf{y}(p-1, j) \end{aligned} \quad (11-7)$$

It is easy to notice that depending on the transformation matrix (group detection scheme)  $\mathbf{F}$ , different group detection schemes can be obtained, namely: the CL-LGMF-PIC, CL-LGDEC-PIC, CL-LGPIC-PIC and finally CL-LGMMSE-PIC detectors.

#### 11.4.1 The CL-LGMF-PIC Detector

It is the simplest scheme, and it is obtained by letting:

$$\mathbf{F}(\mathbf{g}_{eff}) = \mathbf{I} \quad (11-8)$$

where  $\mathbf{I}$  is an  $(U_{g_{eff}} - by - U_{g_{eff}})$  identity matrix. It can be shown that this in fact is the conventional chip-level linear PIC detector.

### 11.4.2 The CL-LGDEC-PIC Detector

For this detector, the linear transformation is given by:

$$\mathbf{F}(\mathbf{g}_{eff}) = \left[ \bar{\mathbf{S}}_{eff}(\mathbf{g}_{eff})^T \bar{\mathbf{S}}_{eff}(\mathbf{g}_{eff}) \right]^{-1} \quad (11-9)$$

Note that if the group size is equal to one, we obtain the conventional chip-level linear PIC detector.

### 11.4.3 The CL-LGMMSE-PIC Detector

For this detector, the linear transformation is given by:

$$\mathbf{F}(\mathbf{g}_{eff}) = \left[ \bar{\mathbf{S}}_{eff}(\mathbf{g}_{eff})^T \bar{\mathbf{S}}_{eff}(\mathbf{g}_{eff}) + \sigma^2 \bar{\mathbf{A}}_{eff}(\mathbf{g}_{eff}, \mathbf{g}_{eff})^{-2} \right]^{-1} \quad (11-10)$$

### 11.4.4 The CL-LGPIC-PIC Detector

The linear transformation is given by:

$$\mathbf{F}(\mathbf{g}_{eff}) = \sum_{i=0}^{N_{PIC}} \left[ \mathbf{I} - \bar{\mathbf{S}}_{eff}(\mathbf{g}_{eff})^T \bar{\mathbf{S}}_{eff}(\mathbf{g}_{eff}) \right]^i \quad (11-11)$$

Where  $N_{PIC}$  denotes the number stages of the PIC detector. The matrix  $\bar{\mathbf{R}}_{eff}$  can be decomposed into three parts, that is:  $\bar{\mathbf{R}}_{eff} = \mathbf{D} - \mathbf{L} - \mathbf{L}^T$ , where  $\mathbf{D}$  is block diagonal matrix, that is  $\mathbf{D} = \text{diag} \left[ \bar{\mathbf{R}}_{eff}(1,1), \bar{\mathbf{R}}_{eff}(2,2), \dots, \bar{\mathbf{R}}_{eff}(\mathbf{g}_{eff}, \mathbf{g}_{eff}), \dots, \bar{\mathbf{R}}_{eff}(GW, GW) \right]$ , and  $\mathbf{L}$  and  $\mathbf{L}^T$  are the remaining lower-left and upper-right block triangular parts of  $\bar{\mathbf{R}}_{eff}$ , respectively. Recall from Chapter 5 that the block Jacobi iterative method is given by:

$$\mathbf{y}(p) = \mathbf{y}(p-1) + \mathbf{D}^{-1} \left[ \mathbf{y} - \bar{\mathbf{R}}_{eff} \mathbf{y}(p-1) \right] \quad (11-12)$$

By comparing (11-12) and (7-36), it easy to notice that if  $\mathbf{F}(\mathbf{g}_{eff}) = \left[ \bar{\mathbf{S}}_{eff}(\mathbf{g}_{eff})^T \bar{\mathbf{S}}_{eff}(\mathbf{g}_{eff}) \right]^{-1}$  (CL-LGDEC-PIC), then the CL-LGPIC detector is in fact a realization of the block Jacobi iterative method. On the other hand, if  $\mathbf{F}(\mathbf{g}_{eff}) = \mathbf{I}$  (CL-LGMF-PIC), then the CL-LGPIC detector is in fact a realization of the Jacobi iterative method.

## 11.5 Convergence Behavior and Conditions of Convergence

From (7-37), it easy to show that as the number of stages tends to infinity the vector of decision variables tends to that of the decorrelator detector, that is:

$$\begin{aligned}
 \lim_{p \rightarrow \infty} \mathbf{y}(p) &= \lim_{p \rightarrow \infty} \sum_{i=1}^p \left( \mathbf{I} - \mathbf{F} \overline{\mathbf{S}}_{eff}^T \overline{\mathbf{S}}_{eff} \right)^{i-1} \mathbf{F} \overline{\mathbf{S}}_{eff}^T \mathbf{q} \\
 &= \left( \mathbf{F} \overline{\mathbf{S}}_{eff}^T \overline{\mathbf{S}}_{eff} \right)^{-1} \mathbf{F} \overline{\mathbf{S}}_{eff}^T \mathbf{q} \\
 &= \left( \overline{\mathbf{S}}_{eff}^T \overline{\mathbf{S}}_{eff} \right)^{-1} \mathbf{F}^{-1} \mathbf{F} \overline{\mathbf{S}}_{eff}^T \mathbf{q}
 \end{aligned} \tag{11-13}$$

Hence if the matrix  $\mathbf{F}$  is nonsingular then, (7-41) is equivalent to:

$$\lim_{p \rightarrow \infty} \mathbf{y}(p) = \left( \overline{\mathbf{S}}_{eff}^T \overline{\mathbf{S}}_{eff} \right)^{-1} \overline{\mathbf{S}}_{eff}^T \mathbf{q} \tag{11-14}$$

This is in fact the decorrelator detector. Therefore, if the proposed CL-LGPIC detector converges, it converges to the decorrelator detector.

The parallel interference cancellation detector is well known to suffer from severe convergence issues ([129] and [134]). By observing the iteration matrix,  $\mathbf{B}$ , of the proposed detector:

$$\mathbf{B} = \left( \mathbf{I} - \mathbf{F} \overline{\mathbf{S}}_{eff}^T \overline{\mathbf{S}}_{eff} \right) \tag{11-15}$$

It is easy to show that determine the condition of convergence of the proposed scheme is given by:

$$0 < \lambda_{\max} \left( \mathbf{F} \overline{\mathbf{S}}_{eff}^T \overline{\mathbf{S}}_{eff} \right) < 2 \tag{11-16}$$

This is not always satisfied and hence the convergence problem of the CL-LGPIC scheme. To overcome this problem, a relaxation scheme is introduced to ensure convergence of this detector. This is the subject of the next section.

## 11.6 The Chip-Level Linear Weighted Group-Wise PIC (CL-LWGPIC) Detector

The interference cancellation unit of the CL-LWGPIC scheme is modified by inserting a weighting factor. The proposed weighted scheme is shown in Figure 11.3.

Following the same procedure as for the CL-LGPIC, it is easy to show that the vector of decision variables at the  $p^{th}$  stage is given by:

$$\mathbf{y}(p) = \omega \sum_{i=1}^p \left( \mathbf{I} - \omega \mathbf{F} \overline{\mathbf{S}}_{eff}^T \overline{\mathbf{S}}_{eff} \right)^{i-1} \mathbf{F} \overline{\mathbf{S}}_{eff}^T \mathbf{q} \tag{11-17}$$

However, it can be shown that if the proposed structure converges it converges to the decorrelator detector only if the following condition is satisfied:

$$0 < \omega < \frac{2}{\lambda_{\max} \left( \mathbf{F} \overline{\mathbf{S}}_{eff}^T \overline{\mathbf{S}}_{eff} \right)} \tag{11-18}$$

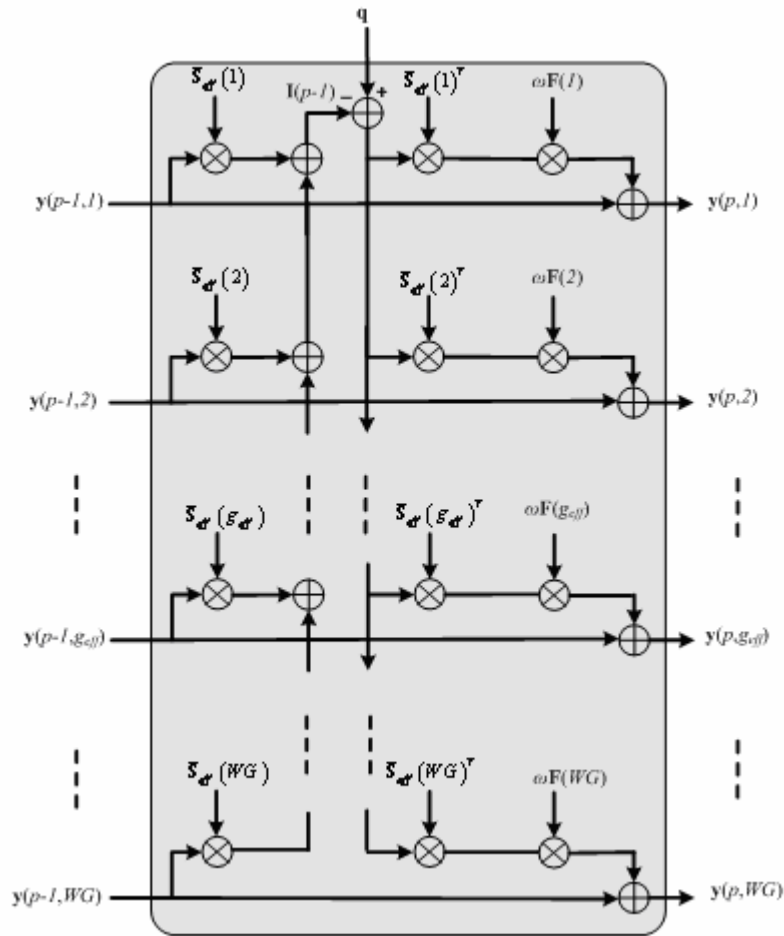


Figure 11.3: The  $p^{th}$  stage interference cancellation unit of the CL-LWGPIC detector.

### 11.7 The CL-LGPIC Detector for the Case of an Asynchronous CDMA Multi-Path Fading Channel

For the case of multipath fading, the diagonal of the cross-correlation matrix is not an identity matrix, hence the CL-LGMF-PIC and CL-LGPIC-PIC group-detection schemes detailed before are changed to the following expressions:

#### 11.7.1 The CL-LGMF-PIC Detector

It is the simplest scheme, and it is obtained by letting:

$$\mathbf{F}(\mathbf{g}_{eff}) = \text{diag} \left[ \bar{\mathbf{S}}_{eff}^b(\mathbf{g}_{eff})^H \bar{\mathbf{S}}_{eff}^b(\mathbf{g}_{eff}) \right]^{-1} \quad (11-19)$$

where  $\mathbf{I}$  is an  $(U_{g_{eff}} - by - U_{g_{eff}})$  identity matrix. It can be shown that this in fact is the conventional chip-level linear PIC detector.

### 11.7.2 The CL-LGPIC-PIC Detector

Thus the linear transformation is given by:

$$\mathbf{F}(\mathbf{g}_{eff}) = \sum_{i=0}^{N_{pic}} \left\{ \mathbf{I} - \text{diag} \left[ \bar{\mathbf{S}}_{eff}^b(\mathbf{g}_{eff})^H \bar{\mathbf{S}}_{eff}^b(\mathbf{g}_{eff}) \right]^{-1} \bar{\mathbf{S}}_{eff}^b(\mathbf{g}_{eff})^H \bar{\mathbf{S}}_{eff}^b(\mathbf{g}_{eff}) \right\}^i \quad (11-20)$$

Note that all the convergence analysis and conditions of convergence determined previously apply here as well.

### 11.8 Computational Complexity

The computational complexity of the proposed detector is given by the following expression:

$$\begin{aligned} PW & \left( 2 \sum_g^G U_g + (WN + \max_{1 \leq k \leq K}(\tau^k) + \max_{1 \leq l_k \leq K}(\tau_{l_k})) \sum_{g=1}^G (2U_g - 1) + \right. \\ & \left. \left( 2WN + 2 \max_{1 \leq k \leq K}(\tau^k) + 2 \max_{1 \leq l_k \leq K}(\tau_{l_k}) - 1 \right) \sum_{g=1}^G U_g \right) \\ & + P(WG - 1) \left( WN + \max_{1 \leq k \leq K}(\tau^k) + \max_{1 \leq l_k \leq K}(\tau_{l_k}) \right) + 2P \left( WN + \max_{1 \leq k \leq K}(\tau^k) + \max_{1 \leq l_k \leq K}(\tau_{l_k}) \right) \\ & + W \sum_{g=1}^G \left( 11U_g^3 + \frac{3}{2}U_g^2 + U_g \right) + 2W \left( WN + \max_{1 \leq k \leq K}(\tau^k) + \max_{1 \leq l_k \leq K}(\tau_{l_k}) \right) \sum_{g=1}^G (U_g)^2 \end{aligned} \quad (11-21)$$

It is compared to the computational complexity of the symbol-level linear weighted group-wise PIC (SL-LWGPIC) detector which is an extension of the SL-LWPIC detector proposed in [84] and its interference cancellation unit for the  $g^{th}$  group of users is shown in Figure 11.4.

Its computational complexity is given by:

$$\begin{aligned} & \left( 2WN + 2 \max_{1 \leq k \leq K}(\tau^k) + 2 \max_{1 \leq l_k \leq K}(\tau_{l_k}) - 1 \right) WK + 2 \left( WN + \max_{1 \leq k \leq K}(\tau^k) + \max_{1 \leq l_k \leq K}(\tau_{l_k}) \right) (WK)^2 \\ & + PW \left( W \sum_{g=1}^G U_g \sum_{j=1}^G (2U_j - 1) + \sum_{g=1}^G (U_g - 1)U_g + \sum_{g=1}^G (2U_g - 1)U_g + 2 \sum_{g=1}^G U_g \right) \\ & + W \left( \sum_{g=1}^G \left( 11U_g^3 + \frac{3}{2}U_g^2 + U_g \right) + 2 \sum_{g=1}^G U_g^2 \right) \end{aligned} \quad (11-22)$$

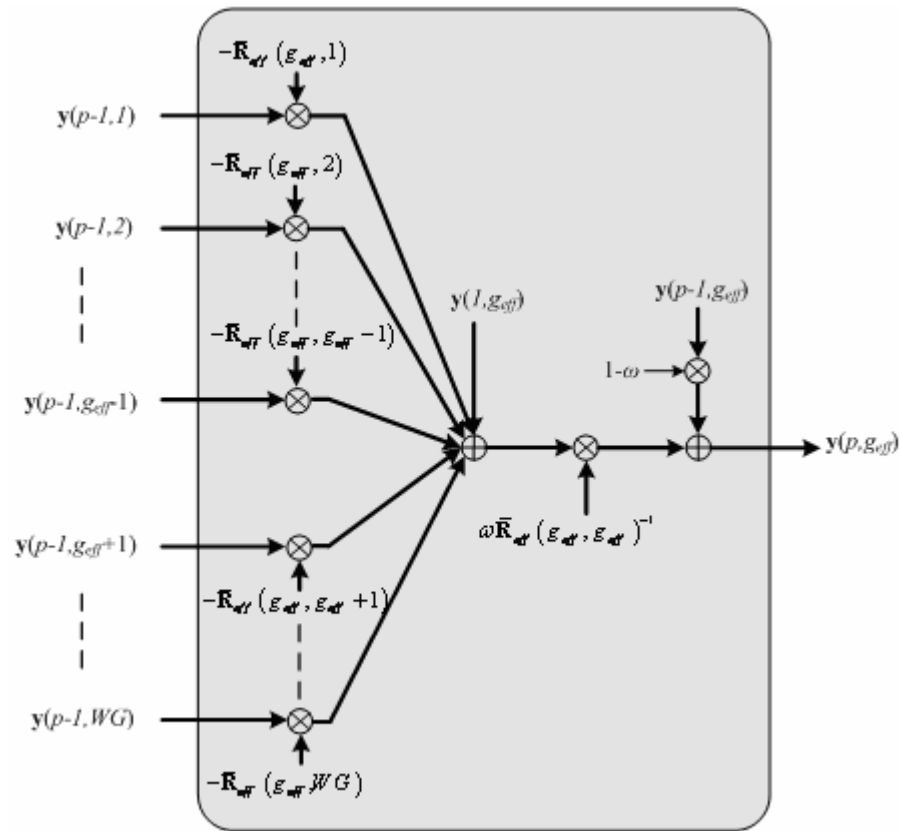


Figure 11.4: SL-LWGPIC unit of the  $g^{\text{th}}$  effective group of users.

### 11.9 Simulation Results

In this section, the above discussed multiuser detectors are simulated and the results obtained are commented. We simulate the convergence behavior of the chip-level interference cancellation detectors and compare their computational complexity to their symbol-level counterparts. Two different scenarios are considered, a synchronous CDMA AWGN channel and an asynchronous CDMA multipath Rayleigh fading channel. The simulation parameters are presented in Table 7.1.

In Figure 11.5, the average BER (average of all users) is plotted versus the number of chip-level linear group-wise PIC stages.

Table 11.1: Simulation parameters

Channel	Synchronous CDMA AWGN	Asynchronous CDMA multipath Rayleigh fading
Performance measure	Average BER versus number of stages	Average BER versus number of stages
$K$	20	10
$N$	31	31
SNR	4dB	4dB
$W$	1	5
Spreading codes	Gold	Gold
Power control	Perfect	Perfect
Power delay profile	Not applicable	Vehicular A outdoor Channel for WCDMA
Length of ISI+MAI	0	$\max_{1 \leq k \leq K}(\tau^k) + \max_{1 \leq k \leq K}(\tau_{l_k}) \leq N$

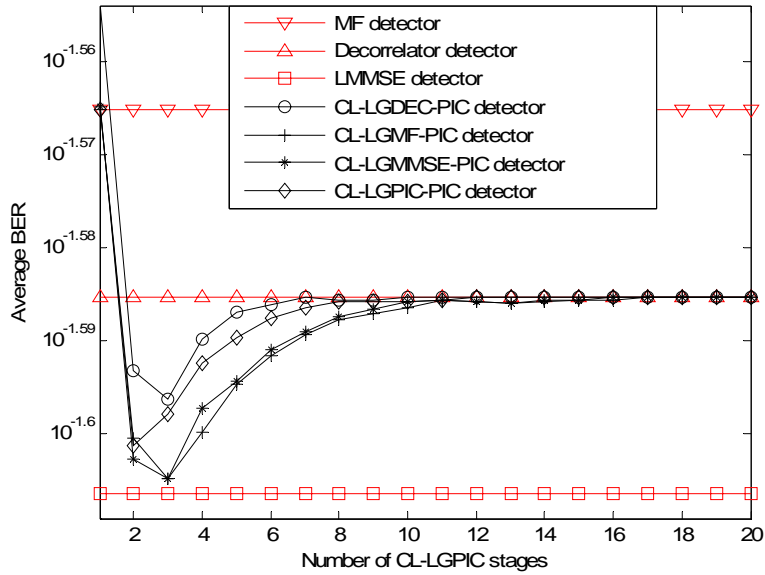


Figure 11.5: Convergence behavior of the CL-LGPIC detector.

Different detection schemes are considered. For the CL-LGDEC-PIC detector, a 2-stage PIC detector is used. It is easy to note that the CL-LGDEC-PIC converges faster than the other group-detection schemes, it needs only 7 stages whereas the CL-LGPIC-PIC detector, the CL-LGMMSE-PIC detector and the CL-LGMF-PIC detector needs 8 stages, 10 stages and 11 stages, respectively. However, the linear CL-LGMF-PIC and the CL-LGMMSE-PIC detectors achieve the lowest average BER level among all detection schemes. Moreover, it is important to notice that lower average BER levels are achieved prior to convergence, this is more noticeable for highly loaded systems and it has also been reported in other works such as [121].

The effect of grouping is analyzed and is depicted in Figure 11.6, 11.7, 11.8 and 11.9. It can be seen that while the convergence speed of the CL-LGDEC-PIC, the CL-LGMMSE-PIC and the CL-LGPIC-PIC detectors increases with decreasing number of groups, the convergence speed of the CL-LGMF-PIC detector is independent of grouping and is constant for any grouping. This is because the CL-LGMF-PIC detector is equivalent to the conventional linear PIC detector and hence the grouping in this case is  $G = K$ . However, the average BER difference between different groupings is small and is of theoretical importance only.

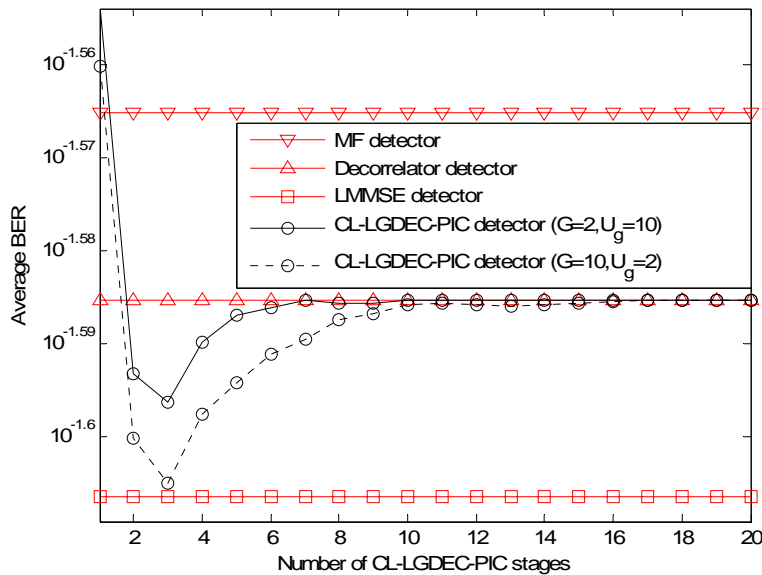


Figure 11.6: Convergence behavior of the CL-LGDEC-PIC detector for  $G = 2$  and  $G = 10$ .

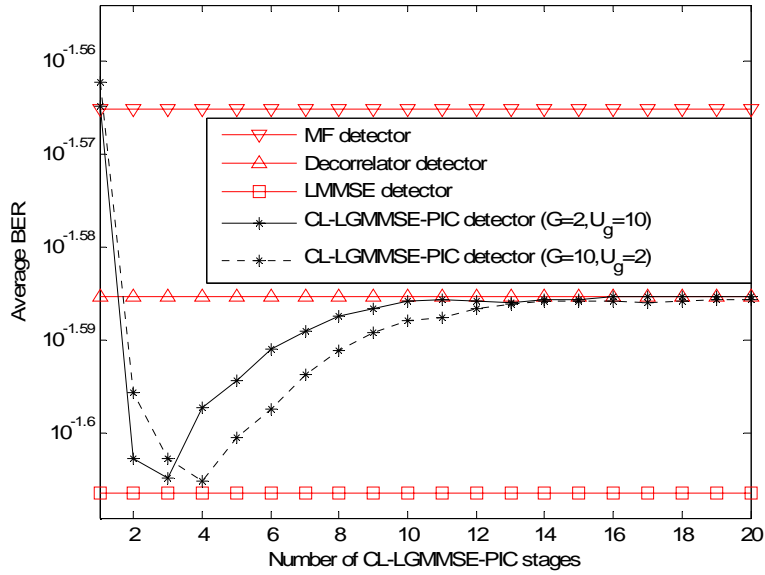


Figure 11.7: Convergence behavior of the CL-LGMMSE-PIC detector for  $G = 2$  and  $G = 10$ .

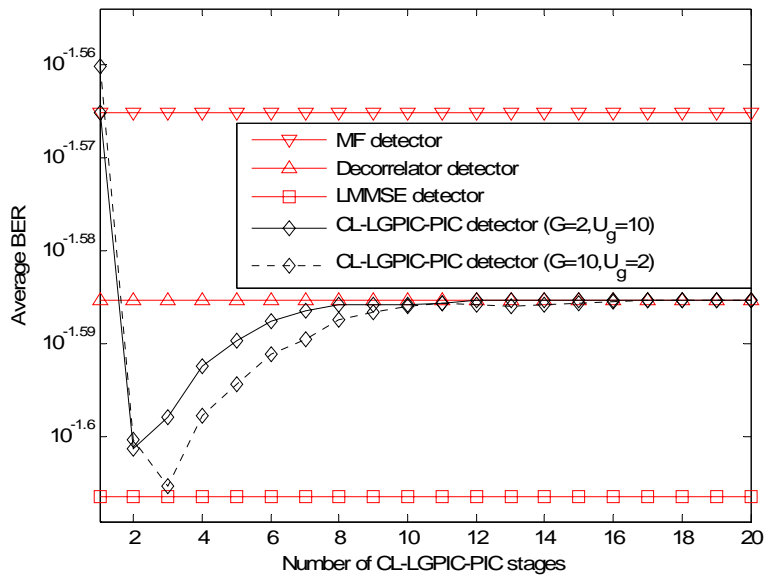


Figure 11.8: Convergence behavior of the CL-LGPIC-PIC detector for  $G = 2$  and  $G = 10$ .

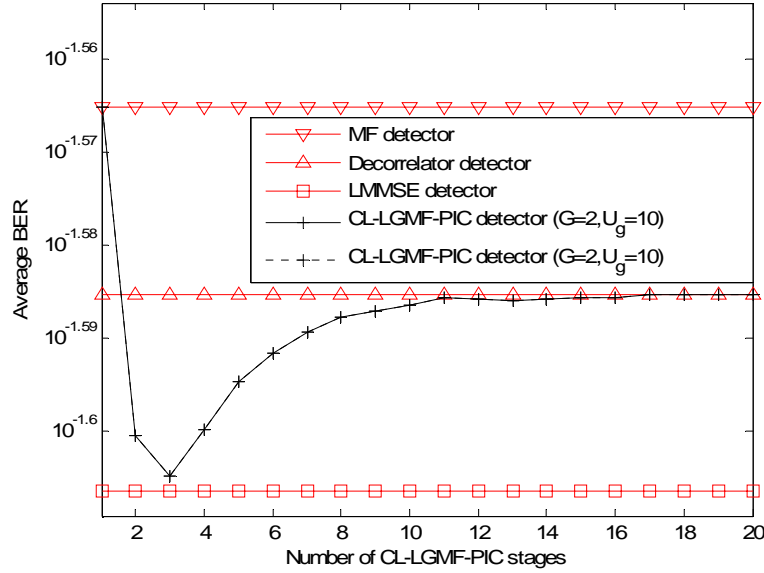


Figure 11.9: Convergence behavior of the CL-LGMF-PIC detector for  $G = 2$  and  $G = 10$ .

To study the instability of some detectors, a set of 10 highly correlated codes are used for spreading and despreading. Their cross-correlation matrix is given by:

$$\bar{\mathbf{R}}_{eff} = \begin{bmatrix} 1 & -0.6 & 0.2 & -0.4 & 0.6 & -0.2 \\ -0.6 & 1 & -0.2 & 0.4 & -0.6 & 0.2 \\ 0.2 & -0.2 & 1 & -0.8 & 0.6 & -0.6 \\ -0.4 & 0.4 & -0.8 & 1 & -0.8 & 0.8 \\ 0.6 & -0.6 & 0.6 & -0.8 & 1 & -0.6 \\ -0.2 & 0.2 & -0.6 & 0.8 & -0.6 & 1 \end{bmatrix}$$

The six users are divided into two equally sized groups of 3 users each. It is evident from Figure 11.10 that while the CL-LGDEC-PIC and the CL-LGMMSE-PIC detectors are converging to the decorrelator detector's performance, the CL-LGMF-PIC and the CL-LGPIC-PIC detectors are exhibiting an oscillatory/smooth divergence behaviors, respectively. Different modes of convergence and divergence are discussed in detail in [134].

It is clear also that even though the CL-LGMF-PIC detector, which is equivalent to the conventional linear PIC detector, diverges the CL-LGDEC-PIC and CL-LGMMSE-PIC detectors converge. This means that group-wise detection is an alternative to relaxation for stabilizing the conventional linear PIC detector.

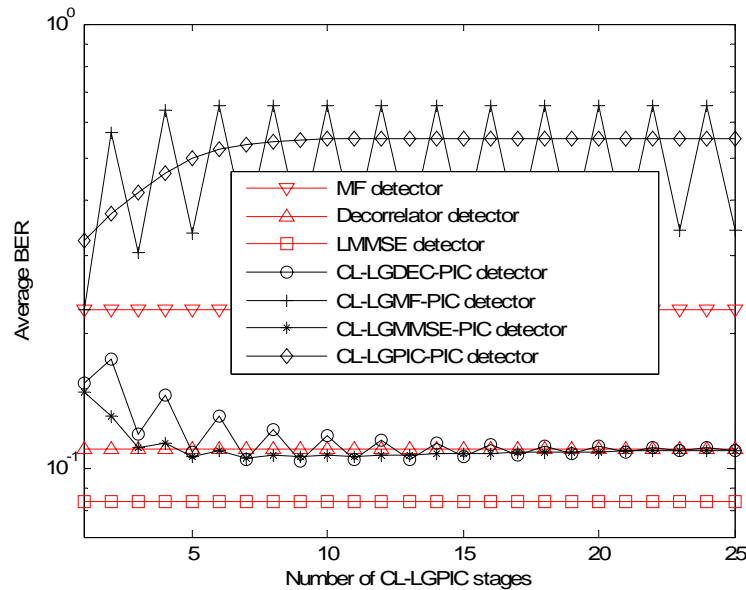


Figure 11.10: Divergence behavior of some chip-level linear interference cancellation detectors due to highly correlated codes.

Another interesting characteristic of the CL-LGPIC detector is its smoothing effect. The ping-pong effect of the divergent CL-LGMF-PIC detector is removed in the divergent CL-LGPIC-PIC detector. This suggests that group-wise detection is an alternative to relaxation for removing the ping-pong effect of the conventional CL-LPIC detector.

In Figure 11.11, the convergence behavior of different CL-LGPIC detection schemes is evaluated in an asynchronous CDMA multipath fading channel. The simulation parameters are depicted in Table 7.1. Here, 10 users are divided into two equally sized groups. In addition, a two-stage PIC detector is used for the CL-LGPIC-PIC detector.

The figure shows that the CL-LGMF-PIC detector which is equivalent to the CL-LPIC detector is divergent. This result is similar to that obtained for the simulation of the CL-LPIC detector in Chapter 7. The CL-LGPIC-PIC detector is also divergent as expected since the group-detection scheme used is the linear PIC detector which is already divergent as shown before. The CL-LGDEC-PIC detector and the CL-LGMMSE-PIC detector on the other hand are convergent and they need only few stages to converge to the decorrelator detector's performance.

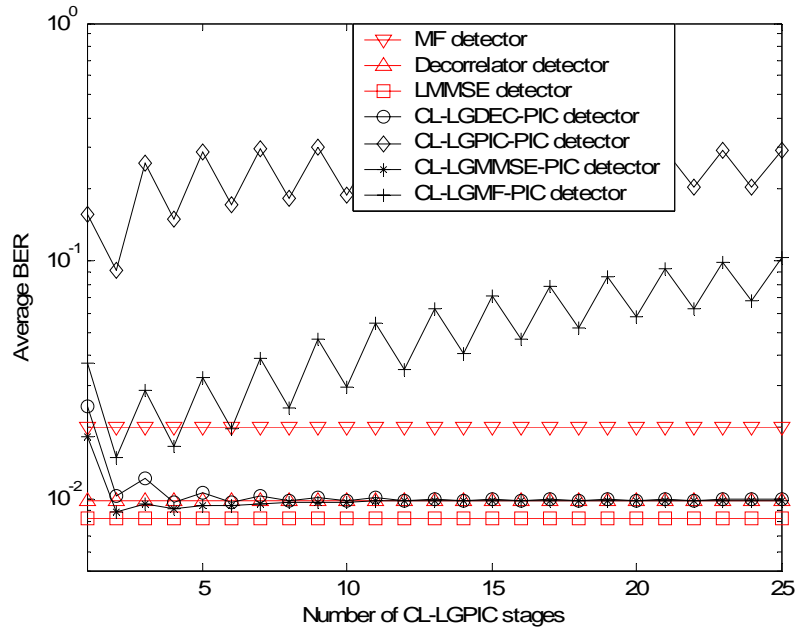


Figure 11.11: Convergence behavior of the CL-LGPIC detector.

As mentioned earlier, the group-wise detection is an alternative to relaxation for stabilizing the conventional linear PIC detector. Here, in Figure 11.11, the CL-LGPF-PIC detector, which is equivalent to the conventional linear PIC detector, diverges whereas the CL-LGDEC-PIC and CL-LGMMSE-PIC detectors converge. Hence, preconditioning (group-wise detection) is an alternative to relaxation (both under-relaxation and over-relaxation).

Finally, the computational complexity of the proposed CL-LPIC detector is compared to its symbol-level counterpart (SL-LPIC). Again, two cases are considered and are depicted in Figure 11.12. In case of Figure 11.12 (a), the number of stages needed for the SL-LPIC/CL-LPIC to converge to the decorrelator detector is assumed to be  $P = (WK)/2$ , whereas for case of Figure 11.12 (b), the number of stages needed for the SL-LPIC/CL-LPIC to converge to the decorrelator detector is assumed to be  $P = (WK)/4$ .

It is clear that the proposed CL-LGPIC structure exhibits less computational complexity than its symbol-level counterpart. Hence, for a long-code system, it is preferable to use this scheme.

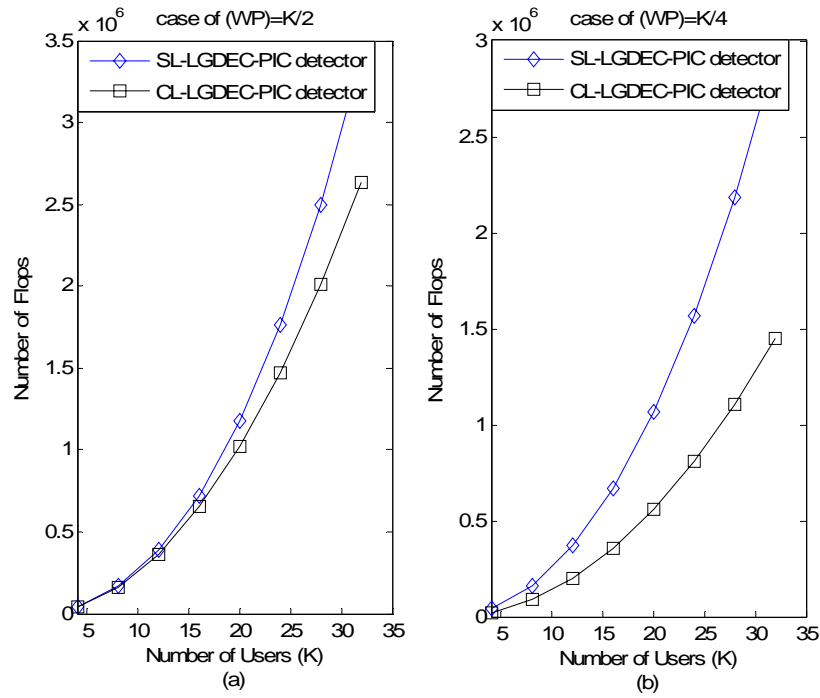


Figure 11.12: Computational complexity of the CL-LGDEC-PIC detector compared to that of the SL-LGDEC-PIC detector.

### 11.10 Conclusion

In this chapter, the principle of group-detection is extended from successive interference cancellation to parallel interference cancellation through the introduction of the CL-LGPIC detector. Different group-detection schemes were derived and their convergence behavior and conditions of convergence were detailed. A weighted version of the CL-LGPIC detector was also derived to ensure the convergence of the proposed structure. A very interesting result is obtained and it consists of using the preconditioning principle as an alternative to the relaxation principle. Finally, the proposed structure was simulated and the results obtained corroborate well with our theoretical findings.

## Chapter 12

### Conclusion and Future Work

#### 12.1 Chapter's Contents

12.1 Chapter's Contents .....	234
12.2 Conclusion.....	234
12.3 Future Work .....	235

#### 12.2 Conclusion

This dissertation has stepped forward into the direction of making use of mathematical tools in the field of engineering. By doing so, new achievements can be accomplished and new results can be obtained. This dissertation exploited the close relation between linear interference cancellation and linear iterative methods to develop new chip-level linear interference cancellation detectors that are suitable for long-code CDMA systems. By noting that symbol-level linear interference cancellation detectors are not suitable for actual long-code CDMA systems because they need to use the cross-correlation matrix, which is computationally expensive for long-code CDMA systems, many chip-level interference cancellation detectors were derived. Some of the chip-level linear structures developed here are:

- SIC/GSIC structures that can converge to either the decorrelator detector or the LMMSE detector.
- SIC/GSIC structures that are equivalent to the linear SOR/linear BSOR iterative methods.
- SIC/GSIC structures that are suitable for the case of asynchronous CDMA multipath fading channel and they are derived using the under-relaxation principle.
- GPIC/weighted GPIC structures were derived for the first time.

Moreover, the convergence behavior analysis and conditions of convergence for all the aforementioned structures are derived. Thanks again to the rich theory of linear iterative methods that made such analysis easy and efficient. In fact, establishing the connection between interference cancellation structures and linear iterative methods makes their convergence analysis straightforward and simple. This was particularly illustrated in Chapter 9 where the conditions of convergence are

determined using two different approaches that led to the same result. It was clear that the approach using the theory of iterative methods is more tractable and facilitated considerably the convergence analysis than the other one.

Furthermore, establishing the analogy between iterative methods and interference cancellation detectors allowed the identification of some of the structures as hybrid or modified linear iterative methods. Such a case was illustrated in Chapter 10 where the chip-level linear group-wise SIC structure was identified as a linear BSOR iterative method but with a relaxation matrix instead of a relaxation factor. With the help of the iterative methods theory conditions of convergence were derived.

Finally, during the phase of this dissertation some by-product contributions have been made such as the development of a new linear asynchronous CDMA multi-path fading channel model, which can be in fact used to develop new multiuser detectors.

### **12.3 Future Work**

Many new avenues and directions for research have been opened by this dissertation, just to name a few:

- Many new multiuser detection structures can be derived using the novel linear asynchronous CDMA multi-path fading channel model proposed in Chapter 4.
- Recently, the connection is also established between nonlinear interference cancellation detectors and nonlinear iterative methods used within the optimization field, by studying such connection, new structures can be developed.
- In Chapter 9, simulation results showed that chip-level linear SIC/GSIC structures attain their minimum achievable average BER within the region of under-relaxation (0,1) for the case of an asynchronous CDMA multi-path fading channel. This is unexpected and needs more investigation.

---

## Appendix A: Probability of error of a linear transformation of the received chip-matched signal/matched filter output

Recall from section 6.7.1 that the  $k^{\text{th}}$  effective user's output of a linear transformation applied to the received signal is given by:

$$y(k_{\text{eff}}) = \mathbf{V}(:, k_{\text{eff}})^T \mathbf{q} = \mathbf{v}_{k_{\text{eff}}}^T (\bar{\mathbf{S}}_{\text{eff}} \bar{\mathbf{A}}_{\text{eff}} \bar{\mathbf{b}} + \bar{\mathbf{n}}) \quad (\text{A-1})$$

where  $\bar{\mathbf{n}}$  is a vector of AWGN I.I.D samples of zero mean and variance  $\sigma^2$ . By using the total probability theorem, we can write:

$$\begin{aligned} P(b_{k_{\text{eff}}} \neq \hat{b}_{k_{\text{eff}}}) &= P(b_{k_{\text{eff}}} = 1, y(k_{\text{eff}}) < 0) + P(b_{k_{\text{eff}}} = -1, y(k_{\text{eff}}) > 0) \\ &= P(b_{k_{\text{eff}}} = 1)P(y(k_{\text{eff}}) < 0 | b_{k_{\text{eff}}} = 1) + P(b_{k_{\text{eff}}} = -1)P(y(k_{\text{eff}}) > 0 | b_{k_{\text{eff}}} = -1) \\ &= \frac{1}{2}P(y(k_{\text{eff}}) < 0 | b_{k_{\text{eff}}} = 1) + \frac{1}{2}P(y(k_{\text{eff}}) > 0 | b_{k_{\text{eff}}} = -1) \\ &= P(y(k_{\text{eff}}) < 0 | b_{k_{\text{eff}}} = 1) \end{aligned} \quad (\text{A-2})$$

thus:

$$\begin{aligned} P(b_{k_{\text{eff}}} \neq \hat{b}_{k_{\text{eff}}}) &= P(\mathbf{V}(:, k_{\text{eff}})^T (\bar{\mathbf{S}}_{\text{eff}} \bar{\mathbf{A}}_{\text{eff}} \bar{\mathbf{b}} + \bar{\mathbf{n}}) < 0 | b_{k_{\text{eff}}} = 1) \\ &= P(\mathbf{v}_{k_{\text{eff}}}^T \bar{\mathbf{n}} < -\mathbf{v}_{k_{\text{eff}}}^T \bar{\mathbf{S}}_{\text{eff}} \bar{\mathbf{A}}_{\text{eff}} \bar{\mathbf{b}} | b_{k_{\text{eff}}} = 1) \end{aligned} \quad (\text{A-3})$$

Due to the symmetry of the Gaussian (Normal) function we have:

$$\begin{aligned} P(\mathbf{V}(:, k_{\text{eff}})^T \bar{\mathbf{n}} < -\mathbf{V}(:, k_{\text{eff}})^T \bar{\mathbf{S}}_{\text{eff}} \bar{\mathbf{A}}_{\text{eff}} \bar{\mathbf{b}} | b_{k_{\text{eff}}} = 1) &= \\ P(\mathbf{V}(:, k_{\text{eff}})^T \bar{\mathbf{n}} > \mathbf{V}(:, k_{\text{eff}})^T \bar{\mathbf{S}}_{\text{eff}} \bar{\mathbf{A}}_{\text{eff}} \bar{\mathbf{b}} | b_{k_{\text{eff}}} = 1) & \end{aligned} \quad (\text{A-4})$$

hence:

$$\begin{aligned} P(b_{k_{\text{eff}}} \neq \hat{b}_{k_{\text{eff}}}) &= P(\mathbf{V}(:, k_{\text{eff}})^T \bar{\mathbf{n}} > \mathbf{V}(:, k_{\text{eff}})^T \bar{\mathbf{S}}_{\text{eff}} \bar{\mathbf{A}}_{\text{eff}} \bar{\mathbf{b}} | b_{k_{\text{eff}}} = 1) \\ &= Q\left(\frac{\mathbf{V}(:, k_{\text{eff}})^T \bar{\mathbf{S}}_{\text{eff}} \bar{\mathbf{A}}_{\text{eff}} \bar{\mathbf{b}} - E[\mathbf{V}(:, k_{\text{eff}})^T \bar{\mathbf{n}}]}{\sqrt{\text{var}[\mathbf{V}(:, k_{\text{eff}})^T \bar{\mathbf{n}}]}}\right) \end{aligned} \quad (\text{A-5})$$

we have:

$$E[\mathbf{V}(:, k_{\text{eff}})^T \bar{\mathbf{n}}] = 0 \quad (\text{A-6})$$

and:

$$\begin{aligned} \text{var} \left[ \mathbf{V}(:, k_{\text{eff}})^T \bar{\mathbf{n}} \right] &= E \left[ \mathbf{V}(:, k_{\text{eff}})^T \bar{\mathbf{n}} \left( \mathbf{V}(:, k_{\text{eff}})^T \bar{\mathbf{n}} \right)^T \right] \\ &= E \left[ \mathbf{V}(:, k_{\text{eff}})^T \bar{\mathbf{n}} \bar{\mathbf{n}}^T \mathbf{V}(:, k_{\text{eff}}) \right] \\ &= \sigma^2 \mathbf{V}(:, k_{\text{eff}})^T \mathbf{V}(:, k_{\text{eff}}) \end{aligned} \quad (\text{A-7})$$

thus:

$$P(b_{k_{\text{eff}}} \neq \hat{b}_{k_{\text{eff}}}) = Q \left( \frac{\mathbf{V}(:, k_{\text{eff}})^T \bar{\mathbf{S}}_{\text{eff}} \bar{\mathbf{A}}_{\text{eff}} \bar{\mathbf{b}} - E \left[ \mathbf{V}(:, k_{\text{eff}})^T \bar{\mathbf{n}} \right]}{\sqrt{\text{var} \left[ \mathbf{V}(:, k_{\text{eff}})^T \bar{\mathbf{n}} \right]}} \right) = Q \left( \frac{\mathbf{V}(:, k_{\text{eff}})^T \bar{\mathbf{S}}_{\text{eff}} \bar{\mathbf{A}}_{\text{eff}} \bar{\mathbf{b}}}{\sigma \sqrt{\mathbf{V}(:, k_{\text{eff}})^T \mathbf{V}(:, k_{\text{eff}})}} \right) \quad (\text{A-8})$$

Conditioning over all interfering bits, the probability of error of the  $k^{\text{th}}$  effective user can be written as:

$$\begin{aligned} P_{k_{\text{eff}}}(\sigma) &= \sum_{b_1 \in \{-1, 1\}} \dots \sum_{\substack{b_j \in \{-1, 1\} \\ j \neq k_{\text{eff}}}} \dots \sum_{b_{K^w} \in \{-1, 1\}} Q \left( \frac{\mathbf{V}(:, k_{\text{eff}})^T \bar{\mathbf{S}}_{\text{eff}} \bar{\mathbf{A}}_{\text{eff}} \mathbf{b}}{\sigma \sqrt{\mathbf{V}(:, k_{\text{eff}})^T \mathbf{V}(:, k_{\text{eff}})}} \right) \\ &= \frac{1}{2^{WK-1}} \sum_{\substack{\text{all } \mathbf{b} \\ b_{k_{\text{eff}}} = 1}} Q \left( \frac{\mathbf{V}(:, k_{\text{eff}})^T \bar{\mathbf{S}}_{\text{eff}} \bar{\mathbf{A}}_{\text{eff}} \mathbf{b}}{\sigma \sqrt{\mathbf{V}(:, k_{\text{eff}})^T \mathbf{V}(:, k_{\text{eff}})}} \right) \end{aligned} \quad (\text{A-9})$$

For a linear transformation applied to the matched filter output, the decision variable is given by (section 6.8.1):

$$\mathbf{y}(k_{\text{eff}}) = \mathbf{V}(:, k_{\text{eff}})^T \mathbf{y}_{MF} = \mathbf{V}(:, k_{\text{eff}})^T \left( \bar{\mathbf{R}}_{\text{eff}} \bar{\mathbf{A}}_{\text{eff}} \bar{\mathbf{b}} + \bar{\mathbf{S}}_{\text{eff}}^T \bar{\mathbf{n}} \right) \quad (\text{A-10})$$

Following the same procedure above and taking in consideration that:

$$E \left[ \mathbf{V}(:, k_{\text{eff}})^T \bar{\mathbf{S}}_{\text{eff}}^T \bar{\mathbf{n}} \right] = 0 \quad (\text{A-11})$$

and

$$\begin{aligned} \text{var} \left[ \mathbf{V}(:, k_{\text{eff}})^T \bar{\mathbf{S}}_{\text{eff}}^T \bar{\mathbf{n}} \right] &= E \left[ \mathbf{V}(:, k_{\text{eff}})^T \bar{\mathbf{S}}_{\text{eff}}^T \bar{\mathbf{n}} \left( \mathbf{V}(:, k_{\text{eff}})^T \bar{\mathbf{S}}_{\text{eff}}^T \bar{\mathbf{n}} \right)^T \right] \\ &= E \left[ \mathbf{V}(:, k_{\text{eff}})^T \bar{\mathbf{S}}_{\text{eff}}^T \bar{\mathbf{n}} \bar{\mathbf{n}}^T \bar{\mathbf{S}}_{\text{eff}} \mathbf{V}(:, k_{\text{eff}}) \right] \\ &= \sigma^2 \mathbf{V}(:, k_{\text{eff}})^T \bar{\mathbf{R}}_{\text{eff}} \mathbf{V}(:, k_{\text{eff}}) \end{aligned} \quad (\text{A-12})$$

It easy to show that the probability of error of the  $k^{\text{th}}$  effective user can be written as:

$$P_{k_{\text{eff}}}(\sigma) = \frac{1}{2^{WK-1}} \sum_{\substack{\text{all } \mathbf{b} \\ b_{k_{\text{eff}}} = 1}} Q \left( \frac{\mathbf{V}(:, k_{\text{eff}})^T \bar{\mathbf{R}}_{\text{eff}} \bar{\mathbf{A}}_{\text{eff}} \mathbf{b}}{\sigma \sqrt{\mathbf{V}(:, k_{\text{eff}})^T \bar{\mathbf{R}}_{\text{eff}} \mathbf{V}(:, k_{\text{eff}})}} \right) \quad (\text{A-13})$$

---

## Appendix B: Asymptotic multiuser efficiency of a linear transformation of the received chip-matched signal/matched filter output

Recall from Appendix A that for  $k^{\text{th}}$  effective user's output of a linear transformation applied to the received signal, the probability of error of the is given by:

$$\begin{aligned}
 P_{k_{\text{eff}}}(\sigma) &= \frac{1}{2^{WK-1}} \sum_{\substack{\text{all } \mathbf{b} \\ b_{k_{\text{eff}}}=1}} Q \left( \frac{\mathbf{V}(:, k_{\text{eff}})^T \bar{\mathbf{s}}_{\text{eff}} \bar{\mathbf{A}}_{\text{eff}} \mathbf{b}}{\sigma \sqrt{\mathbf{V}(:, k_{\text{eff}})^T \mathbf{V}(:, k_{\text{eff}})}} \right) \\
 &= \frac{1}{2^{WK-1}} \sum_{\substack{\text{all } \mathbf{b} \\ b_{k_{\text{eff}}}=1}} Q \left( \frac{\bar{\mathbf{A}}_{\text{eff}}(k_{\text{eff}}, k_{\text{eff}}) \mathbf{V}(:, k_{\text{eff}})^T \bar{\mathbf{s}}_{\text{eff}}(k_{\text{eff}}) + \sum_{\substack{j=1 \\ j \neq k_{\text{eff}}}}^{WK} \bar{\mathbf{A}}_{\text{eff}}(j, j) \mathbf{V}(:, k_{\text{eff}})^T \bar{\mathbf{s}}_{\text{eff}}(j) b_j}{\sigma \sqrt{\mathbf{V}(:, k_{\text{eff}})^T \mathbf{V}(:, k_{\text{eff}})}} \right) \quad (\text{B-1})
 \end{aligned}$$

As  $\sigma \rightarrow 0$ , equation (B-1) is dominated by the smallest argument [30], that is,:

$$\lim_{\sigma \rightarrow 0} P_{k_{\text{eff}}}(\sigma) = \frac{1}{2^{WK-1}} Q \left( \frac{\bar{\mathbf{A}}_{\text{eff}}(k_{\text{eff}}, k_{\text{eff}}) \mathbf{V}(:, k_{\text{eff}})^T \bar{\mathbf{s}}_{\text{eff}}(k_{\text{eff}}) - \sum_{\substack{j=1 \\ j \neq k_{\text{eff}}}}^{WK} \bar{\mathbf{A}}_{\text{eff}}(j, j) \left| \mathbf{V}(:, k_{\text{eff}})^T \bar{\mathbf{s}}_{\text{eff}}(j) \right|}{\sigma \sqrt{\mathbf{V}(:, k_{\text{eff}})^T \mathbf{V}(:, k_{\text{eff}})}} \right) \quad (\text{B-2})$$

The latter goes to zero as  $\sigma$  goes to zero if and only if the argument of  $Q$ -function is positive, that is,:

$$\bar{\mathbf{A}}_{\text{eff}}(k_{\text{eff}}, k_{\text{eff}}) \mathbf{V}(:, k_{\text{eff}})^T \bar{\mathbf{s}}_{\text{eff}}(k_{\text{eff}}) > \sum_{\substack{j=1 \\ j \neq k_{\text{eff}}}}^{WK} \bar{\mathbf{A}}_{\text{eff}}(j, j) \left| \mathbf{V}(:, k_{\text{eff}})^T \bar{\mathbf{s}}_{\text{eff}}(j) \right| \quad (\text{B-3})$$

which is known as the open eye condition, hence, for the determination of the AME, two cases exist:

- Closed eye condition  $(\bar{\mathbf{A}}_{\text{eff}}(k_{\text{eff}}, k_{\text{eff}}) \mathbf{V}(:, k_{\text{eff}})^T \bar{\mathbf{s}}_{\text{eff}}(k_{\text{eff}}) < \sum_{\substack{j=1 \\ j \neq k_{\text{eff}}}}^{WK} \bar{\mathbf{A}}_{\text{eff}}(j, j) \left| \mathbf{V}(:, k_{\text{eff}})^T \bar{\mathbf{s}}_{\text{eff}}(j) \right|)$ :

Recall from section 6.3.2, that the AME is defined as:

$$\eta_{k_{eff}} = \sup \left\{ 0 \leq r \leq 1 : \lim_{\sigma \rightarrow 0} \frac{P_{k_{eff}}(\sigma)}{Q\left(\frac{\sqrt{r}\bar{\mathbf{A}}_{eff}(k_{eff}, k_{eff})}{\sigma}\right)} < +\infty \right\} \quad (\text{B-4})$$

$$= \frac{2}{\bar{\mathbf{A}}_{eff}(k_{eff}, k_{eff})^2} \lim_{\sigma \rightarrow 0} \sigma^2 \log\left(\frac{1}{P_{k_{eff}}(\sigma)}\right)$$

Using the relation [30]:

$$2 \lim_{\sigma \rightarrow 0} \sigma^2 \log\left(\frac{1}{Q(z/\sigma)}\right) = ([z]^+)^2, \text{ where } [z]^+ = \max(0, z) \quad (\text{B-5})$$

we obtain:

$$\eta_{k_{eff}} = 0 \quad (\text{B-6})$$

- Open eye condition  $(\bar{\mathbf{A}}_{eff}(k_{eff}, k_{eff}) \mathbf{V}(:, k_{eff})^T \bar{\mathbf{s}}_{eff}(k_{eff}) > \sum_{\substack{j=1 \\ j \neq k_{eff}}}^{WK} \bar{\mathbf{A}}_{eff}(j, j) |\mathbf{V}(:, k_{eff})^T \bar{\mathbf{s}}_{eff}(j)|)$ :

From equation (B-4), we get:

$$\lim_{\sigma \rightarrow 0} \frac{P_{k_{eff}}(\sigma)}{Q\left(\frac{\sqrt{r}\bar{\mathbf{A}}_{eff}(k_{eff}, k_{eff})}{\sigma}\right)} = \frac{1}{2^{WK-1}} Q\left(\frac{\bar{\mathbf{A}}_{eff}(k_{eff}, k_{eff}) \mathbf{V}(:, k_{eff})^T \bar{\mathbf{s}}_{eff}(k_{eff}) - \sum_{\substack{j=1 \\ j \neq k_{eff}}}^{WK} \bar{\mathbf{A}}_{eff}(j, j) |\mathbf{V}(:, k_{eff})^T \bar{\mathbf{s}}_{eff}(j)|}{\sigma \sqrt{\mathbf{V}(:, k_{eff})^T \mathbf{V}(:, k_{eff})}}\right) \quad (\text{B-7})$$

$$\lim_{\sigma \rightarrow 0} \frac{1}{Q\left(\frac{\sqrt{r}\bar{\mathbf{A}}_{eff}(k_{eff}, k_{eff})}{\sigma}\right)}$$

By using [30]:

$$\lim_{x \rightarrow \infty} \frac{Q(\alpha x)}{Q(\beta x)} = \begin{cases} +\infty, & [\alpha]^+ < \beta \\ 0, & [\beta]^+ < \alpha \end{cases} \quad (\text{B-8})$$

$$\text{where } \alpha = \frac{\bar{\mathbf{A}}_{eff}(k_{eff}, k_{eff}) \mathbf{V}(:, k_{eff})^T \bar{\mathbf{s}}_{eff}(k_{eff}) - \sum_{\substack{j=1 \\ j \neq k_{eff}}}^{WK} \bar{\mathbf{A}}_{eff}(j, j) \left| \mathbf{V}(:, k_{eff})^T \bar{\mathbf{s}}_{eff}(j) \right|}{\sqrt{\mathbf{V}(:, k_{eff})^T \mathbf{V}(:, k_{eff})}}, \quad \beta = \sqrt{r} \bar{\mathbf{A}}_{eff}(k_{eff}, k_{eff})$$

and  $x = \frac{1}{\sigma}$ , we get:

$$\lim_{\sigma \rightarrow 0} \frac{P_{k_{eff}}(\sigma)}{Q\left(\frac{\sqrt{r} \bar{\mathbf{A}}_{eff}(k_{eff}, k_{eff})}{\sigma}\right)} = \begin{cases} 0, & \sqrt{r} \bar{\mathbf{A}}_{eff}(k_{eff}, k_{eff}) < \frac{\bar{\mathbf{A}}_{eff}(k_{eff}, k_{eff}) \mathbf{V}(:, k_{eff})^T \bar{\mathbf{s}}_{eff}(k_{eff}) - \sum_{\substack{j=1 \\ j \neq k_{eff}}}^{WK} \bar{\mathbf{A}}_{eff}(j, j) \left| \mathbf{V}(:, k_{eff})^T \bar{\mathbf{s}}_{eff}(j) \right|}{\sqrt{\mathbf{V}(:, k_{eff})^T \mathbf{V}(:, k_{eff})}} \\ +\infty, & \sqrt{r} \bar{\mathbf{A}}_{eff}(k_{eff}, k_{eff}) > \frac{\bar{\mathbf{A}}_{eff}(k_{eff}, k_{eff}) \mathbf{V}(:, k_{eff})^T \bar{\mathbf{s}}_{eff}(k_{eff}) - \sum_{\substack{j=1 \\ j \neq k_{eff}}}^{WK} \bar{\mathbf{A}}_{eff}(j, j) \left| \mathbf{V}(:, k_{eff})^T \bar{\mathbf{s}}_{eff}(j) \right|}{\sqrt{\mathbf{V}(:, k_{eff})^T \mathbf{V}(:, k_{eff})}} \end{cases} \quad (\text{B-9})$$

Hence, the largest value of  $r$  from the interval  $[0, 1]$  for which  $\lim_{\sigma \rightarrow 0} \frac{P_{k_{eff}}(\sigma)}{Q\left(\frac{\sqrt{r} \bar{\mathbf{A}}_{eff}(k_{eff}, k_{eff})}{\sigma}\right)} < +\infty$  is :

$$\sqrt{r} \bar{\mathbf{A}}_{eff}(k_{eff}, k_{eff}) = \frac{\bar{\mathbf{A}}_{eff}(k_{eff}, k_{eff}) \mathbf{V}(:, k_{eff})^T \bar{\mathbf{s}}_{eff}(k_{eff}) - \sum_{\substack{j=1 \\ j \neq k_{eff}}}^{WK} \bar{\mathbf{A}}_{eff}(j, j) \left| \mathbf{V}(:, k_{eff})^T \bar{\mathbf{s}}_{eff}(j) \right|}{\sqrt{\mathbf{V}(:, k_{eff})^T \mathbf{V}(:, k_{eff})}} \quad (\text{B-10})$$

Consequently:

$$r = \frac{1}{\mathbf{V}(:, k_{eff})^T \mathbf{V}(:, k_{eff})} \left( \mathbf{V}(:, k_{eff})^T \bar{\mathbf{s}}_{eff}(k_{eff}) - \sum_{\substack{j=1 \\ j \neq k_{eff}}}^{WK} \frac{\bar{\mathbf{A}}_{eff}(j, j)}{\bar{\mathbf{A}}_{eff}(k_{eff}, k_{eff})} \left| \mathbf{V}(:, k_{eff})^T \bar{\mathbf{s}}_{eff}(j) \right| \right)^2 \quad (\text{B-11})$$

Combining both cases of closed and open eye conditions, we obtain the following expression of the AME:

$$\eta_{k_{eff}} = \frac{1}{\mathbf{V}(:, k_{eff})^T \mathbf{V}(:, k_{eff})} \max^2 \left( 0, \mathbf{V}(:, k_{eff})^T \bar{\mathbf{s}}_{eff}(k_{eff}) - \sum_{\substack{j=1 \\ j \neq k_{eff}}}^{WK} \frac{\bar{\mathbf{A}}_{eff}(j, j)}{\bar{\mathbf{A}}_{eff}(k_{eff}, k_{eff})} \left| \mathbf{V}(:, k_{eff})^T \bar{\mathbf{s}}_{eff}(j) \right| \right) \quad (\text{B-12})$$

For the case of a linear transformation applied to the matched filter outputs, we have from Appendix A:

$$P_{k_{eff}}(\sigma) = \frac{1}{2^{WK-1}} \sum_{\substack{\text{all } \mathbf{b} \\ b_{k_{eff}}=1}} \mathcal{Q} \left( \frac{\mathbf{V}(:, k_{eff})^T \bar{\mathbf{R}}_{eff} \bar{\mathbf{A}}_{eff} \mathbf{b}}{\sigma \sqrt{\mathbf{V}(:, k_{eff})^T \bar{\mathbf{R}}_{eff} \mathbf{V}(:, k_{eff})}} \right) \quad (\text{B-13})$$

Following the same procedure above and taking in consideration that:

$$E \left[ \mathbf{V}(:, k_{eff})^T \bar{\mathbf{S}}_{eff}^T \bar{\mathbf{n}} \right] = 0 \quad (\text{B-14})$$

and

$$\begin{aligned} \text{var} \left[ \mathbf{V}(:, k_{eff})^T \bar{\mathbf{S}}_{eff}^T \bar{\mathbf{n}} \right] &= E \left[ \mathbf{V}(:, k_{eff})^T \bar{\mathbf{S}}_{eff}^T \bar{\mathbf{n}} \left( \mathbf{V}(:, k_{eff})^T \bar{\mathbf{S}}_{eff}^T \bar{\mathbf{n}} \right)^T \right] \\ &= E \left[ \mathbf{v}_{k_{eff}}^T \mathbf{V}(:, k_{eff})^T \bar{\mathbf{S}}_{eff}^T \bar{\mathbf{n}} \bar{\mathbf{n}}^T \bar{\mathbf{S}}_{eff} \mathbf{V}(:, k_{eff}) \right] \\ &= \sigma^2 \mathbf{V}(:, k_{eff})^T \bar{\mathbf{R}}_{eff} \mathbf{V}(:, k_{eff}) \end{aligned} \quad (\text{B-15})$$

It easy to show that the AME of the  $k^{th}$  effective user can be written as:

$$\eta_{k_{eff}} = \frac{1}{\mathbf{V}(:, k_{eff})^T \bar{\mathbf{R}}_{eff} \mathbf{V}(:, k_{eff})} \max^2 \left( \begin{array}{l} 0, \mathbf{V}(:, k_{eff})^T \bar{\mathbf{R}}_{eff}(:, k_{eff}) \\ - \sum_{\substack{j=1 \\ j \neq k_{eff}}}^{WK} \frac{\bar{\mathbf{A}}_{eff}(j, j)}{\bar{\mathbf{A}}_{eff}(k_{eff}, k_{eff})} \left| \mathbf{V}(:, k_{eff})^T \bar{\mathbf{R}}_{eff}(:, j) \right| \end{array} \right) \quad (\text{B-16})$$

where  $\bar{\mathbf{R}}_{eff}(:, j)$  is the  $j^{th}$  column of the cross-correlation matrix  $\bar{\mathbf{R}}_{eff}$ .

---

## References

- [1] G. C. Di Piazza, A. Plitkins and G. I. Zysman, “The Cellular Concept,” Bell Systems Technical Journal, vol. 58, N<sup>o</sup>. 1, pp: 215–248, January 1979.
- [2] R. Nelson and D. Westin, “The Evolution of the North American Cellular Network” Telecommunications (International Edition), vol. 26, N<sup>o</sup>. 9, pp: 24–28, September 1992.
- [3] V. H. MacDonald, “The Cellular Concept” Bell Systems Technical Journal, vol. 58, N<sup>o</sup>. 1, pp: 15–42, January 1979.
- [4] F. H. Blecher, “Advanced Mobile Phone Service”, IEEE Transactions on Vehicular Technology, vol. VT-29, N<sup>o</sup>. 2, pp. 238–244, May 1980.
- [5] E. S. K. Chien, “A T&T Cellular System-System Description and System Trial Results”, Proceedings of the ICC, vol. 3, pp: 1207–1213, May 1984.
- [6] D. C. Cox, “A Radio System Proposal for Widespread Low Power Tetherless Communications”, IEEE Transactions on Communications, vol. 39, N<sup>o</sup>. 2, pp: 324–335, February 1991.
- [7] D. L. Huff, “A T&T Cellular Technology Review”, Proceedings of MILCOM 1985, vol. 2, pp: 490–494, October 1985.
- [8] J. E. Padgett, C. G. Günther and T. Hattori, “Overview of Wireless Personal Communications”, IEEE Communications Magazine, pp: 28–41, January 1995.
- [9] JA Knottnerus “GSM base stations”, The Hague: Health Council of the Netherlands, 2000; publication N<sup>o</sup>. 2000/16E, ISBN: 90-5549-331-7.
- [10] L. R. Maciel and H. L. Bertoni, “Cell Shape for Microcellular Systems in Residential and Commercial Environments”, IEEE Transactions on Vehicular Technology, vol. 43, No. 2, pp. 270–278, May 1994.
- [11] T. S. Rappaport, *Wireless Communications: Principles and Practice*, Prentice-Hall, NJ, 1996, ISBN: 0133755363.
- [12] W. C. Y. Lee, “Smaller Cells for Greater Performance”, IEEE Communications Magazine, vol. 29, N<sup>o</sup>. 11, pp. 19–23, November 1991.

- 
- [13] W. C. Y. Lee, "Cellular Telephone System," U.S. Patent 4, 932,049, June 1990, Patent Assigned on June 05, 1990.
- [14] J. Korhonen, *Introduction to 3G Mobile Communications*, Second Edition 2003, Artech House mobile communications series, ISBN 1-58053-507-0.
- [15] W. O. Malcom, "The Mobile Phone Meets the Internet", IEEE Spectrum, pp. 20- 28, August 1999.
- [16] Shannon, "A Mathematical Theory of Communication," Bell System Technical Journal, vol. 27, pp. 379-423 and 623-656. 1948.
- [17] Scholtz, "The Evolution of Spread-Spectrum Multiple-Access Communications," in Code Division Multiple Access Communications (S. G. Glisic and P. A. Leppanen, Eds., Kluwer Academic Publishers, 1995.
- [18] "A conversation with Claude Shannon," IEEE Commun. Mag., Vol. 22, N<sup>o</sup>. 5, pp.123-126, May 1984,
- [19] Cooper and R. W. Nettleton, "A spread-spectrum techniques for high capacity mobile communications", IEEE Transactions on Vehicular Technology, vol. 27, N<sup>o</sup>. 4, pp. 264-275. Nov. 1978.
- [20] S. Verdu, "Minimum Probability of Error for Asynchronous Gaussian Multiple Access," IEEE Transactions on Information Technology, vol. IT-32, N<sup>o</sup>. 1, pp. 85-96, Jan. 1986.
- [21] Ojanpera, "Overview of Research Activities for Third Generation Mobile Communication," in Wireless Communications TDMA vs. CDMA (S.G. Glisic and P.A. Leppanen, Eds.), Kluwer Academic Publishers, pp. 415-446, 1997.
- [22] IEEE Communications Surveys, vol. 1 N<sup>o</sup>. 1, pp: 1-29. Fourth Quarter 1998.
- [23] R. Prasad and T. Ojanperä, "An Overview of CDMA Evolution Toward Wideband CDMA", IEEE Communications Surveys, vol. 1, N<sup>o</sup>. 1, pp: 1-29. Fourth Quarter 1998.
- [24] W.C.Y. Lee, "Overview of cellular CDMA," IEEE Transactions on Vehicular Technology, vol. 40, pp. 291-302, May 1991.
- [25] L. R. Pickholtz, L. B. Milstein and D. L. Schilling, "Spread spectrum for mobile communications", IEEE transactions on vehicular technology, vol. 40, N<sup>o</sup> 2, pp. 313-322. 1991.

- 
- [26] A.J. Viterbi, "CDMA Principles of Spread Spectrum Communication", Reading, MA, Addison-Wesley, 1995.
- [27] K. Sh. Zigangirov, *Theory of Code Division Multiple Access Communication*, IEEE Press 2004.
- [28] M. Patzold, *Mobile Fading Channels - Modelling, Analysis & Simulation*, Wiley, 2002, ISBN: 0471495492.
- [29] F.Simpson and J.M. Holtzman, "Direct Sequence CDMA Power Control, Interleaving, and coding", IEEE Journal on Selected Areas on Communication, vol. 11, N<sup>o</sup>. 7, pp. 1085-1095, 1993.
- [30] S. Verdu, *Multi-user Detection*, Cambridge University Press. 1998.
- [31] J. G. Proakis, *Digital Communications*, McGraw-Hill, New York, 3<sup>rd</sup> edition, 1995, ISBN: 0070517266.
- [32] E. H. Dinan and B. Jabbari, "Spreading Codes for Direct Sequence CDMA and Wideband CDMA Cellular Networks", IEEE Communications Magazine, pp.48–54, September 1998.
- [33] M. K. Simon, J. K. Omura, R. A. Scholtz and B. K. Levitt, *Spread Spectrum Communications Handbook*, McGraw-Hill, New York, 1994, ISBN:0071369643.
- [34] H. F. A. Roefs, *Binary Sequences for Spread-Spectrum Multiple-Access Communications*, Ph.D. thesis, University of Illinois, Urbana, Illinois, 1997.
- [35] R. Gold, "Optimal Binary Sequences for Spread Spectrum Multiplexing," IEEE Transactions on Information Theory, vol. IT-13, pp. 619–621, October 1967.
- [36] J. H. Lindholm, "An Analysis of the Pseudo-Randomness Properties of Subsequences of Long  $m$ -Sequences," IEEE Transactions on Information Theory, vol. IT-14, pp. 569–576, July 1968.
- [37] S. Vembu and A.J. Viterbi, "Two different philosophies in CDMA - a comparison", 46 IEEE Veh. Tech. Conference, vol. 2, pp. 869-73, May 1996.
- [38] Kärkkäinen K.H.A. & Laukkanen M.J. & Tarnanen H.K., "Performance of Asynchronous DS-CDMA System with Long and Short Spreading Codes", Electronics Letters, vol. 30, N<sup>o</sup>. 13, pp. 1035-1036, Jun. 1994.
- [39] G. A. Jeffrey, "Interference Cancellation for Cellular Systems: A Contemporary Overview", IEEE Wireless Communication, vol. 12, issue 2, pp: 19-29, April 2005
-

- 
- [40] S. Parkvall, "Long vs short spreading codes in cellular DS-CDMA", in Proceedings of the International Symposium on Spread-Spectrum Techniques and Applications, 1998, pp. 681–685.
- [41] S. Parkvall, "Variability of user performance in cellular DS-CDMA-long versus short spreading sequences," IEEE Transactions on Communications, vol. 48, pp. 1178-1187, July 2000.
- [42] M. Chryssomallis, "Simulation of mobile fading channels", IEEE Antennas and Propagation Magazine, vol 44, issue 6, pp.172–183, 2002.
- [43] R. Gustafsson and A. Mohammed, "Simulation of Wireless Fading Channels", Research report N°: 2003:02, May 2003.
- [44] W. Stallings. "Wireless Communications and Networks", Prentice-Hall, New Jersey, 2002.
- [45] S. Haykin. *Adaptive Filter Theory*. Prentice Hall, 4<sup>th</sup> edition, 2002.
- [46] A. U. Sheikh and A. Zerguine, "Adaptive Suppression of Multiuser Interference in a 3G W-CDMA System", Final Report, KACST, AT-21-58, November, 2006.
- [47] R. H. Clarke. "A statistical theory of mobile-radio reception", Bell Syst. Tech. Journal, vol. 47, pp. 957–1000, July/Aug 1968.
- [48] J. Nordberg and Hai Huyen dam. "Evaluation of different Rayleigh fading channel simulators", Technical report, ATRI, Curtin University, Australia, 2001.
- [49] R.B. Ertel, P. Cardieri, K.W. Sowerby, T.S. Rappaport and J.H. Reed, "Overview of spatial channel models for antenna array communication systems", IEEE Personal Communications, vol. 5, issue 1, pp: 10–22, Feb 1998.
- [50] David Huo, "Proposal of the Basic Fading Channel Model for the Link Level Simulation", technical report proposed to assist the IEEE 802.20 Working Group on Mobile Broadband Wireless Access, 2004-04-26.
- [51] ETSI TR 101 112, UMTS 30.03, V3.2.0, Annex B, Sections 1.2.3, 1.3, 1.4, 1998.
- [52] 3GPP, "Deployment aspects", 3GPP Technical Report 25.943 v5.1.0, Sophia Antipolis, France, 2002.
- [53] Alpha Concept Group, "Wideband Direct Sequence CDMA (WCDMA) Evaluation Document (3.0) ", Technical Document SMG 905/97, December 15-19, 1997, Madrid, Spain.

- 
- [54] J. C.Silva, N.S. Souto, F.C. Cercas, A. Correia and A. J. Rodrigues; “Efficient simulation of tapped delay channel models using converted discrete time channel models”, Proc. Conference on Telecommunications – Conf Tele , vol. 1 ,pp. 231 - 234, June 2003. Aveiro , Portugal
- [55] W. C. Jakes, *Microwave Mobile Communications*, IEEE, Inc., New York, 1974.
- [56] C. Komninakis, “A Fast and Accurate Rayleigh Fading Simulator”, in IEEE Globecom 2003, GC01-8, vol. 6, pp. 3306-10, San Francisco, CA, December 1-5, 2003.
- [57] X. Chengshan and Y.R.Zheng, “A statistical simulation model for mobile radio fading channels”, IEEE Wireless on Communications and Networking, vol.1, pp: 144- 149, 2003.
- [58] P. Dent, G. E. Bottomley and T. Croft, “Jakes fading model revisited” Electronics Letters, vol. 29, N°. 13, pp. 1162-1163, June 1993.
- [59] M. F. Pop and N. C. Beaulieu, “Limitations of sum-of-sinusoids fading channel simulators” IEEE Transactions on Communications, vol. 49, pp. 699-708, Apr. 2001.
- [60] Wu, Z., “Model of independent Rayleigh faders”, Electronics Letters, vol 40, issue. 15, pp: 949-951, July 2004.
- [61] Y. B. Li and Y. L. Guan, “Modified Jakes model for simulating multiple uncorrelated fading waveforms,” in Proceedings of IEEE ICC'00, pp. 46-49. 2000
- [62] Y. X. Li and X. Huang, “The simulation of independent Rayleigh faders”, IEEE Transactions on Communications, vol. 50, pp. 1503-1514, Sept. 2002.
- [63] Y. R. Zheng and C. Xiao, “Improved models for the generation of multiple uncorrelated Rayleigh fading waveforms,” IEEE Communication Letters, vol. 6, pp. 256-258, June 2002.
- [64] Y. R. Zheng and C. Xiao, “Simulation models with correct statistical properties for Rayleigh fading channels”, IEEE Transactions on Communications, vol. 51, issue. 6, pp: 920- 928, June 2003.
- [65] D.R. Brown, D.L. Anair and C.R. Johnson, Jr. , “Fractionally Sampled Linear Detectors for DS-CDMA”, Proc. Asilomar Conf. on Signals, Systems, and Computers (Pacific Grove, CA), pp. 1873- 1877, Nov. 1998.
- [66] L. K. Rasmussen, P. D. Alexander, and T. J. Lim, “CDMA techniques for third generation mobile systems” a book chapter in *A Linear Model for CDMA Signals Received with Multiple*

- 
- Antennas over Multipath Fading Channels*, F. Swarts, P. van Rooyan, I. Opperman, and M. P. L'otter, Eds. Dordrecht, The Netherlands: Kluwer, pp. 23–57, 1999.
- [67] M. Latva-aho, *Advanced Receivers for Wideband CDMA Systems*, Phd thesis, Faculty of Technology, University of Oulu, 1998.
- [68] M. Lava-aho and M.J. Jantti, "LMMSE Detection for DS CDMA Systems in Fading Channels", *IEEE Transactions on Communications*, vol.48, N<sup>o</sup>.2, Feb 2000.
- [69] I. S. Duff, "Combining direct and iterative methods for the solution of large systems in different application areas", technical report RAL-TR-2004-033.
- [70] Y. Saad and H.A. van der Vorst, "Iterative solution of linear systems in the 20th century", *Journal of Computational and Applied Mathematics*, vol. 123, N<sup>o</sup> 1, 1, pp. 1-33. Nov. 2000.
- [71] Y. Saad, *Iterative Methods for Sparse Linear Systems*, Second Edition 2003, publisher: Society for Industrial and Applied Mathematics (SIAM).
- [72] J. Xu, "The method of subspace corrections", *Journal of Computational and Applied Mathematics*, vol. 128, issue 1-2, pp: 335 - 362, March 2001.
- [73] T. Steihaug and Y. Yalcinkaya, "Deteriorating Convergence for Asynchronous Methods on Linear Least Sqare Problems", *European Conference on Parallel Processing*, pp. 750-759, 1997.
- [74] D. Kincaid and W. Cheney, "Numerical Analysis", 1991. Brooks/Cole, Pacific Grove.
- [75] I. S. Duff and H. A. van der Vost, "Preconditioning and parallel preconditioning", technical report RAL-TR-1998-052.
- [76] C.J. Zarowsky, *An introduction to numerical analysis for electrical and computer engineers* Wiley, 2004.
- [77] A. Bjoerck and G. Dahlquist, vols. 2 and 3, *Numerical mathematics and scientific computation*, (web draft), 1999.
- [78] M. Juntti. *Multiuser demodulation for DS-CDMA systems in fading channels*, PhD thesis, Oulu University, Department of Electrical Engineering, Oulu, Finland, 1998.
- [79] G.H. Golub, C.F. van Loan *Matrix computations*, 3ed, The Johns Hopkins University Press, 1996. ISBN0-8018-5413-X.

- 
- [80] R. S. Varga, *Matrix iterative analysis*, 2<sup>nd</sup> edition 2000.
- [81] H. B. Keller, "On the Solution of Singular and Semidefinite Linear Systems by Iteration", *Journal SIAM of Numerical Analysis*. Ser. B, vol. 2, N<sup>o</sup> 2, pp: 280-290, 1965.
- [82] M. H. Hayes. "Statistical digital signal processing and modeling", John wiley & sons, Inc. 1996.
- [83] A. Hadjidimos, "Successive overrelaxation (SOR) and related methods", *Journal of Computational and Applied Mathematics*, vol. 123, N<sup>o</sup> 1-2, p 177-199. Nov, 2000.
- [84] A. Grant and C. Schlegel, "Convergence of Linear Interference Cancellation Multiuser Receivers", *IEEE Transactions on Communications*, vol 49, N<sup>o</sup> 10, pp: 1824-1834, Oct. 2001
- [85] O. Axelsson, *Iterative Solution Methods*, Cambridge, U.K.: Cambridge Univ. Press, 1994.
- [86] B. Parhami, *Introduction to Parallel Processing Algorithms and Architectures*, Kluwer Academic Publishers, 2002, ISBN 0-306-45970-1.
- [87] R.M. Buehrer, N.S. Correal-Mendoza, B.D. Woerner, "Simulation Comparison of Multi-user Receivers for Cellular CDMA", *IEEE Transactions on Vehicular Technology*, vol. 49, issue. 4, pp: 1065 –1085. Jul 2000.
- [88] D. Koulakiotis and A. H. Aghvami, "Data Detection Techniques for DS/CDMA Mobile Systems: A Review," *IEEE Personal Communication.*, vol. 7, pp. 24-34, June 2000.
- [89] Upamanyu Madhow, "Multiuser Detection: An Overview and a New Result" invited paper, *Proc. International Workshop on Independent Component Analysis and Blind Signal Separation*, pp. 257- 266, Helsinki, Finland, June 2000.
- [90] Q. Xue, J. F. Weng, T. Le-Ngoc and S. Tahar, "Multiuser Detection Techniques: An Overview", *Technical Report*, Concordia University, Department of Electrical and Computer Engineering, October 1998.
- [91] R. Lupas and S. Verdu, "Linear multiuser detectors for synchronous code-division multiple-access channels" *IEEE Transactions on Information Theory*, vol. 35, N<sup>o</sup>. 1, pp. 123-136, Jan. 1989.
- [92] M. J. Juntti, B. Aazhang and J. O. Lilleberg, "Linear Multiuser Detection for R-CDMA", in *Proc. Commun. Theory Mini-Conf.*, *IEEE Global, Telecommun. Conf.*, London, England, pp. 127–131, Nov. 1996.

- 
- [93] H. C. Huang and S. C. Schwartz, "A comparative analysis of linear multi-user detectors for fading multi-path channels," Proc. IEEE GLOBECOM, pp. 11-15, 1994.
- [94] A. Yener, "Nonlinear Programming Based Detectors for Multiuser Systems", International Conference on Information Technology: Coding and Computing (ITCC '01), pp: 327-331. Las Vegas, NV, USA, 2001.
- [95] M. Honig, U. Madhow, and S. Verdu, "Blind adaptive multiuser detection," IEEE Transactions on Information Theory, vol. 41, N<sup>o</sup>. 4, pp. 944-960, July 1995.
- [96] U. Madhow, "Blind adaptive interference suppression for direct-sequence CDMA", Proc. IEEE, vol. 86, pp. 2049-2069, Oct. 1998.
- [97] J.J. Murillo-Fuentes, M. Sanchez-Fernandez and F. J. Gonzalez-Serrano, "Adaptive blind multiuser detection in asynchronous CDMA", IEEE VTS 53<sup>rd</sup> Vehicular Technology Conference, 2001. Spring VTC 2001. vol. 3, pp: 1844 – 1848, 6-9 May 2001.
- [98] P. Yuvapoositanon and A. J. Chambers, "Adaptive step-size constant modulus algorithm for DS-SS CDMA receivers in nonstationary environments", Signal Processing, vol. 82, N<sup>o</sup> 2, pp. 311-315, 2002.
- [99] T. Ojanperä, R. Prasad, and H. Harada, "Qualitative Comparison of Some Multiuser Detector Algorithms for Wideband CDMA," Proceedings of VTC'98, pp. 46-50. Ottawa, Canada, May 1998.
- [100] P.H. Tan and L.K. Rasmussen, "Multiuser Detection in CDMA – A Comparison of Relaxations, Exact and Heuristic Search Methods", IEEE Transaction on Wireless Communications, vol. 3, issue 5, pp. 1802-1809, September 2004.
- [101] F. Hasegawa, J. Luo, K. Pattipati, P. Willett, and D. Pham, "Speed and accuracy comparison of techniques for multiuser detection in synchronous CDMA", IEEE Transaction on Wireless Communications, vol. 52, pp. 540-545, Apr. 2004.
- [102] S. Verdu, "Computational complexity of optimum multiuser detection", Algorithmica, vol. 4, pp. 303–312, 1989.
- [103] T. J. Lim, D. Guo and L. K. Rasmussen, "Noise enhancement in the family of Decorrelating detectors for multiuser CDMA", in Proc. IEEE Asia-Pac. Conf. Comms. Int'l Conf. Comm. Systems (APCC/ICCS), pp. 401-405, Singapore, Nov. 1998.
-

- 
- [104] R. Lupas and S. Verdu, "Near-far resistance of multiuser detectors in asynchronous channels", IEEE Transaction on Wireless Communications, vol. 38, pp. 496-508, Apr. 1990.
- [105] H. V. Poor and S. Verdu, "Probability of Error in Multiuser Detection," IEEE Transactions on Information Theory, vol. 43, N<sup>o</sup>. 3, pp: 858–871, May 1997.
- [106] R. Price and P. E. Green, Jr., "A Communication Technique for Multipath Channels," Proc. IRE, vol. 46, pp. 55-570, Mar. 1958.
- [107] S. Striglis, *A Multistage RAKE Receiver for CDMA Systems*, Masters Thesis in Electrical Engineering, Virginia Polytechnic Institute and State University, Blacksburg, VA, Aug. 1994.
- [108] H. Elders-Boll, H. D. Schotten, and A. Busboom, "Efficient implementation of linear multiuser detectors for asynchronous CDMA systems by linear interference cancellation" European Transactions on Telecommunications, vol. 9, N<sup>o</sup>. 4, pp. 427-437, Sept./Nov. 1998.
- [109] Y. Ma, P. H. Tan, and T. J. Lim, "Systematic approach to multistage linear successive interference cancellation for multiuser detection in dynamic asynchronous CDMA systems", IEE Electronics Letters, vol. 35, issue 3, pp. 208-209, Feb. 1999.
- [110] Y. Ma and T. J. Lim, "Multistage linear successive interference cancellation for multipath decorrelating detection in fading channels" in Proc. IEEE W'kshop on Signal Proc. Advances in Wireless Comms. (SPAWC), (Annapolis, MD), pp. 186 - 189, May 1999.
- [111] N. Albeanu and T. J. Lim, "Optimization of linear iterative interference-cancellation receivers for CDMA communications", IEEE Transactions on Communications, vol. 52, N<sup>o</sup>3, pp. 376-379. March 2004.
- [112] P. H. Tan and L. K. Rasmussen, "Linear interference cancellation in CDMA based on iterative solution techniques for linear equation systems", IEEE Transaction on Communications, vol. 48, pp. 2099-2108, Dec. 2000.
- [113] P. H. Tan and L. K. Rasmussen, "Linear interference cancellation in CDMA based on block iterations", in the proceedings of the IEEE Veh. Tech. Conf. (Tokyo, Japan), pp. 740-744, May 2000.
- [114] P. J. Lanzkron, *Convergence of Nested Iterative Methods for Linear Systems*, PhD thesis Duke University, 1989.

- 
- [115] V. Migallón and J. Penadés, “Convergence of two-stage iterative methods for Hermitian positive definite matrices”, *Appl. Math. Lett.* vol. 10, No. 3, pp. 79-83, 1997.
- [116] N. K. Nichols, “On the Convergence of Two-Stage Iterative Processes for Solving Linear Equations”, *SIAM Journal of Numerical Analysis*, vol. 10, N<sup>o</sup>. 3, June 1973.
- [117] K. Jamal and E. Dahlman, “Multi-stage serial interference cancellation for DS-CDMA”, *IEEE 46<sup>th</sup> Vehicular Technology Conference*, 1996. vol. 2, pp: 671 –675. 28 Apr-1-May 1996.
- [118] L. K. Rasmussen, T. J. Lim, and A.-L. Johansson, “Convergence of linear successive interference cancellation in CDMA,” in *Proc. 3<sup>rd</sup> MMT Workshop* pp. 13–27, Melbourne, Australia, Dec. 1997,
- [119] L.K. Rasmussen, T.J. Lim and A.L Johansson, “One-shot filtering equivalence for linear successive interference cancellation in CDMA”, *IEEE 47<sup>th</sup> Vehicular Technology Conference*, vol. 3, 4-7, pp. 2163 -2167. May 1997.
- [120] H. Sugimoto, L. K. Rasmussen, T. J. Lim and T. Oyama, “Mapping functions for successive interference cancellation in CDMA”, in the *Proceedings of the IEEE Vehicular Technology Conference*, pp. 2301-2305, (Ottawa, Canada), May 1998.
- [121] L.K. Rasmussen, T.J. Lim and A.L Johansson, “A matrix-algebraic approach to successive interference cancellation in CDMA”. *IEEE Transactions on Communications*, vol: 48, issue: 1, pp: 145 –151. Jan 2000.
- [122] M. Ammar, T. Chonavel, S. Saoudi, “Asynchronous Multi-Stage SIC Detector For DS-CDMA Systems Over Multipath Fading Channels”, *Third IEEE Signal Processing Workshop on Signal Processing Advances in Wireless Communications*, pp: 190-193, Taoyuan, Taiwan, March 20-23, 2001.
- [123] M. Ammar, T. Chonavel, S. Saoudi, “Multi-Stage SIC Structure for Uplink UMTS Multiuser Receiver over Multipath Rayleigh Channels”, *IEEE VTS 53<sup>rd</sup> Vehicular Technology Conference*, vol.4, pp: 2514-2518. 2001.
- [124] A. L. Johansson and L. K. Rasmussen, “Linear group-wise successive interference cancellation in CDMA”, in the *Proceedings of the IEEE Int. Symp. Spread Spectrum Techniques and Appl.* pp. 121-126, Sun City, South Africa, Sept. 1998.

- 
- [125] S. Sun, L. K. Rasmussen, T. J. Lim, and H. Sugimoto, "A matrix-algebraic approach to linear hybrid interference canceller in CDMA", in the Proceedings of the IEEE Int. Conf. Univ. Personal Commun. pp. 1319-1323, Florence, Italy, Oct. 1998.
- [126] A. Bentrucia, A.U. Sheikh, A. Zerguine, "An improved HIC using a new ordering and grouping algorithm", Seventh International Symposium on Signal Processing and Its Applications ISSPA2003, Proceedings 2003. vol. 1, pp: 49 – 52. July 1-4, 2003.
- [127] A. Bentrucia, A. U. Sheikh, and A. Zerguine, "A New Ordering and Grouping Algorithm for the Linear Weighted Group Matched Filter Successive Interference Canceller" IEEE Transactions on Vehicular Technology, vol. 55, N<sup>o</sup>. 2, pp. 704-708, March 2006.
- [128] D. Guo, L. K. Rasmussen, S. Sun, and T. J. Lim, "A Matrix-Algebraic Approach to Linear Parallel Interference Cancellation in CDMA", IEEE Transactions on Communications, vol. 48, N<sup>o</sup>. 1, January 2000.
- [129] L. K. Rasmussen and I. J. Oppermann, "Convergence behaviour of linear parallel cancellation in CDMA", IEEE Global Telecom. Conf. San Antonio, Texas, pp. 3148-3152, Dec. 2001.
- [130] L. K. Rasmussen, D. Guo, T. J. Lim and Y. Ma, "Aspects on linear parallel interference cancellation in CDMA", Proceedings 1998 IEEE International Symposium on Information Theory, pp. 37, Cambridge, MA, USA, Aug. 1998.
- [131] D. Guo, L. K. Rasmussen and T. J. Lim, "Linear Parallel Interference Cancellation in Long-Code CDMA Multiuser Detection", IEEE Journal on Selected Areas on Communications, vol. 17, N<sup>o</sup> 12, pp. 2074-2081, Dec. 1999.
- [132] D. Guo, L. K. Rasmussen, S. Sumei, T. J. Lim and C. Cheah, "MMSE-based linear parallel interference cancellation in CDMA" in Proc. IEEE Int. Symp. Spread Spectrum Techniques and Appl., pp. 917–921. Sun City, South Africa, Sept. 1998.
- [133] D. Guo, L. K. Rasmussen and T. J. Lim, "MMSE-based parallel interference cancellation for long-code CDMA", in the proceedings of the The Zurich Seminar on Broadband Commun. pp. 31-38, Zurich, Switzerland, Feb. 2000.
- [134] L. K. Rasmussen and I. J. Oppermann, "Ping-pong effects in linear parallel interference cancellation for CDMA", IEEE Transactions on Wireless Communications, vol. 2, pp. 357-363, Mar. 2003.

- 
- [135] W. Kahan, *Gauss-Seidel Methods of Solving Large Systems of Linear Equations*, Doctoral Thesis, University of Toronto, Toronto, Canada, 1958.
- [136] S. Sun, L.K. Rasmussen, H. Sugimoto and T.J. Lim. "A hybrid interference canceller in CDMA". IEEE 5<sup>th</sup> International Symposium on Spread Spectrum Techniques and Applications. Proceedings 1998, vol. 1, pp: 150 -154, 2-4 Sep 1998.
- [137] A. Bentrchia, A. Zerguine, A.U. Sheikh and W.A. Saif, "A linear group polynomial expansion successive interference cancellation detector", 14<sup>th</sup> IEEE Proceedings on Personal, Indoor and Mobile Radio Communications, 2003. PIMRC 2003. vol. 2, pp: 1546 – 1550. Sept. 7-10, 2003.
- [138] D. J. Kim, S. R. Kwon, and C. E. Kang, "Multiuser detection using blockwise successive interference cancellation in DS/CDMA systems," in Proc. IEEE VTC'98, May 1998, pp. 1835-1838.
- [139] L. Rossi, C. H. Hwang and C. C. J. Kuo, "Performance analysis of multistage linear groupwise interference cancellation via graphical approach", Proc. of IEEE WCNC'03, pp: 883-887, New Orleans, Louisiana, USA, March 16-20, 2003.